ISSN (Print) : 2277-7261

PRATIBHA

INTERNATIONAL JOURNAL OF SCIENCE, SPIRITUALITY, BUSINESS & TECHNOLOGY (IJSSBT)

Vol.1, No.1, March 2012

www.ijssbt.org

SHRAM SADHANA BOMBAY TRUST's

COLLEGE OF ENGINEERING & TECHNOLOGY, BAMBHORI, JALGAON (INDIA)

PRATIBHA : INTERNATIONAL JOURNAL OF SCIENCE,SPIRITUALITY, BUSINESS & TECHNOLOGY (IJSSBT) Vol.1,No.1, March 2012 ISSN (Print) : 2277-7261

Smt Pratibha Devisingh Patil
President of India

Our inspiration
to impart Quality Education for
societal development.

PRATIBHA

INTERNATIONAL JOURNAL OF SCIENCE, SPIRITUALITY, BUSINESS & TECHNOLOGY
Vol.1, No.1, March 2012 | ISSN (Print) : 2277-7261

- 25 March 2012 -

PRATIBHA: INTERNATIONAL JOURNAL OF SCIENCE, SPIRITUALITY, BUSINESS AND TECHNOLOGY

(IJSSBT)

Vol.1, No.1, March 2012

ISSN (Print) : 2277-7261

www.ijssbt.org

EDITOR(s)-IN-CHIEF:

Prof. Dr. Kishor S. Wani

Prof. Dr. Shailendra Kumar Mittal

IJSSBT

PRATIBHA: INTERNATIONAL JOURNAL OF SCIENCE, SPIRITUALITY, BUSINESS AND TECHNOLOGY (IJSSBT)

PRATIBHA: INTERNATIONAL JOURNAL OF SCIENCE, SPIRITUALITY, BUSINESS AND TECHNOLOGY (IJSSBT) is a research journal published by Shram Sadhana Bombay Trust's COLLEGE of ENGINEERING & TECHNOLOGY, Bambhori, Jalgaon (MAHARASHTRA, INDIA). College was founded by PRESIDENT, GOVT. of INDIA, Honorable Excellency **Sau. PRATIBHA DEVI SINGH PATIL.**

College is awarded as **Best Engineering College of Maharashtra State** by Engineering Education Foundation Pune in year 2008-09.

The College has ten full-fledged departments. The Under Graduate programs in 7 courses are accredited by National Board of Accreditation, All India Council for Technical Education, New Delhi for 5 years with effect from 19/07/2008 vide letter number NBA/ACCR-414/2004. QMS of the College conforms to ISO 9001:2008 and is certified by JAAZ under the certificate number: 1017-QMS-0117.The college has been included in the list of colleges prepared under Section 2(f) of the UGC Act, 1956 vide letter number F 8-40/2008 (CPP-I) dated May, 2008 and 12(B) vide letter number F. No. 8-40/2008(CPP-I/C) dated September 2010. UG courses permanently affiliated to North Maharashtra University are: Civil Engineering, Chemical Engineering, Computer Engineering, Electronics and Telecommunication Engineering, Electrical Engineering, Mechanical Engineering, Information Technology. Two years Post Graduate courses are Mechanical Engineering in specialization with Machine Design, Civil Engineering in specialization with Environmental Engineering, Computer Engineering in specialization with Computer Science and Engineering, Electronics and Telecommunication in specialization with Digital Electronics. Civil Engineering Department and Mechanical Engineering Department labs are registered for Ph.D. Programs. Spread over 25 Acres, the campus of the college is beautifully located on the bank of River Girna.

The International Journal of Science, Spirituality, Business and Technology (IJSSBT) is an excellent, intellectual, peer reviewed journal that takes scholarly approach in creating, developing, integrating, sharing and applying knowledge about all the fields of study in Engineering, Spirituality, Management and Science for the benefit of humanity and the profession.

The audience includes researchers, managers, engineers, curriculum designers administrators as well as developers.

AIM AND SCOPE

Our philosophy is to map new frontiers in emerging and developing technology areas in research, industry and governance, and to link with centers of excellence worldwide to provide authoritative coverage and references in focused and specialist fields. The journal presents its readers with broad coverage across all branches of Engineering, Management Spirituality and Science of the latest development and applications.

All technical or research papers and research results submitted to IJSSBT should be original in nature. Contributions should be written for one of the following categories:

1. Original research
2. Research Review / Systematic Literature Review
3. Short Articles on ongoing research
4. Preliminary Findings
5. Technical Reports / Notes

IJSSBT publishes on the following topics but NOT LIMITED TO:

SCIENCES

- Computational and industrial mathematics and statistics, and other related areas of mathematical sciences
- Approximation theory
- Computation
- Systems control
- Differential equations and dynamical systems
- Financial math
- Fluid mechanics and solid mechanics
- Functional calculus and applications
- Linear and nonlinear waves
- Numerical algorithms
- Numerical analysis
- Operations research
- Optimization
- Probability and stochastic processes
- Simulation
- Statistics
- Wavelets and wavelet transforms
- Inverse problems
- Artificial intelligence
- Neural processing
- Nuclear and particle physics
- Geophysics
- Physics in medicine and biology
- Plasma physics
- Semiconductor science and technology
- Wireless and optical communications
- Materials science
- Energy and fuels
- Environmental science and technology
- Combinatorial chemistry
- Natural products
- Molecular therapeutics
- Geochemistry
- Cement and concrete research,
- Metallurgy
- Crystallography and
- Computer-aided materials design

COMPUTER ENGINEERING AND INFORMATION TECHNOLOGY

- Information Systems
- e-Commerce
- Intelligent Systems
- Information Technology
- e-Government
- Language and Search Engine Design
- Data Mining and Web Mining
- Cloud Computing
- Distributed Computing
- Telecommunication Systems
- Artificial Intelligence
- Virtual Business and Enterprise
- Computer Systems
- Computer Networks
- Database Systems and Theory
- Knowledge Management

- Computational Intelligence
- Simulation and Modeling
- Scientific Computing and HPC
- Embedded Systems
- Control Systems

ELECTRONICS AND TELECOMMUNICATION ENGINEERING

- 3D Vision
- 3D TV
- Biometrics
- Graph-based Methods
- Image and video indexing and database retrieval
- Image and video processing
- Image-based modeling
- Kernel methods
- Model-based vision approaches
- Motion Analysis
- Non-photorealistic animation and modeling
- Object recognition
- Performance evaluation
- Segmentation and grouping
- Shape representation and analysis
- Structural pattern recognition
- Computer Graphics Systems and Hardware
- Rendering Techniques and Global Illumination
- Real-Time Rendering
- Fast Algorithms
- Fast Fourier Transforms
- Digital Signal Processing
- Wavelet Transforms
- Mobile Signal Processing
- Statistical Signal Processing
- Optical Signal Processing
- Data Mining Techniques
- Motion Detection
- Content-based Image retrieval
- Video Signal Processing
- Watermarking
- Signal Identification
- Detection and Estimation of Signal Parameters
- Nonlinear Signals and Systems
- Signal Reconstruction
- Time-Frequency Signal Analysis
- Filter Design and Structures
- Spectral Analysis
- Adaptive and Clustering Algorithms
- Fast Fourier Transforms
- Virtual, Augmented and Mixed Reality
- Geometric Computing and Solid Modeling
- Game Design and Engine Development
- 3D Reconstruction
- GPU Programming
- Graphics and Multimedia
- Image Processing
- Interactive Environments
- Software and Web accessibility
- Graphics & Perception
- Computational Photography
- Pattern recognition and analysis
- Medical image processing
- Visualization
- Image coding and compression
- Face Recognition
- Image segmentation
- Face recognition
- Radar Image Processing
- Sonar Image Processing
- Signal Identification
- Super-resolution imaging
- Signal Reconstruction
- Filter Design
- Adaptive Filters
- Multi-channel Filtering
- Noise Control
- Control theory and practice

CIVIL ENGINEERING

- Geotechnical
- Structures
- Transportation
- Environmental Engineering
- Earthquakes
- Water Resources
- Hydraulic and Hydraulic Structures
- Construction Management, and Material
- Structural mechanics
- Soil mechanics and Foundation Engineering
- Coastal engineering and River engineering

- Ocean Engineering
- Fluid-solid-structure interactions, offshore engineering and marine structures
- Constructional management and other civil engineering relevant areas
- Surveying
- Transportation Engineering

CHEMICAL ENGINEERING

- Organic Chemistry
- Inorganic Chemistry
- Physical Chemistry
- Analytical Chemistry
- Biological Chemistry
- Industrial Chemistry
- Agricultural & Soil Chemistry
- Petroleum Chemistry
- Polymers Chemistry
- Nanotechnology
- Green Chemistry
- Forensic
- Photochemistry
- Computational
- Chemical Physics
- Chemical Engineering
- Wastewater treatment and engineering
- Biosorption
- Chemisorptions
- Heavy metal remediation
- Phytoremediation
- Novel treatment processes for wastewaters
- Land reclamation methods
- Solid waste treatment
- Anaerobic digestion
- Gasification
- Landfill issues
- Leachate treatment and gasification
- Water and Wastewater Minimization
- Mass integration
- Emission Targeting
- Pollution Control
- Safety and Loss Prevention
- Conceptual Design
- Mathematical Approach
- Pinch Technology
- Energy Audit
- Production Technical Knowledge

ELECTRICAL ENGINEERING

- Power Engineering
- Electrical Machines
- Instrumentation and control
- Electric Power Generation
- Transmission and Distribution
- Power Electronics
- Power Quality & Economic
- Renewable Energy
- Electric Traction, Electromagnetic Compatibility and Electrical Engineering Materials
- High Voltage Insulation Technologies
- High Voltage Apparatuses
- Lightning Detection and Protection
- Power System Analysis, SCADA and Electrical Measurements

MECHANICAL ENGINEERING

- Fluid mechanics
- Heat transfer
- Solid mechanics
- Refrigeration and air conditioning
- Renewable energy technology
- Materials engineering
- Composite materials
- Marine engineering
- Petroleum and mineral resources engineering
- Textile engineering
- Leather technology
- Industrial engineering
- Operational research
- Manufacturing processes
- Machine design
- Quality control
- Mechanical maintenance
- Tribology

MANAGEMENT

- Accounting and Finance
- Marketing
- Operations Management
- Human resource management
- Management Strategy
- Information technology
- Business Economics
- Public Sector management
- Organizational behavior
- Research methods

SPIRITUALITY

- Relevance of Science & Spirituality in decision & Policy making
- Rigors in Scientific Research & Insights from Spiritual wisdom
- Dividends from Scientific research & Spiritual Temper
- Spiritual Wisdom in disaster management
- Techno-Spiritual aspects of development

BIO-TECHNOLOGY

- Molecular biology and the chemistry of biological process to aquatic and earth environmental aspects as well as computational applications
- Policy and ethical issues directly related to Biotechnology
- Molecular biology
- Genetic engineering
- Microbial biotechnology
- Plant biotechnology
- Animal biotechnology
- Marine biotechnology
- Environmental biotechnology
- Biological processes
- Industrial applications
- Bioinformatics
- Biochemistry of the living cell
- Bioenergetics

IJSSBT prides itself in ensuring the high quality and professional standards.
All submitted papers are to be peer-reviewed for ensuring their qualities.

Frequency : Two issues per year
Page charges : There are no page charges to individuals or institutions.
ISSN : 2277-7261 (Print version)
Subject Category : Science, Engineering, Business and Spirituality
Published by : Shram Sadhana Bombay trust's College of Engineering and Technology, Bambhori, Jalgaon

REQUIREMENTS FOR MANUSCRIPT PREPARATION

The following information provides guidance in preparing manuscript for IJSSBT.

- Papers are accepted only in English.
- Papers of original research, research review/systematic literature review, short articles on ongoing research, preliminary findings, and technical reports/notes should not exceed 15 typeset, printed pages.
- Abstracts of 150-200 words are required for all papers submitted.
- Each paper should have three to six keywords. Section headings should be concise and numbered sequentially as per the following format.
- All the authors (maximum three authors) of a paper should include their full names, affiliations, postal address, telephone and fax numbers and email address on the cover page of the manuscript as per following format. One author should be identified as the Corresponding Author.

- Biographical notes on contributors are not required for this journal.
- For all manuscripts non-discriminatory language is mandatory. Sexist or racist terms should not be used.
- Authors must adhere to SI units . Units are not *italicized*.
- The title of the paper should be concise and definitive (with key words appropriate for retrieval purposes).

Manuscript Format

Document : The **Manuscript** should be prepared in English language by using MS Word (.doc format). An IJSSBT paper should not exceed 15 typeset, printed pages including references, figures and abstract etc.

Paper : Use A4 type paper page (8.27″x 11.69″).

Paper format: two columns with equal width and spacing of 0.25″.

Margins : Leave margins of article 1.3" at the left and for top, bottom, and right sides 1″.

Font Size & Style: 10 Point Times new roman, and typed in single space, Justified.

Title Page :

- Title of the paper should be in bold face, Title case: font size 16, Times New Roman, centered.

- Name of the authors in normal face, Title case: font size 11 italic, Times New Roman.
- Addresses and affiliations of all authors: normal face, title case font size 10, Times New Roman.
- Email address: normal face, lower case font size 10, Times New Roman.

Abstract (Font size 10, bold face)
Abstract should be in brief and structured. The abstract should tell the context, basic procedure, main findings and principal conclusions. It should emphasize new aspect of study or research. Avoid abbreviation, diagram and references in abstract. It should be single spaced and should not exceed more than 200 words.

Keywords: **(Font size 10, bold face, italic)**

I. INTRODUCTION (Font size 10, bold face)

Provide background, nature of the problem and its significance. The research objective is often more sharply focused when stated as a question. Both the main and secondary objectives should be clear. It should not include data or conclusions from the work being reported.

All Main Heading with Roman numbers (Font size 10, bold face)

With Subheading of (Font size 10, bold face, Title Case with A, B, C…..Numbering)

Picture / Figure : Pictures and figures should be appropriately included in the

main text, e.g. Fig No. 1 (Font size 9).

Table format : Font: Times New Roman, font size: 10
e.g. Table No. 1 (Font size 9)

References (font size 8, Times New Roman)

References should be arranged alphabetically with numbering. References must be complete and properly formatted. Authors should prepare the references according to the following guidelines.

For a book:
References must consist of last name and initials of author(s), year of publication, title of book (italicized), publisher's name, and total pages.

[1] Name and initial of the Author, "Topic Name", title of the book, Publisher name, Page numbers, Year of publication.

For a chapter in a book:
References must consist of last name and initials of author(s), year of publication, title of chapter, title of book (italicized), publisher's name, and inclusive pages for the chapter.

[1] Name and initial of Author, "Title of chapter", *title of the book*, Publisher name, total pages of chapter, year of publication.

For a Journal article:
Journals must consist of last name and initials of author(s), year of publication of journal, title of paper, title of journal (italicized),volume of journal, page numbers (beginning of article - end of article).

[1] Name and initial of the Author, "topic name", *title of journal*, volume & issue of the journal; Page numbers of article, year of publication.

Conference Proceedings:
References must consist of last name and initials of author(s), year of publication, title of paper, indication of the publication as proceedings, or extended abstracts volume; name of the conference (italicized or underlined), city and state and Country where conference was held, conference sponsor's name, and pages of the paper.

[1] Name and initial of the Author, title of the paper, Proceedings, *name of the conference*, City, State, country, page numbers of the paper, Year of publication.

The title of the journal is italicized and font size 8, Times New Roman.

Final Submission:
Each final full text paper (.doc, .pdf) along with corresponding signed copyright transfer form should be submitted by email
editor@ijssbt.org,
mittalsai@rediffmail.com

Website: www.ijssbt.org/com

S.S.B.T.'S COLLEGE OF ENGINEERING & TECHNOLOGY, BAMBHORI, JALGAON

GOVERNING BODY

Dr. D. R. Shekhawat	***Chairman***
Shri Rajendrasingh D. Shekhawat	***Managing Trustee & Member***
Shri V. R. Phadnis	***Member***
Shri Jayesh Rathore	***Member***
Mrs. Jyoti Rathore	***Member***
Dr. R. H. Gupta	***Member***
Arch. Shashikant R. Kulkarni	***Member***
Dr. K.S. Wani	***Principal & Ex-Officio Member Secretary***
Shri S. P. Shekhawat	***Asstt. Prof. & Member***
Shri Shantanu Vasishtha	***Asstt. Prof. & Member***

LOCAL MANAGEMENT COMMITTEE

Dr. D. R. Shekhawat	***Chairman***
Shri Rajendrasingh D. Shekhawat	***Managing Trustee & Member***
Shri V. R. Phadnis	***Member***
Dr. R. H. Gupta	***Member***
Arch. Shashikant R. Kulkarni	***Member***
Dr. K.S. Wani	***Principal & Ex-Officio Member Secretary***
Shri S. P. Shekhawat (Representative of Teaching Staff)	***Asstt. Prof. & Member***
Shri Shantanu Vasishtha (Representative of Teaching Staff)	***Asstt. Prof. & Member***
Shri S. R. Girase (Representative of Non-Teaching Staff)	***Member***

EDITOR(s)-IN-CHIEF

Prof. (Dr.) K. S. WANI,
M. Tech. (Chem. Tech.), D.B.M., Ph. D.
LMISTE, LMAFST, MOTAI, LMBRSI
Principal,
S.S.B.T.'s College of Engineering and Technology,
P.B. 94, Bambhori,
Jalgaon-425001 Maharashtra, India
Mobile No. +919422787643
Phone No. (0257) 2258393,
Fax No. (0257) 2258392,
Email id: wani.kishor@gmail.com

Dr. SHAILENDRA KUMAR MITTAL
Ph.D. (Electrical Engineering)
Professor
Member IEEE, Senior Member IACSIT, LMISTE
Director - Research and Development
S.S.B.T.'s College of Engineering and Technology,
P.B. 94, Bambhori,
Jalgaon-425001 Maharashtra, India
Mobile No. +91 9422788382
Phone No. (0257) 2258393,
Fax No. (0257) 2258392.
Email id : editor@ijssbt.org
mittalsai@rediffmail.com

Web Address : www.ijssbt.org/com

EDITORIAL BOARD

Prof. SUBRAMANIAM GANESAN
Director, Real Time & DSP Lab.,
Electrical and Computer Engineering Department,
Oakland University, Rochester, MI 48309, USA.
IEEE Distinguished Visiting Speaker (2005-2009) and Coordinator.
IEEE SEM CS chapter Chair, Region 4 and CS Society Board member
SAE, ASEE, ACM member

Prof. ALOK VERMA
Old Dominion University
Norfolk
Virginia, USA

Prof. EVANGELINE GUTIERREZ
Programme Manager, Global Science and Technology Forum Pvt. Ltd
10 Anson Road, Singapore

Dr. G.P. PATIL
Distinguish Professor of Mathematics Statistics
Director, Center for Statistical Ecology and Environmental Statistics
Editor-in-Chief, Environmental and Ecological Statistics
Department of Statistics
The Pennsylvania State University, USA

Dr. ABAD A. SHAH
Professor**,** Department of Computer Science & Engineering
University of Engineering and Technology
G. T. Road Lahore, Pakistan

Dr. ANSHUMAN TRIPATHI
Ph. D.
Principal Engineer
VESTAF, SINGAPORE

Dr. MUHAMMAD MASROOR ALI
Professor, Department of Computer Science and Engineering
Bangladesh University of Engineering and Technology
Dhaka-1000, Bangladesh mmasroorali@cse.buet.ac.bd

Dr. RAMESH CHANDRA GOEL
Former Director General
Deharadun Institute of Technology
Deharadun, Uttarakhad, India

Dr. DINESH CHANDRA
Ph. D.
Professor
Department of Electrical Engineering
Motilal Nehru National Institute of Technology
Allahabad-U.P., India

Dr. BHARTI DWIVEDI
Ph. D.
Professor
Department of Electrical Engineering
Government Institute of Engineering & Technology
Luknow, India

Dr. L. A. Patil
Ph. D.
Professor & Head
Dept of Physics
Pratap College Amalner
Jalgaon, India

Dr. M. QASIM RAFIQ
Ph. D. (Computer Engineering)
Professor
Senior Member IEEE (USA)
FIETE, FIE, LMCSI
Department of Computer Engineering
Z.H. College of Engineering & Technology
Aligarh Muslim University (A.M.U.)Aligarh, India

Dr. RAZAULLHA KHAN
Ph. D. (Civil Engineering)
Professor
Department of Civil Engineering
Z.H. College of Engineering & Technology
Aligarh Muslim University (A.M.U.)
Aligarh, India

Dr. K. HANS RAJ
Professor
Department of Mechanical Engineering
Faculty of Engineering
Dayalbagh Educational Institute, Dayalbagh
AGRA-India

Dr. DURGESH KUMAR MISHRA
Professor and Head (CSE), Dean (R&D)
Acropolis Institute of Technology and Research, Indore, MP, India
Chairman, IEEE Computer Society, Bombay Chapter
Chairman IEEE MP Subsection
Chairman CSI Indore Chapter

Dr. SUDHIR CHINCHOLKAR
Ph.D. Microbiology
Professor & Head (Microbiology)
N.M.U. University, Jalgaon, India

Dr. M. A. LOKHANDE
Ph. D.
Professor and Head
Department of Commerce
Member Indian Commerce Association
Dr. Babasaheb Ambedkar Marathwada University, Aurangabad, India

Dr. K. K. SHUKLA
Ph.D.
Professor
Department of Civil Engineering
Motilal Nehru National Institute of Technology
Allahabad- U.P., India

Dr. RAHUL CAPRIHAN
Ph.D.
Professor
Department of Mechanical Engineering
Faculty of Engineering
Dayalbagh Educational Institute
Dayalbagh, Agra, India

Dr. SATISH KUMAR
Ph. D.
Professor
Department of Electrical Engineering
Faculty of Engineering
Dayalbagh Educational Institute
Dayalbagh, Agra, India

Dr. VED VYAS J. DWIVEDI
Professor (Electronics and Communication Engineering)
Director
Noble Group of Institutions, Junagadh, Gujarat, India
Editor-in-Chief
International Journal on Science and Technology

Dr. RAM PAL SINGH
Ph.D.
Professor
Department of Civil Engineering
Motilal Nehru National Institute of Technology
Allahabad- India

Dr. ANURAG TRIPATHI
Ph.D.
Professor
Department of Electrical Engineering
Government Institute of Engineering & Technology
Luknow, India

Dr. (Mrs.) ARUNIMA DE
Ph.D.
Professor
Department of Electrical Engineering
Government Institute of Engineering & Technology
Luknow, India

Dr. A.P. DONGRE
Ph. D.
Department of Management Studies
North Maharashtra University, Jalgaon India

Dr. V. VENKATACHALAM
Principal, The Kavery Engineering College,
Mecheri. Salem District.

Dr. T. RAVICHANDRAN
Research Supervisor,
Professor & Principal
Hindustan Institute of Technology
Coimbatore, Tamil Nadu, India

Dr. BHUSHAN TRIVEDI
Professor & Director, GLS-MCA, Ahmedabad.

Dr. NEERAJ BHARGAVA
HoD, Department of Computer Science,
MDS University, Ajmer.

Dr. CRISTINA NITA-ROTARU
Purdue University

Dr. RUPA HIREMATH
Director, IIPM, Pune

Dr. A. R. PATEL
HoD, Department of Computer Science,
H. North Gujarat University, Patan. Gujarat

Dr. PRIYANKA SHARMA
Professor, ISTAR, VV Nagar,
Gujarat.

Dr. V.P.ARUNACHALAM
Principal
SNS College of Technology
Sathy Main Road,
Coimbatore - 35.

Dr. B. S. AGRAWAL
Gujarat

Dr. SATYEN PARIKH
Professor, Dept of Comp Sci.
Ganpat University, Mehsana. Gujarat.

Dr. P. V. VIRAPARIA
VV Nagar, Gujarat.

Dr. ARUMUGANATHAN
Professor, Department of Mathematics and Computer Applications
PSG College of Technology, Coimbatore-641 004
Tamilnadu, INDIA.

Dr. H. B. BHADKA
Director (I/c)
C. U. Shah College of Master of Computer Application
Campus of C. U. Shah College of Engineering & Technology
Surendranagar-Ahmedabad

Dr. MOHAMMED MUSSADIQ
Ph. D.
Professor & Head, Department of Microbiology,
Shri Shivaji College of Arts, Commerce & Science, Akola.

Dr. ZIA-UL HASAN KHAN
Ph. D.
Professor & Head, Department of Biochemistry,
Shri Shivaji College of Arts, Commerce & Science, Akola.

PUBLICATION SECRETARY

SUHAS M. SHEMBEKAR
Assistant Professor
Electrical Engineering Department
S. S. B. T.'s College of Engineering and Technology, Bambhori, Jalgaon (M.S.)

DHANESH S. PATIL
Assistant Professor
Electrical Engineering Department
S. S. B. T.'s College of Engineering and Technology, Bambhori, Jalgaon (M.S.)

LOCAL REVIEW COMMITTEE

Dr. K. S. Wani
Principal
S.S.B.T.'s College of Engineering & Technology,
Bambhori, Jalgaon

S. R. Suralkar
Associate Professor & Head
Department of Electronics & Telecommunication Engineering

Dr. M. Husain
Professor & Head
Department of Civil Engineering

J. R. Chaudhary
Associate Professor & Head
Department of Mechanical Engineering

Dr. I.D. Patil
Professor & Head
Department of Bio-Technology

K. P. Adhiya
Associate Professor & Head
Department of Computer Engineering

Dr. S.L. Patil
Associate Professor & Head
Department of Applied Science

D. U. Adokar
Associate Professor & Head
Department of Electrical Engineering

Dr. M. N. Panigrahi
Professor
Department of Applied Science

S. S. Gharde
Assistant Professor & Head
Department of Information Technology

Dr. V.R. Diware
Assistant Professor
Department of Chemical Engineering

V. S. Rana
Assistant Professor & Head
Department of Business Administration

PRATIBHA: INTERNATIONAL JOURNAL OF SCIENCE, SPIRITUALITY, BUSINESS AND TECHNOLOGY
(IJSSBT)
Table of Contents

Volume 1, No.1, March, 2012

PRATIBHA: INTERNATIONAL JOURNAL OF SCIENCE, SPIRITUALITY, BUSINESS AND TECHNOLOGY (IJSSBT), Vol. 1, No.1, March 2012
ISSN (Print) 2277—7261

Luus Jaakola Algorithm Based Order Reduction of Discrete Interval Systems

Vinay Pratap Singh[1], *Dinesh Chandra*[2], *Robin Rastogi*[3]
[1,3]EED, M. N. National Institute of Technology, Allahabad-211004, India
[2]Professor, EED, M. N. National Institute of Technology, Allahabad-211004, India
Emails: [1]vinaymnnit@gmail.com, [2]dinuchandra@rediffmail.com, [3]robinrastogi@gmail.com

Abstract: This paper presents a method for order reduction of discrete interval systems in which the denominator of the model is obtained by pole-clustering while the numerator is derived by retaining first *m* time moments/Markov parameters of high-order discrete interval system as well as minimizing errors between subsequent *n* time moments/Markov parameters of high-order discrete interval system and model, such that *m* + *n* = *r*, where *r* is the order of model. The inverse distance measure criterion is used for pole clustering. The algorithm due to Luus Jaakola is used for minimization of objective function which is weighted squared sum of errors between n time moments/Markov parameters of high-order discrete interval system and those of the model. The proposed method is validated by a worked example.

Keywords: Interval system, Kharitonov Polynomials, Order reduction, Padé approximants, Pole-clustering method.

I. INTRODUCTION

Various methods have been proposed for order reduction of continuous-time and discrete-time systems. Out of these methods, the methods based on power series expansion [1]-[10] of the system transfer function have received considerable attention of researchers. One of these methods, which is known as Padé approximation [1] has been found to very useful in theoretical physical research [11]-[12] due to its simplicity. But the model obtained using Padé approximation often leads to be unstable even though the high-order system is stable. To overcome this problem, Routh approximant [4] was introduced. However, this method tends to approximate only low frequency behavior of high-order system [13]. Therefore, Routh approximant does not always lead to good model. Various attempts [5]-[9] have been made to improve the Routh approximant method.

Some of the above methods have been applied for order reduction of high-order interval systems [14]-[20]. Bandypadhyay *et al.* [14] presented Routh-Padé approximation for order reduction of high-order continuous interval systems in which the denominator is obtained by direct truncation of the Routh-table and the numerator is obtained by matching the time moments of the high-order interval system and model. In [20], a method is presented for obtaining the model of high-order discrete interval system (HODIS) in which the denominator of model is determined by retaining dominant poles of the HODIS and the numerator is obtained by matching first r time moments of the HODIS and model. However, in this method only time moments are considered for obtaining the model. For good overall response, Markov parameters should also be considered in addition to time moments as the transient state and steady state matching depend on Markov parameters and time moments, respectively.

In this paper, a method for order reduction of HODIS in which the denominator of the model is determined [21]-[23] by pole-clustering and the numerator is derived by retaining first m time moments/Markov parameters of HODIS as well as minimizing errors between subsequent n time moments/Markov parameters of HODIS and model, such that $m + n = r$. The Luus Jaakola algorithm is used for minimization of objective function which is weighted squared sum of errors between n time moments/Markov parameters of HODIS and those of the model. The IDM criterion is used for pole clustering. The brief outline of this paper is organized as follows: section-II covers problem formulation, section-III contains Luus Jaakola algorithm, a worked numerical example is included in section-IV to illustrate the method and finally, paper is concluded in section-V.

II. PROBLEM FORMULATION

Consider a HODIS given by the transfer function

$$\left.\begin{aligned} G_n(z) &= \frac{[b_0^-, b_0^+] + [b_1^-, b_1^+]z + \cdots + [b_{n-1}^-, b_{n-1}^+]z^{n-1}}{[a_0^-, a_0^+] + [a_1^-, a_1^+]z + \cdots + [a_n^-, a_n^+]z^n} \\ &= \frac{N(z)}{D(z)} \end{aligned}\right\} \quad (1)$$

where $[a_i^-, a_i^+]$ for $i = 0,1,\cdots,n$ are denominator

coefficients of $G_n(z)$ with a_i^- and a_i^+ as lower and upper bounds of interval $[a_i^-, a_i^+]$, respectively, and $[b_i^-, b_i^+]$ for $i = 0,1,\cdots,n-1$ are numerator coefficients of $G_n(z)$ with b_i^- and b_i^+ as lower and upper bounds of interval $[b_i^-, b_i^+]$, respectively.

The transfer function $G_n(z)$ can also be expanded in its power series expansion around $z=1$ and $z=\infty$ as:

$$\left.\begin{aligned} G_n(z) = [\zeta_0^-, \zeta_0^+] + [\zeta_1^-, \zeta_1^+](z-1) + \cdots \\ + [\zeta_n^-, \zeta_n^+](z-1)^n + \cdots \end{aligned}\right\} \quad (2)$$

(expansion around $z=1$)

$$\left.\begin{aligned} G_n(z) = [M_1^-, M_1^+]z^{-1} + [M_2^-, M_2^+]z^{-2} + \cdots \\ + [M_n^-, M_n^+]z^{-n} + \cdots \end{aligned}\right\} \quad (3)$$

(expansion around $z=\infty$)

where $[\zeta_i^-, \zeta_i^+]$ for $i = 0,1,\cdots$ are proportional to the time moments of HODIS, and $[M_i^-, M_i^+]$ for $i = 1,2,\cdots$ are Markov parameters of HODIS.

Assuming $[b_i^-, b_i^+] = \boldsymbol{b}_i$ for $i = 0,1,\cdots,n-1$, $[a_i^-, a_i^+] = \boldsymbol{a}_i$ for $i = 0,1,\cdots,n$, $[\zeta_i^-, \zeta_i^+] = \zeta_i$ for $i = 0,1,\cdots$ and $[M_i^-, M_i^+] = \boldsymbol{M}_i$ for $i = 1,2,\cdots$, (1), (2) and (3) are identified to be, respectively, (4), (5) and (6).

$$G_n(z) = \frac{\boldsymbol{b}_0 + \boldsymbol{b}_1 z + \cdots + \boldsymbol{b}_{n-1} z^{n-1}}{\boldsymbol{a}_0 + \boldsymbol{a}_1 z + \cdots + \boldsymbol{a}_n z^n} \quad (4)$$

$$= \zeta_0 + \zeta_1(z-1) + \cdots + \zeta_n(z-1)^n + \cdots \quad (5)$$

$$= \boldsymbol{M}_1 z^{-1} + \boldsymbol{M}_2 z^{-2} + \cdots + \boldsymbol{M}_n z^{-n} + \cdots \quad (6)$$

Suppose, it is desired to obtain a rth -order ($r < n$) model given by the transfer function

$$\left.\begin{aligned} G_r(z) &= \frac{[\hat{b}_0^-, \hat{b}_0^+] + [\hat{b}_1^-, \hat{b}_1^+]z + \cdots + [\hat{b}_{r-1}^-, \hat{b}_{r-1}^+]z^{r-1}}{[\hat{a}_0^-, \hat{a}_0^+] + [\hat{a}_1^-, \hat{a}_1^+]z + \cdots + [\hat{a}_r^-, \hat{a}_r^+]z^r} \\ &= \frac{\hat{N}_r(z)}{\hat{D}_r(z)} \end{aligned}\right\} \quad (7)$$

where $[\hat{a}_i^-, \hat{a}_i^+]$ for $i = 0,1,\cdots,r$ and $[\hat{b}_i^-, \hat{b}_i^+]$ for $i = 0,1,\cdots,r-1$ are, respectively, denominator and numerator coefficients of $G_r(z)$.

The transfer function $G_r(z)$ can also be expanded in its power series expansion around $z=1$ and $z=\infty$ as:

$$\left.\begin{aligned} G_r(z) = [\hat{\zeta}_0^-, \hat{\zeta}_0^+] + [\hat{\zeta}_1^-, \hat{\zeta}_1^+](z-1) + \cdots \\ + [\hat{\zeta}_r^-, \hat{\zeta}_r^+](z-1)^r + \cdots \end{aligned}\right\} \quad (8)$$

(expansion around $z=1$)

$$\left.\begin{aligned} G_r(z) = [\hat{M}_1^-, \hat{M}_1^+]z^{-1} + [\hat{M}_2^-, \hat{M}_2^+]z^{-2} + \cdots \\ + [\hat{M}_r^-, \hat{M}_r^+]z^{-r} + \cdots \end{aligned}\right\} \quad (9)$$

(expansion around $z=\infty$)

where $[\hat{\zeta}_i^-, \hat{\zeta}_i^+]$ for $i = 0,1,\cdots$ are proportional to the time moments of model, and $[\hat{M}_i^-, \hat{M}_i^+]$ for $i = 1,2,\cdots$ are Markov parameters of model.

Assuming $[\hat{b}_i^-, \hat{b}_i^+] = \hat{\boldsymbol{b}}_i$ for $i = 0,1,\cdots,r-1$, $[\hat{a}_i^-, \hat{a}_i^+] = \hat{\boldsymbol{a}}_i$ for $i = 0,1,\cdots,r$, $[\hat{\zeta}_i^-, \hat{\zeta}_i^+] = \hat{\zeta}_i$ for $i = 0,1,\cdots$ and $[\hat{M}_i^-, \hat{M}_i^+] = \hat{\boldsymbol{M}}_i$ for $i = 1,2,\cdots$, (7), (8) and (9) are identified to be, respectively, (10), (11) and (12).

$$G_r(z) = \frac{\hat{\boldsymbol{b}}_0 + \hat{\boldsymbol{b}}_1 z + \cdots + \hat{\boldsymbol{b}}_{r-1} z^{r-1}}{\hat{\boldsymbol{a}}_0 + \hat{\boldsymbol{a}}_1 z + \cdots + \hat{\boldsymbol{a}}_r z^r} \quad (10)$$

$$= \hat{\zeta}_0 + \hat{\zeta}_1(z-1) + \cdots + \hat{\zeta}_r(z-1)^r + \cdots \quad (11)$$

$$= \hat{\boldsymbol{M}}_1 z^{-1} + \hat{\boldsymbol{M}}_2 z^{-2} + \cdots + \hat{\boldsymbol{M}}_r z^{-r} + \cdots \quad (12)$$

A. Calculation of Poles of HODIS

Consider interval polynomial $E(z)$ given by

$$\left.\begin{aligned} E(z) &= [e_0^-, e_0^+] + [e_1^-, e_1^+]z + \cdots + [e_{n-1}^-, e_{n-1}^+]z^{n-1} + z^n \\ &\equiv \boldsymbol{e}_0 + \boldsymbol{e}_1 z + \cdots + \boldsymbol{e}_{n-1} z^{n-1} + z^n \end{aligned}\right\} \quad (13)$$

The poles [20] of discrete interval polynomial $E(z)$ are calculated as:

Let F be the interval matrix given as

$$F = \begin{bmatrix} 0 & 1 & 0 & \cdots & 0 \\ 0 & 0 & 1 & \cdots & 0 \\ \vdots & \vdots & \vdots & \ddots & \vdots \\ 0 & 0 & 0 & \cdots & 1 \\ -\boldsymbol{e}_0 & -\boldsymbol{e}_1 & -\boldsymbol{e}_2 & \cdots & -\boldsymbol{e}_{n-1} \end{bmatrix} \quad (14)$$

The matrix F can be written as

$$F = F_c - \Delta F, F_c + \Delta F \quad (15)$$

where

$$\left.\begin{aligned} f_{cij} &= \frac{1}{2}\left[f_{ij}^{-} + f_{ij}^{+} \right] \\ \Delta f_{cij} &= \frac{1}{2}\left[f_{ij}^{+} - f_{ij}^{-} \right] \end{aligned}\right\} \quad i, j = 1, 2, \cdots, n \qquad (16)$$

and f_{ij}^{-}, f_{ij}^{+} are the lower and upper bounds of ijth element of F.

The real part λ_i^{σ} and imaginary part λ_i^{ω} of the ith eigenvalue λ_i^{H} of F are given as

$$\left.\begin{aligned} \lambda_i^{\sigma}(F) &= \left[\lambda_i^{\sigma}\left[F_c - \Delta F \circ S^i \right] \;,\; \lambda_i^{\sigma}\left[F_c + \Delta F \circ S^i \right] \right] \\ \lambda_i^{\omega}(F) &= \left[\lambda_i^{\omega}\left[F_c - \Delta F \circ T^i \right] \;,\; \lambda_i^{\omega}\left[F_c + \Delta F \circ T^i \right] \right] \\ & \qquad\qquad i = 1, 2, \cdots, n \end{aligned}\right\} \qquad (17)$$

where $\circ$ denotes component wise multiplication and elements of matrices S^i and T^i are given by

$$\left.\begin{aligned} S_{k,j}^i &= \operatorname{sgn}\left[t_{\sigma k}^i s_{\sigma j}^i + t_{\omega k}^i s_{\omega j}^i \right] \\ T_{k,j}^i &= \operatorname{sgn}\left[t_{\sigma k}^i s_{\omega j}^i - t_{\omega k}^i s_{\sigma j}^i \right] \end{aligned}\right\} \qquad (18)$$

where s and t are, respectively, the ith eigenvector and reciprocal eigenvector of F_c, with σ and ω denoting the real and imaginary parts, respectively.

B. Procedure to Obtain Time Moments of HODIS and Model

Putting $z = \ell + 1$ in (4), $G(z)$ becomes

$$G(\ell) = \frac{\boldsymbol{b}_0 + \boldsymbol{b}_1(\ell+1) + \cdots + \boldsymbol{b}_{n-1}(\ell+1)^{n-1}}{\boldsymbol{a}_0 + \boldsymbol{a}_1(\ell+1) + \cdots + \boldsymbol{a}_n(\ell+1)^n} \qquad (19)$$

$$= \frac{\boldsymbol{B}_0 + \boldsymbol{B}_1\ell + \cdots + \boldsymbol{B}_{n-1}\ell^{n-1}}{\boldsymbol{A}_0 + \boldsymbol{A}_1\ell + \cdots + \boldsymbol{A}_n\ell^n} \qquad (20)$$

Expansion of (20) through interval arithmetic (Appendix I) around $\ell = 0$ is given as:

$$G(\ell) = \boldsymbol{t}_0 + \boldsymbol{t}_0\boldsymbol{t}_1\ell + \boldsymbol{t}_0\boldsymbol{t}_1\boldsymbol{t}_2\ell^2 + \cdots + \left(\prod_{i=0}^{n} \boldsymbol{t}_i \right)\ell^n + \cdots \qquad (21)$$

$$= \zeta_0 + \zeta_1\ell + \zeta_2\ell^2 + \cdots + \zeta_n\ell^n + \cdots \qquad (22)$$

where

$$\zeta_k = \prod_{i=0}^{k} \boldsymbol{t}_i \qquad k = 0, 1, 2, \cdots \qquad (23)$$

with

$$\boldsymbol{t}_k = \begin{cases} \boldsymbol{B}_0 / \boldsymbol{A}_0 & k = 0 \\ \boldsymbol{c}_1 - \boldsymbol{d}_1 & k = 1 \\ \left((\boldsymbol{c}_k - \boldsymbol{d}_k) - \sum_{i=1}^{k-1} \boldsymbol{d}_i \left(\prod_{j=1}^{k-i} \boldsymbol{t}_j \right) \right) \div \left(\prod_{l=1}^{k-1} \boldsymbol{t}_l \right) & k \geq 2 \end{cases} \qquad (24)$$

where

$$\boldsymbol{c}_i = \begin{cases} \dfrac{\boldsymbol{B}_i}{\boldsymbol{B}_0} & \forall\, i \in [0, n-1] \\ 0 & \forall\, i \geq n \end{cases} \qquad (25)$$

and

$$\boldsymbol{d}_i = \begin{cases} \dfrac{\boldsymbol{A}_i}{\boldsymbol{A}_0} & \forall\, i \in [0, n] \\ 0 & \forall\, i \geq n+1 \end{cases} \qquad (26)$$

Putting $\ell = z - 1$ in (22), $G(z)$ then can be obtained as follows:

$$\left.\begin{aligned} G(z) = \zeta_0 + \zeta_1(z-1) + \zeta_2(z-1)^2 + \cdots \\ + \zeta_n(z-1)^n + \cdots \end{aligned}\right\} \qquad (27)$$

Therefore, the time moments of HODIS [24]-[25], in terms of ζ_i parameters, are

$$\boldsymbol{T}_{i+1} = \begin{cases} \zeta_i & i = 0 \\ (-1)^i \sum_{j=1}^{i} \dfrac{1}{j!} (T_s)^j w_{ij} \;\; \zeta_j & i = 1, 2, \cdots \end{cases} \qquad (28)$$

where T_s is the sampling frequency and w_{ij} is defined as

$$w_{ij} = \begin{cases} 1 & j = 1 \\ 0 & i < j \\ 1 & i = j \\ w_{i-1,j-1} + j\, w_{i-1,j} & i > j \end{cases} \qquad (29)$$

Similarly, time moments of the model are given as

$$\hat{\boldsymbol{T}}_{i+1} = \begin{cases} \hat{\zeta}_i & i = 0 \\ (-1)^i \sum_{j=1}^{i} \dfrac{1}{j!} (T_s)^j w_{ij} \;\; \hat{\zeta}_j & i = 1, 2, \cdots \end{cases} \qquad (30)$$

where T_s is sampling frequency, w_{ij} is given by (29) and $\hat{\zeta}_i$ for $i = 0, 1, 2, \cdots$ have the same meaning as ζ_i for $i = 0, 1, 2, \cdots$ in (23) for HODIS.

C. Procedure to Obtain Markov Parameters of HOIS and Model

Expansion of (4) through interval arithmetic (Appendix I) around $z=\infty$ is given as:

$$\left.\begin{aligned} G(z) &= \varpi_1 z^{-1} + \varpi_1\varpi_2 z^{-2} + \varpi_1\varpi_2\varpi_3 z^{-3} + \cdots \\ &\quad + \left(\prod_{i=1}^{n}\varpi_i\right) z^{-n} + \cdots \end{aligned}\right\} \tag{31}$$

$$\left.\begin{aligned} &= \boldsymbol{M}_1 z^{-1} + \boldsymbol{M}_2 z^{-2} + \boldsymbol{M}_3 z^{-3} + \cdots \\ &\quad + \boldsymbol{M}_n z^{-n} + \cdots \end{aligned}\right\} \tag{32}$$

where

$$\boldsymbol{t}_k = \begin{cases} \boldsymbol{B}_0 / \boldsymbol{A}_0 & k=0 \\ \boldsymbol{c}_1 - \boldsymbol{d}_1 & k=1 \\ P/Q & k\geq 2 \end{cases} \tag{33}$$

with

$$P = \left((\boldsymbol{c}_k - \boldsymbol{d}_k) - \sum_{i=1}^{k-1}\boldsymbol{d}_i\left(\prod_{j=1}^{k-i}\boldsymbol{t}_j\right)\right)$$

$$Q = \left(\prod_{l=1}^{k-1}\boldsymbol{t}_l\right)$$

$$\boldsymbol{C}_i = \begin{cases} \dfrac{\boldsymbol{b}_i}{\boldsymbol{b}_{n-1}} & \forall\, i\in[0,n-1] \\ 0 & \forall\, i\geq n \end{cases} \tag{34}$$

and

$$\boldsymbol{D}_i = \begin{cases} \dfrac{\boldsymbol{a}_i}{\boldsymbol{a}_n} & \forall\, i\in[0,n] \\ 0 & \forall\, i\geq n+1 \end{cases} \tag{35}$$

Hence, the Markov parameters of HODIS are

$$\boldsymbol{M}_k = \prod_{i=1}^{k}\varpi_i \qquad k=1,2,\cdots \tag{36}$$

Similarly, Markov parameters of the model are given as

$$\hat{\boldsymbol{M}}_k = \prod_{i=1}^{k}\hat{\varpi}_i \qquad k=1,2,\cdots \tag{37}$$

where $\hat{\varpi}_i$ for $i=1,2,\cdots$ have the same meaning as ϖ_i for $i=1,2,\cdots$ in (33) for HODIS.

D. Procedure to Obtain Denominator Polynomial of Model

The cluster center using pole clustering technique [21]-[23] is obtained by grouping the poles of HODIS. In this process, separate cluster partitions should be made for real poles and complex conjugate poles and then cluster centers for these cluster partitions are obtained. Each real cluster center or pair of complex conjugate cluster centers are, respectively, replaced by real pole or pair of complex conjugate poles of model, respectively. The inverse distance measure (IDM) criterion is used for clustering the poles of HODIS.

For obtaining rth order model, r cluster centers should be obtained from r cluster partitions. The steps for IDM criterion follow as:

Step 1: Arrange the poles of HODIS in r cluster partitions collecting the real and complex conjugate poles in separate cluster partitions.

Step 2: Obtain the cluster centers:
The cluster center for real poles is obtained as

$$\rho^C = \left\{\left(\sum_{i=1}^{k}\left(\frac{1}{\alpha_i}\right)\right)\div k\right\}^{-1} \tag{38}$$

where ρ^C is cluster center of cluster partition containing k real poles $(\alpha_1,\alpha_2,\cdots,\alpha_k)$ of HODIS.
The pair of cluster centers for complex conjugate poles in the form of $\rho^R \pm j\rho^I$ is obtained as

$$\left.\begin{aligned} \rho^R &= \left\{\left(\sum_{i=1}^{l}\left(\frac{1}{\alpha_i^R}\right)\right)\div l\right\}^{-1} \\ \rho^I &= \left\{\left(\sum_{i=1}^{l}\left(\frac{1}{\alpha_i^I}\right)\right)\div l\right\}^{-1} \end{aligned}\right\} \tag{39}$$

where ρ^R and ρ^I are, respectively, real and imaginary parts of cluster pair $\rho^R \pm j\rho^I$ in which l pairs of complex conjugate poles $\alpha_1^R \pm j\alpha_1^I$, $\alpha_2^R \pm j\alpha_2^I$,$\cdots$, $\alpha_l^R \pm j\alpha_l^I$ are grouped.

Step 3: Obtain the denominator of model:
The denominator polynomial $\hat{D}_r(z)$ of rth -order model is given as
Case 1: If all obtained cluster centers are real

$$\hat{D}_r(z) = \prod_{i=1}^{r} z-\rho^C \tag{40}$$

Case 2: If one pair of cluster centers is complex conjugate and $(r-2)$ cluster centers are real

$$\hat{D}_r(z) = \left[z-(\rho_1^R+j\rho_1^I)\right]\left[z-(\rho_1^R-j\rho_1^I)\right]\prod_{i=1}^{r-2}(z-\rho_i^C) \tag{41}$$

Case 3: If all obtained cluster centers are complex conjugates

$$\hat{D}_r(z)=\prod_{i=1}^{r/2} z-(\rho_i^R+j\rho_i^I)\quad z-(\rho_i^R-j\rho_i^I) \qquad (42)$$

The denominator polynomial of the model is obtained by (40), (41) or (42) depending upon the nature of cluster centers.

E. Procedure to Obtain Numerator Polynomial of Model:

Once the denominator polynomial of model is obtained, the numerator polynomial is determined by retaining first m time moments/Markov parameters of HODIS as well as minimizing errors between subsequent n time moments/Markov parameters of HODIS and model such that $m+n=r$. The time moments of the HODIS and model are obtained by (28) and (30), respectively, and the Markov parameters of the HODIS and model are given by (36) and (37), respectively.

The numerator parameters of model are obtained by matching first m time moments/Markov parameters of HODIS to those of model, given as

$$\left.\begin{aligned} \boldsymbol{T}_i-\hat{\boldsymbol{T}}_i&=0 \quad i=1,2,\cdots,p\\ \boldsymbol{M}_j-\hat{\boldsymbol{M}}_j&=0 \quad j=1,2,\cdots,q\\ p+q&=m \end{aligned}\right\} \qquad (43)$$

and minimizing a weighted squared sum of the errors, between subsequent n time moments/Markov parameters of HODIS and those of model, given as

$$J_C'=\sum_{i=p+1}^{u}\lambda_i'(\boldsymbol{T}_i-\hat{\boldsymbol{T}}_i)+\sum_{j=q+1}^{v}\gamma_j'(\boldsymbol{M}_j-\hat{\boldsymbol{M}}_j) \qquad (44)$$

where λ_i' and γ_j' are non-negative numbers, and $u+v=r$.

The objective function (44) is normalized as follows:

$$J_C=\sum_{i=p+1}^{u}\lambda_i\left(1-\frac{\hat{\boldsymbol{T}}_i}{\boldsymbol{T}_i}\right)+\sum_{j=q+1}^{v}\gamma_j\left(1-\frac{\hat{\boldsymbol{M}}_j}{\boldsymbol{M}_j}\right) \qquad (45)$$

However, in (45), it is assumed that $\boldsymbol{T}_i\neq 0$ and $\boldsymbol{M}_j\neq 0$.

III. LUUS JAAKOLA ALGORITHM

The algorithm due to Luus and Jaakola [26] is used for finding the minimum value of objective function (45) obtained in last section. In Luus Jaakola algorithm, initial values for all variables and corresponding search intervals are chosen at random and then in every next iteration, search intervals are contracted by a constant contraction factor. This algorithm has been applied in many problems in optimal control [8],[27].

IV. NUMERICAL SECTION

Let the transfer function [20] of a third-order interval system be given as

$$\left.\begin{aligned} G(z)&=\frac{[8,10]+[3,4]z+[1,2]z^2}{[0.8,0.85]+[4.9,5]z+[9,9.5]z^2+[6,6]z^3}\\ &=\frac{N(z)}{D(z)} \end{aligned}\right\} \qquad (46)$$

Suppose, it is desired to obtain a second-order $(r=2)$ model given by the transfer function

$$\left.\begin{aligned} G_2^P(z)&=\frac{[\hat{b}_0^-,\hat{b}_0^+]+[\hat{b}_1^-,\hat{b}_1^+]z}{[\hat{a}_0^-,\hat{a}_0^+]+[\hat{a}_1^-,\hat{a}_1^+]z+[\hat{a}_2^-,\hat{a}_2^+]z^2}\\ &\equiv\frac{\hat{\boldsymbol{b}}_0+\boldsymbol{b}_1 z}{\hat{\boldsymbol{a}}_0+\hat{\boldsymbol{a}}_1 z+\hat{\boldsymbol{a}}_2 z^2}=\frac{\hat{N}_2(z)}{\hat{D}_2(z)} \end{aligned}\right\} \qquad (47)$$

The poles, calculated using (17), of the HODIS (46) are

$$\left.\begin{aligned} \lambda_1^H&=[-0.5340,-0.2680]\\ \lambda_2^H&=[-0.7125,-0.5361]\\ \lambda_3^H&=[-0.8534,-0.7203] \end{aligned}\right\} \qquad (48)$$

Since poles (48) are real, thus, using (38), the cluster centers obtained by grouping λ_1^H in one cluster partition and λ_2^H and λ_3^H in other cluster partition are

$$\left.\begin{aligned} \rho_1^C&=[-0.5340,-0.2680]\\ \rho_2^C&=[-0.7766,-0.6147] \end{aligned}\right\} \qquad (49)$$

and the denominator obtained using (40) is

$$\left.\begin{aligned} \hat{D}_2(z)&=(z-\rho_1^C)(z-\rho_2^C)\\ &=(z-[-0.5340,-0.2680])(z-[-0.7766,-0.6147])\\ &=[0.1647,0.4147]+[0.8827,1.3106]z+[1,1]z^2\\ &=[\hat{a}_0^-,\hat{a}_0^+]+[\hat{a}_1^-,\hat{a}_1^+]z+[\hat{a}_2^-,\hat{a}_2^+]z^2 \end{aligned}\right\} \qquad (50)$$

First time moment and Markov parameter, as given by (28) and (36), respectively, of the HODIS are

$$\left.\begin{aligned} \boldsymbol{T}_1&=[0.5621,0.7729]\\ \boldsymbol{M}_1&=[0.1667,0.3333] \end{aligned}\right\} \qquad (51)$$

and the first time moment and Markov parameter, as given by (30) and (37), respectively, of the model are

$$\left.\begin{aligned} \hat{\boldsymbol{T}}_1&=\frac{\hat{\boldsymbol{b}}_0+\hat{\boldsymbol{b}}_1}{\hat{\boldsymbol{a}}_0+\hat{\boldsymbol{a}}_1+\hat{\boldsymbol{a}}_2}\\ \hat{\boldsymbol{M}}_1&=\frac{\hat{\boldsymbol{b}}_1}{\hat{\boldsymbol{a}}_2} \end{aligned}\right\} \qquad (52)$$

Using (43), numerator parameters are obtained as

$$\boldsymbol{T}_1=\hat{\boldsymbol{T}}_1\Rightarrow\hat{\boldsymbol{b}}_0+\hat{\boldsymbol{b}}_1=[1.1508,2.1064] \qquad (53)$$

The objective function (45) for this problem is given as:

$$J_C = \sum_{j=1}^{1} \gamma_j \left(1 - \frac{\hat{\boldsymbol{b}}_1 / \hat{\boldsymbol{a}}_2}{[0.1667, 0.3333]} \right) \quad (54)$$

Starting with various initial conditions and ranges, the Luss-Jaakola algorithm converges to following optimal solution

$$\hat{\boldsymbol{b}}_1 = [0.1508, 1.1064] \quad (55)$$

Using (53) and (55), the second-order model obtained is

$$G_2^P(z) = \frac{[0.0107, 0.1054] + [1.1401, 2.0010]z}{[0.1647, 0.4147] + [0.8827, 1.3106]z + z^2} \quad (56)$$

and the second-order model proposed in [20] is

$$G_2^O(z) = \frac{[0.8845, 0.9] + [0.5921, 0.6055]z}{[0.1437, 0.3805] + [0.8041, 1.2465]z + z^2} \quad (57)$$

The step and impulse responses of one of the rational systems constructed with the help of Kharitonov polynomials (Appendix II) of numerator and denominator of (46), (56) and (57) are shown in Fig. 1 and 2, respectively.

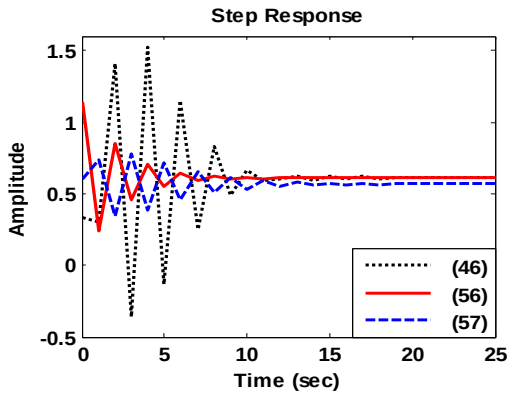

Fig No. 1 Step Responses of HODIS and models.

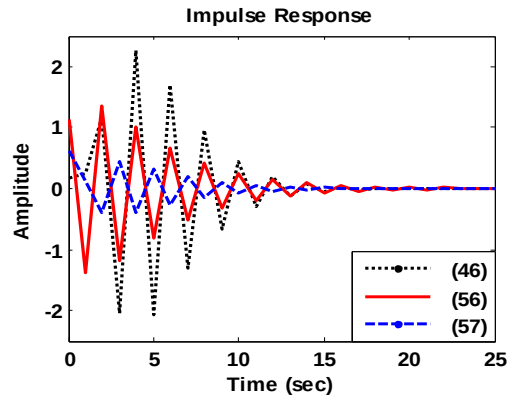

Fig No. 2 Impulse Responses of HODIS and models.

The best-case ISEs (Appendix III) of impulse responses for (56) and (57) are given in Table 1.

Table 1
Best-case ISE for impulse response

Model	Best-case ISE
(56)	4.1521
(57)	8.0926

It is clear from Fig. 1-2 that the responses of proposed model (56) when compared to (46) is better than that of (57) and also, the best-case ISE of (56) is lower than that of (57). This confirms the applicability of proposed method for order reduction of HODIS.

V. CONCLUSION

A method for obtaining model of given HODIS is proposed in which the denominator is obtained by pole clustering and the numerator is determined by minimizing errors between time moments/Markov parameters of HODIS and model in addition to retaining some initial time moments/Markov parameters of HODIS. The objective function which is weighted squared sum of errors between time moments/Markov parameters of HODIS and those of model is minimized using Luus Jaakola algorithm. The proposed method is validated by a numerical example.

APPENDIX I
Interval Arithmetic

The rules of interval arithmetic [17] are defined as follows:

Suppose, $\boldsymbol{c} \equiv [c^-, c^+]$ and $\boldsymbol{d} \equiv [d^-, d^+]$ are two intervals.

Addition:

$$\boldsymbol{c} + \boldsymbol{d} \equiv [c^-, c^+] + [d^-, d^+] = [c^- + d^-, c^+ + d^+]$$

Subtraction:

$$\boldsymbol{c} - \boldsymbol{d} \equiv [c^-, c^+] - [d^-, d^+] = [c^- - d^+, c^+ - d^-]$$

Multiplication:

$$\boldsymbol{c}\,\boldsymbol{d} \equiv [c^-, c^+][d^-, d^+]$$
$$= [\min(c^- d^-, c^- d^+, c^+ d^-, c^+ d^+),$$
$$\max(c^- d^-, c^- d^+, c^+ d^-, c^+ d^+)]$$

Division:

$$\boldsymbol{c} / \boldsymbol{d} \equiv [c^-, c^+] / [d^-, d^+] = [c^-, c^+] / [1/d^+, 1/d^-];$$
$$\boldsymbol{d} / \boldsymbol{d} \equiv [d^-, d^+] / [d^-, d^+] = 1$$

APPENDIX II
Kharitonov Polynomials

Consider a family of real interval polynomials [28]:

$$\left.\begin{aligned} D(z) &= \boldsymbol{\beta}_0 + \boldsymbol{\beta}_1 z + \cdots + \boldsymbol{\beta}_{n-1} z^{n-1} + \boldsymbol{\beta}_n z^n \\ &= [\beta_0^-, \beta_0^+] + [\beta_1^-, \beta_1^+] z + \cdots + [\beta_n^-, \beta_n^+] z^n \end{aligned}\right\}$$

The four Kharitonov polynomials associated with $D(z)$ are given as:

$$D_1(z) = \beta_0^- + \beta_1^- z + \beta_2^+ z^2 + \beta_3^+ z^3 + \beta_4^- z^4 + \cdots$$
$$D_2(z) = \beta_0^+ + \beta_1^- z + \beta_2^- z^2 + \beta_3^+ z^3 + \beta_4^+ z^4 + \cdots$$
$$D_3(z) = \beta_0^+ + \beta_1^+ z + \beta_2^- z^2 + \beta_3^- z^3 + \beta_4^+ z^4 + \cdots$$
$$D_4(z) = \beta_0^- + \beta_1^+ z + \beta_2^+ z^2 + \beta_3^- z^3 + \beta_4^- z^4 + \cdots$$

APPENDIX III
ISE of Impulse Response

The integral-squared-error (ISE) for impulse responses between $G_n(z)$ and $G_r(z)$ is obtained as

$$J = \frac{1}{2\pi i}\oint E(z)E(z^{-1})\frac{1}{z}dz$$

where

$$E(z) = G_n(z) - G_r(z)$$
$$= \frac{B_p(z)}{A_q(z)} \quad p,q = 1,2,\cdots,4.$$

Each of $B_p(z)$ and $A_q(z)$ represents four Kharitonov polynomials (Appendix II).

The ISE can recursively [29],[13] be obtained as

$$J = \frac{1}{A_0^n}\sum_{j=0}^{n}\frac{(B_j^j)^2}{A_0^j}$$

where n is the order of error signal $E(z)$ and A_0^n, B_j^j, and A_0^j are defined in [29].

The best-case ISE [30] is obtained as

$$ISE_{best-case} = \min_{p,q=1,\cdots,4} J(B_p, A_q)$$

REFERENCES

[1] Y. Shamash, "Stable reduced order models using Padé type approximation," IEEE Trans. Auto. Cont., vol. 19, pp. 615-616, 1974.

[2] M. Aoki, "Control of large-scale dynamic systems by aggregation," IEEE Trans. Auto. Cont., vol. 13, pp. 246-253, 1968.

[3] N. K. Sinha, and B. Kuszta, "Modeling and identification of dynamic systems," New York: Van Nostand Reinhold, pp. 133-163, 1983.

[4] M. F. Hutton, and B. Friedland, "Routh approximations for reducing the order of linear time-invariant systems," IEEE Trans. Autom. Control, vol 20, pp. 329-337, 1975.

[5] Y. Shamash, "Model reduction using the Routh stability criterion and the Padé approximation technique," Int. Jr. Control, vol. 21, pp. 475-484, 1975.

[6] S. Rao, S. S. Lamba, and S. V. Rao, "Routh-approximant time-domain reduced-order modelling for single-input single-output systems," IEE Proc., Control Theory Appl., vol. 125, pp. 1059-1063, 1978.

[7] Singh, D. Chandra, and H. Kar, "Improved Routh-Padé approximants: a computer-aided approach," IEEE Trans. on Automatic Control, vol. 49, no. 2, pp. 292-296, 2004.

[8] V. Singh, D. Chandra, and H. Kar, "Optimal Routh approximants through integral squared error minimisation: computer-aided approach," IEE Proceedings-Control Theory and Applications, vol. 151, no. 1, pp. 53-58, 2004.

[9] S. K. Mittal, and D. Chandra, "Stable optimal model reduction of linear discrete time systems via integral squared error minimization: computer-aided approach," Jr. of Advanced Modeling and Optimization, vol. 11, no. 4, pp. 531-547, 2009.

[10] S. K. Mittal, D. Chandra, and B. Dwivedi "Improved Routh-Pade approximants using vector evaluated genetic algorithm to controller design," Jr. of Advanced Modeling and Optimization, vol. 11, no. 4, pp. 579-588, 2009.

[11] G. A. Baker, "Essenstials of Padé approximants," New York: Academic, 1975.

[12] G. A. Baker, and P. R. Graves-Morris, "Padé approximants, Part-II: Extensions and Applications," London: Addison-Wesley, 1981.

[13] Y. Choo, "Suboptimal bilinear Routh approximant for discrete systems," ASME Jr. of Dynamic systems, measurement, and control, vol. 128, pp. 742-745, 2006.

[14] B. Bandyopadhyay, O. Ismail, and R. Gorez, "Routh-Padé approximation for interval systems," IEEE Trans. Auto. Cont., vol. 39, no. 12, pp. 2454-2456, 1994.

[15] Y. Dolgin, and E. Zeheb, "On Routh-Padé model reduction of interval systems," IEEE Trans. on Auto. Control, vol. 48, no. 9, pp. 1610-1612, 2003.

[16] B. Bandyopadhyay, A. Upadhye, and O. Ismail, "$\gamma - \delta$ Routh approximation for interval systems," IEEE Trans. on Automatic Control, vol. 42, no. 8, pp. 1127-1130, 1997.

[17] G. V. K. R. Sastry, G. Raja, and P M. Rao, "Large scale interval system modeling using Routh approximants," IET Journal, vol. 36, no. 8, pp. 768-769, 2000.

[18] O. Ismail, and B. Bandyopadhyay, "Model reduction of linear interval systems using Padé approximation," IEEE International Symposium on Circuits and Systems (ISCAS), vol.2, pp. 1400 – 1403, 1995.

[19] V. P. Singh, and D. Chandra, "Routh approximation based model reduction using series expansion of interval systems," IEEE Inter. Conf. on Power, Control & Embedded Systems (ICPCES), pp. 1-4, 2010.

[20] O. Ismail, B. Bandyopadhyay, and R. Gorez, "Discrete interval system reduction using Padé approximation to allow retention of dominant poles," IEEE Trans. on Circuits and Systems_I: Fundamental theory and applications, vol. 44, no. 11, pp.1075-1078, 1997.

[21] K. Sinha, and J. Pal, "Simulation based reduced order modeling using a clustering technique," Comput. Elect. Eng., vol. 16, no. 3, pp. 159-169, 1990.

[22] B. Vishwakarma, and R. Prasad, "Clustering method for reducing order of linear system using Pade approximation," IETE Journal of Research, vol. 54, no. 5, pp. 326-330, 2008.

[23] W. T. Beyene, "Pole-clustering and rational-interpolation techniques for simplifying distributed systems," IEEE Trans. on Circuits and Systems-I: Fundamental Theory and Applications, vol. 46, no. 12, pp.1468-1472, 1999.

[24] C. Hwang, and Y. P. Shih, "On the time moments of discrete systems," Int. J. Contr., vol. 34, pp. 1227-1228, 1981.

[25] Y. Shamash, "Continued fraction methods for the reduction of discrete-time dynamic systems," Int. J. Contr., vol. 20, pp. 267-275, 1974.

[26] R. Luus and T. H. I. Jaakola, "Direct search and systematic reduction of size of search region," AIChE J., vol. 19, pp. 760-766, 1973.

[27] V. Singh, "Obtaining Routh-Pade approximants using the Luus-Jaakola algorithm," IEE Proceedings - Control Theory and Applications, vol. 152, no. 2, pp. 129-132, 2005.

[28] V. L. Kharitonov, "Asymptotic stability of an equilibrium position of a family of system of linear differential equation," Differential'Nye Uravenia, vol. 14, pp. 1483-1485, 1978.

[29] K. J. Astrom, E. I. Jury, and R. G. Agniel, "A numerical method for evaluation of complex integrals," IEEE Trans. on Auto. Contr., vol. 15, pp. 468-471, 1970.

[30] C.-C. Hsu, and C.-H. Yu, "Design of optimal controller for interval plant from signal energy point of view via evolutionary approaches," IEEE Trans. On Systems, Manand Cybernetics-Part B: Cybernetics, vol. 34, no. 3, pp.1609-1617, 2004.

PRATIBHA: INTERNATIONAL JOURNAL OF SCIENCE, SPIRITUALITY, BUSINESS AND TECHNOLOGY (IJSSBT), Vol. 1, No.1, March 2012
ISSN (Print) 2277—7261

Continuous Wavelet Transform for Discrimination between Inrush and Fault Current Transients in Transformer

S. R. Paraskar[1], M. A. Beg[2], G. M. Dhole[3]
[1,2,3]Department of Electrical Engineering, S.S.G.M. College of Engineering Shegaon. (M.S.), 44203, India.
[1]srparaskar@ gmail.com, [2]beg_m_a@rediffmail.com, [3]gmdhole@gmail.com

Abstract: This paper presents the characterization of fault transient in transformer using Continuous wavelet transform (CWT). This characterization will add the diagnostic of internal fault in transformer. The detection method can provide information of internal turns to turns fault in winding. CWT analysis provides discrimination of inrush current and fault from terminal parameter. This will add advance concept of on line monitoring of transformer from terminal quantity.

Keywords: Continuous wavelet transform (CWT), inrush, turns to turns fault, transformer.

I. INTRODUCTION

The trends towards a deregulated global electricity market has put the electric utility under severe stress to reduce operating costs, enhance the availability of generation, transmission and distribution equipment, and improve supply of power and service to customers. Using efficient methods of detection and classification of transients will help the utilities to accomplish these objectives.

Transformers are essential and important elements of power systems and whose unexpected outage can cause the total disruption of electrical supply and subsequent major economic loss. Hence, detection and classification of faults through certain intelligent procedure can provide early warning of electrical failure and could prevent catastrophic losses.

Fault detection in transformer has been conducted in several manners. The existing methods can be classified in following major groups like Electrical Based Technique and Oil Based Technique. The electric based methods decide the condition of transformer by means of differential relaying techniques, and oil based technique is mainly represented by Dissolved gas Analysis (DGA). The fault diagnosis with this procedure requires complex and, expensive sensors capable of detecting the different gases dissolved in transformer oil as a consequence of failure.

Several industrial methods exits for online and offline fault diagnosis of transformer, but all of them are expensive, complex and time consuming.
To take the diagnostic decisions, transformer fault must be characterized by analyzing quantities of data, which could be generated through computer simulation or field experiments.
The power transformer protection is one of the critical issues in power system. Since minimization of frequency and duration of unwanted outages, is very desirable, this high demand imposed on power transformer protective relays; this includes the requirement of dependability associated with no false tripping and operating speed associated with short fault clearing time.
One of the main concerns in protecting this particular component of power system lies in the accurate and rapid discrimination of magnetizing inrush current from other different faults. This is because the magnetizing inrush current, which occurs during the energizing the transformers, generally results in several times full, load current and therefore can cause mal operation of relay. Such mal operation of a differential relays can affect both reliability and stability of the whole power system.
Traditionally transformer protection methods that use its internal behavior are based on differential protection and the studies for improvement of transformer protection have focused on discrimination between internal short circuit faults and inrush currents in transformer, [4], [5].
But incipient faults in equipment containing insulation material are also very important. Detection of these types of faults can provide information to predict failure ahead of time. The major cause of incipient faults is the deterioration of insulation in the electrical equipment. When the condition of system equipment degrades because of electrical, thermal or chemical effects, intermittent incipient fault begin to persist in the system, leading to more frequent outages degraded the quality of service and eventually longer outages. Until finally a catastrophic failure occurs and service cannot be restored until the source of failure is repaired [6].

The basic philosophy of protective device is different for incipient faults than for short circuits. The classical short circuit methods can not detect incipient faults by using the terminal

behavior of transformer unless a major arcing fault occur that will be detected by protective device such as fuse and relay protection.

Since incipient faults develop slowly there is a time for careful observation and testing. Conventional protective device cannot detect these faults. Supplementary protective system and methods, which may not be based on terminal behavior of transformers, are needed for power system transformer [5].

Over the years various incipient fault detection techniques, such as dissolved gas analysis and partial discharge analysis [15] have been successfully applied to large power transformer fault diagnosis. On line condition monitoring of transformers can give early warning of electrical failure and could prevent catastrophic losses. Hence a powerful method based on signal analysis should be used in monitoring. This method should discriminate between normal and abnormal operating cases that occur in distribution system related to the transformers such as external faults, internal faults, magnetizing inrush, load changes, aging, arcing, etc.

There have been several methods based on time domain and frequency domain techniques. In previous study researchers have used Fourier Transform or Windowed Fourier Transform. Since FT gives only frequency information of signal, time information is lost. In Windowed FT or short time FT has the limitation of a fixed window width, so it does not provide good resolution in both time and frequency. A wide window, for example gives good frequency resolution but poor time resolution, where as a narrow window gives good time resolution but poor frequency resolution. Wavelets on the other hand provide greater resolution in time for high frequency components of a signal and greater resolution in frequency components of signal. In a sense Wavelet have a window that automatically adjusts to give the appropriate resolutions. Therefore in recent studies Wavelet transform based methods have been used for analysis of characteristics of terminal current and voltages, [4], [8].

Traditional Fourier analysis, which deals with periodic signals and has been the main frequency domain analysis tool in many applications, fails to describe the eruptions commonly existing in transient processes such as magnetic in rush and incipient faults.

The Wavelet transform (WT) on the other hand can be useful in analyzing the transient phenomenon associated with the transformer faults.

II. METHODOLOGY/METHODS IN DETAILS

A case study on custom built transformer will be presented in this paper. The laboratory experimental works will focuses mainly on the inter turn short circuits in the transformer and inrush currents. The acquired data will be analyzed as per the fundamentals of signal processing. The probable and possible methods are briefly discussed below.

A. Fourier Transform

It is well known from Fourier theory that a signal can be expressed as the sum of a, possibly infinite, series of sines and cosines. This sum is also referred to as a Fourier expansion. The main disadvantage of a Fourier expansion is that it has only frequency resolution and no time resolution. This means that although we might be able to determine all the frequencies present in a signal, we do not know when they are present. To overcome this problem in the past decades several solutions have been developed which are more or less able to represent a signal in the time and frequency domain at the same time.

The idea behind these time-frequency joint representations is to cut the signal of interest into several parts and then analyze the parts separately. It is clear that analyzing a signal this way will give more information about the when and where of different frequency components, but it leads to a fundamental problem as well: how to cut the signal? Suppose that we want to know exactly all the frequency components present at a certain moment in time. We cut out only this very short time window using a Dirac pulse [2], transform it to the frequency domain and ... something is very wrong. The problem here is that cutting the signal corresponds to a convolution between the signal and the cutting window. Since convolution in the time domain is identical to multiplication in the frequency domain and since the Fourier transform of a Dirac pulse contains all possible frequencies the frequency components of the signal will be smeared out all over the frequency axis. (Please note that we are talking about a two-dimensional time-frequency transform and not a one-dimensional transform.) In fact this situation is the opposite of the standard Fourier transform since we now have time resolution but no frequency resolution whatsoever. The underlying principle of the phenomena just described is due to Heisenberg's uncertainty principle, which, in signal processing terms, states that it is impossible to know the exact frequency and the exact time of occurrence of this frequency in a signal. In other words, a signal can simply not

be represented as a point in the time-frequency space. The uncertainty principle shows that it is very important how one cuts the signal. The *wavelet transform* or *wavelet analysis* is probably the most recent solution to overcome the shortcomings of the Fourier transform. In wavelet analysis the use of a fully scalable modulated window solves the signal-cutting problem. The window is shifted along the signal and for every position the spectrum is calculated. Then this process is repeated many times with a slightly shorter (or longer) window for every new cycle. In the end the result will be a collection of time-frequency representations of the signal, all with different resolutions. Because of this collection of representations we can speak of a multiresolution analysis.

In the case of wavelets we normally do not speak about time-frequency representations but about time-scale representations, scale being in a way the opposite of frequency, because the term frequency is reserved for the Fourier transform. Since from literature it is not always clear what is meant by small and large scales, I will define it here as follows: the large scale is the big picture, while the small scales show the details. Thus, going from large scale to small scale is in this context equal to zooming in.

Following sections presents the wavelet transform and develop a scheme that will allow us to implement the wavelet transform in an efficient way on a digital computer.

B. The continuous Wavelet Transform

The continuous wavelet transform was developed as an alternative approach to the short time
Fourier transforms to overcome the resolution problem. The wavelet analysis described in the introduction is known as the *continuous wavelet transform* or *CWT*. More formally it is written as:

$$\gamma(s,\tau) = \int f(t)\psi^*_{s,\tau}(t)dt \quad \text{--(1)}$$

Where * denotes complex conjugation. This equation shows how a function $f(t)$ is decomposed into a set of basis functions , called the wavelets. The variables s and, scale and translation, are the new dimensions after the wavelet transform. For completeness sake (2) gives the inverse wavelet transform.

$$f(t) = \int\int \gamma(s,\tau)\psi_{s,\tau}(t)d\tau ds \quad \text{---------- (2)}$$

The wavelets are generated from a single basic wavelet ψ **(*t*),** the so-called *mother wavelet*, by scaling and translation:

$$\psi_{s,\tau}(t) = \frac{1}{\sqrt{s}}\psi\left(\frac{t-\tau}{s}\right) \quad \text{------ (3)}$$

In (3) **s** is the scale factor, **τ** is the translation factor and the factor *s*-1/2 is for energy normalization across the different scales. It is important to note that in (1), (2) and (3) the wavelet basis functions are not specified. This is a difference between the wavelet transform and the Fourier transform, or other transforms. The theory of wavelet transforms deals with the general properties of the wavelets and wavelet transforms only. It defines a framework within one can design wavelets to taste and wishes.

C. Wavelet Properties

The most important properties of wavelets are the admissibility and the regularity conditions and these are the properties which gave wavelets their name.

Functions **ψ (*t*)** satisfying the *admissibility condition*

$$\int \frac{|\Psi(\omega)|^2}{|\omega|}d\omega < +\infty \quad \text{----- (4)}$$

can be used to first analyze and then reconstruct a signal without loss of information. In (4) **ψ (ω**) stands for the Fourier transform of **ψ(*t*)**. The admissibility condition implies that the Fourier transform of **ψ(*t*)** vanishes at the zero frequency, i.e.

$$|\Psi(\omega)|^2\Big|_{\omega=0} = 0 \quad \text{---------- (5)}$$

This means that wavelets must have a band-pass like spectrum. This is a very important observation, which we will use later on to build an efficient wavelet transform.

A zero at the zero frequency also means that the average value of the wavelet in the time domain must be zero,

$$\int \psi(t)dt = 0 \quad \text{---------- (6)}$$

and therefore it must be oscillatory. In other words, **ψ(*t*)** must be a *wave*.

As can be seen from (1) the wavelet transform of a one-dimensional function is two-dimensional; the wavelet transform of a two-dimensional function is four-dimensional. The time-bandwidth product of the wavelet transform is the square of the input signal and for most practical applications this is not a desirable property. Therefore one imposes some additional conditions on the wavelet functions in order to make the wavelet transform decrease quickly with decreasing scale *s*. These are the *regularity Conditions* and they state that the wavelet function should have some smoothness and concentration in both time and frequency domains. Regularity is a quite complex concept and we will try to explain it a little using the concept of *vanishing moments*. If we expand the wavelet transform (1) into the Taylor series at $t = 0$ until order n (let $\gamma = 0$ for simplicity) we get :

$$\gamma(s,0) = \frac{1}{\sqrt{s}}\left[\sum_{p=0}^{n} f^{(p)}(0)\int \frac{t^p}{p!}\psi\left(\frac{t}{s}\right)dt + O(n+1)\right] \quad \text{---------- (7)}$$

Here $f(p)$ stands for the *pth* derivative of f and $O(n+1)$ means the rest of the expansion. Now, if we define the *moments* of the wavelet by Mp,

$$M_p = \int t^p \psi(t)dt \quad \text{---------- (8)}$$

then we can rewrite (7) into the finite development

$$\gamma(s,0) = \frac{1}{\sqrt{s}}\left[f(0)M_0 s + \frac{f^{(1)}(0)}{1!}M_1 s^2 + \frac{f^{(2)}(0)}{2!}M_2 s^3 + \ldots + \frac{f^{(n)}(0)}{n!}M_n s^{n+1} + O(s^{n+2})\right] \quad \text{---------- (9)}$$

From the admissibility condition we already have that the 0th moment $M0 = 0$ so that the first term in the right-hand side of (9) is zero. If we now manage to make the other moments up to Mn zero as well, then the wavelet transform coefficients (s,) will decay as fast as $sn+2$ for a smooth signal $f(t)$. This is known in literature as the vanishing moments[4] or *approximation order*. If a wavelet has N vanishing moments, then the approximation order of the wavelet transform is also N. The moments do not have to be exactly zero, a small value is often good enough. In fact, experimental research suggests that the number of vanishing moments required depends heavily on the application . Summarizing, the admissibility condition gave us the wave, regularity and vanishing moments gave us the fast decay or the *let*, and put together they give us the wavelet.

III. EXPERIMENT SETUP

The main component of the experiment setup is 230V/230V, 50Hz 2KVA single phase transformer. The transformer is having 5 tap on primary winding, first four tap after each 10turns and on secondary having total 27 tap, each of 10turns. The taps are especially provided for turns to turns fault application. The primary winding was connected across rated voltage at rated frequency. The transformer was loaded at 50% of its full load. The application of fault on primary, secondary and both winding was done with the help of external contactor.

A portable data acquisition system was used to collect the instant of faulted samples. The primary and secondary current and voltage were measured with help of current transformer (CT) and Potential transformer (PT), suitable for data acquisition system. The current and voltage signal were recorded at sampling rate of 10000 sample/s. The experimental circuit and labortory set up is as shown in Fig. 2(a) and Fig. 2(b).

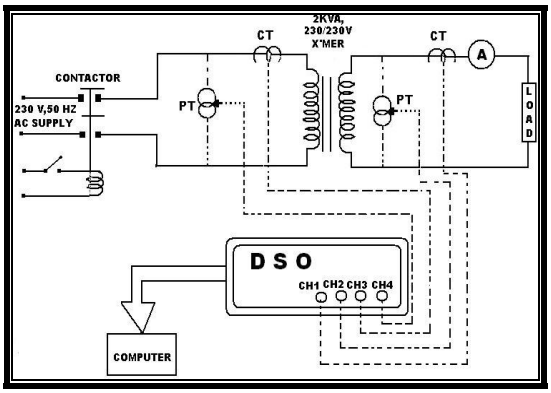

Fig No. 2(a) Experimental Circuit

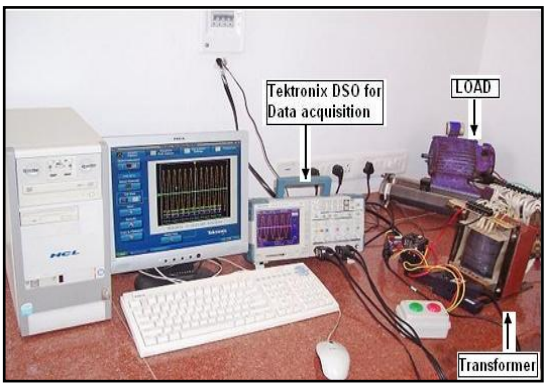

Fig No. 2(b) Laboratory Setup

IV. RESULTS AND DISCUSSION

A. Inrush Transients

When a transformer is de-energized, a permanent magnetization of the core remains due to hysteresis of the magnetic material. This "residual flux" is influenced by the transformer core material .When a transformer is energized the instantaneous magnitude of core flux at the instant of energization is the residual flux. The amount of offset of the sinusoidal flux generated by the applied voltage depends upon the point of voltage wave where the transformer is energized. The core flux can therefore reach a value double the normal flux plus residual flux. The most severe case where energization at voltage zero, the peak transient core is more than two time higher than the peak normal core flux. Experimental readings for inrush current are taken accordingly. Fig.3. Shows CWT of Inrush current.

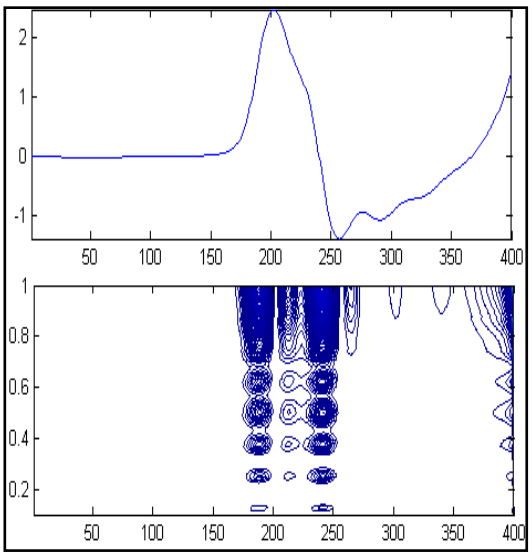

Fig No. 3 CWT of Inrush current.

B. Internal Short Circuit Transient

Internal fault are the fault that occurs within protective zone and protective scheme suppose to sense the fault and take action on it. Internal fault is generally turns to turns short circuit fault.

Fig.4. shows the CWT result from turns to turns fault on primary side. The fault was created with help of external contactor. The turns to turns fault was done between 10 to 20 turns of primary winding on rated voltage and loaded condition.

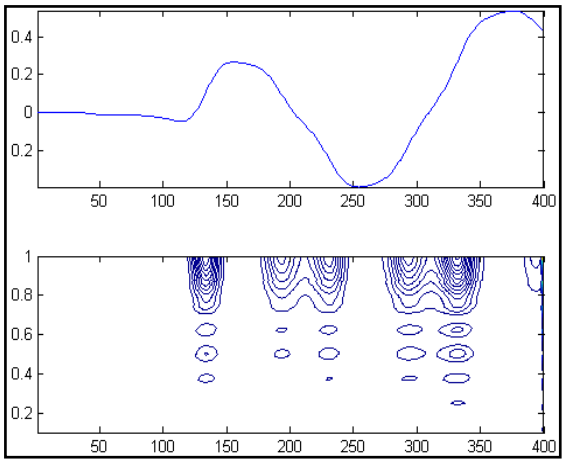

Fig. No. 4 CWT for Interturn fault

V. CONCLUSION

This paper presents a new approach for discrimination between inrush current and internal faults in power transformer by pattern recognition technique using CWT. The CWT gives the contours for inrush current and internal fault very distinctly. The obtained results clearly show that the scheme can provide accurate discrimination between Inrush and fault condition in transformer. The online implementation of this technique needs to be explored using suitable artificial intelligence method.

REFERENCES

[1] Karen L Butter-pury & Mustafa bagriyanik, "Characterization of transients in Xmer using DWT" IEEE Transactions on power system, Vol.18 No.2 may 2003.

[2] Jawed Faiz, "A Novel Wavelet-based algorithm of internal faults" from magnetizing inrush currents in power transformers." IEEE Transactions on power delivery, Vol.21 No.4 Oct 2006.

[3] Karen L Butter-pury, "Identifying Transformer Incipient Events fir maintaining Distribution system reliability" Proceedings of the 36th Hawai International Conference on system sciences 2003.

[4] M.A.Rahman and B Jeyarurya "A state of art reviews of transformer protection algorithm, "IEEE Transactions on power delivery, Vol.3 PP 534-544 Apr-1988.

[5] P.M.Anderson, Power system protection. Piscataway NJ: IEEE press 1999.

[6] H.Wang and K.L.Butter "Modelling transformers with internal incipient faults." IEEE Transactions on power delivery, Vol.17 PP 500-509 Apr-2002.

[7] P.L.Mao and R.K Agrawal, "A wavelet transform base decision making logical method for dissemination between internal faults and inrush currents in power transformers," Electrical Power and Energy system," Vol.22 PP 389 – 395, 2000.

[8] P.L.Mao and R.K.Agrawal "A novel approach to the classification of the transient phenomena's in power transformers using combine wavelet transform and neural network, "IEEE Transactions on power delivery, Vol.16 No.4 PP 654-660 Oct 2001.

[9] Y.Y.Hong & C.W.Wang, "Switching detection/classification using discrete wavelet transform and self organizing mapping network"IEEE Transactions power delivery, Vol.20 No.2PP1662– 1668 APR – 2005.

[10] S.A.Saleh and M.A.Rahman , "Modelling and protection of three phase power transformer using wavelet packet transform" IEEE Transactions on power delivery, Vol.20 No.2pt II PP 1273 – 1282 APR – 2005.
[11] O.A.S.Yousef, "A wavelet based technique for discrimination between faults and magnetizing inrush currents in transformer" IEEE Transactions on power delivery, Vol.18 No.1 PP 170 – 176 Jan – 2003.
[12] C.K.Chui, ed: Wavelets: - A tutorial in theory and application academic Press. Inc. 1992.
[13] G.Kaiser, A Friendly guide to wavelets, Birk base 1994.
[14] S Mallat, "A theory for multi resolution signal decomposition: the wavelet representation," IEEE Transactions on power Anal and much Intel, Vol.111 PP 674 – 693 Jul 1989.
[15] C.E.Lin, J.M. Ling and C.L.Haury "Expert system for new fault diagnoses using dissolved gas analysis, "IEEE Transactions on power delivering , Vol.08 PP 231 – 236 Jan l 1993.

PRATIBHA: INTERNATIONAL JOURNAL OF SCIENCE, SPIRITUALITY, BUSINESS AND TECHNOLOGY (IJSSBT), Vol. 1, No.1, March 2012
ISSN (Print) 2277—7261

Anti-Microbial Susceptibility Patterns of Enterobacteriaceae Isolated from Tertiary Care Unites in Akola City

M. Musaddiq[1]*, and Snehal Nemade*[2]
[1,2]P.G. Department of Microbiology, Shri Shivaji College, Akola 444001, (M.S.) India.
Emails: [1]dr_m.musaddiq@rediffmail.com, [2]snehalnemade1987@gmail.com

Abstract: The development of antibiotic resistance can be viewed as global problem in microbial genetic ecology. Bacterial infection is the most common cause for hospital visits. Most of members of the Enterobacteriaceae family are a leading cause of infectious diseases in both the community and acute care settings. Monitoring antibiotic susceptibility patterns of uropathogens at a local level yields important information regarding emerging problems of antibiotic resistance and provides assistance in managing empirical therapy. The existence of large concern over the increasing resistance to antibiotics for clinically important pathogens which cause varied number of diseases has led to monitor the prevailing resistance pattern microbes in a study which was carried out in the city of Akola. In the present study, different one four nine clinical samples were collected from government hospitals and different pathological laboratories. Isolation and identification of isolates belonging to family Enterobacteriaceae was done based on their morphologic, cultural and biochemical characteristics .The prominent isolates then evaluated for antimicrobial resistance by Disc Diffusion Method. The samples 51% were positive and 48.99% were negative to the infection. The highest causative organism was E.coli followed by Klebsiella. Antibiotic resistance profile obtained revealed high resistance of isolates to Ampicillin , Amoxicillin, Nalidixic Acid, Ciprofloxacin .In contrast organisms showed susceptibility to Chloramphenicol and then to Colistin. These findings indicate that continued surveillance at a local level is essential to maintaining the efficacy and safety of empirical therapy.

Keywords: Antibiotics, Enterobacteriaceae, multi drug resistance.

I. INTRODUCTION

Enterobacteriaceae belong to the normal enteric flora in humans and may cause infections. *E.coli* is the leading urinary tract pathogens with septicaemia potential, whereas *Klebsiella pneumonia* causes opportunistic infections and often outbreaks in hospital settings. Beta lactam are the first choice for treatment of infections caused by the Enterobacteriaceae and might be destroyed by extended spectrum of β-lactamases. ESBL producing Enterobacteriaceae are a challenge to clinical microbiology laboratory and infection control teams.

Multi drug resistance has significantly increased in recent years. The existence of enzymes of extended spectrum β-lactamases producing organism that are resistant to virtually all β-lactam antibiotics have been reported (Philippon *et al*.,1989).ESBLs are plasmid mediated class A enzymes commonly found in the family Enterobacteriaceae mainly *Klebsiella pneumonia* and *E.coli.* Infections caused by ESBLs- producing bacteria often involve immunocompromise patients, making it difficult to eradicate the organisms in high risk wards, such as intensive care units.(Bonnet *et al*.,2000).The emergence and spread of resistance in Enterobacteriaceae are complicating the treatment of serious nosocomial infections and threatening to create species resistant to all currently available agents. The present increase in resistance to second and third generation cephalosporin observed in medical institutions as a result of the acquisition and expression of extended spectrum β-lactam enzymes among Enterobacteriaceae has posed a serious public health problem. The clinical implications are extremely serious and lack of sensitive diagnostic method needed to guide therapy, monitor resistance developments and implementing intervention strategies have complicating the problem(Brad ford;2001; Stureburg and Merck,2003). The ESBL producing bacteria are increasingly causing urinary tract infections both in hospitalized and outpatients. The increase of drug resistance among these organisms has made therapy difficult and has led greater use of expensive broad spectrum antibiotics such as third generation of cephalosporin. The vast majority of Entaerbacteriaceae , including ESBL producers, remains susceptible to carbapenems and these agents are considered preferred empiric therapy for serious Enterobacteriaceae infections, carbapenem resistance, although rare, appears to be increasingly.

Better antibiotic stewardship and infection control are needed to prevent further spread of ESBLs and other forms of resistance in Enterobacteriaceae throughout the world. Area

specific monitoring studies aimed to gain knowledge about the type of pathogens responsible for specific infections and their resistance patterns may help the clinicians to choose the correct empirical treatment. Hence, this study was undertaken to fine out the antibiotic susceptibility pattern of the isolated pathogenic Enterobacteriaceae from various specimens from hospital acquired infections.

II. MATERIALS AND METHODS

Clinical samples (viz urine, skin swabs, blood etc) were collected in sterilized tryptone soya broth and exposed to further analysis. Prior incubation loopfull of each enriched culture was streaked on MacConkey Agar and Blood Agar plates. All plates were incubated at 37^{o}C for 24hrs.Colonies with different morphological characters, nature of haemolysis, and Gram characters were selected and inoculated on respective selective or differential media viz. Endo Agar, C.L.E.D Agar, Hekton Enteric Agar etc. All plates were incubated at 37^{o}C for 24hours.

Antibiogram in presence of usually recommended antibiotics was studied by Kirby-Bauer Disc Diffusion Method (1966). Isolates were categorized as susceptible, moderately susceptible and resistant based upon interpretative criteria developed by the clinical and laboratory standards institute (CLSI) and results were recorded as per zone of inhibition. The antibiotic used were-Nalidixic acid (30 mcg), Amoxicilin (10 mcg), Ampicillin (30mcg), Ciprofloxacin (30mcg),Norfloxacin(30 mcg) , Chloramphenicol (50 mcg) ,Tetracyclin (30 mcg),Colistin(10mcg).

III. RESULTS

Out of 149 samples were recorded which showed 51% positive for the presence of infection caused by organisms and 48.99% showed negative which is the absence of organisms.
In the present study highest causative organism isolated was *E.coli*(52.63%), followed by *K.pneumonia* (17.10%), *Enterobacter sps.* (10.52%) , *Morganella sps.*(1.31%), *Proteus sps*.(14.47%), and *Citrobacter sps*. (1.31%), *Salmonella sps*. Figure.1

Frequency of isolation of pathogenic organisms from various specimens is depicted in Table –I . It can be observed that with urine as the specimen source, highest infective organism isolated was *E.coli*(51.06%) followed by *K.pneumonia*(17.02%), *Enterobacter sps*. (12.75%), *Proteus sps*. (17.07%) and *Citrobacter sps.* (2.12%).

In burn swabs highest infective organism isolated was *E.coli(*55%) followed by *K.pneumonie* (20%), *Enterobacter sps*.(10%), *Proteus sps.(*15%).

In pus only three organisms, *E.coli* (66.66%) followed by *K.pneumonae*(16.66%) and *Morganella*(16.66%). *E.coli* and Salmonella was the only organism isolated from blood and serum respectively.

The positive culture reports showed varied responses to different antibiotics by the organisms in the biological samples. Since, Urinary tract infections are the most common among the infections, frequent and primary testing of urine samples is advised by the practitioners. Thus, the study concentrates on the antibiotic susceptibility of obtained predominant isolates. The resistance percentage for the antibiotics was highest than the sensitive percentage from the results it was revealed that all the isolates analyzed were sensitive to Chloramphenicol followed by colistin.
Tetracyclin was also found to have considerable inhibition against all obtained isolates except *E.coli* and *K. pneumoniae*(83.84%).
Ciprofloxacin inhibited (90%) considerably all the isolates of Morganella, *Citrobacter sps.* ,*Salmonella sps.*and all *Proteus species* while few isolates of *E.coli* (87.5%), *K. pneumonia* (38.46%),*Enterobacter* sps. (37.5%), were found resistant to it.

Ampicillin and Nalidixic acid resistance was revealed by all the obtained isolates with variable percentage viz. *E.coli*(100%)isolates were resistant to Ampicillin while 95% isolates exhibited resistance towards Nalidixic acid, few strains of *K.pneumoniae* (61.53%), *Enterobacter sps*(87.5%),*Morganella*(100%),*Proteus sps*. (36.36%), *Citrobacter sps* and *Salmonella sps.* (100%), were found resistance to Nalidixic acid.
E.coli was found to show high resistance to Norfloxacin followed by *K.pneumoniae*(46.15%),*Enterobacter sps.*(75%), *Morganella sps.* (100%), *Proteus sps.*(27.27%) ,*Citrobacter sps.(*100%),*Salmonella sps*.(100%) resistance pattern in response to it and least inhibition was recorded in presence of amoxicillin. All bacterial isolates exhibited variable percentage of resistance towards it.

Table No. 1 Frequency distribution of isolated predominant pathogenic organisms

Isolates	Percentage Occurrence
E.coli	52.63
K.pneumoniae	17.10
Enterobacter sps	10.52
Morganella sps	1.31
Proteus sps	14.47
Citrobacter sps	1.31
Salmonella sps.	2.73

Figure 1 : Rrequency Distribution of Isolated Prominant Pathogens

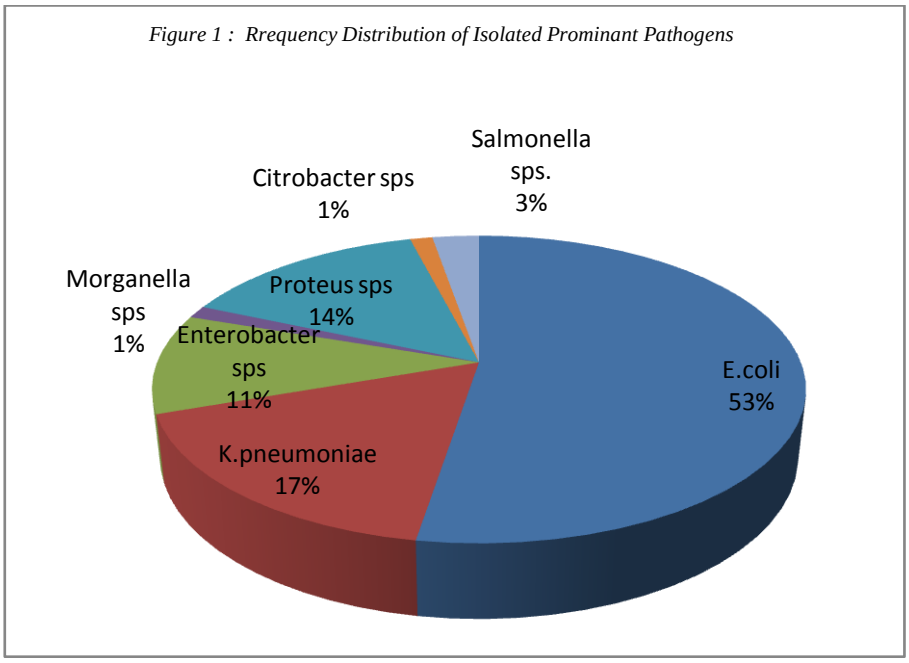

Table No. 2: Antibacterial resistance pattern (%) exhibited by obtained isolates.

Name of Antibiotics	Name of organism						
	E.coli	*K. pneumoniae*	*Enterobacter sps*	*Morganella sps*	*Proteus sps*	*Citrobacter sps*	*Salmonella sps.*
Nalidixic acid	95	61.53	87.5	100	36.36	100	100
Amoxicillin	97.5	92.3	62.5	100	45.45	100	100
Ampicillin	100	92.3	75	100	63.63	100	100
Ciprofloxacin	87.5	38.46	37.5	0	27.27	0	0
Norfloxacin	82.5	46.15	75	100	27.27	0	0
Chloramphenicol	62.5	61.52	25	0	36.36	0	0
Tetracyclin	85	83.84	37.5	0	18.18	0	0
Colistin	70	23.7	0	0	0	0	100

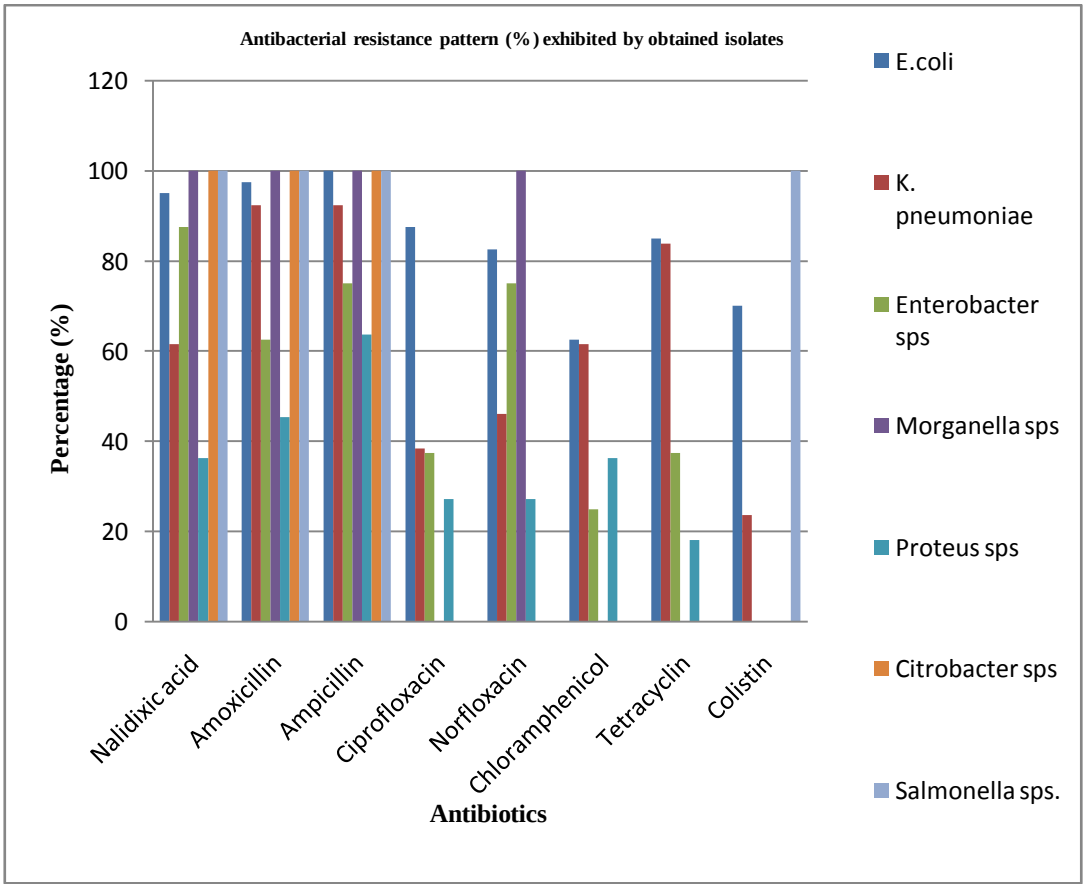

Out of 76 cultures positive specimens isolates, 61.84% (47 specimens) were urine samples indicating that urinary tract infection (UTI) is the most common hospital acquired infection. A high isolation rate of pathogens from urine samples of clinically suspected UTI show a good correlation between clinical findings and microbiological methods. UTI is one of the most important causes of morbidity in general population and is the second most common cause of hospital visits. Gram negative organisms were the commonest organisms present in specimens, amongst which *E.coli* , *Klebsiella sps.* , *Enterobacter sps.* , *Proteus sps.*, *Morganella sps*. *Salmonella sps*. Were confirmed by standard conventional tests. In the present study *E.coli* 40(52.63%) and *Klebsiella* 13(17.10%) are the most prominent organisms isolated from different samples of infected patients (Fig: 1) Similar study was conducted among 1020 pathogen from 11308 urine sample, revealed that 620 strains(60.78%) of *E. coli* and 115 strains(11.27%) of *K. Pneumoniae* (Ava Behrooozi *et al*.,2010) were isolated from urine specimens of patients correlates our present study. The study was formulated for an outlay of the clinical sources at specified areas. Various studies on antibiotic resistance are emerging with an intention to bring into lime light about the resistance that is developing among the microorganisms towards the antibiotics. Organisms showing different responses towards antibiotics .However reasons for the cause of this resistant activity can be framed out as either more frequent and unnecessary usage of antibiotics or prescribing newer antibiotics with newer antibiotics with newer combination for faster recovery of infections. In the present study, the top resistance percentage was observed by ampicillin (100%), Amoxicillin (97.5), Nalidixic acid (95%), Ciprofloxacin(87.5%), Tetracycline (85%). Penicillin group of antibiotics are drugs of choice for a wide variety of infectious diseases. Unfortunately these drugs are readily hydrolyzed by broad spectrum β-lactamases that are found with increasing frequency in clinical isolates of these gram negative bacteria. Many reports in the literature suggest an increased resistance to ampicillin (80-100%). A study from western Nepal reported high prevalence of resistance to ampicillin, nalidixic acid and norfloxacin (Das *et al.*,2006). Studies conducted in Eastern Jorden was similar to the present study in organism profile in urine sample and resistance pattern was high to Co-trimoxazole (59.5%), Gentamycin (43.2%), Nalidixic acid (29.3%) and least to Norfloxacin (11%) and Ciprofloxacin (3.8%) (Younis *et al.*,2009). A retrospective study in a tertiary care setting in Bangalore had high resistance to Co-trimoxazole, Amicillin, Amoxicillin and fluroquinolones by *E. coli* (Priya *et al.*,2002). It is worth to note that maximum organisms exhibited multiple drug resistance specially E.coli and Klebsiella. These pathogens have been reported as major cause of nosocomial infection. A nosocomial infection surveillance system may be introduce to reduce the rate nosocomial infections and for better therapeutic options. From present investigation, we can say that there are increasing instances where the resistance to antimicrobials acquired by previously susceptible organisms is the cause of treatment failure or requires administration of larger doses and toxic agents. Irrational and inappropriate use of antibiotics has been a major cause in development of drug resistance. Therapeutic decisions in infections involve consideration of susceptibility resistance patterns.Prophylactic/combined antibiotic therapy and adverse reaction of drug etc.

REFERENCES

[1] Ava Behrooozi, Mohammad Rahbar, and Jalil Vand Yousefi, 2010. Frequency of Extended Spectrum Beta-Lactamase (ESBLs) producing *Escherichia coli* and *Klebseilla pneumonia* isolated from urine in an Iranian 1000-bed tertiary care hospital. *African Journal of* Microbiology *Research*,4:881-884.

[2] Abu Shaqra Q. Occurrence and antibiotic sensitivity of Enterobacteriaceae isolated from a group of Jordanian patients with community acquired urinary tract infections. Cytobios 2000;101:15-21. (s)

[3] Bonnet, R., Sampaio, J.L.M. and Chana,L. C. 2000. A novel class A extended-spectrum *β*- lactamase (BES-1) in *Serratia marcescens* isolated in Brazil. *Antimicrobial Agents and Chemotherapy*, 44:3061–3068.

[4] Bradford, P.A. 2001. Extended – spectrum beta – lactamases in the 21st century: characterization, epidemiology, and detection of this important resistance threat. *Clin.Microbiol*. Rev., 14: 933 - 51. Sturenburg, E. and Mack, D. 2003. Extended Spectrum b- lactamases: implications for the clinical microbiology laboratory. *J. Infection*., 47: 273 - 95.

[5] Chitnis SV, Chitnis V, Sharma N, Chitnis DS. Current status of drug resistance among gram negative bacilli isolated from admitted cases in a tertiary care centre. JAPI 2003;51:28-32. (s)

[6] Das RN, Chandrashekhar TS, Joshi HS, Gurung M, Shrestha N, Shivananda PG. Frequency and Susceptibility profile of pathogens causing urinary tract infections at a tertiary care hospital in western Nepal. Singapore Med J 2006;47:281-5. (s)

[7] Jones RN, Kugler KC, Pfaller MA, Winokur PL. Characteristics of pathogens causing urinary tract infections in hospitals in North America: results from the SENTRY Antimicrobial Surveillance Program 1997. Diagn Microbiol Infect Dis 1999;35:55-63. (s)

[8] Kamini W. (2006) *Emerging Problem of Antimicrobial Resistance in Developing Countries: Interwining Socio economic Issues. Regional Health Forum WHO South-East Asia Region*, 7(1), 2006.

[9] National Committee for Clinical Laboratory Standards. Performance standards for antimicrobial disk susceptibility tests. Approved standard M2 A7 NCCLS, Villanova, PA. 1995; 15. (s)

[10] Navaneeth BV, Belwadi S, Suganthi N. Urinary pathogens resistance to common antibiotics: a retrospective analysis. Trop Doct 2002;32:20-2. (s)

[11] Philippon, A., Labia, R. and Jacoby, G. 1989. Extended spectrum beta lactamases. *Antimicrob. Agents Chemother*., 33 :1131-1136.
[12] Priya P., Khurana R. and George J. (2002) *Indian J. Pharma*., 34; 278-280
[13] Shrinivasa H, Parija SC, Bhattacharya S, Sehgal R. Incidence of ciprofloxacin resistance in urinary isolates Eastern Nepal. J comm Dis 1999;31:45-7. (S)
[14] Tambekar DH, Dhanorkar DV, Gulhane SR, Khandelwal VK, Dudhane MN. Antibacterial susceptibility of some urinary tract pathogens to commonly use antibiotics. African J Biotech 2006; 5 (17): 1562-5. (S)
[15] Younis N., Quol K., Momani T, Awaisheh F.A. and Kayed D.A. (2009) *J. Nepal Med. Assoc*., 48(173): 14-19.

PRATIBHA: INTERNATIONAL JOURNAL OF SCIENCE, SPIRITUALITY, BUSINESS AND TECHNOLOGY (IJSSBT), Vol. 1, No.1, March 2012
ISSN (Print) 2277—7261

A New U-Shaped Heuristic for Disassembly Line Balancing Problems

Shwetank Avikal[1], *and P. K. Mishra*[2]
[1,2]MED, M. N. National Institute of Technology, Allahabad, India
Emails: [1]shwetank@mnnit.ac.in, [2]pkm@mnnit.ac.in

Abstract: The product recovery operations are fully based on disassembly line balancing. The disassembly line is a best chaise of automated disassembly or returned product. It is very difficult to find the optimal balance of a disassembly line because of its N-P hard nature. In this paper a new U-shaped heuristic is proposed to assign the parts to the disassembly work stations under precedence constraints and we compared the proposed heuristically obtained solutions with the other heuristically solutions to see that this is performing well or not. The heuristic tries to minimize the minimum number of workstations while addressing the hazardous, high demand and low disassembly cost components. Examples are considers to illustrate the methodology of the proposed heuristics. For the problem tested, we observe that the heuristic described in this paper generated significantly better result.

Keywords: Disassembly, Heuristic, Line balancing, U-shape assembly line.

I. INTRODUCTION

Now a day's more and more manufacturers are beginning to recycle and remanufacturer their post-consumed products due to insertion of new product, more rigid environment legislation, increased public awareness and extended manufacturer responsibility. In addition, the economic attractiveness of reusing product, subassemblies or parts instead of disposing of them has further fueled this effort. Recycling is a process performed to retrieve the material contents of used and non-functioning products.

Remanufacturing, on the other hand, is also an industrial process in which warm-out products are restored to like-new product's conditions. Thus, remanufacturing provides the quality standards of new product with used parts [18].

In order to minimize the amount of waste sent to landfills, product recovery seeks to obtain materials and component from old or outdated products through recycling and remanufacturing – this includes the reuse of components and products. There are many attributes of a product that enhance product recovery; examples include: ease of disassembly, modularity, type and compatibility of materials used, material identification markings, and efficient cross-industrial reuse of common parts/materials. The first crucial step of product recovery is disassembly [14].

End-of life processing of complex products such as electronic product is becoming increasingly important, because they contain a large variety of hazardous, useful as well as valuable components and materials. Disassembly is often used to separate such components and materials. A disassembly precedence graph (DPG) is frequently used to describe a disassembly process. Box in this graph refer to operations, typically the detachments of components. Arcs represent the precedence relationships. Both yield and costs are associated with every operation [19].

Disassembly is defined as the methodical extraction of valuable parts/subassemblies and materials from discarded products through a series of operations. After disassembly, reusable parts/subassemblies are cleaned, refurbished, tested and directed to inventory for remanufacturing operations. The recyclable materials can be sold to raw-material suppliers, while the residuals are sent to landfills [14].

Recently, disassembly has gained a great deal of attention in the literature due to its role in product recovery. A disassembly system faces many unique challenges; for example, it has significant inventory problems because of the disparity between the demands for certain parts or subassemblies and their yield from disassembly. The flow process is also different. As opposed to the normal "convergent" flow in regular assembly environment, in disassembly the flow process is "divergent" (a single product is broken down into many subassemblies and parts). There is also a high degree of uncertainty in the structure and the quality of the returned product. The conditions of the products received are usually unknown and the reliability of the components is suspects. Some parts of the product may cause pollution or may be hazardous. These parts tend to have a higher chance of being damaged and hence may require

special handling, which can also influence the utilization of the disassembly workstations. For example, an automobile slated for disassembly contents a variety of parts that are dangerous to remove and/or present a hazard to the environment such as the battery, airbags, fuel and oil. Various demanded sources may also lead to complications in disassembly line balancing. The reusability of parts creates a demand for these parts, however, the demands and availability of the reusable parts is significantly less predictable than what is found in the assembly process. Finally, disassembly line balancing is critical in minimizing the use of valuable recourses (such as time and money) invested in disassembly and maximizing the level of automation of the disassembly and the quality of the parts (or material) removed [18].

In this paper an analysis of U-shaped disassembly line has been carried out using proposed heuristic. In section II, the relevant literature has reviewed, while section III depicts precise description of the U-shaped and traditional straight-line layout. In section IV, disassembly line balancing problems has been described and in section V, the proposed heuristic has been described and in section VI a practical example and computational results have been shown while the conclusion in section VII.

II. LITERATURE REVIEW

Product recovery involves a number of steps [1]. The first crucial step is disassembly. Disassembly is a methodical extraction of valuable parts/subassemblies and materials from post-used products through a series of operations [2] [3]. After disassembly, re-usable parts/subassemblies are cleaned, refurbished, tested and directed to the part/subassembly inventory for remanufacturing operations. The recyclable materials can be sold to raw-material suppliers and the residuals are disposed of [14].

The basic disassembly line balancing problem (DLBP) can be stated as the assignment of disassembly tasks to workstations such that all the disassembly precedence relations are satisfied and some measure of effectiveness is optimized.
Gungor and Gupta presented the first introduction to the disassembly line-balancing problem [4-6] and developed an algorithm for solving the DLBP in the presence of failures with the goal of assigning tasks to workstations in a way that probabilistically minimizes the cost of defective parts [7]. Tang et al. developed an algorithm to facilitate disassembly line design and optimization [10]. McGovern et al. first applied combinatorial optimization techniques to the DLBP [9], [14].
Gungor and Gupta [11, 12] described the DLBP and developed a heuristic algorithm for solving the DLBP with the goal of minimizing the cost of defective parts [20]. McGovern & Gupta [18] presented a disassembly solution and that was found first by greedy modal then improving the solution with the help of 2-opt heuristic. Gupta and Lambert [3] provide a heuristically solution for the disassembly line balancing problems that incorporating sequencing dependent part removal costs. McGovern et al. [13] first proposed applying combinatorial optimization techniques to the DLBP. Later, various combinatorial optimization techniques to solve DLBP were compared by McGovern and Gupta [14]. The fact that even a simple disassembly line balancing problem is NP-complete was proven in literature [15], and a genetic algorithm was presented for obtaining optimal solutions for DLBP. Ranky et. al. [16] proposed a dynamic disassembly line balancing algorithm that aims at smoothing the load of the shop floor. In order to solve the profit-oriented DLBP, Altekin et. al. [17] developed the first mixed integer programming algorithm for the DLBP [20]. Ding et.al. [20] Proposed a multi objective disassembly line balancing problem and then solve this by an ant colony algorithm.
The benefits of the U-line as compared to a straight line include reduction in the wasted movement of operator, work-in-process inventory, and improved productivity, easier implementation of zero-defects comparing, higher flexibility in workforce planning in the face of changing demand, and improvement in material handling. Several authors have provided an explanation of U-shaped production lines and the way they operate, as well as the benefits realized by their implementation [15].

So a lot of research on U-shaped assembly line balancing has been done but no research is available on U-shaped disassembly line balancing.

III. U-SHAPED AND TRADITIONAL STRAIGHT-LINE LAYOUT

The traditional straight line layout allows to organize the tasks sequentially in one direction to form stations. A U-line, however, permits tasks located on both side of the line to form stations. Fig. 1 (a, b) illustrate the fundamental difference between the straight line and U-line layouts. When using a straight line layout, operator performs one or more tasks on a continuous portion of the line. When using a U-shaped layout, operators are allowed to work across both legs of the line, while partially assembled units follow the U-shaped

configuration. By allowing operators to work across both legs of the line, the U-shaped layout in fig. 1 requires fewer workstations then the comparable straight line layout [24].

The U-line balancing problem is to assign tasks to stations arranged in a U-shaped production line [13]. The U-shaped assembly line balancing problem may be define as: assigning all the tasks on the U-line to form a minimal number of work stations while the work contents in each station should not be greater than the given cycle time.

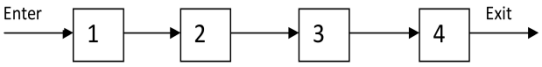

Fig 1.a. Traditional straight assembly line layout

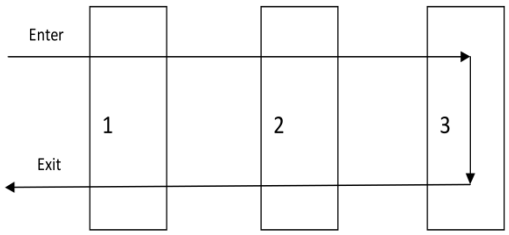

Fig 1.b. U-shaped assembly line layout

Notations:

J	$= 1, 2, 3, 4\ldots$
NWS	= Number of Workstations
CT	= Cycle Time
WS	= Work Load
Z	= Total Idle Time
K	$= 1, 2, 3, \ldots$
n	= Number of Parts to Remove
PRT	= Total Part Removal Time
$NWS_{\min}$	= Minimum No of Workstations
$NWS_{\max}$	= Maximum No of Workstations
h	= Part's Hazardous or not (0, 1)
H	= Part Hazardousness
PS_k	= Position of Part in Removal Sequence
D_k	= Demand of Part K
D	= Demand of Total Parts
C_k	= Part Removal Cost
T_k	= Part Removal Times

IV. DISASSEMBLY LINE BALANCING PROBLEM DESCRIPTION

Problem assumptions include the following:

1. Part removal times are deterministic,
2. Part removal times are constant,
3. Each product undergoes complete disassembly,
4. All products contain all parts with no additions, deletions, or modifications,
5. All the parts are assigned,
6. Each part is assigned to one and only one workstation,
7. The sum of the part removal times of all the parts those are assigned to a workstation must not exceed CT.
8. The precedence relationships among the parts must not be violated.
9. Any part can be assign to any workstation.

The main objective of the work is to Minimizing the sum of the workstation idle times, which will also minimize the total number of workstations. This objective is represented as:

$$\text{Minimize } Z = \sum_{j=1}^{NWS} CT - WS_j \quad ^2$$

The perfect line balance, $Z = 0$

Line balancing seeks to achieve Perfect Balance (all idle times equal to zero). When this is not achievable, either line Efficiency (IE) or the Smoothness Index (SI) is used as a performance evaluation tool for disassembly line balancing, Elsayed and Boucher [3].

In addition, we find:

The maximum number of workstations can be calculated as:

$$NWS_{\max} = n$$

The minimum number of workstations can be calculated as:

$$NWS_{\min} = \frac{\sum_{k=1}^{n} PRT_k}{CT}$$

A hazardous measure has developed to quantify each solution sequence performance, with a lower calculated value being more desirable. This measure is based upon binary variables that indicates whether the part is considered to contain hazardous material (the binary variable is equal to one if hazardous, otherwise zero) and its position is the sequence. A given solution sequence hazard measure is define as the sum of hazard binary variables multiplied by their position in the sequence, thereby rewarding the removal of hazardous part early in the part removal sequence [18]. The position in sequence is calculated as the number of predecessors of the component or the number of components which are necessary to remove earlier to the hazardous component. This measure is represented as:

$$H = \sum_{k=1}^{n} h_k * PS_k$$

$$h_k = \begin{cases} 1, & hazardous \\ 0, & otherwise \end{cases}$$

If individual hazardous measure of a component is required then it can be calculated as

$$H = h_k * PS_k$$

A demand measure has developed to quantify each solution sequence performance, with a lower

calculated value being more desirable. This measure is based upon positive integer values that indicate the quantity required of this part after it is removed (or zero if not desired) and its position in the sequence. Any given solution sequence demand measure is defined as the sum of the demand value multiplied by their component's position in the sequence. Position in sequence is calculated as the number of predecessors of the component or the number of components which are necessary to remove earlier to refer component, rewarding the removal of high demand parts early in the part removal sequence [18].

$$D = \sum_{k=1}^{n} d_k * PS_k$$

If individual demand measure of a component is required then it can be calculated as

$$D = d_k * PS_k$$

V. PROPOSED HEURISTIC

The heuristic is developed to achieve following objectives:

1. Minimize the total minimum number of disassembly work stations to decrease total idle time,
2. Balance the disassembly line,
3. Remove hazardous parts/components early in the disassembly sequence,
4. Remove high demand components before low demand components ,
5. Remove low disassembly cost components before high disassembly cost components,
6. Remove the parts which have large part removal time before the parts which have small part removal time and
7. Assign same type of parts at same workstations (e.g. hazardous component at same work stations, high demand component at same workstations).

The proposed heuristic is a U-shaped heuristic where the parts are assigned to the workstations which are arranged in U-shaped. The product comes from one direction to disassemble and the parts are removed at each workstation.

The proposed heuristic is based on some simple priority rules that are based on knowledge. The first priority rule assign the parts which are hazardous, then second rule assign the part to the workstation, that have highest demand and then in decreasing order, then third rule is based on pert removal cost, and it assign the part from minimum part removal cost to high part removal cost or in increasing order of part removal cost and in the last the forth rule assign the part to the workstation in order of decreasing part removal time.

The priority rules on which the proposed heuristic is based are as follows:

1. Maximum part hazardous
2. High part demand
3. Low disassembly cost
4. Maximum part removal time

The heuristic ranking procedure is as follows:

1. Find the hazardous parts and rank them according to their decreasing order of hazardousness,
2. Find the parts that have demand and list them in decreasing demand order,
3. List the parts in order of their increasing part removal cost order, and
4. List the parts in order of their decreasing part removal time

Then assign a rank to all the parts, based on above priority rules. Assign the first rank to that part that is hazardous and have high demand, low part removal cost and have highest part removal time in case of tie. It means if two parts have property of same hazardous then it is a case of tie, so now check for their demand, if one of them have more demand than other one, assign it at first rank but if the demands of both parts are same then check for their part removal cost, if one of them have lower cost than other one , assign it at first rank and if the part removal cost is again same and it is again case of tie, so check for their part removal time and assign them rank in order of their part removal time.

After assigning rank to all parts, start the assignment of parts to the workstations in order of decreasing their rank and their precedence constraints. If a task has first rank but it cannot be assigned to workstations because of precedence constraints, then check for next part in the rank list and again check for assignment. If task is eligible for assignment but the time available at the current workstation is not enough then check next assignable task and no if part can be assign on current workstations, start a new workstation with full of cycle time and repeat the same till all parts get assigned to workstations.

VI. COMPUTATIONAL EXAMPLE

The developed algorithm has been investigated on a variety of test cases to confirm its performance and to optimize parameters. The proposed U-shaped heuristic has been used to provide a solution to the disassembly line balancing problem based on the disassembly sequencing problem presented by Kongar and Gupta [25] where the objective is to completely disassemble a given product (see Figure 1) consisting of n = 10 components and several precedence relationships (e.g., parts 5 and 6 need to be removed prior to part

7). The problem and its data were modified with a disassembly line operating at a speed which allows CT = 40 seconds for each workstation to perform its required disassembly tasks. This provided an application to a previously explored disassembly problem. This practical and relevant example consists of the data for the disassembly of a product as shown in Table 1. It consists of ten subassemblies with part removal times of T_k = {14, 10, 12, 18, 23, 16, 20, 36, 14, 10}, hazardousness as h_k = {0, 0, 0, 0, 0, 0, 1, 0, 0, 0}, part demand d_k = {0, 500, 0, 0, 0, 750, 295, 0, 360, 0}, and part removal cost as C_k = {27, 63, 48, 62, 24,18, 83,77, 93, 10}, The disassembly line is operated at a speed that allows 40 seconds for each workstation [18].

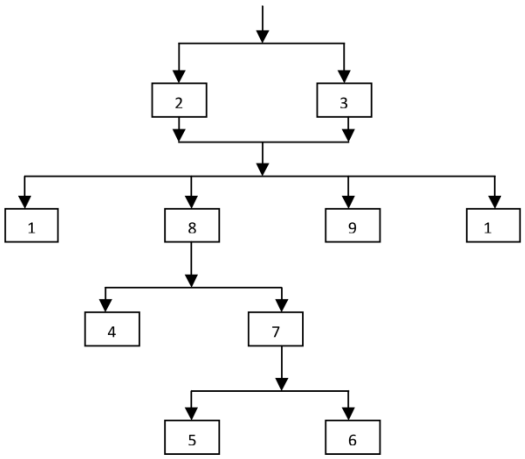

Fig. 2: example of product precedence relationships

Table 1: Knowledge based of the example from literature

Part	Time	Hazardous	Demand	Cost
1	14	0	0	27
2	10	0	500	63
3	12	0	0	48
4	18	0	0	62
5	23	0	0	24
6	16	0	485	18
7	20	1	295	83
8	36	0	0	77
9	14	0	360	93
10	10	0	0	10

After applying proposed heuristic a ranking is provide to all the tasks and then assign them according to their rank from higher to lower order and according to their precedence constraints.

The final ranking of the parts removal is as follows:

Table 2. Ranking of tasks

Tanks No.	1	2	3	4	5	6	7	8	9	10
Rank	7	3	8	9	6	2	1	10	4	5

In this list the part number 7 is ranked first because it has hazardous property and it also have some demand, after this part number 6 is assigned at rank 2 cause of it has no hazardous property but it have maximum demand over demand of all the parts. Then part number 2 is assigned at rank 3 and part number 9 at rank 4, because of part number 2 have much more demand and it require minimum 8 removed parts to remove it and part number 9 do not require any removed part to remove it. Part number 10 and 5 are also assigned at rank 5 and 6, these tasks do not have hazardous property and demand also, so here, there part removal cost is consider as decision variable and according to their part removal cost they are assigned ranking. This process is also repeated for the part number 1,3,4,8 and they got assign their respective rank.

After assigning rank to all the parts to remove, the assignment of part to the workstations is started. Start first workstation with the cycle time as CT=40, and check the rank list for the assignment of parts to the workstations that are arranged in U-shaped. Task number 7 hast first rank in the list but it cannot be assign to the workstation because of its precedence constraints, so move to next one and the next part i.e. part number 6, and it can be assign to the work station. After this, again check the list from starting and the part number 7 is again not assignable, so move to next one. The next part is part number 2 and it can be assign to same workstation, and the next part that is part number 9, can also be assign to the same workstation. Now first workstation has been completed because it has no idle time so no more parts can be assign on this workstation, so start a new workstation with CT=40, and start the assignment procedure again. For this new workstation, check the rank list from start, and task number 7 is again not assignable, so again move to next part and assign part number 5, and again check the rank list because of same part number 7 cannot be assign so assign the part number 1 at second workstation. The idle time left on second workstation is 3 seconds and no task can be assign in this workstations, so again start a new workstation with CT=40, and repeat the procedure of parts assignments. Now at this third workstation, part number 7 is assigned which was not earlier assigned because of its precedence relations, and then check for the next not assigned

parts in the rank list, and assigned the part number 10 at the same workstation. Now the idle time of third workstation is 10 seconds and no part in the list can be assigned on this workstation, start a new forth workstation with CT=40 sec, and again check for assignment and assign the part number 4 & 3 at this workstation and idle time left at forth workstation is 10 sec, here no task can be assign on forth workstation, so start a new one with CT=40, and assign the last part i.e. part number 8 at fifth workstation and the remaining idle time on this workstation is 4 sec and there is no more task available in the rank list to be assign, so the procedure of assignment of parts on the workstations is now completed and the assignment of parts to the work station has shown in Fig. 3.

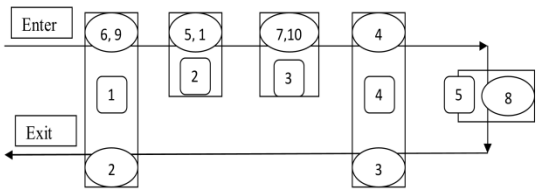

Fig. 3: Assignment of parts on the workstations

Table 3: Solution by Proposed Heuristic

W/S No.	Part assigned	Part removal time	Idle time
1.	6 2 9	16 10 14	24 14 00
2.	5 1	23 14	17 3
3.	7 10	20 10	20 10
4.	3 4	12 18	28 10
5.	8	36	4

The problem solved by proposed heuristic is also solved by 2-opt heuristic by Mc.Govern & Gupta. The comparison of results of this problem, with result of Mc.Govern & Gupta is given as:

Table 4: Comparison of Solutions

S. No.	Bases	Mc.Govern & Gupta	Proposed
1.	Number of Workstations	Five	Five
2.	Cycle Time	40 Seconds	40seconds
3.	Line Efficiency	73%	73%
4.	Workstations Efficiency	1. 97.5% 2. 85% 3. 80% 4. 90% 5. 80%	1. 100% 2. 92.5% 3. 75% 4. 75% 5. 90%
5.	Heuristic Based on	1. Hazardous Part 2. Part Demand 3. Part Removal Time	1. Hazardous Part 2. Part Demand 3. Part Removal Cost 4. Part Removal Time
6.	Objectives	1. Minimize The No. of Workstations 2. Balance The Line 1. 3.Remove Hazardous Part First 3. Remove High Demand Parts Before Low Demand Parts	1. Minimize The No. of Workstations 2. Balance The Line 3. 3.Remove Hazardous Part First 4. Remove High Demand Parts Before Low Demand Parts 5. Remove Same Parts At Same Workstation (Hazardous Part At Same, High Demand Parts At Same Workstation)
7.	Line Type	Straight Line	U-Shaped Line

VII. CONCLUSION

An efficient, near optimal, multi objective heuristic is presented for U-shaped deterministic disassembly line balancing. The proposed heuristic is able to achieve all of the objectives and provide an efficient solution with minimum number of workstations. It disassemble all high demands parts at the same workstation then try to remove hazardous part at the same workstations then assign the part to the workstations with respect to their minimum part disassembly costs and then according to their part removal time. The comparisons shows that the proposed heuristic performs better then the heuristic provided by M. McGovern and Gupta while achieving one more objective i.e. assign the same parts at same workstations (high demanded parts at same and hazardous parts at same workstations). It is because of its U-shape and arrangement of its priority rules. The U-shape of the line allows the assignment of parts on both sides of the line. If we compare this U-shaped line to straight line then, in U-shaped, parts are assigned from both directions and it can be seen that task no 8 that is assigned at fifth workstation cannot be possible at straight line because of precedence resections and it can only possible in U-shaped line. So because of U-shaped and arrangement of priority rules the proposed heuristic performs better and provides optimal/near optimal significant solutions. This proposed heuristic provides an additional advantage i.e. the workers are allowed to move to any workstations, so that they can work freely.

REFERENCES

[1] A. Gungor, and S. M. Gupta, "Issues in Environmentally Conscious Manufacturing and Product Recovery: A Survey", *Computers and Industrial Engineering*, Vol. 36, No. 4, pp. 811-853, 1999.

[2] L. Brennan, S. M. Gupta, and K. N. Taleb, "Operations Planning Issues In An Assembly/Disassembly Environment", *International Journal of Operations and Production Planning*, Vol. 14, No. 9, pp. 57-67, 1994.
[3] S. M. Gupta, and K. N. Taleb, "Scheduling Disassembly", *International Journal of Production Research*, Vol. 32, pp. 1857-1866, 1994.
[4] A. Gungor, and S. M. Gupta, "Disassembly Line Balancing", Proceedings of the 1999 *Annual Meeting of the Northeast Decision Sciences Institute*, Newport, Rhode Island, March 24-26, pp. 193-195, 1999.
[5] A. Gungor, and S. M. Gupta, "A Systematic Solution Approach to the Disassembly Line Balancing Problem", Proceedings of the 25th *International Conference on Computers and Industrial Engineering*, New Orleans, Louisiana, March 29-April 1, pp. 70-73, 1999.
[6] A. Gungor, and S. M. Gupta, "Disassembly Line In Product Recovery", *International Journal of Production Research*, Vol. 40, No. 11, pp. 2569-2589, 2002. 9.
[7] S. M. Gupta, and K. N. Taleb, "Scheduling disassembly", *International Journal of Production Research*, Vol. 32, pp. 1857-1866, 1994.
[8] A. Gungor, and S. M. Gupta, "A Solution Approach to The Disassembly Line Problem In The Presence Of Task Failures", *International Journal of Production Research*, Vol. 39, No. 7, pp. 1427-1467, 2001.
[9] S. M. McGovern, et.al., "Solving Disassembly Sequence Planning Problems Using Combinatorial Optimization", Proceedings of the 2003 *Annual Meeting of the Northeast Decision Sciences Institute*, Providence, Rhode Island, pp. 178-180, March 2003.
[10] Y. Tang, M, et.al., "A Systematic Approach to Disassembly Line Design", Proceedings of the 2001 *IEEE International Symposium on Electronics and the Environment*, Denver, Colorado, May 7-9, pp. 173-178, 2001.
[11] Gungor A & Gupta SM, "A Solution Approach To The Disassembly Line Problem In The Presence Of Task Failures", *International Journal of Production Research*, Vol. 39, No.7, pp. 1427–1467, 2001.
[12] Gungor A, Gupta SM, "Disassembly Line in Product Recovery", *International Journal of Production Research*, Vol. 40, No.11, pp. 2569–2589, 2002.
[13] McGovern SM et.al., "Solving Disassembly Sequence Planning Problems Using Combinatorial Optimization", Proceedings of the 2003 Annual Meeting of Northeast Decision Sciences Institute, Providence, Rhode Island, pp 178–180, 2003.
[14] McGovern SM, Gupta SM, "Combinatorial Optimization Methods For Disassembly Line Balancing", Proceedings of the 2004 SPIE International Conference on Environmentally Conscious Manufacturing, Philadelphia, Pennsylvania, pp 53–66, 2004.
[15] McGovern SM, Gupta SM, "A Balancing Method And Genetic Algorithm For Disassembly Line Balancing", *European journal of Operation Research*, Vol. 179, pp.692–708, 2007.
[16] Ranky RJ et.al. (2003), "Dynamic Scheduling And Line Balancing Methods, And Softwaretools For Lean And Reconfigurable Disassembly Cells And Lines", Proceedings of the IEEE International Symposium on Electronics and Environment, Boston, Massachusetts, pp 234–239
[17] Altekin FT et. al., "Profit-Oriented Disassembly-Line Balancing", *International Journal of Production Research*, vol. 46, pp.2675–2693, 2008.
[18] Seamus M.McGovern & Surendra M.Gupta, "2-Opt Heuristic For The Disassembly Line Balancing Problem", Iris, Northeastern University, Boston, USA, January 1, 2003.
[19] Surendra M.Gupta & A.J.D.lambert, "A Heuristic Solution for Disassembly Line Balancing Problem Incorporating Sequence Dependent Costs", Iris, Northeastern University, Boston, USA, January 1, 2005.
[20] Ding et.al., "A New Multi-Objective Ant Colony Algorithm For Solving The Disassembly Line Balancing Problems", *International Journal of Advance Manufacturing Technology*, Vol. 48, pp. 761-771, 2010.
[21] Chiang & Urban, "The Stochastic U-Shaped Balancing Problem: A Heuristic Procedure", *European Journal of Operational Research*, vol. 175, pp. 1767-1781, 2005.
[22] Hadi et.al., "A Shortest Route Formulation Of Simple U-Type Assembly Line Balancing Problem", *Applied Mathematical Modeling*, vol. 29, pp. 373-380, 2005.
[23] Toksari et.al., "Simple And U-Type Assembly Line Balancing Problems With A Learning Effect", *Applied Mathematical Modeling*, vol. 32, pp. 2954-2961, 2008.
[24] Aase et.al., "U-Shaped Assembly Line Layout and Their Impact on Labor Productivity: An Experimental Study". *European Journal of Operation Research*. Vol. 156, pp. 698-711, 2004.
[25] Kongar, E. & Gupta. S. M., "A genetic algorithm for disassembly process planning", *proceedings of the 2001 SPIE International Conference on Environmentally Concious Manufacturing II, Newton, Massachusetts*, October 28-29, pp. 54-62, 2001

PRATIBHA: INTERNATIONAL JOURNAL OF SCIENCE, SPIRITUALITY, BUSINESS AND TECHNOLOGY (IJSSBT), Vol. 1, No.1, March 2012
ISSN (Print) 2277—7261

Modified Cadmium Stannate Nanostructured Thin Films Prepared by Spraying Technique for the Detection of Chemical Warfares

L. A. Patil[1], V. V. Deo[2], and M. P. Kaushik[3]
[1] Nanomaterials Research Lab., Department of Physics, Pratap College, Amalner, 425 401, India.
[2] Defence Research and Development Establishment, Gwalior 474 002, India.
Emails: [1]plalchand_phy_aml@yahoo.co.in

Abstract: In present study spray pyrolysis technique was employed to prepare pure and doped $CdSnO_3$ thin films. The spray pyrolyzed thin films were observed to be nanostructured in nature with particle size less than 10 nm and characterized to investigate its structural, microstructural and chemical properties by means of XRD, SEM/EDS, TEM and surface profilometry. Pure and Zn doped $CdSnO_3$ nanostructured thin films were tested against THE simulants of chemical warfare agents (CWA). The Zn doped nanostructured thin films showed good sensing performance towards the simulants as compared to the pure thin films. The effect of nanocrystalline nature on simulant-sensing properties of pure $CdSnO_3$ and Zn-doped $CdSnO_3$ thin films was discussed and interpreted.

Keywords: Spray pyrolysis technique, Nanostructured $CdSnO_3$ thin films, Zn doping, CWA simulant, simulant response, speed of response and recovery.

I. INTRODUCTION

Nanostructured metal oxide-based gas sensors have been a major area of extensive research because of their use in detecting several toxic, inflammable, odorless gases and deadly Chemical warfare agents (CWA) and it's simulants over the past decades [1-11]. Chemical warfare agents can be defined as , a chemical which is intended for use in military or civilized area operations to kill, seriously injure, or incapacitate humans or animals through its toxicological effects[12,13]. As a result of high toxicity of chemical warfare agents (CWAs), fast and correct detection of CWAs is a great urge to protect living beings. Due to high toxicity of CWA, structural analogs i.e. simulants are generally used for research purpose.

The gas sensing properties are totally dependent upon the reaction between semiconducting metal oxides and target gas. Mechanism of gas-sensing involves the redox reaction at the metal oxide surface, leading to the change in the depletion layer of the grains that ultimately change the electrical resistance of the metal oxide. For the change in electrical resistance of the metal oxide, there are many possible reactions; the most commonly accepted reaction that leads to changes in electrical resistance is the adsorption of gases on the metal oxide surface. Adsorption is nothing but a surface effect and nanostuctured metal oxides possess high surface to volume ratio, which enhances this effect [14-16].

Metal oxide gas sensors improve their sensitivity and response/recovery time due to nanocrystalline nature of the material associated, which is the most attractive quality of nanomaterials. Basically the improvements are because of the high surface area to volume ratio and smaller crystallite size compared to conventional microcrystalline materials [17]. Despite of binary semiconducting metal oxide e.g. ZnO, SnO_2, TiO_2 etc, perovskites (ABO_3) with good thermal stability are also interesting materials for gas sensing. The flexibility for introduction of variety of dopant for the enhancement of sensing properties is only due to the cations size difference between A and B. These interesting characteristics of perovskites also make them promising candidate for catalytic applications [18]. Cadmium Stannate ($CdSnO_3$) based gas sensors are efficient for detection of reducing gases such as Cl_2, C_2H_5OH gas and ammonia [19-21] etc. Various techniques such as thermal decomposition, ball milled, co-precipitation method, low-temperature ion exchange, solid-state reaction, CVD, Sputter deposition, Electron Beam Technique [22-28] etc. have been employed to prepare $CdSnO_3$ thin films. In the present investigation, spray pyrolysis technique was employed to prepare pure and zinc doped $CdSnO_3$ thin films because the technique is simple and involves low cost equipments and raw materials. The technique involves a simple technology in which an ionic solution (containing the constituent elements of a compound in the

form of soluble salts) is sprayed over heated substrates [29]. By this method, dopants can be easily introduced into the matrix of the film by using appropriate precursors [30]. Additives or dopants enhance the properties of the sensors, such as sensitivity, selectivity, lowering the operating temperature, response and recovery time etc [31-33]. The morphology and microstructure of the films were investigated by x-ray diffraction (XRD) , energy dispersive x-ray (EDX) analyzer, transmission electron microscopy (TEM) and surface profilometry. In this work we tested sensors to sense dimethyl methylphosphonate (DMMP), a simulant -Sarin gas (Nerve agent), 2-chloroethyl ethyl sulfide (2-CEES) and chloroethyl phenyl sulfide (CEPS) - simulants of - Mustard gas (blister agent) namly, [34]. The electrical and gas sensing tests were carried out by indigeneous gas sensing system [35]. Measurements were carried out at different operating temperatures, ranging from 250 to 400 ^{0}C. The operating temperature of the sensors was adjusted by a regulated dc power supply to the heater.

II. EXPERIMENTAL

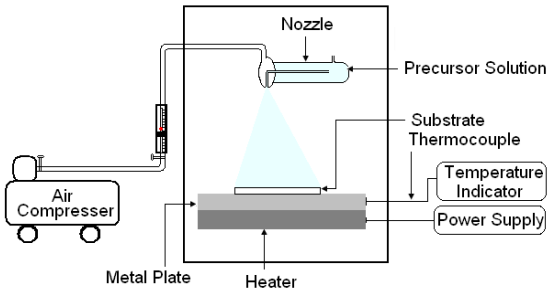

Figure1. Spray pyrolysis setup.

Figure 1 shows the schamatic diagram of spray pyrolysis system. Samples were prepared by simlpe and versatile spray pyrolsis technique. In this technique, the precursor solution was sprayed onto a heated substrate using air as carrier gas. The setup consists of spray nozzle, heater, air compresssor, flow meter, power supply, temperature indicator and thermocople. The $CdSnO_3$ thin films were prepared by spraying the solution mixure of aqueous solutions of: cadmium tertranitrate ($Cd(NO_3)_2{\cdot}4H_2O$ - 0.1 M) and tin pentachloride ($SnCl_4{\cdot}5H_2O$ - 0.1 M) with 1:1 proportions. Few drops of HCl were added to get the transparent solution. The stock solution was delivered to nozzle with the help of compressed air. The aerosol produced by nozzle was sprayed onto the heated glass substrate (300 ^{0}C). The spraying time was kept as 5 min and the thin film was referred to as S1.

To obtain the three types of zinc doped films, 1, 2.5 and 5 vol.% solutions of Zn $(NO_3)_2{\cdot}3H_2O$ were added into the equal proportion of solution mixture of: cadmium tertranitrate ($Cd(NO_3)_2{\cdot}4H_2O$ - 0.1 M) and tin pentachloride ($SnCl_4{\cdot}5H_2O$ - 0.1 M) . Each solution was sprayed for 5 minutes and the films so obtained were referred to as Z1, Z2 and Z3 respectively. The undoped and doped films were fired at 500 ^{0}C for 1h, prior to characterization and gas sensing studies. CEES/DMMP/CEPS (4 ppm) in gaseous form was used to test sensing performance of the pure and Zn-$CdSnO_3$ based sensors.

The gas response of the sensor to reducing gases is defined as S = Ig/Ia which Ia and Ig are the current in air and in test gas, respectively. The response time is defined as the times needed for the sensor-current to change by 90% of the difference from the maximum value to the minimum after the test gas injection. The recovery time is the times required for the sensor current to change by 90% of the difference from the minimum value to the maximum after exposure of gas [36].

III. RESULTS AND DISCUSSION

A. Structural Analysis

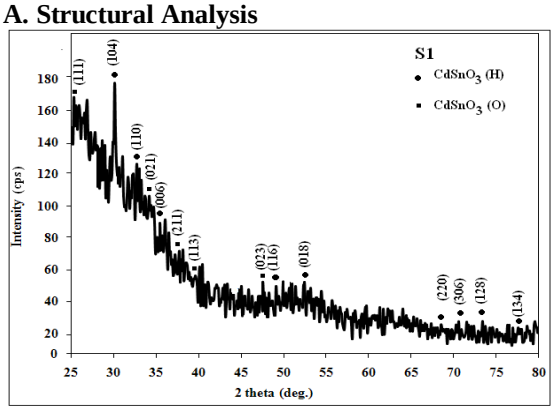

Figure2. XRD of sample S1.

Figure 2 shows the X-ray diffraction of sample S1. Several peaks in graph for S1 were observed to be nearly matching with to perovskite type $CdSnO_3$ (JCPDS file No. 34-0758 and 34-0885). The symbols, sphere and square corresponds to hexagonal and orthorhombic phase of $CdSnO_3$ in figure 2. Hexagonal phase is the most dominant, whilst the orthorhombic phase is present to a lesser extent. The diffractogram (figure2) indicates that the prepared $CdSnO_3$ thin films are amporphus in nature. The Zn doped X-ray diffraction doesnot show any peak corresponding to the zinc. The reason may be the very low content of zinc in $CdSnO_3$.

B. Quantitative elemental analysis

Table1. Elemental composition data of sample S1 and Z1.

Sample	at %			
	Cd	Sn	O	Zn
S1	19.53	33.88	46.5	---
Z1	09.97	21.83	67.90	0.31

The table 1 shows the Elemental composition of pure and doped samples. The films were observed to be nonstoichiometric in nature.

C. Thickess Measurement

Thickess of the samples were measured using surface profiler. Table 2 shows the thickness and roughness of samples as follows:

Table2. Thickness and roughness of samples.

Sample	Thickness (nm)	Roughness (nm)
S1	454	110.1
Z1	417.8	73.2

It is clear from the table that the Zinc doping has lowered the thickness and surface roughness as compared to the undoped samples.

D. Microstructural Study:

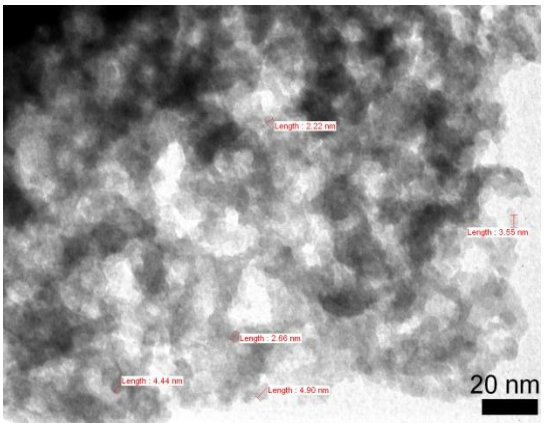

Figure3(a). Transmission electron microscopic image of sample S1

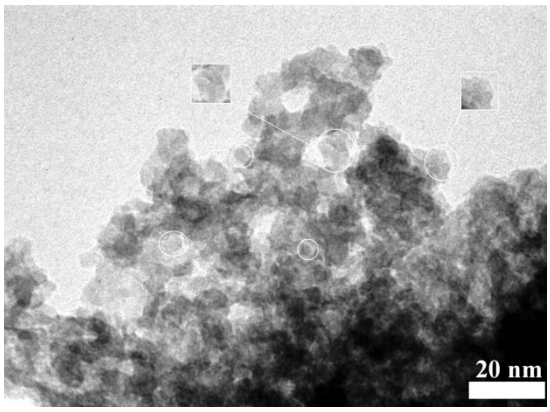

Figure3(b). Transmission electron microscopic image of sample Z1.

Figure 3 (a) and (b) shows the transmission electron microscopic images of sample S1 and Z1 respectively. Average particle size for sample S1 and Z1 were calculated from TEM images are 3.55 and 4.33 nm respectively. It is clear from the image 3 (b) that the zinc doping in CdSnO3 transforms the particle shapes into specific morphology- like hexagonal and square .

IV. ELECTRICAL PROPERTIES OF THE SENSORS

A. I-V Characteristics:

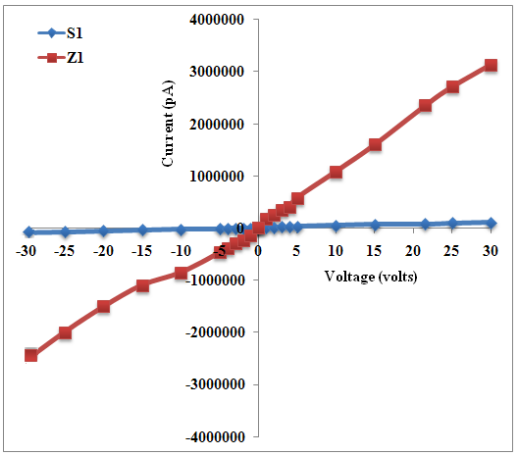

Figure4. I-V curves of sample S1 and Z1.

The working temperature was varied within the range of 250 ^{o}C - 450 ^{o}C. Figure 4 depicts I-V curves of S1 and Z1 samples. Linear nature of I-V curve of sensor shows good ohmic contact. The ohmic contact is very important to the gas sensing properties, b ecause the sensitivity of the gas sensor is affec ted by contact resistance [37].

B. Sensing responses of modified and unmodified samples:

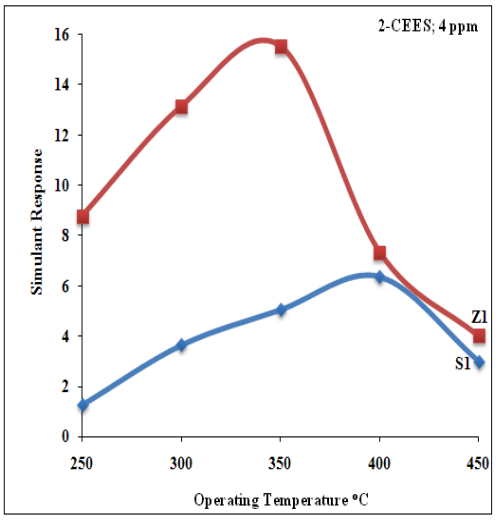

Figure5(a). Response of S1and Z1 to 2-CEES,

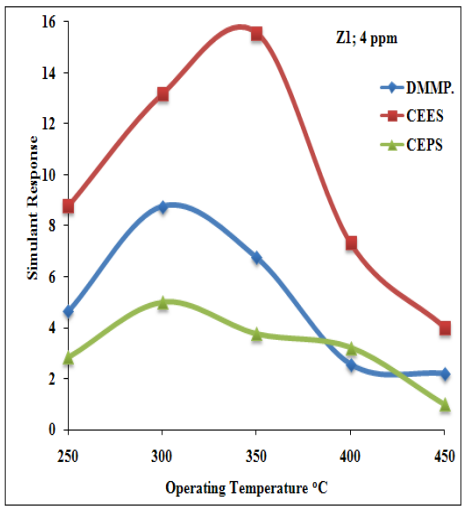

Figure 5(b). Response of Z1 to 2-CEES, DMMP and CEPS

Figure 5(a) shows the responses of the S1 (undoped) and Z1(Zn doped) sensors upon exposure to 4 ppm DMMP, 2-CEES and CEPS. The response to 2-CEES in case of S1 (S = 6) and Z1 (S = 15.56) were higher than the response to DMMP and CEPS. Also, Zn doping in $CdSnO_3$ enhances the simulant response. Sample Z1 observed to be more sensitive and selective to 2-CEES than the other two simulants as shown in figure 5(b).

C. Selectivity and speed of response of modified and unmodified sensors

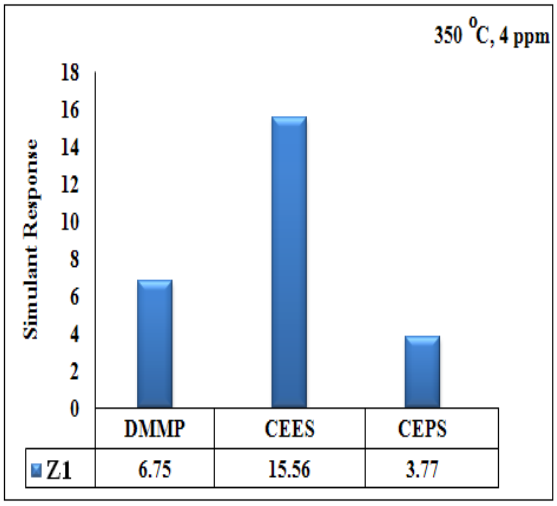

Figure 6(a). Selectivity profile of Z1

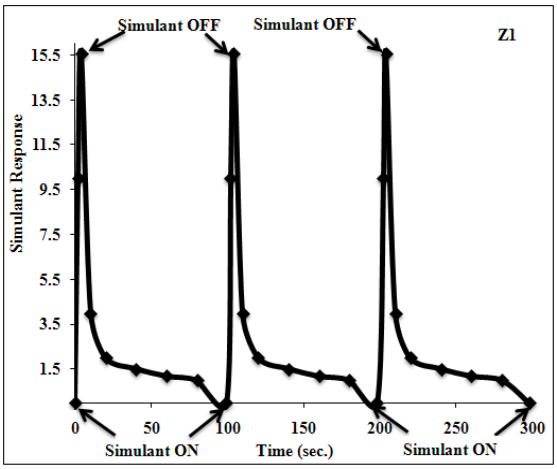

Figure 6(b). Response and recovery profile of Z1.

Figure 6 (a) shows the selectivity profile of sample Z1 for 2-CEES (4 ppm) at 350 °C. The dynamic response transients are shown in figure 6 (b). The response time of Z1 to 2-CEES was observed to be 4 sec. While the recovery time to of Z1 to 2-CEES was recorded as 100 sec.

V. DISCUSSION

The sensing mechanism is based on the effect of surface reactions of gas species on electron/hole concentration on the conduction band of the sensing material and creating a space charge layer, depending on whether it is an n- or p-type semiconductor. Such a depletion layer modifies the electrical conduction barrier at the grain boundaries. The bulk conductivity of the sensing material is the average of resistivity of bulk particles and grain boundaries. In microcrystalline materials the depth of the space charge layer is negligible compared to the grain diameter. In nanocrystalline materials, however, the depth of the space charge layer could be comparable to the

grain radius and the whole grain could be considered as a depleted layer. The electrical conduction is therefore controlled by the whole grain conductivity and the material becomes sensitive for very small gas concentrations in the surrounding atmosphere. This sensing mechanism relies on the fact that the electrical characteristics of materials depend on the amount of chemisorbed molecules. In air, the surface of a semiconducting material is covered with adsorbed oxygen layer. The process involves as shown in equations (1) and (2), physisorption of oxygen molecules in air, which then capture electrons from the near-surface region of the semiconductor[38]:

$$1/2\ O_2(g) \rightleftharpoons O(ads)$$

$$O(ads) + 2e \rightleftharpoons O^{2-}(ads)$$

The well accepted sensing mechanism for n-type semiconductor sensors involves three-step process i.e. an adsorption-oxidation-desorption process.

An ion radius of Zn^{2+} (0.073 nm) has similar to that of Sn^{4+} (0.071 nm) and smaller than Cd^{2+} (0.095 nm), so that it can be incorporated into the $CdSnO_3$ lattice easily by substituting for Sn^{4+} or Cd^{2+}. Zn as dopant results in surface modification and the formation of more oxygen vacancies, which can facilitate the enhancement of gas-sensing properties. It may be due to an ability of Zn ion to substitute Sn/Cd ions easily.It may be because of smaller ionic radius of Zn^{2+} (0.073 nm) than Cd^{2+} (0.095 nm) and close to Sn^{4+} (0.071 nm) [39-41].

The resistance of the film is very high when oxygen ions are adsorbed on heated Zn doped $CdSnO_3$ (sample Z1) surface at higher temperatures above 300 ^{0}C due to abstraction of surface electrons. The exposed 2-$ClCH_2CH_2SCH_2CH_3$ (2-CEES), would be first divided into the $\bullet SCH_2CH_3$ and $ClCH_2CH_2\bullet$ radicals as eq. (3). Through both chorine and sulfur moieties (which have unpaired electrons), these radicals would try to adsorb onto the film onto Lewis acid sites (i.e. metal ions). The radicals would act as a Lewis base (electron donors) and could interact with Lewis acid sites (i.e. metal ion) in the process of adsorption. Due to oxidation, the byproducts like CO_2, Cl_2, H_2O, and SO_2 would be released and electron would return back to metal oxide surface shown in eq (4) and (5). The process may be represented in scheme [42].

Decomposition of 2-chloroethyl ethyl sulphide (2-CEES)

$$2\text{-CEES} \longrightarrow ClCH_2CH_2^{\bullet}{}^{\bullet}SCH_2CH_3 \quad (3)$$

Oxidation of chloroethylene and return of electrons back to the film

$$2\ CH_2CH_2Cl + 8\ O^- \longrightarrow 2CO_2 + Cl_2 + 4\ H_2O + 8\ e^- \quad (4)$$

Oxidation of ethylsulphide and return of electrons back to the film

$$2\ CH_3CH_2S + 13\ O^- \longrightarrow 2\ SO_2 + 5\ H_2O + 2\ CO_2 + 13\ e^- \quad (5)$$

Thus, in whole process of adsorption, dissociation and oxidation, electrons are returned back to material and film resistance is increased. This process is therefore for detection of exposed CEES.

VI. CONCLUSIONS

Pure and Zn doped $CdsnO_3$ thin films, prepared using a simple spray pyrolysis technique, were observed to be nanostructured in nature. The particle size of the films was observed to be below 10 nm. Due to nanocrystillinity and Zn doping, the $CdSnO_3$ sensor showed good response to 2-CEES at an operating temperature 350 ^{o}C as compared to pure $CdSnO_3$ sensor. The sensor responded rapidly to 4 ppm of 2-CEES (response time 4 sec). The recovery time was 100 sec. The Zn doped nanostructured $CdSnO_3$ thin films prepared by using spray pyrolysis technique is a promising sensor candidate for the detection of CWA simulants.

ACKNOWLEDGEMENTS

The authors are thankful to the Defence Research & Development Establishment (DRDE), Gwalior, Defence Research Development Organization (DRDO), Government of India, New Delhi for providing financial support. The authors are also thankful to the Head, Department of Physics and Principal, Pratap College, Amalner for providing laboratory facilities for this work.

REFERENCES

[1] Park J and Lee J 2009 *Sens Actuators B* 136 151.
[2] Kapse V, Ghosh S, Chaudhari G, Raghuwanshi F and Gulwade D 2009 *Vacuum* 83 346.
[3] Sarala Devi G, Manorama S and Rao VJ 1995 *Sens Actuators B* 28 31.
[4] Jimenez I, Arbiol J, Dezanneau G, Cornet A and Morante JR 2003 *Sens Actuators B* 93 475.
[5] Zhua BL, Xie CS, Wu J, Zeng DW, Wang AH and Zhao XZ 2006 *Mater Chem Phys* 96 459.
[6] Chaudhari GN, Bende AM, Bodade AB, Patil SS and Sapkal VS 2006 *Sens Actuators B* 115 297.
[7] Kugishima M, Shimanoe K and Yamazoe N 2006 *Sens Actuators B* 118 171.
[8] Berger F, Brunol E, Planade R, Chambaudet A 2003 *Thin Solid Films* 436 1.
[9] Tomchenko A, Harmer G and Marquis B 2005 *Sens Actuators B* 108 41.
[10] Brunol E, Berger F, Fromm M and Planade R 2006 *Sens Actuators B* 120 35.

[11] Kanu A, Haigh P and Hill H 2005 *Analytica Chimica Acta* 553 148.
[12] Kim D, Gweon B, Moon S and Choe W 2009 *Curr App Phys* 9 1093.
[13] Wang Y, Zhou Z, Yang Z, Chen X, Xu D and Zhang Y 2009 *Nanotechnology* 20 345502.
[14] Wilson DM, Dunman K, Roppel T and Kalim R 2000 *Sens Actuators B* 62 199.
[15] Gaidi M, Chenevier B and Labeau M. 2000 *Sens Actuators B* 62 43.
[16] Wada K and Egashira M 2000 *Sens Actuators B* 62 211.
[17] Cadena G, Riu J and Rius F 2007*Analyst* 132 1083.
[18] Ghasdi M and Alamdari H 2010 *Sens Actuators B* 148 478.
[19] Shannon R, Gillson J and Bouchard R 1977 *J. Phys. Chem. Solids* 38 877.
[20] Cardile C, Meinhold R, MacKenzie K 1987 *J. Phys. Chem. Solids* 48 881.
[21] Chu X and Cheng Z 2004 *Sens. Actuators B* 98 215 .
[22] Sharma Y, Sharma N, Subba Rao G and Chowdari B 2009 *J Power Source* 192 627.
[23] Natu G and Wu Y 2010 *J Phys Chem C* 114 6802.
[24] X Jia, Fan H, Lou X and Xu 2009 *J Appl Phys A* 94 837.
[25] Tang Y, Jiang Y, Jia Z, Li B, Luo L and Xu L 2006 *Inorg Chem* 45 10774.
[26] Zhang T, Shen Y, Zhang R and Liu X 1996 *Mater Lett* 27 161.
[27] Haacke G, Mealmaker W and Siegel L 1978 *Thin Solid Films* 55 67.
[28] Ali H, Mohamedy H, Wakkad M, and Hasaneen M 2009 *Jap J App Phy* 48 041101.
[29] Prajapati C, Pandey S and SahayP 2011 *Physica B* 406 2684.
[30] Mardare D, Iacomi F, Cornei N, Girtan M and Luca D 2010 *Thin Solid Films* 518 4586.
[31] Bai S, Tong Z, Li D, Huang X, Luo R and Chen A 2007 *Sci in China Series E: Tech Sci* 50 18.
[32] Korotcenkov G, Boris I , Cornet A , Rodriguez J , Cirera A , Golovanov V, Lychkovsky Y and Karkotsky G 2007 Sens Actuators B 120 657.
[33] Tan R, Guo Y, Zhao J, L, Xu T and Song W 2011 *Trans. Nonferrous Met. Soc. China* 21 1568.
[34] Bartelt-Hunt S, Knappe D and Barlaz M 2008 *Criti Rev Environ Sci Techno* 38 112.
[35] Patil L A, Shinde M D, Bari A R, Deo V V, Patil D M and Kaushik M P 2011 *Sens Actuators B* 155 174.
[36] Wang D, Hu P, Xu J and Dong X and Pan Q 2009 *Sens Actuators B* 140 383.
[37] Faglia G, Comini E, Sberveglieri G, Rella R, Siciliano P and Vasanelli L 1998 *Sens Actuators B* 53 69.
[38] Gaskov M and Rumyantseva M 2000 *Inorg Mater* 36 293.
[39] Zhang G and Liu M 2000 *Sens Actuators B* 69 144.
[40] Neri G, Bonavita, Galvagno S, Li X, Galatsis K and Wlodarski W 2003 *IEEE SENS J* 3 195.
[41] Tian S, Gao Y, Zeng D and Xie C 2012 *J Am Ceram Soc* 95 436.
[42] Martyanov and Klabunde K 2003 *Environ. Sci. Technol* 37 3448.

PRATIBHA: INTERNATIONAL JOURNAL OF SCIENCE, SPIRITUALITY, BUSINESS AND TECHNOLOGY (IJSSBT), Vol. 1, No.1, March 2012
ISSN (Print) 2277—7261

Discrimination of Capacitor Switching Transients Using Wavelet

M.A.Beg[1], *Dr.M.K.Khedkar*[2], *Dr.G.M.Dhole*[3]
[1,3] Shri Sant Gajanan Maharaj College of Engineering, Shegaon
[2]Vice Chancellor, Sant Gadege Baba Amravati University.

Abstract: Switchable shunt capacitor banks are in extensive use to improve loading of the lines as well as to support system voltages. As these capacitor banks are frequently switched in and out of duty, energization and de-energization transients are produced and raise concern. These are the most common transient events present in power systems. This paper presents a method to distinguish between transients arising out of isolated capacitor switching and back-to-back capacitor switching. The DWT (Discrete Wavelet Transform) of modal voltage signal is used to extract distinguishing features from the voltage waveform of these events.

Keywords: Transients, Discrete Wavelet Transform (DWT), Multi Resolution Analysis (MRA), power quality (PQ).

I. INTRODUCTION

Due to their widespread applications, capacitor switching transients are the most common transient events on the power system, second only to voltage sag disturbances. Capacitor switching operations are frequently correlated with problems such as nuisance tripping of adjustable speed drives, process controls, and any load that cannot tolerate subcycle overvoltage transients. Unfortunately, most utilities have very limited resources to identify these problems and correlate them with the capacitor switching operations.

Switching of transmission capacitor banks may cause high phase to phase voltages on transformers and the magnification of transient at consumer end distribution capacitor. Problems are common in plants with capacitor and dc drive systems. The advent of pulse width –modulated (PWM) inverters created a whole new concern for capacitor switching

The application of shunt capacitors can lead to following additional side effects:

1) Bring about severe harmonic distortion, and resonance with load –generated harmonics;
2) Increase in the transient inrush current of power transformer in the system, create overvoltage, and prolong its decay rate;
3) Capacitor themselves can be stressed due to switching transient;
4) Increase the duty on switching devices , which may be stressed beyond the specified ratings in American National Standards Institute (ANSI)/IEEE standards;
5) Discharge into an external fault , and produce damaging over voltages across current transformer (CT) secondary terminals; and
6) Impact sensitive loads, i.e. drive system, and bring about the shut down.

The wavelet transform (WT) can be used to detect PQ problems and identify their occurrences in terms of time, generating data in both time and frequency domains, via the multi resolution analysis (MRA). These data will also be crucial to the classification of these events, as unique features of the various types of disturbance can be identified in the data emerging from the different levels of resolution, available in the MRA. The results obtained may be dealt with by a variety of techniques, including artificial neural networks (ANNs) in order to classify them.

Parsons [1] investigated the disturbance energy flow during the transient period and the polarity of the initial peak of the disturbance power to find out the relative but not the exact location of the switched capacitor bank. Sochuliakova [2] presented an analytical expression of the position of a switched capacitor as a function of transient frequency. Kim [3] applied a backward Kalman filter to find the location of a switched capacitor bank by estimating the voltage rise of capacitor bank. Unfortunately, this solution is also impractical to implement because it is based on the assumption that an exact power system dynamic model exists.

T. E Grebe presents power quality issues arising out of application of utility capacitor banks, such as capacitor switching transients and power system harmonics in,[4]. Makram et al in [5] described a frequency domain based approach for the analysis of shunt capacitor switching transients in the presence of harmonic sources, unbalanced feeder configuration, and combinations of single- and three-phase loads. Chang et al analyzed the effect of transients arising due to utility capacitor switching, on mass rapid transit(MRT),using

EMTP simulations considering ,size ,location, and switching instant, in [6].In this paper a single modal voltage signal is generated by combining all the three phase voltages. This modal signal is than decomposed using DWT up to five detail levels. The spectral energy density of the fifth detail level coefficients is used to discriminate between isolated and back to back capacitor switching events. This paper is organized as follows. Wavelet transform is briefly discussed in section I. Features for discrimination is presented in section II. Finally the conclusion is presented in section III.

II. WAVELET TRANSFORM AND MULTI RESOLUTION ANALYSIS

A wavelet is a short-term duration wave. These functions have been proposed in connection with the analysis of signals - primarily *transients* - in a wide range of applications. The basic concept of wavelet analysis is the use of a wavelet as a kernel function in integral transforms and in series expansions much like the sinusoid is used in Fourier analysis or the Walsh functions in Walsh analysis. Unlike Fourier analysis which uses one basis function, wavelet analysis relies on wavelets of a rather wide functional form. The basis wavelet is termed a *mother wavelet.* An informal statement of conditions for a function to be a wavelet are that the function:

- Must be oscillatory.
- Must decay quickly to zero (can only be non-zero for a short period of the wavelet function).
- must integrate to zero (i.e., the dc frequency component is zero)

In most cases, a band pass type signal (limited in time and frequency) is admissible. These conditions allow the wavelet transform to translate a time-domain function into a representation that is localized in both time (space) and frequency (scale). The term t*ime-frequency* is used to describe this type of multi resolution analysis.

Wavelet transform expands a signal in terms of a wavelet, generated using translation and dilation of a fixed wavelet function called the ‘‘mother wavelet”. A mother wavelet is defined as

$$\Psi_{j,k}(t) = 2^{-j/2}\Psi(2^{-j}t-k) \qquad (1)$$

Wavelets analyze any signal by using an approach called the multi resolution analysis (MRA), i.e., it analyzes the signal at different frequencies with different resolutions. MRA is designed to give good time resolution and poor frequency resolution at high frequencies and good frequency resolution and poor time resolution at low frequencies. Discrete wavelet transform (DWT) can be implemented using a tree-structured filter bank. An input signal x[n] is decomposed as

$$y_{high}[k] = \sum_n x[n] \cdot g[2k-n] \qquad (2)$$

$$y_{low}[k] = \sum_n x[n] \cdot h[2k-n] \qquad (3)$$

Where, $y_{high}[k]$ and $y_{low}[k]$ are the outputs of the high pass and low pass filter at a given level, after sub-sampling by 2. Here, g[n] is a high pass filter; h[n]is a low pass filter.

The selection of the mother wavelet depends on the application.

In this paper Daubeschies, with four filter coefficients (db4) has been used.db4 is very well suited to analyze power system transients.

III. FEATURE FOR DISCRIMINATION

An existing 132 kv transmission network of state transmission company has been simulated in PSCAD-EMTDC and analysis is done using wavelet tool box in MATLAB.

A modal voltage signal-

$$\boldsymbol{E}_m = \mathrm{M}\, \mathrm{E}^{abc} \qquad (4)$$

Where $\mathrm{E}^{abc} = [\, \mathrm{E}_a \;\mathrm{E}_b \;\mathrm{E}_c \,]^{\mathrm{T}}$

E_m is modal voltage signal ,E_a, E_b, E_c are three phase voltages and M a column vector of modal coefficient having 1x3 dimensions, has been used in this method.

MRA of wavelet transform of modal signal provides the following information –

$$A_n, d_1, d_2, .., d_i, .., d_n = DWT\{E_m\} \qquad (5)$$

Where, An is the set of approximate wavelet coefficients at level n.

d1, d2… dn is the set of detailed coefficients of wavelet transform at first, second…n^{th} decomposition level. Fig.1 and 2 shows the MRA wavelet decomposition of modal voltage signal of (4) for isolated and back to back capacitor switching. The top figure is the modal voltage signal,a_5 represent the approximate coefficients of the fifth level and d_1 to d_5 are the detail coefficients. Horizontal axis is time in seconds. Close examination of these provides no

distinguishing features between these events, except changes in magnitudes of coefficients. However, microscopic inspection of detailed level 5 coefficients provides some hope for distinguishing feature extraction.

Let 'i' be the level where possible discrimination is found (in this case fifth level) and corresponding wavelet coefficients are denoted by 'd_i'. The spectral energy density of d_i coefficients for level 5 can be calculated using

$$S_{xx}(n) = d_i^2(n) \quad (6)$$

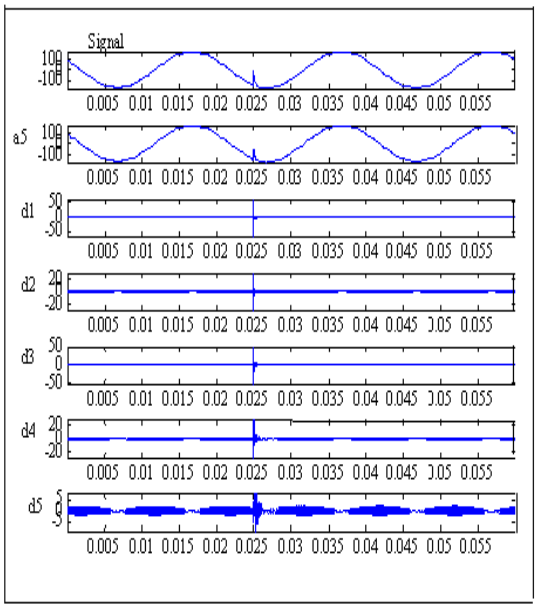

Figure 1 Wavelet decomposition of isolated capacitor switching transient

Energy contained in the detail coefficients of DWT has effectively been used in the past for the characterization of power quality disturbances. However it is observed that these methods do not always work, particularly when analyzing voltage signals. Hence it is necessary to map the energy into another domain to extract distinguishing features.

Therefore, the spectral energy density $S_{xx}(n)$ of d_i coefficients is mapped as follows-

$$S_{xx}(n) \rightarrow (0,1] \quad (7)$$

using the following membership function-

$$\mu_A(n) = \frac{1}{1+S_{xx}(n)} \quad (8)$$

compliment of (8) can be obtained from (9)

$$\overline{\mu_A(n)} = 1 - \frac{1}{1+S_{xx}(n)} \quad (9)$$

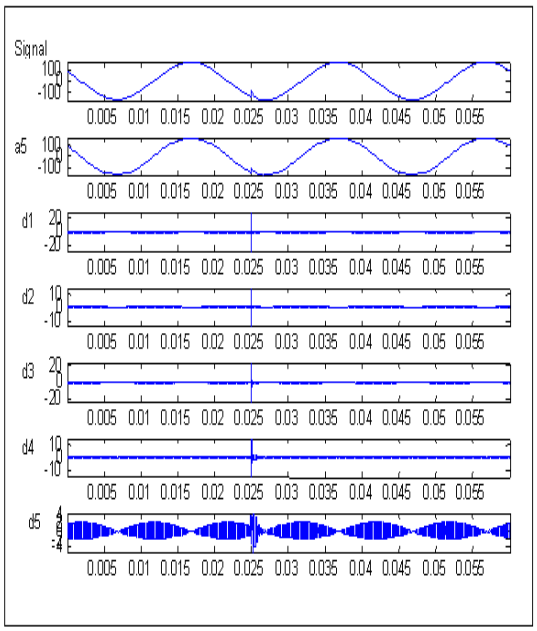

Figure 2 Wavelet decomposition of back to back capacitor switching transient

Fig. 3 provides the comparative graph of spectral energy density for level 5 (i.e. d5) coefficients for these two cases. Variation of spectral energy density follows the same pattern for dominant coefficients up to certain duration of time, but difference is observed in transient decay time. Back to back capacitor switching transients decays faster than isolated case. Smaller magnitude oscillations are observed in isolated switching case (marked with rectangle in Fig.3) which is a distinct feature.

Equation (9) provides discrete sequence where low magnitude long duration transients acquire higher membership than the high magnitude transients. Hence, low magnitude long duration transients which are not easy to detect directly from the wavelet coefficients are clearly visible in mapped domain, and are shown in Fig. 4 marked with rectangles. Hence isolated capacitor switching can be discriminated from back to back capacitor switching.

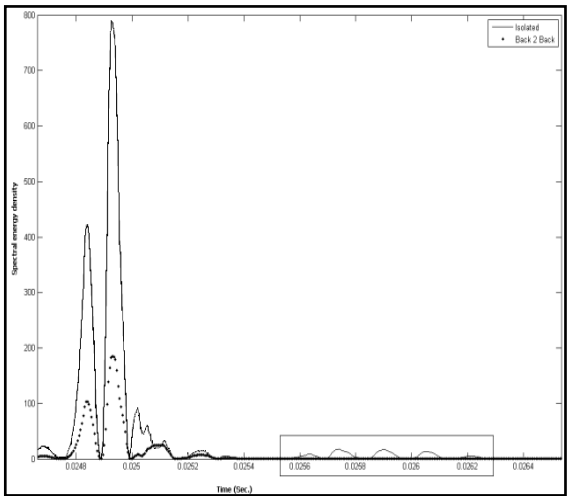

Figure 3 Spectral energy density plot for isolated and back to back capacitor switching

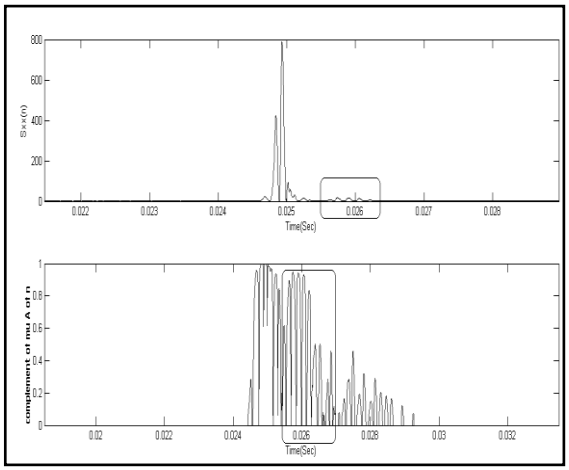

Figure 4 Feature extraction

IV. Conclusion

Distinguishing feature for identification of isolated capacitor switching and back to back capacitor switching is extracted in this paper using wavelet analysis. Wavelet is capable of extracting low frequency as well high frequency components from the power system transients and hence it is superior to Fourier analysis.

REFERENCES:

1. C. Parsons, W. M. Grady, E. J. Powers, and J. C. Soward, "A direction finder for power quality disturbances based upon disturbance power and energy," *IEEE Trans. Power Del.*, vol. 15, no. 3, pp. 1081–1085, Jul. 2000.
2. D. Sochuliakova, D. Niebur, C. Nwankpa, R. Fischl, and D. Richardson, "Identification of capacitor position in a radial system,"*IEEE Trans. Power Del.*, vol. 14, no. 4, pp. 1368–1373, Oct. 1999.
3. J. S. Kim, W. M. Grady, A. Arapostathis, J. C. Soward, and S. C. Bhatt, "A time domain procedure for locating switched capacitors in power distribution systems," *IEEE Trans. Power Del.*, vol. 17, no. 4,pp. 1044–1049, Oct. 2002 }.
4. T.E. Grebe, "Application of Distribution system capacitor banks and their impacts on power quality", IEEE transactions on industry applications,vol..32, No.3, pp.714-719 May/June1996.
5. E.B.Makram, et al. "Transient analysis of capacitor switching in unbalanced distribution system with harmonic distortion", Electric power components and systems, vol...17, issue 2, pp.75-92,1989.
6. C.S.Chang, et al. "Determination of worst case capacitor switching overvoltage of MRT system using genetic algorithm", Electric power components and systems, vol.27, issue 11, pp. 1161-1170, Oct 1999}.

PRATIBHA: INTERNATIONAL JOURNAL OF SCIENCE, SPIRITUALITY, BUSINESS AND TECHNOLOGY (IJSSBT), Vol. 1, No.1, March 2012
ISSN (Print) 2277—7261

Study of Profitability and Break-Even Analysis For Glycolytic Depolymerization Of Poly (Ethylene Terephthalate) (PET) Waste During Chemical Recycling Of Value Added Monomeric Products

Dr. V.R. Diware[1], A. S. Goje[2], Dr. S. Mishra[3]

[1]SSBT's College of Engineering and Technology, Bambhori, Jalgaon, M.S., (INDIA).
[2]G.H.Raisoni College of engineering and Management, Ahmednagar, M. S., India.
[3] Department of Chemical Technology, North Maharashtra University, Jalgaon, M.S., India.
E-mail: vrdiware65@rediffmail.com[1], asgoje@rediffmail.com[2], profsm@rediffmail.com[3]

ABSTRACT: Cost estimation, profitability and break-even analysis for glycol tic depolymerization of poly (ethylene terephthalate) (pet) waste was carried out using a batch reactor. different costs were determined. obtained data was used to decide the feasibility of the process technology for its commercialization. the break-even point was estimated for the process that showed much more adequate return on the investment, which has an industrial significance.

Key words: poly (ethylene terephthalate) depolymerisation, material balance, cost, profit, return, break-even point

I. INTRODUCTION

The growing interest in pet waste recycling is due to the widespread use for various domestic and engineering applications. Ecological and economical considerations advocate the introduction of wide-scale recycling. Market is increasing rapidly and will further be boosted by current developments of pet grades, and produces high waste pet materials after use or during pet synthesis. Hence, among different methods of pet waste recycling, chemical recycling has recently been paid much more attention. [1–2] various researchers [3–12] has studied depolymerization of pet. application of these methods depends on end use of recovered products. appreciable amounts of monomeric products were recovered during chemical recycling of pet. [3–8] results of their studies did not report the feasibility of the method of recovery of monomers for commercialization. [1–12] hence, there were no required data available about cost estimation and profitability analysis that are essential for process selection during plant design for a new product. In absence of a reliable and sufficient necessary data of profitability and break-even analysis, reaction and mass transport engineers are forced to scale-up the established reactors and or separating equipments in economically undesirable small steps. Additionally, the available reaction and or mass transport data are insufficient for designing new reactor and or separation equipment concepts with justifiable expenditure. for process selection as well as process development for optimal plant design, the knowledge of cost estimation, profitability and break-even analysis is required. hence, this study is undertaken to fulfill the industrial requirements for commercialization. however, literature does not show these types of study for glycol tic depolymerization of pet at optimal conditions. in this work cost estimation, profitability and the break-even analysis are studied for glycolytic depolymerization of pet waste at various optimal reaction conditions.

A. Theory

Although the technical parameters are influencing the selection and design of a given type of process may be unique, cost is usually only parameter relevant to all processes. Cost is often the parameter used to select the optimum process from the alternatives available. Economical information plays an important role in setting many states of the process. However, cost analysis is used to determine the minimum economic way of achieving the desired goal. An understanding of the economics involved in the process is important in making decision at both the engineering and management levels. Every engineer should be able to execute an economical evaluation of a proposed project. If the project is not profitable, it should obviously not be pursued and the earlier such a project can be identified, the fever is the resources that will be wasted. Before the cost of a process can be evaluated, the factors contributing to the cost must be recognized. [13] An acceptable plant design must present a process that is capable of operating under conditions that will yield a

significant profit. Since net profit equals total income minus all expenses, it is essential that the chemical process engineer be aware of the different types of costs involved in manufacturing processes. Capital must be allocated for direct plant expenses, such as those for raw materials, labour, and equipment. Besides direct expenses, many other indirect expenses are incurred, and these must be included if a complete analysis of the total cost is to be obtained. Some examples of these indirect expenses are administrative salaries; product distribution costs, and costs for interplant communications.[13– 15] The selection of process using cost analysis is normally based on capital and operating cost. All equipment costs were reported [13] to be accurate to within 20 %. Variations in the total cost can be attributed to a number of variable factors such as cost of auxiliary equipment, new installation, local labour cost, engineering overhead, location and accessibility of plant site, and type of industry (installation work). [13]

A capital investment is required for any industrial process, and determination of the necessary investment is an important part of a plant design project. The total investment for any process consists of fixed capital investment for physical equipment and facilities in the plant alongwith working capital that must be available to pay salaries, keep raw materials and products on hand, and handle other special items requiring a direct cash outlay. Moreover, in an analysis of costs in industrial processes, capital investment costs, manufacturing costs, and general expenses including income taxes must be taken into consideration. [13, 14] The flow chart for the glycolytic depolymerization of PET using ethylene glycol (EG) was developed for complete recovery of monomers (Figure 9) [8] at various optimal process conditions. Based on the various information of glycolytic depolymerization process of PET, [8] the material balances were evaluated for raw materials as well as products.

In present study, costing of fixed capital investment was under taken by calculating initially the total equipment costs for the depolymerization process. Then using the percentage of purchased equipment costs the fixed capital investment was evaluated. Then total product cost and hence total expenses were calculated. Total annual income, gross profit, and net profit were computed. Finally, payback period, rate of return and break-even point analysis were computed.

II. EXPERIMENTAL

A. Material, Chemicals And Reagents

PET used was procured from Garaware Polyesters, Aurangabad, M.S., (INDIA). Here waste just mean materials left over after some products were made from raw material that was free from any additives / plasticizers. The other materials used were neutral water, methanol, HCl, CaO, sodium sulfate, ethylene glycol, zinc acetate, urea, etc., obtained from s. d. Fine Chemicals (INDIA). These chemicals were used as received without further purification.

B. Glycolysis of PET

Glycolysis reactions [8] were carried out in a 1 L four-necked batch reactor at various temperatures ranging from 100-220 ^{O} C at the interval of 10 ^{O}C and 1 atm pressure. Reactor was equipped with a thermometer and two reflux condensers. A stirrer was put in reactor to ensure proper mixing. Reaction was carried out by taking 10 g PET in 40 mL of ethylene glycol (EG) using glycolysis catalyst (i.e., 0.002 mol of zinc acetate) with 4 pieces of porcelain for different periods of time ranging from 30 to 150 min. Different particle sizes ranging from 50 to 512.5 µm of PET were taken for this reaction (separately). After completion of glycolysis reaction of PET, the batch reactor was removed from heating mantel and 50 mL of boiling neutral water was slowly introduced into reaction mixture. Whole reaction mixture was quickly filtered.

Unreacted PET was collected, washed with neutral water, dried in controlled oven at 95 ^{O}C until its constant weight that was recorded.

Remaining filtrate was methanolized (second step required in process) with additional catalyst (i.e., 0.002 mol of urea) for 30 min at 190 ^{O}C and 1 atm pressure. Reaction mixture was cooled in an ice-bath. White crystalline flakes of DMT were formed. It was filtered and washed with 50 mL of cooled neutral water in order to remove catalysts, and dried in a controlled oven at 95 ^{O}C until its constant weight, which was recorded.

From remaining liquid phase, EG was separated using salting-out method [2, 8] by introduction of sodium sulfate. Both monomeric products (DMT and EG) were analyzed qualitatively and quantitatively. Percent depolymerization of PET, yield of DMT and yield of EG were determined by gravimetry and defined in following ways.

A. Depolymerization of PET (%)

$$= \{(W_{PET,i} - W_{PET,R}) / W_{PET,i}\} \times 100 \quad (1).$$

Yield of DMT (%)

$$= \{m_{DMT,O} / m_{PET,i}\} \times 100 \quad (2).$$

Yield of EG (%)

$$= (m_{EG,O} / m_{PET,i}) \times 100 \quad (3).$$

Where $W_{PET,i}$ is initial weight of PET, $W_{PET,R}$ is weight of unreacted PET, $m_{DMT,O}$ is number of moles of DMT, $m_{EG,O}$ is number of moles of EG, and $m_{PET,i,}$ is initial number of moles of PET monomeric units.

Process Reaction For Glycolysis Of PET

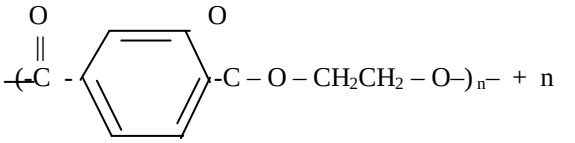

(PET)

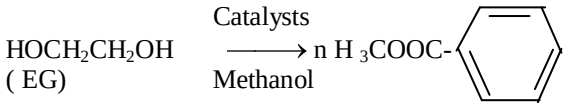

$$-COOCH_3 + n\ HOCH_2CH_2OH$$
(DMT) (EG)

Analyses Of Depolymerized Products (EG And DMT) Of PET

Liquid and solid products obtained from depolymerization of PET were analyzed [8] by determining their various physical properties (like melting point, boiling point, molecular weight, acid value, etc.) to confirm them.

Material Balance For Glycolytic Depolymerization Of PET:

Maximum PET Weight % loss = 98.78 %.
Molecular Weight of PET = 16703 g mol $^{-1}$.
Mol.Wt. of Dimethyl Terephthalate (DMT) = 194 g mol $^{-1}$.
Mol.Wt. of Ethylene Glycol (EG) = 62 g mol $^{-1}$.
Mol.Wt. of DMT + EG = 194 + 62 = 256 g mol $^{-1}$.
Mol.Wt. of DMT + EG – H_2O = 194 + 62 –18 = 256 – 18 = 238 g mol $^{-1}$.
From 238 = 1 Water molecule was liberated.
From 16703 = 70.2 Water molecule will liberate.
100 % Material = 10 g PET.
98.78 % Conversion of Material = 9.878 g PET.
16703 give 70.2 Water molecules.
9.878 g give 0.042 g Water molecules.
Total weight of products (DMT + EG) = 9.878 + 0.042 = 9.92 g.
In 256 g, EG is 62 g (Theoretical).
In 9.92 g, EG is 2.4025 g (Theoretical).
Wt. of DMT = 9.92- 2.4025 = 7.5175 g (Theoretical).
Wt. of EG = 2.3722 g (Experimental).
Wt. of DMT = 7.4213 g (Experimental).

Basis of calculation: Plant Production capacity of 76800 Kg DMT per Annum.

Raw materials required to produce 76800 Kg DMT:

PET = 103486 Kg.
EG = 413944 L.
CaO = 35000 Kg.
Neutral Water = 537600 L.
HCl = 19200 L.
Na_2SO_4 = 76800 Kg.
Z. A. (Zinc Acetate, Catalyst for glycolysis) = 5175 Kg.
Urea, Catalyst for methanolysis (second step required in process) = 1243 Kg.
Methanol = 206972 L.

Monomeric Products Produced That Were Recovered:

DMT = 76800 Kg.
EG = 24549 L.

Costs Estimation:

Total Equipment Costs:

Sr. No.	***Equipment***	No.	Cost per equipment (Rs)	Cost (Rs)
1	Reactor	1	82000	82000
2	Evaporator	1	78000	78000
3	Filter	2	51000	10200
4	Dryer	1	72000	72000
5	Centrifugal Pump	3	25000	75000
6	Vacuum Pump	1	42000	42000
7	Rectangular Tank	10	22000	220000
Total Equipment Costs (TEC):				671000

Capital Investment:

Fixed Capital Investment:
Direct Costs:

Sr. No.	***Item***	% TEC	Cost (Rs)
1	Purchased Equipment	100	671000
2	Purchased Equipment Installation	39	261690
3	Instrumentation & Controls (Installed)	13	87230
4	Piping (Installed)	31	208010
5	Electrical (Installed)	10	67100
6	Building (Including Services)	29	194590

7	Yard Improvements	10	67100
8	Service Facilities (Installed)	55	369050
9	Land	6	40260
	Total Direct Cost (TDC)		Rs 1966030

Indirect Costs:

Sr. No.	***Item***	% TEC	Cost (Rs)
1	Engineering And Supervision	32	214720
2	Construction Expenses	34	228140
3 Total Indirect Cost: T I D C:			Rs 442860

Total Direct Costs And Indirect Costs:
Rs 2408890

Other Charges:

Sr. No.	***Item***	% TD&IDC	Cost (Rs)
1	Contractors Fees	5	120445
2	Contingency	10	240889

Fixed Capital Investment = Rs 2770224.
Working Capital Investment = 74 % TEC = Rs 496540.
Total Capital Investment = Rs 3266764.
Total Product Cost:
Manufacturing Cost:
Direct Production Costs: Raw Materials Cost:

Sr. No.	Raw Material	Raw Material (Kg / Yr)	Cost (Rs / Kg)	Cost (Rs / Yr)
1	PET	103486	22	2276692
2	EG	413944	200	82788800
3	CaO	35000	70	2450000
4	Neutral Water	537600	5	2688000
5	HCl	19200	40	768000
6	Na_2SO_4	76800	54	4147200
7	Zinc Acetate	5175	200	1035000
8	Urea	1243	60	74580
9	Methanol	206972	55	41383460

Total Raw Materials Costs = Rs 107611732.

Operating Labour Costs:

Sr. No.	Post	**1) No.of Posts**	Pay (Rs/ Month)	Pay (Rs /yr)
1		1	12000	144 000
2	Plant Manager	1	6000	720 00
3	Shift Engineer	3	4000	144 000
4	Shift Supervisor	3	3000	108 000
5	Operator	15	2500	450 000
6	Skilled Labour	10	2000	240 000
7	Unskilled Labour	30	1500	540 000

Total Operating Labour Costs = Rs 1698000.
Office Materials And Clerical Expenses = 10 % TOLC = Rs 169800.
Utilities = 75 % TOLC = Rs 1273500.
Maintenance And Repairs = 2 % FCI = Rs 55405.
Operating Supplies = 10 % M & R = Rs 5541.
Laboratory Charges = 10 % TOLC = Rs 169800.
Patents And Royalties = 10 % TOLC = Rs 169800.
Fixed Charges:
Depreciation = 10 % FCI + 2 % Building Value = 277023 + 3892 = 280915.
Local Taxes = 1 % FCI = Rs 27703.
Insurance = 0.4 % FCI = Rs 11080.
Plant Overhead = 50 % TOLC = Rs 849000.
General Expenses:
Administrative Costs = 15 % TOLC = Rs 849000.
Distribution And Selling Costs = 15 % TOLC = Rs 254700.
Research And Development Costs = 15 % TOLC = Rs 254700.
Financing (Interest) Costs = 10 % FCI = Rs 277023.
Total Product Costs = Manufacturing Costs + General Expenses.
Total Product Costs = Rs 113957699.
Total Expenses = Total Capital Investment + Total Product Costs
Total Expenses = 3266764 + 113957699 = Rs 117224463.
Profitability Analysis:
Total Product Annual Income:

Sr. No.	**1) Prod- 2) ucts**	Production (Kg/Yr)	Cost (Rs/Kg)	Income (Rs/Yr)
1	**3) DMT**	76800	1500	115200000
2	EG	24549	200	4909800

Total Product Annual Income = Rs 120109800.
B. Gross Profit = TPAI – Total Expenses = 120109800 – 117224463
= Rs 2885337.
C. Net Profit = Gross Profit – Income Tax. = Gross Profit – 40 % Gross Profit
= 60 % Gross Profit = Rs 1731202.

Payback Period = (FCI / NP) = (2770224 / 1731202) = 1.6 Yrs = 19.2 Months.
Rate of Return = (NP / FCI) x 100 = (1731202 / 2770224) x 100 = 62.5 %.

Break Even Analysis:

Break Even Point (Units) = [FCI / (Selling Price per Unit - Variable Cost per Unit)].
= [2770224 / (1500 – 1350)] = 18468.16 Kg.
Break Even Point (as a % capacity) = [BEP (units) / Total capacity of Product] x 100.
= (18468.16 / 76800) x 100. = 24 %.

Conclusion

Cost estimation, profitability and break-even analysis for glycolytic depolymerization of poly (ethylene terephthalate) (PET) waste was revealed that the rate of return on investment and payback period is pretty good that has an industrial significance. Various cost analysis data is used to decide the feasibility of the process for industrial application. The break-even point (as a % capacity), payback period and rate of return were estimated that were recorded as 24 %, 1.6 years and 62.5 % respectively for the process. Payback period, rate of return and break-even point values indicates that the much more excellent viability of the process of glycolytic depolymerization of PET at various optimal conditions.

References

[1] Paszun, D.; Spychaj, T.; Nowaczek, N. Chemical recycling of Poly (Ethylene Terephthalate) -PET. *Ekoplast*. 1, 259, 1993 (in Polish).
[2] Paszun, D.; Spychaj, T. Chemical recycling of Poly (Ethylene Terephthalate). *Ind. Eng. Chem. Res.* 36, 1373, 1997.
[3] Mishra, S.; Goje, A. S.; Zope, V. S. Proceedings: International Conference On Plastic Waste Mangt and Environment., 163, New Delhi, March 2001
[4] S. Mishra, V.S.Zope, A.S.Goje. Kinetic and Thermodynamic studies of Depolymerization of Poly (Ethylene Terephthalate) Waste By Saponification Reactions. *Polymer International*.51 (12), 1310, 2002.
[5] S. Mishra, A.S.Goje. Kinetics of Glycolysis of Poly (Ethylene Terephthalate) Waste Powder At Moderate Pressure And Temperature. *J. Appl. Polym. Sci.* 87 (10), 1569, 2003.
[6] S. Mishra, A. S.Goje. Kinetic and Thermodynamic study of Methanolysis of Poly (Ethylene Terephthalate) Waste Powder. *Polymer International*. 52 (3), 337, 2003.
[7] S. Mishra, A.S.Goje, and V.S.Zope. Chemical Recycling, Kinetics and Thermodynamics of Poly (Ethylene Terephthalate (PET) Waste Powder by Nitric Acid Hydrolysis. *Polymer Reaction Engg.* 11 (1), 79, 2003.
[8] A.S.Goje, S. Mishra. Chemical Kinetics, Simulation and Thermodynamics of Glycolytic Depolymerization of Poly (Ethylene Terephthalate) Waste with Catalyst Optimization for Recycling of Value added Monomeric Products. *Macromolecular Materials and Engg*. 288 (4), 326-336, 2003.
[9] Chen, J. Y.; Ou, C. F.; Hu, Y. C.; Lin, C.C. Depolymerization of PET Resin Under Pressure. *J. Appl. Polym. Sci.* 42, 1501, 1991.
[10] Yoshioka, T.; Sato, T.; Okuwaki, A. J. Hydrolysis of Waste PET by NaOH at 150 ^{o}C for a Chemical Recycling. *J. Appl. Polym*. Sci.52, 1353, 1994.
[11] Ben-Zu, Wan., Chih-Yu, Kao., and Wu-Hsun, Cheng.; Kinetics of Depolymerization of PET in a Potassium Hydroxide Solution. *Ind. Eng. Chem. Res.* 40, 509, 2001.
[12] Oku, A.; Hu, L. C.; Yamade, E. Alkali Decomposition of PET with Sodium Hydroxide in Non-aqueous Ethylene Glycol: A Study on Recycling of TPA and EG. *J. Appl. Polym. Sci*. 63, 595, 1997.
[13] Maycock, J. C.; McKenna, J.D.; Theodore, L. *Hand book of Air Pollution Control Engg. And Technology*. Lewis Publishers, New York,p-277, 1995.
[14] Peter; M. S.; Timmerhaus, K.D. *Plant Design and Economics for Chemical Engineers*. McGraw-Hill Publication, Singapore, p 183, edn 1991.
[15] Vilbrandt, F, C.; Dryden, C, E. *Chemical Engineering Plant Design*. McGraw Hill, Kogakusa, Ltd, 4Th edn, p – 84, 1959.

PRATIBHA: INTERNATIONAL JOURNAL OF SCIENCE, SPIRITUALITY, BUSINESS AND TECHNOLOGY (IJSSBT), Vol. 1, No.1, March 2012
ISSN (Print) 2277—7261

Effect of Dot (Direct Observation Treatment) Therapy on Hepatic Enzymes and Calcium Level in Serum of T.B. Patients

S. S. Warke[1], G V Puranik[2], and Z. H. Khan[3]
[1,2]Department of Pathology, B.Y.L. Nair Ch. Hospital & T.N.Medical College, Mumbai-8 (India)
[3]Department of Biochemistry Shri Shivaji College, Akola-444001 (India.)
Emails: [1]shankarwarke@gmail.com, [2]puranikgv@gmail.com, [3]ziakhan7862@rediffmail.com

Abstract: In the present study, the Biochemical manifestations of liver toxicity caused by co-administration of anti-tuberculosis drugs, rifampicin (RIF), isoniazid (I NH), pyrazinamide (PZA) and Ethembutol (ETH) in TB patients were investigated. Significant alterations were observed in serum glutamate oxaloacetat transaminase (SGOT), Serum glutamate pyruvate transaminase (SGPT), Serum Alkaline phosphatase (ALP), Serum Acidic Phosphatase (ACP) its prostatic factor (APF) and serum calcium on 15th day of treatment. However all the checked parameters came to normal level (equal to control) on 6th months of treatment except SGOT and SGPT.

***Key words: Anti-tuberculosis drug, liver toxiocity, Hepatic Enzymes, DOT therapy*.**

I. INTRODUCTION

In developing countries Tuberculosis is still a major public health problem both in children as well as in adults [1]

In 1956 there were about 15 lakhs patients in India having tuberculosis infection. But now it is estimated that there are about 14 million T. B. patients in our country of whom about 3.5 million are infectious (sputum positive). About 2.2 million T. B. patients are added every year out of which 1 million are sputum positive. Five lakh people in India die due to tuberculosis every year. i.e. one patient with tuberculosis die every minute more than 1000 people every day [2].

There were about 28 thousand T.B. patient in Mumbai in 2008 survey [3].

To combat against such an increasing infectious disease in the country it is imperative that further intensive research is to be undertaken. Hence the present study is proposed to see the effect on Hepatic enzymes levels in T.B. patients undergoing treatment with antituberculosis drug like Rifampacin, Isoniazid, Pyrozinamide and Ethambutol.Most reported cases of hepatic dysfunction due to anti-TB drugs are reported to occur within the first 3 months of starting the treatment [4].Now a days T.B. Patients are subjected to DOTS (Direct Observation Treatment System) therapy thrice a week. It may have effect on liver as it is a main site of drug metabolism, Mc Neill L. *et.al.* [5], reported that In a community setting, we found a threefold increase in the risk of hepatotoxicity among patients receiving pyrazinamide/rifampin (13%) as compared to isoniazid (4%). The risk of severe hepatotoxcity requiring hospitalization was 5% (2 of 43 patients) in the pyrazinamide/rifampin group prior to the more intensive monitoring.

Kristic Buric *et.al.* [6], has also studied levels of serum transaminases in DOT therapy. Deck K.A. *et.al.* [7], have been reported side effects of rifampicin in tuberculosis patients. According to Schare L. Smith J.P. [8], a number of patients receiving antituberculous chemotherapy develop serum transaminase elevations unaccompanied by symptoms. However, the finding that these enzymes rises may be induced by INH alone has not been previously emphasized. Moreover, serum transaminase elevations and histologic evidence of hepatic damage has not been previously reported in asymptomatic subjects receiving isoniazid for chemoprophylaxis.

One set of the asymptomatic reaction in all cases occurred within 2 months of initiating INH. In general, the rise in enzymes appeared sooner in hospitalized patients, who had more frequent blood studies, than in the outpatient group, although early detection does not appear to account for all differences. Indications for interruption of INH based on SGOT and SGPT limits were not established while early experience was being accumulated on the tuberculosis in patients service. As a result, individual physician or patient concern generated by the chemical abnormalities prompted temporary interruption of INH in seven of the eight hospitalized reactors. In one of these cases SGOT was 600 and SGPT, 900 units before the drug was interrupted; whether or not these values represent the potential maximum severity of the reaction is unknown.

It has been found that such studies i.e. levels of liver enzymes with respect to duration have not been yet done. Hence the present study is proposed to see the effect on Hepatic enzymes levels in T.B. Patients undergoing treatment with antituberculosis drugs (INH, Isonizid, Rifanpacin and Ethembutal combinely).

II. MATERIALS AND METHODS

The study was conducted on out-door patients in one of the corporation Hospital, Nair Hospital and T. M. Medical College, Mumbai – 8.
100 Patients were examined in respiratory Medicine Unit. Patients of either sex between age group 15 to 60 year with pulmonary tuberculosis were studies for serum SGOT, SGPT, Alkaline Phosphatase and Acid Phosphatase with respect to duration of treatment.Diagnosis of Tuberculosis (TB) was based on detection of Acid Fast Bacilli (AFB) and direct smear examination by Ziehi Nelson staining and also on culture for AFB [9].
All above diagnostic examination were carried out in Department of Microbiology, Nair Hospital and T. N. Medical College along with chest X-ray in Radiology Department of the Hospital Diagnosis was confirmed clinically in OPD of the Hospital by senior physicians.

Patients were treated with antituberculosis drugs. All the drugs were given thrice a week through out for 6 months under the direct supervision of clinical staff. Patients treated with the following drugs :

1. Cap. Rifanpacin (RIF) on empty stomach 1 Cap. (450 mg).
2. Tab. Isonazid (INH) 2 Tab. (300 mg).
3. Tab. Ethanbutol (ETH) 2 Tab. (600 mg).
4. Tab. Pyrazinamide (PZA) 2 Tab. (750 mg).

All drugs were given for two months. After two months tablets ethanbutal and Tablet Pyrazinamide were ceased but treatment continued with Cap. Rifampacin and Tab. Isoniazid for a period of further four months.Blood samples of all patients were collected on zero day (before start of treatment), 15 days, 1 month, 2 month, 3 month, 4 month and 6 month of treatment period.Approval from Institutional Ethics committees for research work was obtained.

A. Sample Collection :

Various blood samples were collected in plain bulb and serum was separated.Serum AST (SGOT) and serum ALT (SGPT) enzymes were estimated by modified IFCC by kinetic method (10, 11, 12) by using Olympus AU 400 Auto Analyzer in Chemical Pathology Lab of Nair Hospital.Enzymatic Diethalamine Kinetic Method (13) was followed for ALP estimation by using same instrument.Acid Phosphatase was estimated by IFCC method modified from Kind and King Method (14).Serum calcium levels were estimated by cresolphthalein comilexone method (15) by using Auto Analyzer Olympus AU 400

III. PATIENTS SELECTION CRITERIA

A. Inclusion Criteria

1. Patients of either sex in the age group 18-60 years.
2. New cases of Pulmonary T.B. as diagnosed by using Revised National Tuberculosis Control Programme (RNTCP) diagnostic algorithum.

B. Exclusion Criteria

1. Retreatment cases of Pulmonary T.B. relapse, failure, treatment after defaulter with Cagetory II.
2. Sputum smear negative for pulmonary T.B.
3. Patients suffering from active liver disease.
4. Patients suffering from severe renal cardiac disease admitted in ICU of the Hospital.
5. Patients suffering from other associated pulmonary diseases.
6. Pregnant and lactating female.
7. Patients suffering from HIV

C. Selection of Control

1. Healthy 10 male / female volunteers in the age group of 15-60 years.
2. On the basis of following Lab investigations within the normal range;
   a) Hb / CBC, ES
   b) LFT and AST, ALT. S. Bilirubin
   c) BUN and Serum creatinin

IV. RESULT AND DISCUSSION

Table No. 1 Effect of Antituberculosis Drugs* on SGOT and SGPT in IU/Lit. in Serum of Patients with Respect to Duration of Treatment.

Duration of Treatment	SGOT	Percentage changes	SGPT	Percentage Changes
Control	20.66 ± 0.88 1	--	19.17 ± 0.94	--
Zero Days	34.80 ± 2.46 P < 0.001	+ 68.44	25.76 ± 3.40 Z = 1.88 P > 0.05	+ 34.37
15 Days	42.22 ± 4.93 P < 0.001	+ 104.35	27.91 ± 3.45 P < 0.01	+ 45.58
1 Month	29.95 ± 3.27 P < 0.001	+ 44.96	23.86 ± 2.89 1.57, P < 0.001	+ 24.46
2 Months	27.76 ± 2.45 P < 0.01	+ 34.36	28.43± 3.62 2.47, P < 0.05	+ 48.30
3 Months	31.53 ± 3.13 P < 0.001	+ 52.61	24.95 ± 2.51 2.15, P < 0.05	+ 30.15
4 Months	26.30 ± 2.01 P < 0.01	+ 27.29	25.02 ± 2.56 2.13, P < 0.05	+ 30.51
6 Months	29.64 ± 3.14 P < 0.001	+ 43.46	30.17 ± 5.02 Z = 2.2, P < 0.05	+ 57.38

Values are Mean ± SE (N = 100)
* (1) Cap. Rifanpacin (RIF) on empty stomach 1 Cap. (450 mg). (2) Tab. Isonazid (INH) 2 Tab. (300 mg). (3) Tab. Ethanbutol (ETH) 2 Tab. (600 mg). (4) Tab. Pyrazinamide (PZA) 2 Tab. (750 mg). For 2 Months Durgs 3 + 4 continued upto 6 months.
P < 0.001 Highly Significant, P < 0.01 More Significant,
P < 0.05 Significant, P > 0.05 Not Significant.

Table No. 2 Effect of Antituberculosis Drugs* on Alkaline phosphatase, Acid Phosphatase and Prostetic acid Phosphatase IU/Lit. In patients with Respect to Duration of Treatment.

Duration of Treatment	Alkaline Phosphatase	% change	Acid Phosphatase	% change	Protatic Acid Phosphatase	% change
Control	156.5 ± 3.06	--	1.806± 0.06	--	0.92 ± 0.04	--
Zero Days	279.14 ± 22.83 P < 0.001	+78.36	3.23 ± 0.25 P < 0.001	+78.8	1.28 ± 0.07 P < 0.001	+39.13
15 Days	285.63 ± 24.17 P < 0.001	+82.51	2.78± 0.24 P < 0.001	+53.9	1.71 ± 0.08 P < 0.001	+85.86
1 Month	240.16 ± 21.00 P < 0.001	+53.45	2.71± 0.17 P < 0.001	+50.0	1.04 ± 0.05 P < 0.05	+13.04
2 Months	232.50 ± 18.65 P < 0.001	+48.56	2.46± 0.15 P < 0.001	+36.2	0.92 ± 0.05 P > 0.05	0
3 Months	223.32 ±17.92 P < 0.001	+42.69	2.39± 0.13 P < 0.001	+32.2	0.96 ± 0.05 P > 0.05	+4.34
4 Months	192.52 ± 16.56 P < 0.05	+23.01	2.11 ± 0.07 P < 0.001	+16.8	0.99 ± 0.04 P > 0.05	+7.60
6 Months	186.15 ± 19.35 P > 0.05	+18.94	1.80 ± 0.06 P > 0.05	-1.0	0.92 ± 0.04 P > 0.05	0

Values are Mean ± SE (N = 100)
* (1) Cap. Rifanpacin (RIF) on empty stomach 1 Cap. (450 mg). (2) Tab. Isonazid (INH) 2 Tab. (300 mg). (3) Tab. Ethanbutol (ETH) 2 Tab. (600 mg). (4) Tab. Pyrazinamide (PZA) 2 Tab. (750 mg). For 2 Months Durgs 3 + 4 continued upto 6 months.

P < 0.001 Highly Significant, P < 0.01 More Significant,
P < 0.05 Significant, P > 0.05 Not Significant.

Table No. 3 Effect of antituberculosis drugs* on serum calcium in mg/dl in serum of patient with respect to duration of treatment.

Duration of Treatment	Serum calcium		Percentage change
Control	9.66 ± 0.10		
Zero Days	8.60 ± 0.10	P < 0.001	- 11
15 Days	8.71 ± 0.10	P < 0.001	- 10
1 Month	8.66 ± 0.10	P < 0.001	- 11
2 Months	8.49 ± 0.09	P < 0.001	- 13
3 Months	\8.39 ± 0.10	P < 0.001	- 14
4 Months	8.64 ± 0.14	P < 0.001	- 18
6 Months	8.49 ± 0.12	P < 0.001	- 13

Values are Mean ± SE (N = 100)
* (1) Cap. Rifanpacin (RIF) on empty stomach 1 Cap. (450 mg). (2) Tab. Isonazid (INH) 2 Tab. (300 mg). (3) Tab. Ethanbutol (ETH) 2 Tab. (600 mg). (4) Tab. Pyrazinamide (PZA) 2 Tab. (750 mg). For 2 Months Durgs 3 + 4 continued upto 6 months.
P < 0.001 Highly Significant, P < 0.01 More Significant,
P < 0.05 Significant, P > 0.05 Not Significant.

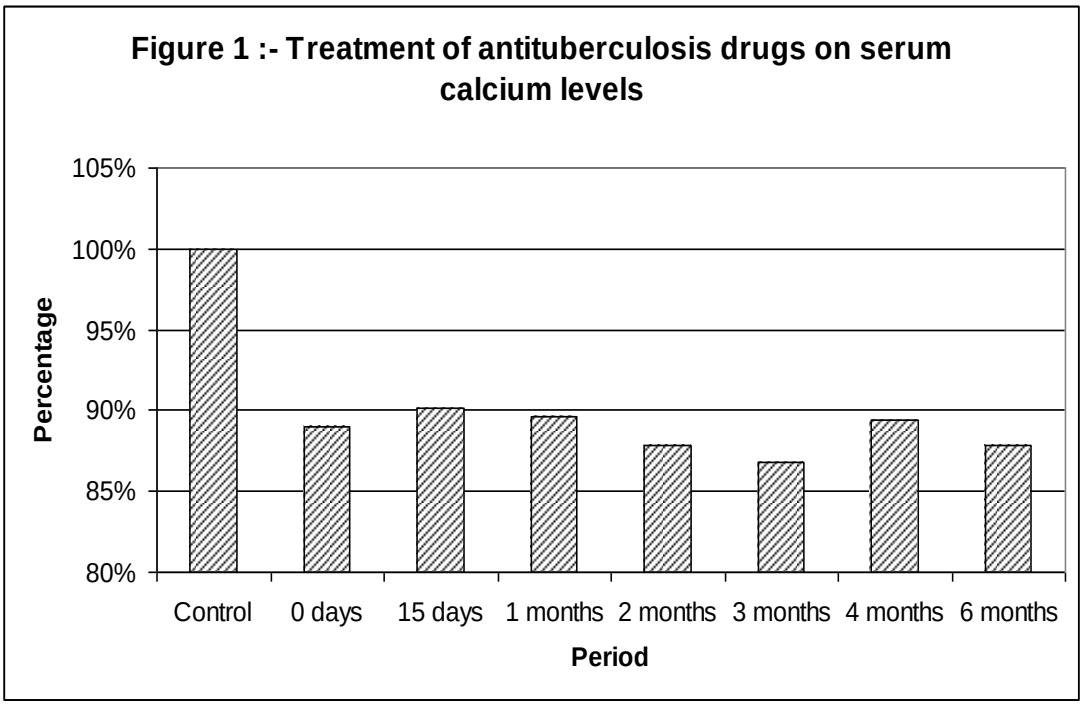

V. RESULTS

Table I shows the effect of anti-tuberculosis drugs on serum transferases i.e. SGOT and SGPT which are marker of liver function.

In control group of patients SGOT level was found to be 20.66 ± 0.88 IU/L which significantly increased in pretreated T.B. patients to 34.80 ± 2.46 which was 68.45% higher. The value further increases on treatment with T.B. drugs and it reaches to 42.22 ± 4.93 on 15th day. The magnitude of increase being 104% higher as compared to control.

Afterward the SGOT level remains some what constant from 1 month post treatment to 2 months, 3 months, 4 month and upto 6 months. On 6th month value was 29.64 which was still significantly high (43.46%) with respect to control.

Similar pattern have been observed in SGPT also. In control group the SGPT level was 19/17 ± 0.94 IU/L which increased to 25.76 ± 3.4 IU/L in T.B. Patients prior to start of treatment. The rise being 34.37%. A significant rise was observed on 15 days post-treatment period by 45.59%. The value remain almost increased in all post-treatment groups i.e. 1 month, 2 month, 3 month, 4 month and 6 month post treatment. On 6th month the value was 30.16 ± 5.02 IU/L which in 57.38% higher than control group.

Table II indicates the effects of anti-T.B drugs on serum Alkaline phsophatase, Acid Phosphatasea and Prostatic factor of Acid phsophatase in T.B. patients. The healthy subjects of control group showed 156.5 ± 3.06. 1.806 ± 0.06, 0.92 ± 0.04 IU/L values of Alkaline phosphatase, Acid Phosphatase and prostatic factor of acid phosphatase respectively. Significant increase was found in all three parameters in pretreated T.B. patients. The value being 279.14 ± 22.83, 3.23 ± 0.25 and 1.28 ± 0.07 respectively in Alkaline Acid and Prostatic acid phosphatase respectively.

The percent increase was 78.36%, 78.8% and 39.13% respectively in Acid, Alkaline and Prostatic acid Phosphatases.

All parameters reaches to highest value on 15th day post treatment. The Alkaline phosphatase was reached to 285.63 ± 24.17 IU/L which was 82.5% higher than control. The Acid phsophatase increased to 2.78 ± 0.24 IU/I which was 53.9 % higher and Prostatic factor of acid phsophatase reached to 1.71 ± 0.08 IU/L which was 85.86% higher than control.

After one month treatment of T.B. drugs till 6 months through 2, 3, 4 month the gradual decrease in all three parameters observed, which reached to normal level on 6th month post-treatment.

Table III represents the serum calcium level in T.B. patiets on treatment with DOT therapy. The healthy group of subjects showed 9.66 ± 0.10 mg/dl serum calcium. As compared to it the T.B. patients group prior to treatment shows significant decreased of 11%, the magnitude being 8.60 ± 0.10 mg/dl. The decrease in level was persistent till period of investigation. It was -10%. –11%, -13%, -14%, -11% and -13% on 15 days post-treatment, 1, 2, 3, 4 and 6th month post treatment period of T.B. drug.

VI. DISCUSSION

The results showed that biomarkers of toxicity in serum of Tuberculosis patients were stimulated significantly after administration of anti-T.B. drug.

In normal i.e. control group serum SGOT and SGPT levels were found 20.5 IU/Lit and 19.1 IU/Lit respectively. The normal levels of ALP was 156.7 IU/L, whereas serum calcium content was 9.71 mg%. The acid phosphatase level and prostatic acid phosphatase levels in control groups were 1.80 and 0.92 IU/L respectively. In tuberculosis patients on zero day i.e. prior to treatment all values were significantly high. All the parameters reached to highest level on 15th day of treatment but start to decline till 6th month post-treatment (through 1, 2, 3, 4 months post treatment values).

The present study revealed that the hepatic injury by anti-TB drugs (in combination) is due to membrane damage as indicated by increase serum markers (13). However decline in levels of serum marker after 1 month till 6 months, through 2nd, 3rd, 4th month of treatment may be due to aquantance in development of detoxifying mechanism in hepatic cells for Sr. Acid and Alkaline phosphatase. However SGOT and SGPT levels remains almost constant from 1 month to 6 month through 2nd, 3rd and 4th month of treatment. The reason is that the theraphy was continued till 6 months. SGOT and SGPT might have been came to normal after end of therapy. Further research is in progress regarding aspect.

In conclusion a temporary rise in ALP, ACP, APF and Sr. Calcium have been observed till 15 days post treatment which come to normal at one month onwards. However SGOT and SGPT remained high significantly till end of experiment.

The out come of hepatic adverse effect is often made more severe by continued administration of the offending drugs after the onset of the first manifestation of liver damage. Therefore, both physician and patients should be educated about the possibility of hepatiotoxicity during antitubercular treatment and about the necessity of monitoring liver status (14).

ACKNOWLEDGEMENT

The authors are thankful to Dr. Sanjay N. Oak, The Director, BMC, Medical Education and Major Hospital for providing collected Blood samples from T.B. patients of attending DOTS medicine, Nair Hospital and to Dr. Jaya Deshpande, Ex. Head of Department of Pathology, for Providing the laboratory facility to carry out the work.

Thanks are also due to Providing chemical facilities by Nana Parkar Smriti Samiti, Parel and Rupchand Bansari and also Lab Incharge Miss Ajita Kulkarni, Sr. Biochemist and V. D. Rane, Lab. Tech, Gurunath Shinde, Umesh Shinde and Laxman Chougule and Dhodke, Kuwar and all lab technician for their co-operation and for invaluable help and important suggestion.

REFERENCES

[1] Udani P. M. (1961): Incidence of tuberculosis in children. *Indian J. Child Helath*, : **10** : 566 – 575.
[2] M. M. Puri (2003) : Stop TB-use dots. Employment News Weekly 29 March – 4 April/ XXVII No. 52. 1.
[3] Health Department Survey (2008) : Maharashtra Times 24 – 9 – 2008.
[4] Davies D. M. Editor (1999) : Text book of adverse drug reactions. London Oxford Medical Publications.
[5] Mc Neill L. *et al.,* (2003) : Pyraznamide and Rifampicin vs Isoniazid for the treatment of Lattent tuberculosis. *Chest*, 123 (1) – 102 – 06.
[6] Krastic Buric *et al.,* (1980) : The activity of Transminase (GOT) and (GPT), Alkaline phosphatase. *Plucne bolesti Tuberk* : 92 (3), 132 – 8.
[7] Deck K. A. *et al.,* (1976) : Frequency Diagnosis and course of Kepatoxic efforts of Rifampicin. *Med. Klln*., 71 (4) : 1836 – 41.
[8] Seharer L., Smith J. P. (1969) : Serum transminase elevation and other hepatic abnormalities in patients receiving Isoniazid. *Ann. Intern. Med*., 71 (6) : 1113 – 20.
[9] Warke S. S. and Khan Z. H. (2004) :Effect of anti tuberculosis drug on serum electrolytes levels osmolarity, Blood pH and PCO_2 levels in tuberculosis patients. *Asian Jr. of Microbiol Env. Sc*. Vol. **5**, No.(1): 89 – 91.
[10] Bergmete H. U., Horder M, Rej R.(1986) : Approved Recommendation (1985) on IFCC Method for the measurement of catalytic concentration of enzymes part 3. IFCC Method for L/ Aspartate aminstransferase. *J. Clin. Chem. Clin biochem*.; 24, 497 – 510.
[11] Penttila, I. M. *et al.,* (1975) : *Scand. J. Clin. Lab. Invest*, 36, 2751.
[12] Hafkensheild, J. C. M *et al.,* (1979): *J. Clin. Chem. Clin biochem*.; 17, 219.
[13] Klin Lab (1992) : Age-dependent reference Limits of Several enzymes in Plsama at different measuring termeratures/ 38, 555-61.
[14] Seiler, D., Nagel. Tritschler W. and Lsoser S. (1983) : *J. Clin. Chem. Clin. Biochem*., 21 : 519.
[15] Young S.D., Pestaner L.C., and Gibbeman V. (1975) : *Clin. Chem*.Vol 21, No. 5.
[16] Sheikh A., Tasduq Kaiser Peerzada,. Supriya Kaul, Rinku Bhat, Rakesh K. Johri (2005) : Biochemical Manifestations of antituberculosis drugs induced hepatotoxicity and the effect of silymarin. *Hepatology research*, 31 132 – 135.
[17] Francois Durand, gilles Jebrak Dominique Pesseyre *et al.,* (1996) : Hepatotoxicity of antitubercular treatments. *Drug safety* Des. 15 (6) : 394 – 405.

PRATIBHA: INTERNATIONAL JOURNAL OF SCIENCE, SPIRITUALITY, BUSINESS AND TECHNOLOGY (IJSSBT), Vol. 1, No.1, March 2012
ISSN (Print) 2277—7261

Multimedia Data Mining: A Survey

Sarla More[1], and Durgesh Kumar Mishra[2]
[1]Assistant Professor, Truba Institute of Engineering and information Technology, Bhopal
[2]Professor and Head (CSE), Sri Aurobindo Institute of Technology, Indore
Emails: [1]sarlamore@gmail.com, [2]drdurgeshmishra@gmail.com

Abstract: Multimedia data mining (MDM) can be defined as the process of finding interesting patterns from media data such as audio, video, image and text that are not ordinarily accessible by basic queries and associated results. MDM is the mining of knowledge and high level multimedia information from large multimedia database system. MDM refers to pattern discovery, rule extraction and knowledge acquisition from multimedia database. To extract knowledge from multimedia database multimedia techniques are used. We compare MDM techniques with the state of the art data mining techniques involving clustering, classification, sequence pattern mining, association rule mining and visualization. This paper is a survey on the problems and solution of MDM it elaborates basic concepts, application at various areas, techniques , approaches and other useful areas which need to be work for MDM. Analyzing this huge amount of multimedia data to discover useful knowledge is a challenging problem which has opened the opportunity for research in MDM.

Keywords: Multimedia Data Mining, Feature Extraction, Knowledge acquisition, visualization.

I. INTRODUCTION

Multimedia data mining can be better understood by its purpose and scope. According to MPEG-7 Standard the kinds of data belong to the multimedia data [1] are of four types audio data, which includes sounds, speech, and music; image data ,video data, which include time-aligned sequences of images; and electronic or digital ink, which is sequences of time aligned 2D or 3D coordinates of a stylus, a light pen, data glove sensors, graphical, temporal, relational and categorical data or a similar device are stored in a multimedia database and used to develop a multimedia system [2]. The meaning of term MDM means several data sources of different modalities are processing at the same time. The MDM's primary purpose is to process media data alone or in a combination with other data for finding patterns useful for business.

Definition1. "MDM is the exploration and analysis, by automatic or semi-automatic means, of large quantities of data in order to discover meaningful patterns and rules"

Definition2. "Multimedia data mining is a subfield of data mining that deals with an extraction of implicit knowledge, multimedia data relationship or other patterns not explicitly stored in multimedia database".

The goals of MDM are to discover useful information from large disordered data and to obtain knowledge from the information. There are mainly six tasks for MDM: summarization, association, classification, clustering, trend analysis and deviation analysis. The working of MDM system is similarity search in multimedia data, Description based retrieval system, build indices and perform object retrieval based on image description such as keywords, caption, size and time of creation, content based retrieval system, support retrieval based on the image content, such as color, histogram, texture, shape, object and wavelet transform. The multimedia mining involves two basic steps:

- Extraction of appropriate features from the data.
- Selection of data mining methods to identify the desired information.

For multimedia information system and retrieval of content based image/audio/video Multimedia database is used and provides search and efficient storage organization. Data mining tool operate on structured data so that powerful tools are required for the unstructured or semi-structured data and dynamic audio-visual features available in multimedia database. Mining of multimedia data requires two or more data types such as text and video or text video and audio. Multimedia mining reaches much higher complexity from huge volume of data such as diversity of sensor, time or condition of acquisition. Mining in multimedia is referred to automatic annotation or annotation mining.

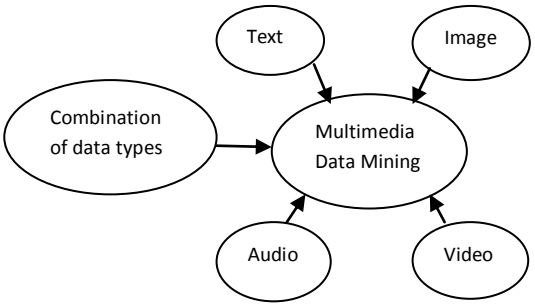

Fig No. 1 Multimedia data mining

Multimedia and data mining are two very interdisciplinary and multidisciplinary areas with independently and simultaneously rapid developments in recent years, for many decision-making applications the need for tools to extract hidden useful knowledge embedded within multimedia collections has become central point for research.

II. RELATED WORK

A. Background of multimedia data mining:

Since 1960 the research in the field of multimedia has begun for combining different media data into one application where text and images were combined in a document. During the research and development process, the synchronization of audio, video, and animation were done using a timeline which specify when they should be played. The problems of multimedia data capture, storage, transmission, and presentation have been investigated in the middle of 1960 where the multimedia standards MPEG-4, X3D, MPEG-7, and MX have continued to grow. Which are adapted and can transparently handle sound, images, videos, and 3-D objects that combined with events, synchronization, and scripting languages and can describe the content of any multimedia object. For multimedia distribution and database applications different algorithms need to be used. Such a database can be queried, for example, with the SQL multimedia and application packages called SQL/MM. The MDM covers the following areas:

- Media compression and storage.
- Delivering streaming media over networks with required quality of service.
- Media restoration, transformation, and editing.
- Media indexing, summarization, search, and retrieval.
- Creating interactive multimedia systems for learning/training and creative art production.
- Creating multimodal user interfaces.

B. Multimedia Mining

1. Processing Text:

The Unstructured text documents can be represented as "bag-of-words" such as huge feature vectors, where each feature encodes the presence or absence of a word from the dictionary common to all documents. a naive Bayesian classifier is used for such vectors to be analyzed to classify documents into

- By predefined groups, or by self organizing maps
- A type of neural networks to cluster documents according to topics
- Trees: we consider the structure of documents expressed using HTML tags
- Multi-valued attributes, which corresponds to some parts of the document instead of single term. for filtering e-mails this approach was used.

2. Processing Graphs:

In the machine learning community processing graphs or trees such as organic molecules or web sites and HTML documents has become an important part of research. Between the classic attribute-value and multi-relational representation of training data graph structures are there. Graph is more expressive than a flat representation this is the motivation for using graph representation in the area of machine learning, and directly learning from graphs is potentially more efficient than multirelational learning.

3. Processing Images:

In the field of pattern recognition a number of approaches to image processing can be used for feature extraction. Texture analysis, line detection, edge detection, segmentation and region of interest processing are some of the tasks solved in image processing. Fourier transformation, smoothing, color histograms, contour representations are tools that are used to solve these tasks. The images decomposed into segments or regions can then be represented in relational form and machine learning algorithms can be applied.

4. Processing Audio:

In multimedia applications audio data plays an important role. Band energy, zero crossing rate, frequency centroid, Band-width and pitch period are most frequently used features for audio processing. Audio signals can also be decomposed using wavelet transformation.

5. Processing Video:

The tasks of digital video processing are automatic segmentation, indexing, content-based retrieval and classification. High-level information from video includes detecting trigger events.

C. Multimedia data mining goals and methods:

Dissecting a set of objects, uncovering rules, decision trees, pattern recognition, trend prediction, and dimensionality reduction are some goals in MDM [3].

1. *Dissecting a Set of objects*

The most popular goal in data mining is dissecting a set of objects which is described by high-dimensional data into small comprehensive units, classes, substructures, or parts. These substructures give better understanding and control, and based on suitable information can assign a new situation to one of these classes, which can be classified as supervised or unsupervised. Each object originates from one of the predefined classes and is described by a data vector. But it is unknown to which class the object belongs, and this class must be reconstructed from the data vector. In unsupervised classification (clustering), according to the object content without a priori knowledge a new object is classified into a cluster of objects. It used in MDM early processes.

2. Uncovering rules:

An association rule method is used If goal of MDM is to be expressed as uncovering interesting rules [3]. An association rule takes a form of an implication X→Y, where X *and Y* denote antecedent and consequent of the rules respectively. X and Y belong to set of objects I, X ∩ Y = Φ, and *D* denotes a set of cases. We describe support s and confidence c as two parameters. The rule X→Y has support s in *D*, where s% of the data cases in *D* contains both *X* and *Y* and the rule holds confidence *c* in *D*, where *c*% of the data cases in *D* that support *X* also support *Y*. Association rule mining selects rules which have support greater than user-specified minimum support threshold. Confidence of the rule is at least from 0 to 1 confidence threshold. An association rule mining algorithm works in two steps:

- Finds all large item sets that meet the minimum support constraint
- It generates rules from all large item sets that satisfy the minimum confidence constraints.

III. DATA MINING VERSUS MULTIMEDIA DATA MINING

Current data mining tools operate on structured data, resides in large relational databases whereas data in multimedia databases are semi structured or unstructured. Compared with data mining, multimedia mining reaches much higher complexity resulting from:

- The huge volume of data,
- The variability and heterogeneity of the multimedia data such as diversity of sensors, time or conditions of acquisition
- The content meaning of multimedia is subjective.

Unstructured data: It is simply a bit stream. For example pixel level representation of images, video, and audio, and character level representation for text. To extract semantics from this data substantial processing and interpretation are required. It is difficult to interpret the database as this kind of data is not broken down into smaller logical structures.

IV. ARCHITECTURE OF MULTIMEDIA DATA MINING

To design and develop a MDM system some architecture are available. The first architecture includes Extracting data or metadata from the unstructured database in figure 2 which Store the extracted data in a structured database and apply data mining tools on the structured database.

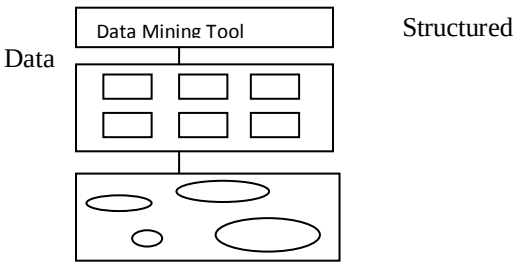

Fig No. 2 Converting unstructured data to structured data for Mining

In Figure 3 architecture as a starting point data collection is considered to be a learning system. The overall achievable performance determines by the quality of raw data. The goal of data pre-processing is to discover important features from raw data. Data cleaning, normalization, transformation, and feature selection comes under data pre-processing. At pre-processing stage if informative features be identified Learning can be straightforward. Detailed procedure depends highly on the nature of raw data and problem's domain. In some cases, prior knowledge can be extremely valuable [4].

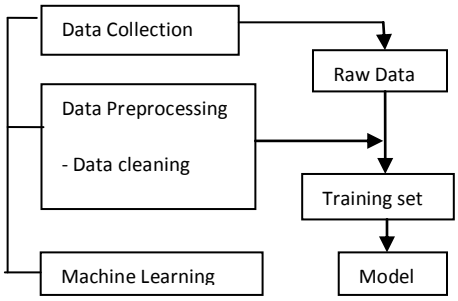

Fig No. 3 Multimedia mining process

For many systems, Domain experts conduct these stages. Training set is the product of data pre-processing. A learning model has to be chosen to learn from training set. The steps of multimedia mining are iterative. In order to improve the results the analyst jump back and forth between major tasks .

Figure 4 present architecture of applying MDM in different multimedia types [2]. The main stages of data mining process are:

A. *Domain Understanding:* It requires learning how the results of data-mining will be used so as to gather all relevant prior knowledge before mining.

B. *Data selection:* This stage requires the user to target a database or select a subset of fields or data records to be used for data mining.

C. *Learning and Pre-processing:* Integrating data from different sources and making choices about representing or coding certain data fields is the task of this stage. It serves as input to the pattern discovery stage. Because certain fields may contain data at levels of details which are not considered suitable for the pattern discovery stage representation choices are needed. In MDM the preprocessing stage is of considerable importance given the unstructured nature of multimedia data.

D. *Discovering Patterns:* The pattern discovery stage is the heart of the entire data mining process. The hidden patterns and trends in the data are actually uncovered in this stage. Several approaches of pattern discovery stage includes association, classification, clustering, regression, time-series analysis and visualization.

E. *Interpretations:* To evaluate the quality of discovery and its value to determine whether previous stage should be revisited or not this stage of data mining process is used.

F. *Reporting and using discovered knowledge:* This final stage reporting and putting to use the discovered knowledge to generate new actions or products and services or marketing strategies as the case may be.

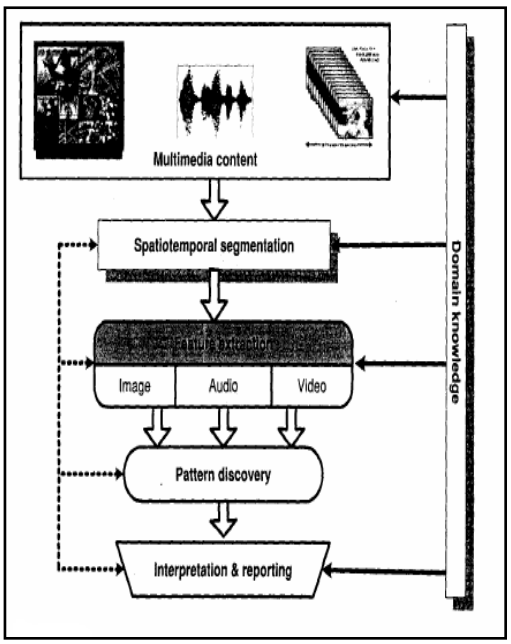

Fig No. 4 Architecture of Multimedia data mining

The above mentioned stages of data mining process such as Data preprocessing, cleaning and transformation, Discovering patterns, Interpretation, and Reporting and using discovered knowledge contains the highest importance and novelty from the MDM perspective. Thus, we can organize Multimedia Data Mining State of the Art review. The proposed scheme achieves the following goals [5].

- Discussion of the existing preprocessing techniques for multimedia data in MDM literature.
- Identifying specific problems encountered during data mining of multimedia data from feature extraction, transformation, representation and data mining techniques perspective.
- Discuss the current approaches to solve the identified problems and their limitations.
- Identification of open issues in the MDM area.

V. ISSUES IN MULTIMEDIA DATA MINING

Before MDM develops into a conventional, mature and trusted discipline some issues have to be addressed. These issues pertain to be the MDM approaches and their limitations. Major Issues in MDM includes content based retrieval and similarity search which are integrated with mining methods, generalization and multidimensional analysis, classification and prediction analysis, and mining associations in multimedia data [6]. Content based retrieval in multimedia is a challenging problem [7]. To gain insight into the meaning contained in databases is objective of multi-dimensional analysis. The multi-dimensional approach makes navigating the database easier, screening for a particular subset of data, or asking for data in a particular way, and being able to define analytical calculations. The speed of these operations is much quicker and more consistent than in other database structures as the data is physically stored in a multi-dimensional structure [8].

Feature Fusion:

With features extracted from multimedia data an important issue is how features should be integrated for mining and other applications. On each modality most of the multimedia analysis is performed separately, and to arrive at the final decision about input data results are brought together at a later stage. This approach is called late fusion or decision-level fusion. This is a simple approach, we lose valuable information about the multimedia events or objects present in the data.

VI. APPROACHES TO MDM

The integration of storage and search techniques with standard data mining methods is required for multimedia database mining. Promising approaches [4] includes Construction of multimedia data cubes, the extraction of multiple features from multimedia data, and similarity based pattern searching.

A. *Multimedia data cube:* Primarily on the basis of visual content this facilitates multiple dimensional analyses of multimedia data. Multimedia Miner as a MDM system prototype has been designed and developed which includes the construction of a multimedia data cube that facilitates multiple dimensional analysis of multimedia data. The mining of multiple kinds of knowledge includes characterization (summarization), discrimination (comparison), classification, association and clustering, in image and video databases.

B. *Feature extraction:* To extract patterns and derive knowledge from large collections of images, audio and video it takes the information contained in multimedia data. Some features that are used include short-time energy, pause rate, zero-crossing rate, normalized harmonicity, fundamental frequency, frequency spectrum, bandwidth, spectral centroid, spectral roll-off frequency and band energy ratio [9].

C. *Similarity based pattern searching:* In multimedia retrieval and data mining Similarity search is a crucial task. It can be defined as searching for a set of similar objects to a given query object.

D. *Database approach:* This approach views multimedia data as structured. Manually or semi-automatically features are extracted. The features or attributes on unstructured data, entail a high level of abstraction. In the features the higher the level of abstraction, the lower the scope for ad-hoc queries.

VII. TECHNIQUES OF MDM

A. *MDM Process Using Classification Rules:*

In this approach, main focus is on discovering the semantic structures. We use the classification rule approaches to perform data mining process because this approach only induce absolutely accurate rules. Examples of this work are:

1. The Hidden Markov Model
2. Detection of soccer goal shots using decision tree

B. *MDM Process Using Clustering:*

Clustering is a process of organizing objects into groups whose members are similar in some way. It is one of the unsupervised learning data mining technique. In unsupervised classification, the problem is to group a given collection of unlabeled multimedia files into meaningful clusters according to the multimedia content without Apriori knowledge. Recent works in this area are:

1. Unsupervised neural nets & staff organizing maps
2. Incremental clustering at various resolutions, using Haar Wavelet transforms and K- means

C. *MDM Process Using Association Rules:*

For discovering interesting relations between variables in large databases Association rule learning is a popular and well researched method. There are different types of associations which are association between image content and non image content features. Some early examples are:

1. Image classification method by using multiple level association rules based on image objects.
2. A multirelational extension to FP-tree algorithm to accomplish association rule mining task effectively

D. MDM Through Statistical Modeling:

In this approach, a collection of annoted images is used to build models for joint distribution of probabilities that link image features and keywords [4]. An early example of this work is:

1. A simple occurrence model to establish links between words and partitioned image regions.

VIII. FEATURES AND STANDARDS FOR MULTIMEDIA DATA MINING

To extract features for mining different image attributes such as Color, edges, shape, and texture are used [6]. Feature extraction based on these attributes performed at the global or local level. To characterize the spatial distribution of color in an image color histograms may be used as features. Similarly, shape of a segmented region may be represented as a feature vector of Fourier descriptors to capture global shape property of the segmented region or a shape could be described in terms of salient points or segments to provide localized descriptions. Global descriptors are generally easy to compute, provide a compact representation, and less prone to segmentation errors.

To uncover subtle patterns or changes in shape such descriptors may fail because global descriptors tend to integrate the underlying information. Local descriptors, on the other hand, tend to generate more elaborate representation and can yield useful results even when part of the underlying attribute, shape of a region is occluded, is missing. In the case of video, additional attributes resulting from object and camera motion are used.

APPLICATIONS OF MDM

There are various applications [2] [9] of MDM some of which are as follows:

A. In Digital Libraries: The retrieval collection storage and preservation of digital data is performed in the digital library. To fulfill this purpose, there is a need to convert different formats of information such as text, images, video, audio, etc. While conversion of the multimedia files into the libraries data mining techniques are popular.

B. For Traffic Video Sequences: To discover important but previously unknown knowledge the analysis and mining of traffic video sequences such as vehicle identification, traffic flow, queue temporal relations of the vehicle at intersection, provides an economic approach for daily traffic monitoring operations.

C. For Automated event analysis of suspicious movements: Surveillance system to monitor movements of employees, visitors and machines are used in many government organizations, multi-nationals companies, shopping malls, banks. Which has an ultimate objective to detect suspicious person based on their movements to maintain security and avoid any casualty?

D. In medical analysis: Application of Data Mining techniques for Medical Image Classification is used.

E. Media Production and Broadcasting: Proliferation of radio stations and TV channels makes broadcasting companies to search for more efficient approaches For creating programs and monitoring their content.

F. Customer Insight: It includes collecting and summarizing information about customer's opinions, products or services, customers' complains, customer's preferences, and the level of customer's satisfaction of products or services. Many companies have help desks or call centers that accept telephone calls from the customers. The audio data serve as an input for data mining to pursue the following goals:

- Topic detection
- Resource assignment
- Evaluation of quality of service

G. Surveillance: Surveillance consists of collecting, analyzing, and summarizing audio, video, or audiovisual information about a particular area, such as battlefields, forests, agricultural areas, highways, parking lots, buildings, workshops, malls, retail stores, offices, homes, etc. [10]. Which is associated with intelligence, security, and law enforcement and the major uses of this

technology are military, police, and private companies that provide security services.

There are several goals of surveillance data mining:

1. Objector event detection/recognition
2. Summarization
3. Monitoring

H. Intelligent Content Service: The Intelligent Content Service (ICS) is "a semantically smart content-centric set of software services that enhance the relationship between information workers and computing systems by making sense of content, recognizing context, and understanding the end user's requests for information" The MDM techniques can help to achieve the following goals:

- Indexing Web media and using advanced media search
- Advanced Web-based services

I. Knowledge Management: Many companies consider their archives of documents as a valuable asset. They spend a lot of money to maintain and provide access to their archives to employees. Besides text documents, these archives can contain drawings of designs, photos and other images, audio and video recording of meetings and multimedia data for training.

XI. CONCLUSION

This paper proposes a survey of multimedia data mining. The key idea is to provide review of MDM, which is an active and growing area of research. While the majority of the work has been devoted to the development of data mining methodologies to deal with the specific issues of multimedia data, Several applications of multimedia data mining have been investigated. Many of the recent MDM applications are focused on traffic monitoring and video surveillance, possibly due to increased attention to homeland security. In the coming years, we expect the MDM applications to grow especially in areas of entertainment and medicine. Almost all of the MDM efforts to date have been with the centralized data mining algorithms; however, this is expected to change as more and more multimedia content is searched and accessed through peers. The MDM is an active and growing area of research.

FUTURE WORK

Our review provides analysis of MDM, methods for MDM and compares the result of them. In future we explore the effect of Multimedia techniques on multimedia database to mine the multimedia components and improve the multimedia database environment. Researchers in multimedia information systems, in the search of techniques for improving the indexing and retrieval of multimedia information, are looking for new methods for discovering indexing information.

REFERENCES

[1] Manjunath BS, Salembier Ph, Sikora T, "Introduction to MPEG-7 Multimedia Content Description Interface" Wiley, New York, 2002.

[2] Manjunath T.N, Ravindra S Hegadi, Ravikumar G .K, "A survey on multimedia data mining and its relevance today", IJCSNS International Journal of Computer Science and Network Security, VOL.10 No.11, November 2010.

[3] Janusz Swierzowicz Rzeszow, "Multimedia Data Mining Trends and Challenges" University of Technology, Poland 2009.

[4] S. Kotsiantis, D. Kanellopoulos, P. Pintelas, "Multimedia Mining, WSEAS Transactions on Systems", Issue 10, Volume 3, December 2004, pp. 3263-3268.

[5] Chidansh Amitkumar Bhatt · Mohan S. Kankanhalli, "Multimedia data mining: state of the art and challenges", Multimed Tools and Applications (2011) 51:35–76.

[6] Sanjeev kumar R. Jadhav, and Praveenkumar Kumbargoudar, "Multimedia Data Mining in Digital Libraries: Standards and Features", ACVIT- 07, Dr. Babasaheb Ambedkar MarathWada University, Aurangabad, MS-India.

[7] Mittal, Ankush, "An overview of multimedia content-based retrieval strategies", Publication: Informatica, October 1 2006.

[8] You, J. Liu, L. Li, and K.H. Cheung, "on data mining and warehousing for multimedia information retrieval", From Proceeding (365) Artificial and Computational Intelligence – 2002.

[9] Valery A. Petrushin and Latifur Khan, "Multimedia Data Mining and Knowledge Discovery", Springer, 2007 pp. 3-17.

[10] Valery A. Petrushin and Latifur Khan "Multimedia Data Mining and Knowledge Discovery", Springer 2007.

PRATIBHA: INTERNATIONAL JOURNAL OF SCIENCE, SPIRITUALITY, BUSINESS AND TECHNOLOGY (IJSSBT), Vol. 1, No.1, March 2012
ISSN (Print) 2277—7261

A dimensionless approach for rate of re-aeration in river Ganges

R. P. Singh
Professor, Department of Civil Engineering, MNNIT, Allahabad-211004, U.P., INDIA

Abstract: This communication presents a methodology to evaluate the re-aeration rate term in basic dissolved oxygen (DO) deficit models by incorporating some important parameters like turbulence, width, depth and length of streams, which are necessary for fast biochemical oxygen demand (BOD) assimilation in streams. A mathematical model based on dimensional approach for rate of re-aeration as well as DO deficits, using basic philosophy of Bhargava (1986) model, is presented. The simulation of data on river Ganges in India, indicate that the predictions of DO deficits are in close agreement with the experimentally observed values. The methodology presented in accounts for all the important factors affecting re-aeration in streams and thus, may offer an alternative to traditionally used approaches for representing re-aeration rate.

Keywords: Dissolved oxygen; BOD assimilation; DO deficit; River Ganges; Pollution reduction

I. INTRODUCTION

Dissolved Oxygen in river is one of the most important indices for assessing the river's health and is a prime consideration in streams assimilation capacity. Many factors affect the dissolved oxygen concentration in river water and can be broadly classified into three main categories, namely 1) Geophysical factors, 2) Bio-chemical factors and 3) Physical factors. Geo-physical factors include river flow, temperature of water body, climatic conditions, surface expanse, turbulence, type and amount of organic matter and depth of the water body. Bio-chemical & physical forces include dilution and dispersion, mass-transfer phenomena, photosynthetic activities, bio-oxidation and reduction and all the natural and man-made sources and sinks of dissolved oxygen. Polluted streams are usually characterized by a decline in DO level, followed by a recovery in the dissolved oxygen level along the length of stream. The initial decrease in DO level occurs due to greater rate of oxygen removal by biological oxidation than that recouped by re-aeration. The rate of biological oxidation is directly proportional to the quantity of organic material present and consequently decreases with time. The minimum DO deficit will occur at a point where the rate of supply of oxygen by re-aeration equals the rate of its consumption by biological oxidation. Thereafter, the re-aeration process dominates and the dissolved oxygen deficit is gradually reduced.

A number of mathematical models for DO deficit [(Streeter and Phelps 1925), (Fair 1939), (Bhatia and Mc. Bean 1986) and (Bhargava 1986)] have been developed to assess the DO behaviour in streams. Little or no attention has been paid towards the modification of re-aeration rate term, which depends upon the number of variables. Also, the river Ganges in India is famous for fast BOD assimilation capacity (Bhargava 1983). Therefore, there is a need to incorporate the important variables affecting the re-aeration phenomenon so that the condition of river can be described in a better way.

In the present paper, the original DO deficit model developed by Bhargava (1986), which was originally derived from Streeter and Phelps (1925) DO model, has been modified by replacing the re-aeration rate term by a new term. In Bhargava (1986) model, the BOD assimilation term was divided into two fractions, i.e. settleable and non-settleable fractions. But, no attention was paid by earlier investigators to modify/replace the rate of re-aeration term (r_R), which is of great significance in fast self purification of streams. From the literature, it is evident that the term 'r_R' is largely influenced by the river's characteristics such as width, depth, turbulence and velocity, and length along the course of river, time of travel as well as initial and saturation DO levels of stream. Keeping these factors in view, a dimensional analysis is performed to derive a dimensionless expression for the re-aeration rate term and the same was used in Bhargava (1986) model, for further prediction of DO deficits in streams. The reported data from the study of Bhargava (1986) on river Ganges in India has been used in predictions and also compared with the observed values. It is believed that the methodology presented in this paper will prove better to represent comprehensively the re-aeration rate rather than representing 'r_R' by a single parameter 'k_R', the re-aeration coefficient, as used by many previous researchers.

II. THEORETICAL BACKGROUND

When an organic effluent is discharged into a stream, it exerts a biochemical oxygen demand (BOD) with the processes of BOD assimilation and

atmospheric re-aeration proceeding simultaneously. In many situations the oxygen demand will initially exceed the re-aeration rate, so the DO concentration will fall rapidly. If the rate of consumption lowers the oxygen concentration, the oxygen mass transfer rate will increase. At some point downstream of point of discharge the rate of re-aeration and the rate of consumption becomes equal and the oxygen concentration stops declining. This is the critical point of the curve, where the oxygen deficit is maximum and the dissolved oxygen concentration is lowest, called as critical DO deficit (D_c) and the corresponding time is called as critical time (t_c). Thereafter, re-aeration phenomenon predominates and the dissolved oxygen concentration rises to approach saturation DO level. As the rate of mass transfer is proportional to the oxygen concentration, the rate of re-aeration slows down near the asymptotic point.

As per Streeter and Phelps (1925), the rate dissolved oxygen (DO) deficit can be expressed as a function of BOD assimilation and re-aeration rates, which is the algebraic sum of rate of de-oxygenation (r_D) and the rate of re-aeration (r_R) and is given by the expression:

$$\frac{dD}{dt} = r_D + r_R \qquad (1)$$

where, both r_D and r_R follow first order kinetics with respect to BOD of waste and DO deficit 'D' respectively and are expressed as:

$$r_D = \frac{dD}{dt} = kS \qquad (2)$$

$$r_R = -k_R D \qquad (3)$$

where, $\frac{dD}{dt}$ = the rate of change of DO deficit, k = de-oxygenation rate constant (d^{-1}), k_R = re-aeration rate constant, (d^{-1}), and *S* = BOD remained after time *t*, mg/L. Therefore, Eq. (1) becomes

$$\frac{dD}{dt} = kS - k_R D \qquad (4)$$

As per Bhargava (1986), the DO Deficit in the river due to discharge of wastewater is affected by the settling of settleable organic particles. If the settleable portion of the initial BOD concentration is $S_{0\text{-}x}$, which would be completely removed within a transition time '$T = \frac{d}{v}$ (days)' where *d*= depth of river, m, *v* = settling velocity of bio-flocculated particles (m/s) and $S_{0\text{-}y}$ is the non-settleable organic fraction (mg/l), then, the total initial BOD, 'S_0' will be given by

$$S_0 = S_{0\text{-}x} + S_{0\text{-}y} \qquad (5)$$

The settled fraction of settleable portion of initial BOD concentration ($S_{o\text{-}x}$), at time *'t'* is given by $S_{o-x}\frac{v}{d}t$. Therefore, the non-settleable fraction (S_1) of settleable portion of initial BOD concentration ($S_{o\text{-}x}$), at time *'t'*, is given by

$$S_1 = S_{o-x} - S_{0-x}\frac{v}{d}t \qquad (6)$$

The non-settleable portion *(S_2)* of total initial BOD concentration (S_0), at time *t* is given by,

$$S_2 = S_{0-y}e^{-kt} \qquad (7)$$

Hence, BOD remaining at time '*t*' will be

$$S = S_1 + S_2 = S_{0-x}\left(1 - \frac{v}{d}t\right) + S_{0-y}e^{-kt} \qquad (8)$$

Bhargava (1986) pointed out that non-settleable organic matter exerts the oxygen demand at a maximum rate equal to the rate of BOD exertion *(k)*. But, the settleable organic matter would exert a part of its oxygen demand before it reaches the bottom of the streams and this rate constant is denoted as *(m)*. It is to be noted that this rate constant of oxygen demand *(m)* may be even more than k_R, such that the maximum value of *(m)* would equal to k_R. Thus, *k* for the first term of the right hand side of the Eq. (8) should be *(m)*, and for the second term of right hand side of the equation (8) would be (k). From Eqs. (4) and (8), we have,

$$\frac{dD}{dt} = mS_{0-x}\left(1 - \frac{v}{d}t\right) + kS_{0-y}e^{-kt} - k_R D \qquad (9)$$

The exact solution of Eq. (9), for *t*< *T* (Transition time), t = T =d/v and t >T can be given respectively by Eqs. (10), (11) and (12).

$$D = \left(\frac{m}{k_R}\right)S_{0-x}\left\{1 - e^{-k_R t}\left[1 + \left(\frac{1}{k_R}\right)\left(\frac{v}{d}\right)\right] - \left(\frac{v}{d}\right)\left(t - \frac{1}{k_R}\right)\right\} \qquad (10)$$

$$\ldots\ldots\ldots\ldots + \left(\frac{k}{k_R - k}\right)S_{0-y}\left(e^{-kt} - e^{-k_R t}\right) + D_0 e^{-k_R t}$$

$$D_T = \left(\frac{m}{k_R}\right)S_{0-x}\left[\left\{1 - e^{\left(-k_R\frac{d}{v}\right)}\right\}\left\{\left(1 + \frac{1}{k_R}\left(\frac{v}{d}\right)\right) - 1\right\}\right] + \left(\frac{k}{k_R - k}\right)S_{0-y}\left\{e^{\left(-k_R\frac{d}{v}\right)} - e^{\left(-k_R\frac{d}{v}\right)}\right\} + D_0 e^{\left(-k_R\frac{d}{v}\right)} \qquad (11)$$

$$D = \frac{k}{k_R - k}S_{0-y}\left[e^{-kt} - e^{\left\{k_R - k\frac{d}{v} - k_R t\right\}}\right] + D_T e^{\left\{-k_R\left(t - \frac{d}{v}\right)\right\}} \qquad (12)$$

where D_T is the DO deficit at T = d/v, d = depth of river and v = settling velocity of bio-flocculated particles. Other model equations developed are available else where (Bhargava 1986).

Bhargava (1986) did not propose any change in the re-aeration rate term (k_RD). For fast river purification, this term has great significance and hence has been taken up in this study. A dimensional approach is followed as described below.

III. A DIMENSIONLESS APPROACH FOR EVALUATION OF RE-AERATION RATE AND DO DEFICIT

It is well known that rate of re-aeration in streams depends upon a number of forces and factors. Among them, some relevant factors are DO deficit (D), re-aeration coefficient (k_R), Reynolds number accounting turbulence *(R)*, initial DO of the river water *(C_i)*, saturation DO of the river water *(C_s)*, acceleration due to gravity *(g)*, length along course of river *(L)*, width of river *(B)*, depth of river *(d)*. Thus, the rate of re-aeration can be assumed as a function of all these parameters and can be expressed as:

$$r_R = f(D, k_R, L, t, C_i, C_s, g, R, d, B) \quad (13)$$

The repeating variables may be taken as *L*, *t*, k_R and C_s. The dimensions of the parameters are given below.

Parameters	*D*	*L*	*T*	*Ci*	*Cs*	*g*	*B*	*R*	*D*	k_R
Dimension	ML^{-3}	*L*	*T*	ML^{-3}	ML^{-3}	LT^{-2}	*L*	$M^0L^0T^0$	*L*	ML^3T^{-1}

Using Buckingham-Pi theorem, the various relevant dimensionless groups formed can be expressed as:

$$\pi_1 = \frac{r_R.t}{C_s} = \frac{k_R.D.t}{C_s} \quad (14)$$

$$\pi_2 = \frac{C_i}{C_s} \quad (15)$$

$$\pi_3 = \frac{gt^2}{L} \quad (16)$$

$$\pi_4 = \frac{B}{L} \quad (17)$$

$$\pi_5 = R \quad (18)$$

$$\pi_6 = \frac{d}{L} \quad (19)$$

Using these dimensionless groups, the parameter, $\frac{k_R.D.t}{C_s}$ can be expressed as function of other dimensionless groups as:

$$\frac{k_R.D.t}{C_s} = f\left[\frac{C_i}{C_s}, \frac{gt^2}{L}, \frac{B}{L}, R, \frac{d}{L}\right] \quad (20)$$

As the variation of rate of re-aeration can be approximated as a power function of variables, therefore, the right hand side of Eq. (20) can be assumed as power function of multiplier of all the dimensionless groups and the resulting equation can be written as:

$$\frac{k_R.D.t}{C_s} = A.\left[R.\frac{C_i}{C_s}.\frac{gt^2}{L^3}Bd\right]^a \quad (21)$$

where A and a are some constants. Eq. (21) can also be written equivalently in terms of velocity of flow (V) in place of L and is given by

$$\frac{k_R.D.t}{C_s} = A.\left[R.\frac{C_i}{C_s}.\frac{g}{V^3.t}Bd\right]^a \quad (22)$$

From Eq. (21) or (22), the rate of re-aeration, r_R (=k_R.D) can be determined by power fitting of the experimental data on streams. In the present work, the parameters required to be used in Eq. (21) or (22) were extracted from the study of Bhargava (1986) on Ganga river. The parameters' values are: m = 9.0 d^{-1}, k = 3.5 d^{-1}, k_R = 9.0 d^{-1}, $S_{0\text{-}x}$ =16 mg/l, $S_{0\text{-}y}$ =12 mg/l, D_0 = 3.75mg/l, T= d/v = 0.025 d^{-1}, V = 0.54 m/s, C_s = 7.75 mg/l, C_i = 4 mg/l, B = 120 m, and d = 5 m. The Reynold's number 'R' was determined using the relation:

$$R = \frac{VBd}{\nu.(B+2d)} \quad (23)$$

where ν =1.01x10^{-6} m^2/s = kinematic viscosity of water.

Using Eq. (23) and parameters value, the Reynold's Number, R was found equal to 2467631. The functional relationship between the parameters of Eq. (21) was derived by power fitting of the data presented in Table 1 using observed DO deficit, D (read from Fig. 1 of the study of Bhargava (1986)) and the time, t as shown in Figure 1. The following functional relationship with R^2 – value of 0.9851 results.

$$\frac{k_R.D.t}{C_s} = 506005.\left[R.\frac{C_i}{C_s}.\frac{gt^2}{L^3}Bd\right]^{-0.8882} \quad (24)$$

From Eq. (24), the value of k_R.D (equal to rate of re-aeration, r_R) was substituted after replacing L by

V.t in Eq. (9) and the modified equation is expressed as:

$$\frac{dD}{dt} = mS_{0-x}\left(1-\frac{v}{d}t\right) + kS_{0-y}e^{-kt} - 506005\,.C_s^{\,1.8882}.\left[R.C_i.\frac{g}{V^3}Bd\right]^{-0.8882}.t^{-0.1118} \quad (25)$$

The exact solution of Eq. (25), for $t < T$ (Transition time), t = T =d/v and t >T can be given respectively by Eqs. (26), (27) and (28) and expressed as:

$$D = mS_{0-x}t - mS_{0-x}\frac{v.t^2}{2d} - S_{0-y}e^{-kt} - 569697\,.C_s^{\,1.8882}.\left[R.C_i.\frac{g}{V^3}Bd\right]^{-0.8882}.t^{0.8882} + D_0 + S_{0-y} \quad (26)$$

$$D = mS_{0-x}.\frac{d}{v} - mS_{0-x}\frac{d}{2v} - S_{0-y}e^{-k\frac{d}{v}} - 569697\,.C_s^{\,1.8882}.\left[R.C_i.\frac{g}{V^3}Bd\right]^{-0.8882}.\left(\frac{d}{v}\right)^{0.8882} + D_0 + S_{0-y} \quad (27)$$

$$D = -S_{0-y}e^{-kt} - 569697\,.C_s^{\,1.8882}.\left[R.C_i.\frac{g}{V^3}Bd\right]^{-0.8882}.t^{0.8882} + D_T + S_{0-y}e^{-k\frac{d}{v}} + 569697\,.C_s^{\,1.8882}.\left[R.C_i.\frac{g}{V^3}Bd\right]^{-0.8882}.\left(\frac{d}{v}\right)^{0.8882} \quad (28)$$

The critical time, t_c for $t_c \leq T$ and $t_c > T$ can be respectively modified to following equations:

$$mS_{0-x}\left(1-\frac{v}{d}t_c\right) + kS_{0-y}e^{-kt_c} = 506005\,.C_s^{\,1.8882}.\left[R.C_i.\frac{g}{V^3}Bd\right]^{-0.8882}.t_c^{\,-0.1118} \quad (29)$$

$$kS_{0-y}e^{-kt_c} = 506005\,.C_s^{\,1.8882}.\left[R.C_i.\frac{g}{V^3}Bd\right]^{-0.8882}.t_c^{\,-0.1118} \quad (30)$$

The critical DO deficit, D_c for $t_c \leq T$ and $t_c > T$ can be determined by first determining t_c from Eqns. (29) and (30) respectively by trial and error and using $t = t_c$ and $D = D_c$ in Eqs. (26) and (28).

IV. RESULTS AND DISCUSSION

The input parameters and the data for prediction of DO deficits were taken from the study of Bhargava (1986) and are presented in the text above and Table 1. The predicted DO deficits were computed using Eqs. (10), (11) and (12) respectively for $t < T$ (Transition time), t = T = $\frac{d}{v}$ d/v and t >T for Bhargava (1986) model and Eqs. (26), (27) and (28) for modified model. Predicted DO deficits for both the models are computed only against the known experimental values and are given in Table 1. The predicted DO deficits along with the observed DO deficits are also plotted in Figure 2. It can be seen that the predictions are comparable and somewhat better by use of the modified equation than those predicted using Bhargava (1986) model. Thus, the modification proposed in the re-aeration rate term has practical utility in modelling DO in rivers like Ganges having fast purification capacity.

The present work demonstrates that a dimensionless approach can be used to replace the rate of re-aeration term in DO deficit modelling. Traditionally, re-aeration coefficient has been the subject of dimensionless analysis. Errors may creep in the representation of re-aeration coefficient and this coupled with D term to represent re-aeration rate may adversely affect the DO deficit computations. Thus, instead of following this line of attack, it was preferred to look into the possibility of representing re-aeration rate term itself. Results from Figs. 1 and 2 clearly indicate that this approach can also work. Due to lack of data on other rivers, the approach has not been tested for other conditions and it is expected that the concept presented in this paper will simulate further interest and applications in DO modelling in streams.

V. CONCLUSIONS

The present study is basically aimed to develop a functional relationship for re-aeration rate using dimensionless approach, which is tested to be applicable to the rivers having fast BOD assimilation capability like river Ganges in India. The concept developed gives satisfactory results in prediction of DO deficits in river Ganges. However, the validity of the approach needs further investigation on other rivers.

ACKNOWLEDGEMENTS

The author is grateful to the Ministry of Human Resources Development (MHRD), Government of India, New Delhi for providing help and assistance in completion of this work. Authors are also thankful to Director, MNNIT, Allahabad, U.P., India, for providing the facilities needed for the work.

Notation

The following symbols are used in this paper:

A , = constant;
a = constant;
B = width of river;
BOD = biochemical oxygen demand;
C_i = initial dissolved oxygen;
C_s = saturation dissolved oxygen;
DO = dissolved oxygen;
D = dissolved oxygen deficit;
D_c = critical dissolved oxygen deficit;
D_T = dissolved oxygen deficit at transition time, T;
D_0 = initial dissolved oxygen deficit;
d = depth of river;
k = biochemical oxygen demand rate constant for settleable organic matter;
k_R = re-aeration rate constant;
L = length of river course;
m = biochemical oxygen demand rate constant for non-settleable organic matter;
R = Reynold's number;
r_D = rate of de-oxygenation;
r_R = rate of re-aeration;
S = biochemical oxygen demand remained after time t;
S_1 = non-settleable fraction of settleable portion of initial BOD concentration at time t;
S_1 = settleable fraction of settleable portion of initial BOD concentration at time t;
S_0 = total biochemical oxygen demand at time t = 0;
$S_{0\text{-}x}$ =settleable biochemical oxygen demand at time t = 0;
$S_{0\text{-}y}$ =non-settleable biochemical oxygen demand at time t = 0;
T = transition time;
t = time
t_c = critical time;
v = settling velocity of bioflocculated particles;
V = velocity of flow;
ν = kinematic viscosity.

Table 1: ***Observed and Predicted DO deficits***

Time, days	Distance from point of discharge[a] , m	Observed DO deficit[b], D , mg/l	Predicted DO deficit[c] , D, mg/l	Predicted DO deficit[d] , D, mg/l
0.000	0.00	3.75	3.750	3.750000
0.010	466.56	6.83	4.920	4.726915
0.020	933.12	5.08	5.418	5.201299
0.025	1166.40	4.80	5.445	5.228913
0.050	2332.80	4.60	5.170	5.021416
0.065	3032.64	4.15	5.000	4.892359
0.075	3499.20	4.55	4.880	4.801045
0.100	4665.60	4.35	4.590	4.549683
0.110	5132.16	4.30	4.520	4.439106
0.125	5832.00	4.95	4.210	4.262094
0.150	6998.40	4.80	4.014	3.937328

[a]computed by multiplying time with velocity of flow.
[b] extracted from study of Bhargava (1986)
[c] using Bhargava (1986) model
[d] using present model

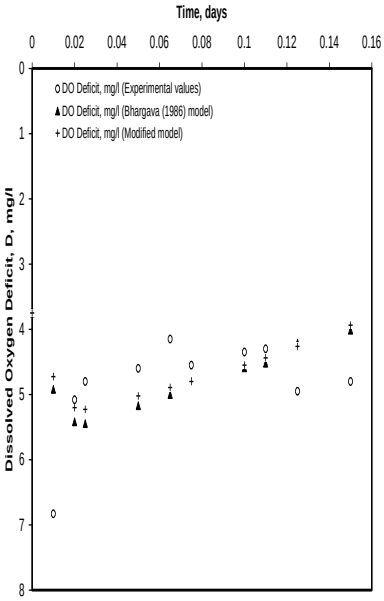

Fig. 1.Variation of dimensionless parameters

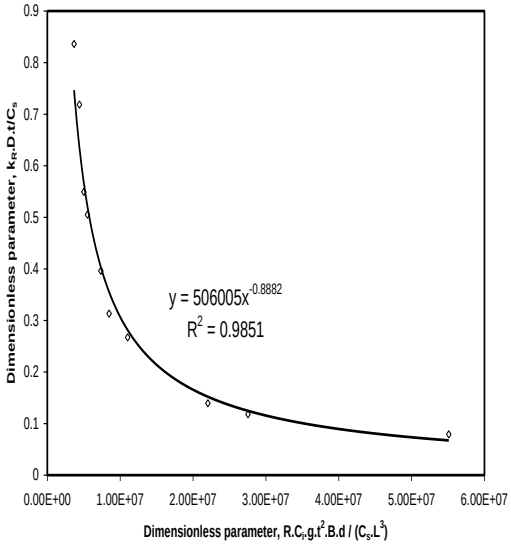

Fig. 2. Variation of dissolved oxygen deficit with time. kR.D.t / Cs with R.Ci.g.t2.B.d / (Cs.L3).

REFERENCES

[1] Bhargava, D. S. (1986). "DO Sag Model for Extremely Fast River Purification." *J. Environ. Engrg, ASCE*, 112(3), 573-585.

[2] Bhargava, D. S. (1983). "Most Rapid BOD Assimilation in Ganga and Yamuna Rivers." *J. Environ. Engrg., ASCE*, 109(1), 174-188.

[3] Bhatia, K. K. S. and McBean, E. A. (1986). "Steady State Modelling of Dissolved Oxygen in River Speed (Canada)." *J. IAH*, 9(4), 11-24.

[4] Fair, G. M. (1939). "The Dissolved Oxygen Sag – An Analysis." *J. Sewage Works*, 11(3), 445.

[5] Streeter, M. W. and Phelps, E. E. (1925). "A Study of the Pollution and Natural Purification of the Ohio Rivers." *U.S. Public Health Bulletin No. 146.*

PRATIBHA: INTERNATIONAL JOURNAL OF SCIENCE, SPIRITUALITY, BUSINESS AND TECHNOLOGY (IJSSBT), Vol. 1, No.1, March 2012
ISSN (Print) 2277—7261

Short Term Load Prediction Considering the Effect of Temperature as a Weather Parameter Using a Combinatorial Model of Wavelet and Recurrent Neural Networks

Anand B. Deshmukh[1], *Dineshkumar U.Adokar*[2]
S.S.P.M's College of Engineering & Technology, Amravati (MS), India
S.S.B.T's College of Engineering & Technology Bambhori, Jalgaon (MS), India
Email:abd_07@rediffmail.com[1], dadokar@gmailmail.com[2]

Abstract:-In this paper, a novel combinatorial model of Wavelet and RNNs is developed for one-day-ahead electrical power load prediction. For this purpose three RNN predictors are modeled on different frequency components such as approximation component and several other detailed components of wavelet transformed load data for one-day-ahead prediction. The best predictor is chosen on each frequency component on the grounds of validation performance with respect to the performance measures on training and testing dataset. The final prediction is achieved by adding the forecast of best predictor on each component in the different seasons. The results offered by the proposed technique are outperformed the traditional statistical technique.

Keywords- short-term load prediction, recurrent neural networks, Daubechies, statistical methods, weather information

.

I. INTRODUCTION

Short-term load prediction relies on historical load, weather condition, and industrial demand, daily and seasonal patterns. Short-term prediction is indeed a complex problem. Conventional methods have been used to predict the hourly load such as autoregressive moving average, linear regression, stochastic time series, and general exponential smoothing [1]. Such methods cannot properly represent the complex nonlinear relationships between the load and a series of stochastic factors such as daily and weekly time rhythms special events and correlation properties of weather conditions which can cause high unpredictable variations in power demand.

ANNs are able to give better performance in dealing with the nonlinear relationships among their input variables [2]-[4]. ANNs could extract implicit nonlinear relationships among the input variables by learning from training data. Combining the wavelet transform with other techniques such as autoregressive modeling, and neural networks for predicting electrical load demand has been studied [5]-[8]. Wavelet analysis provides time and frequency representation simultaneously. The wavelet transform is applied to decompose the original time domain signal into several other scales with different levels of resolution in what is called as multiresolution decomposition [9],[10].

By analyzing the electric load we find that the load curve shows certain periodicities of year, month and day and the periodicities nested in each other. Therefore, the load series can be considered as a linear combination of sub-series characterized by different frequencies. Each sub-series corresponds to a range of frequencies and show much more regularities so they are predicted more precisely than the original load series.

In this research work Db4 has been confirmed as a best mother wavelet. To obtain better results and ensure that the adopted model results in convergence, this paper investigate factors that influence the overall performance of the recurrent neural networks (RNNs) such as the determination of the right network topology, good selection of data patterns and the selection of appropriate and efficient training algorithm and a number of possible combinations of inputs load and various weather variables. Next, a performance analysis is carried out on the basis of performance measures such as mean square error (MSE), correlation coefficient (r) and daily mean absolute percentage error (DMAPE) for different seasonal load series of the year 2009.

II. METHODOLOGY USED

Available electric load time series and weather data is retrieved from the authentic data repositories. The electric load time series pertaining to these data sets reflect the demography, culture, environment that are specific and exclusive for a Vidarbha region of Maharashtra state. The data is conditioned using wavelet transform technique in order to extract prominent features and important statistical parameters of the data sets.

Optimal Recurrent Neural Network model is designed with a view to minimize prediction error, mean square error (MSE), normalized MSE and mean absolute percentage error (MAPE).The neural network model is trained on the training dataset at least five times with different random initialization of connection weights which is usually chosen as very small arbitrary real numbers .The trained network is assessed on different datasets, such as training and testing data sets.

The proposed Recurrent Neural Network architectures that are used for predicting given load time series include-

1. Elman RNN
2. Jordon RNN
3. Fully Recurrent Neural Network based on gamma memory filter

For computer simulation and design of aforementioned RNNs, Matlab 7.0 and Neurosolutions 5.06 are used. The parameters which are set include number of hidden layers, number of neurons in each hidden layer, activation function of neurons in output layer. Appropriate learning algorithms such as standard back propagation with momentum term, conjugate gradient algorithm, quick propagation algorithm and delta bar delta algorithm. Further an exhaustive experimentation has been undertaken in order to set the optimal values of momentum term and step size in hidden as well as in output layer. In addition, the value of gamma parameter and number of taps for FRNN based on gamma memory filter is optimally configured.

III. WAVELET-TRANSFORM BASED LOAD TIME SERIES

The main idea of the wavelet multi-resolution analysis (MRA) is that any function *f (t)* can be approximated step by step, and the approximation of each step is just to smooth *f (t)* by a low-pass function *Φ (t)* which will also expand or contract according to step. Therefore, *f (t)* was approximated in different precision in different steps. In this paper, the Mallat algorithm is adopted to decompose the load signal.

Figure 1 show one week load curve in rainy season. It is seen that, reconstructed sub-series show much more regularities. The approximation A2 (t) varies with the period of a day and the value is relatively big, which is the basic load of the system. D2(t) appears to be small value and strong regularities. for the sub-series A2(t), D2(t) and D1(t), three D1(t) is the random component in the the load, whose value is fairly trivial in the entire load. In this paper, aforementioned RNNs are optimally designed and developed simultaneously on each frequency component to predict them. After getting the prediction result of each sub-series by different optimally designed RNNs, the best RNN is chosen on each component on the basis of their validation performance such as MSE, r and MAPE on the prediction test data set. Finally, prediction of best RNN of each sub-series is added in order to achieve final prediction in all seasons.

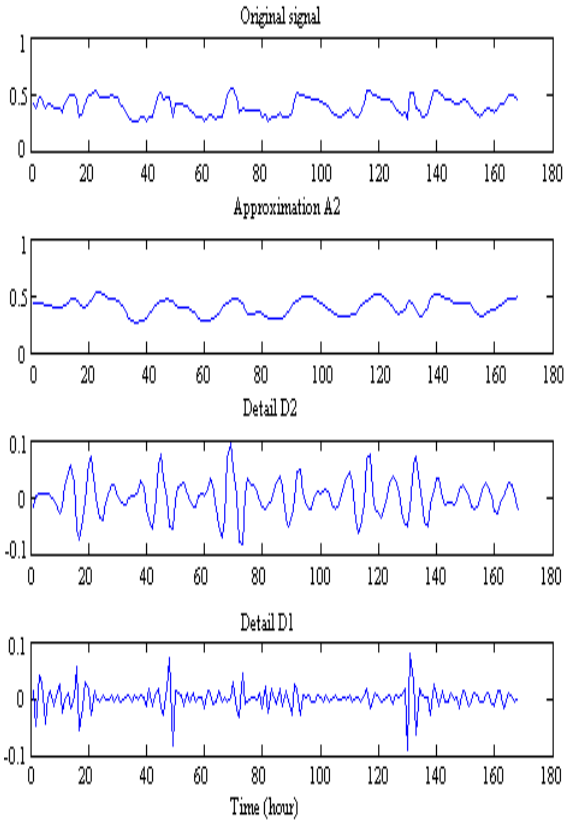

Figure 1 : Wavelet-transformed load time series of one week load data (July 1 to July 7, 2009)

Selection of optimal parameters:

In order to achieve optimally configured RNN, the various optimal parameters of the proposed best RNN predictors are decided for different frequency bands such as approximation component and several other detail components in various seasons, as depicted in Table 1.

Table 1: Optimal parameters for approximation (A2) and details (D2, D1) {1-day-ahead load prediction}

Parameters	**Approx(A2)**			**Detail(D2)**			**Detail(D1)**		
	S	**W**	**R**	**S**	**W**	**R**	**S**	**W**	**R**
TF(O)	LA	LTA	LTA	TA	TA	TA	LTA	TA	A
LR	CG	CG	CG	CG	CG	CG	CG	CG	CG
TH	0.00001	0.00001	0.0001	0.001	0.0001	0.0001	0.001	0.001	0.001
INPUT	2	4	5	6	3	2	5	5	6
TF(CU)	NA	IA	IA	NA	NA	NA	IA	NA	NA
TIME	NA	0.6	0.8	NA	NA	NA	0	NA	NA
GP	0.3	NA	NA	1	1	1	NA	1.1	1
TAPS	6	NA	NA	6	5	6	NA	7	6

(S-summer, W-winter, R-Rainy, TF-transfer function, O-output, LR-learning rule, TH-threshold, CU-context unit, GP-gamma parameter, LA-linear axon, LTA-linear tanh axon, TA-tanh axon, A-axon ,CG-conjugate gradient, NA-not applicable)

IV. THE PROPOSED PREDICTION METHODOLOGY

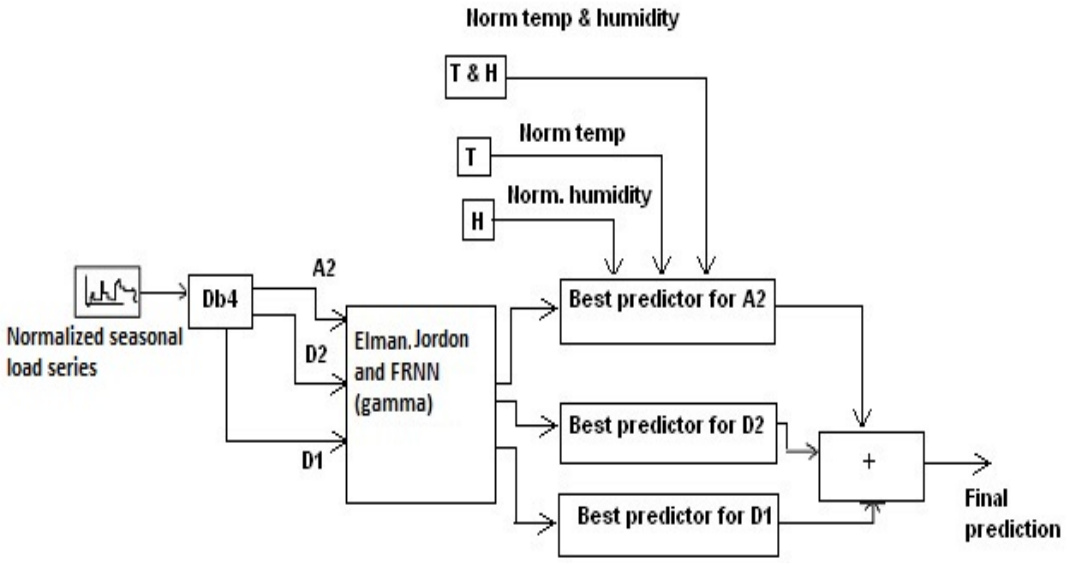

Figure 2: Proposed prediction technique for different seasons.

A typical load profile of one week contains basic component, peak and valley components, average component, periodic component and random component. Conventional techniques like time series methods, regression based methods are able to extract only some of these components from the historic data. But, ANNs by its non-linear nature can extract all the components from the training data. However, RNN when modeled on original load data could not extract all of them in a well

defined manner. A certain regularity of the data is an important precondition for the successful application of neural networks (NNs).

Hence, a novel technique of combinatorial model of wavelet and RNNs is proposed for the prediction of one-day-ahead load prediction for different seasons.

Figure 2 shows block diagram of proposed prediction methodology. Here, idea is to decompose the different seasonal load series using Daubechies 4 with decomposition of levels two and to model it via individual fitting of each level of resolution (frequency bands).The suggested RNNs are modeled on each frequency component and the final prediction is obtained by adding the forecast of best predictor on each frequency band. The best RNN for A2 in the different seasonal load series is chosen on the basis of their validation performance with respect to the performance measures like MSE, r and MAPE. It is observed that, the approximation A2 and all two levels of detail components are taken into account to "reconstruct" the load series.

V. SIMULATION RESULTS AND THE EFFECT OF TEMPERATURE AS A WEATHER PARAMETER

The proposed architecture of best predictor is trained on approximation component for different seasons with and without considering the weather information such as temperature as one of the input variables. The effect of weather parameter on STLP for a typical day in winter season (Friday, October 16, 2009) is investigated without considering temperature as a weather information and considering temperature are shown in figure 3 & figure 4 respectively. The daily mean absolute percentage error (DMAPE) and maximum absolute percentage error (maximum APE) of typical weekdays in a winter season (16 to 22 October 2009) are shown in Table 2.The weather information such as temperature is considered as an input variable only for approximate component .However, temperature as a weather information have not been considered for detail component as it is least significant on detail components.

The results depicted in table 2 show that, on 17/10/09, 19/10/09, 20/10/09 and 22/10/09 the prediction accuracy is improved when lone temperature as one of the input weather variable is considered. Hence from the results it is confirmed that temperature as a weather variable plays significant role in improving the prediction accuracy and the suggested combinatorial model of wavelet and RNNs performs better when temperature as a weather parameter is introduced as an additional input variable. It is worthwhile to notice that the prediction accuracy is degraded significantly on all days when no weather information is given to the adopted models.

Table 2: Effect of temperature as a weather parameter on the performance of best chosen load predictor

Date	Performa-nce metrics	Effect of temperature on prediction error	
		Without considering temperature	With temper-ature
16/10/09	Max(APE)	9.71	10.92
	MAPE (%)	3.67	3.64
17/10/09	Max(APE)	7.86	5.96
	MAPE (%)	2.98	2.60
18/10/09	Max(APE)	7.24	7.61
	MAPE (%)	2.40	2.19
19/10/09	Max(APE)	6.77	5.51
	MAPE (%)	2.55	2.38
20/10/09	Max(APE)	15.68	13.39
	MAPE (%)	4.13	3.98
21/10/09	Max(APE)	12.26	13.11
	MAPE (%)	4.16	4.24
22/10/09	Max(APE)	16.01	15.75
	MAPE (%)	4.271	4.04

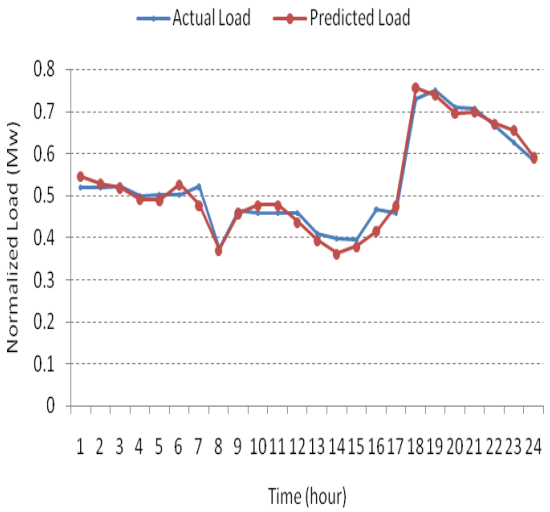

Fig.3:Comparison of the actual load and the predicted load for Friday (16-Oct. 2009) without considering weather variables.

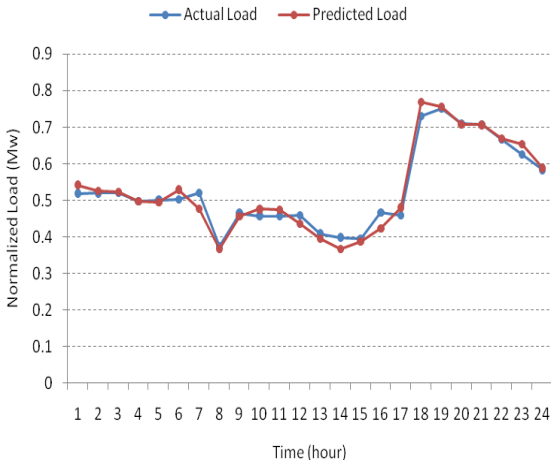

Fig.4: Comparison of the actual load and the predicted load for Friday (16-Oct. 2009) considering with temperature.

From the figures (3 & 4), it is observed that, prediction accuracy is improved when temperature as an additional input variable is considered .However; prediction performance is degraded reasonably when no weather information is given to the RNNs.

VI. CONCLUSION

The major contribution of this research is the increase in the one-day-ahead prediction accuracy in all seasons by employing the proposed combinatorial model of wavelet and RNNs. The exhaustive experimentation is made to explore the best RNN on different frequency component according to the characteristics of each component and finally, prediction is achieved by adding the predictions of best RNNs on different frequency components. The proposed technique offers reliable and encouraging results.

The adopted models in the proposed technique are evaluated with different weather information in order to judge the effect of a particular weather parameter on accurate load prediction. It has been observed from Table 2 that the DMAPE and maximum APE are less when lone predicted weather parameter such as temperature was introduced as one of the input variable.

Finally we could conclude that the proposed novel combination of wavelet and RNN for STLP considering the effect of weather parameters with systematic design procedure of optimal neural network for addressing, one-day-ahead load prediction provides more accuracy than the existing methodologies .

REFERENCES:

[1] I. Moghram and S. Rahman, "Analysis and evaluation of shortterm load forecasting techniques , " IEEE Trans. Power Syst. , vol. 4, no. 4.1484-1491. Nov. 1989.

[2] E. Sanchez-Sinencio and C. Lau. Artificial neural networks. Paradigms, Applications and Hardware Implementations. Piscataway,NJ:IEEE Press, 1992.

[3] B.S. Kermanshahi, C. H. poskar, G. Swift, P. McLaren ,W. Pedrycz, W. Buhr and A. Silik, "Artificial neural networks for forecasting daily loads of a Canadian electricity utility"in Proc IEEE 2nd Int. Forum Applications of Neural Networks to Power Systems , 1993, pp. 302-307.

[4] T. W. S. Chow and C. T. Leung, " Neural Networks based short term load forecasting using weather compensation" IEEE Trans Power Syst., Vol. 11, No. 4, pp. 1736-1742, Nov. 1996.

[5] A. K. Saha, S. Chowdhury, S. P. Chowdhury, Y. H. Song, and G.A. Taylor," Application of Wavelets in Power System Load Forecasting", in Proc. IEEE Power Eng. Soc. General Meeting, 2006.

[6] Y. Bi. J. Zhao and D. Zhang, "Power load forecasting algorithm based on wavelet packet analysis" in Proc. IEEE Int. Conf. Power system technology, 2004, pp. 987-990.

[7] D. Tao, W. Xiuli, and W. Xifan, "a combined model of wavelet and neural network for short term load forecasting," in Proc. IEEE Int. Conf. Power system technology, 2002, pp. 2331-2335.

[8] A. J. R. Reis and A.P.A. da Silva, "Fearure extraction via multi resolution analysis for short term load forecasting, " IEEE Trans Power Syst., Vol. 20, No. 1, pp. 189-198, Feb. 2005.

[9] C.K.Chui,An introduction to wavelets .New York: Academic,1992,pp 6-18.

[10] S.Mallat," A theory for multiresolution signal decomposition –the wavelet representation,"IEEE trans.Pattern Anal.Mach.Intell,vol.11,no.7,pp.674-693,Jul.1989.

PRATIBHA: INTERNATIONAL JOURNAL OF SCIENCE, SPIRITUALITY, BUSINESS AND TECHNOLOGY (IJSSBT), Vol. 1, No.1, March 2012
ISSN (Print) 2277—7261

Human Power: An Earliest Source of Energy and It's Efficient Use

K. S. Zakiuddin[1], H. V. Sondawale[2], J. P. Modak[3]
[1]Dean (Academics), Priyadarshini College of Engineering, Nagpur-440001, India
[2]MED, Smt. Rajshree Mulak College of Engineering for Women, Nagpur-440009, India
[3]Dean (Research and Development), Priyadarshini College of Engineering, Nagpur-440001, India
Emails: [1]qszaki1@rediffmail.com, [2]hvsondawale@rediffmail.com, [3]jpmodak@gmail.com

Abstract: This paper discusses the importance of human power from the earliest times to the present and its future scope. As the use of natural fuel is incresed due to industrial development, it's storage going to end. We need to come with alternate source of energy, i.e non conventional energy. Human power credits its importance in search of an alternative source of energy as it fulfills the requirement of renewable source of energy. More effective use of human power can do by using mechanisms. The technology used to transmit human power to the working unit is termed as human powered machine. The appropriate and most effective technology to use human power efficiently is bicycle technology. In bicycle technology the operator uses the pedal to operate the machine and transmits power through crank, chain and freewheels to the working unit. This machine widely can be used to generate electric power, to operate various home appliances, to drive water pump, harvesting activities in agriculture and for physical fitness.

Keywords: Human Power machine, Bicycle Technology, Dinapod, Flywheel.

I. INTRODUCTION

Manual work involves the natural movements of a human with regards to direction, speed and frequency. A man exerts his physical strength directly by walking, pushing, pulling, pressing, lifting, carrying and throwing activities [1]. When there is a restricted use of natural movements, it causes more fatigue. Also the repetitive movements without an implement results in laborious and tedious task. It recommends the use of tools and equipments to reduce fatigue and to improve human efficiency.

II. NECESSITY OF HUMAN POWERED MACHINES

Growing demands for energy, coupled with expiable natural resources, has resulted in a demand for the development of renewable energy sources. A renewable energy is the energy available in natural form can be replaced by another form by the natural or artificial processes. In natural form it is not in usable form, so some devices are required to transform the energy in usable form. There are so many sources which are qualified as renewable energy sources e.g. solar, water, tides, geothermal, biomass, wind etc. and having endless existence.

Some limitations are noted down to use these energy sources. It requires favorable local geographical and climatic conditions to use efficiently. Also the energy sources required costly equipments to transform the energy in usable form. The equipments like water turbines, windmills, solar energy collectors etc. and also storage media are out of the coverage of general people. The property of endless existence make the renewable energy sources important, but the high initial andmaintenance cost of the equipments is the great obstacle to use these sources.

It's a present need to find out an alternative to these renewable energy sources which will be suitable to use any time and at any place and which is reachable to general user. Human power is one such form of renewable energy that has been used historically to varying degrees. Direct application of human power is

III. HUMAN POWERED MACHINES

These are the human power magnification units driven manually, the units may be driven by hand or foot. Thus, the human powered machines can be categorized as

1. Hand Operated Human Powered Machines: These machines are operated by hand and are available in the following forms
   - i. Hand Crank with Gear Transmission Unit: Rotary motion of crank is transmitted through gear train. Gear train may be used to rise speed and/or torque, e.g. Sugarcane Juice extractor.
   - ii. Hand Crank with Chain Drive: Rotary motion of crank is transmitted through crank and chain drive as in bicycle, e.g. Tri-cycle for orthopedically handicapped person.

2. Foot Operated Human Powered Machines: These machines are operated by foot and following Two basic forms of foot operated human powered machines are available
   i. Treadle Powered Unit: To drive treadle powered unit operator uses one foot to pedal the machine. These machines are available with following mechanical arrangements,
      - Treadle Powered Unit with Crank, Connecting Rod: The oscillating motion of pedal is converted in to rotary motion through crank and connecting rod and then is transmitted to processing unit. Chain and crank or belt and pulley may be used for further transmission, e.g. Sewing Machine

   ii. Bicycle Technology: The rotary motion of foot pedal is transmitted through crank, chain and sprocket to the processing unit.

IV. THE DYNOPOD [2]

Bicycles can sometimes be adapted to drive the devices mentioned above, but the result is often inefficient. It is frequently cheaper in initial and maintenance costs to use a properly designed and constructed dynapod. A dynapod is a portable pedaling device that consists of a stand, saddle, handlebar, pedals, and sprocket wheel. The name comes from the Greek words for "power" and "foot." Dynapod power varies according to the size and fitness of the operator and the length of time spent pedaling.

There are three kinds of dynapods:

1) A one-person dynapod that utilizes belt drive. It can be built either with or without chain drive.

2) A two-person dynapod that can be pedaled either by one person at a time, or by two people together. It is also possible to fit a special adaptor so that a direct shaft drive leads off the unit and powers a flour mill or other machine. (When this is done, only one person can pedal at a time.)

3) A one-person dynapod that has belt drive, chain drive, and direct drive. It is very similar to the two-person dynapod.

The two-person dynapod illustrated below (Figure 5) has been attached to a grain mill, but the unit can be adapted to a wide variety of uses. The dynapod frame can be made of wood or welded steel, depending on cost and availability of materials. Heavily weighted flywheel provides extra power and smoothes out the pedal stroke, reducing operator fatigue.

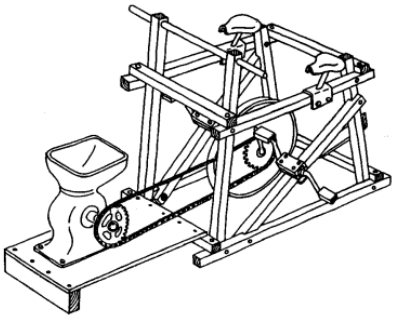

Fig No. 1: Two Person Dynapod with Chaindrive operating a Grain Mill.

V. HUMAN POWER FLYWHEEL MOTOR CONCEPT [3, 4]

The evolved machine system comprised of three subsystems namely (i) Energy Unit : Comprising of a suitable peddling mechanism, speed rise gear pair and Flywheel conceptualized as Human Powered Flywheel Motor (HPFM) (ii) Suitable torsionally flexible clutch and torque amplification gear pair and (iii) a process unit. The suggested machine system uses human energy achieved by peddling and stores this energy in a flywheel at an energy-input rate convenient to the peddler. After storing the maximum possible energy in the flywheel (peddling time could be 1-2 minutes) the same can be made available for the actuation of any process unit by making available the energy stored in the flywheel through a suitable clutch and torque-amplification if needed. Thus the flywheel will decelerate depending on the actual resisting torque offered by the process. It implies that the peddler does not pedal while the flywheel is supplying energy to the process-unit.

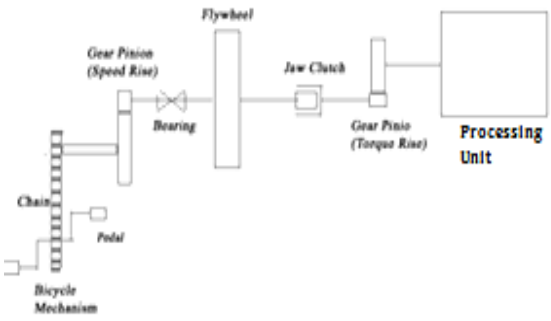

Fig No. 2: Human Powered Flywheel Motor Concept

VI. APPLICATIONS OF HUMAN POWERED MACHINES

1. **Domestic Use:**
   A bicycle-powered soap-making machine,Pedal-powered and hand-cranked grain mills, Coffee mills or Coffee pulpers, Food mills, Strainers and Juicers, Ice cream makers , Washing Machine, Sewing Machine, Water Pump, etc.

2. **Commercial and Industrial Use:**
   Hand-Cranked tool Sharpeners, Pedal Power Grinders and Tool Sharpeners, Foot Powered Scroll Saws, A Stationary Bicycle and Dual Wheel Bench Grinders, A Treadle Powered Lathe, Potter's Wheel, Tire Pumps, etc.

3. **Agricultural Use:**
   Pedal Operated Chaff Cutters, Hand Operated Threshers, Pedal Operated Threshers, Treadle Powered Threshers, Hand Operated Winnowers, Pedal Operated Winnowers, Pedal Operated Irrigation Pumps, Cultivators, Seeders, etc.

4. **Transportation:**
   Bicycle, Bicycle Trailers, Cycle Rickshaw, Hand Cranked Tri-cycle, etc.

5. Electrical Generator: A Pedal Operated AC/DC Electrical Generator Unit.

6. Physical Fitness: A Bicycle Unit for Physical Fitness.

VII. CONCLUSION

From above discussion it can be concluded as

1. Human power is easy to use and no need of special training.
2. As no combustion of fuel takes place so no air pollution.
3. Human powered machines can be manufactured locally.
4. Low initial and maintainance cost.
5. Self dependent source of energy.
6. Best alternative source of energy.

REFERENCES

[1] H. J. Hopfen (1969): Farm Implements for Arid and Tropical Regions Published by Food and Agriculture Organization of the United Nations, Via delle Terme di Caracalla 00100 Rome, Italy. Published in AT Microfiche Reference Library, pp.150

[2] David Gordon Wilson (1986): Understanding Pedal Power, A Technical Paper-51, Published in Volunteers in Technical Assistance, ISBN: 0-86619-268-9, Published by VITA, 1600 Wilson Boulevard, Suite 500, Arlington, Verginia-22209 USA.

[3] J. P. Modak (1982): Manufacture of Lime-Flyash-Sand Bricks using Manually Driven Brick Making Machine, Project Report, Project sponsored by MHADA, Mumbai, Emeritus Professor of Mechanical Engineering and Dean (R&D) Priyadarshini College of Engineering, Near Central Reserve Police Force Campus, Hingna Road, MIDC, NAGPUR 440019 (INDIA), pp 1-50.

[4] Zakiuddin Sayed Kazi, J.P. Modak (2010): Design and Development of Human Energized Chaff Cutter, New York Science Journal, PP. 104-108.

[5] www.ferrari-tractors.com: A treadle powered machine FT 370, Gridley, CA 95948

PRATIBHA: INTERNATIONAL JOURNAL OF SCIENCE, SPIRITUALITY, BUSINESS AND TECHNOLOGY (IJSSBT), Vol. 1, No.1, March 2012
ISSN (Print) 2277—7261

Signal Processing based Wavelet Approach for Fault Detection of Induction Motor

A.U.Jawadekar[1], Dr G.M.Dhole[2], S.R.Paraskar[3]
Department of Electrical Engineering, S.S.G.M. College of Engineering Shegaon. (M.S.),44203, India.
Email:anjali.jawadekar@ gmail.com[1],gmdhole@gmail.com[2],srparaskar@gmail.com[3]

Abstract: Condition monitoring and fault detection of induction motor have been challenging task for engineers and researchers mainly in industries as faults and failures of induction motor can lead to excessive downtimes and generate large losses in terms of maintenance and lost revenue. This motivates motor monitoring, incipient fault detection and diagnosis. Online monitoring of induction motor can lead to diagnosis of electrical and mechanical faults. Most recurrent faults in induction motor are turn to turn short circuit, bearing deterioration, and cracked rotor bar.
This paper presents a signal processing based frequency domain approach using wavelet transform and Artificial neural network based algorithm for multiple fault detection in induction motor .Motor line currents are captured under various fault conditions .DWT is used for data processing and this data is then used for testing and training of ANN. Three different types of wavelets are used for signal processing to demonstrate the superiority of Db4 wavelet over other standard wavelets for accurate fault classification of induction motor. Experimentation results obtained proves the suitability of proposed algorithm.

Keywords : Induction Motor, Discrete wavelet transform, Multiple fault detection.

I. INTRODUCTION

Induction motor possesses advanced features such as simple construction, small volume and light weight, which leads to their wide use in engineering applications. In spite of their robustness and reliability they occasionally fail and hence require constant attention. It is well known that faults on induction motor causes interruption of manufacturing process which induces a significant loss for the firm. Major faults in induction motor includes stator winding faults, bearings faults, rotor faults and external faults such as voltage unbalance ,phase failure, single phasing. Bearing faults are responsible for approximately one fifth of all faults .Interturn short circuit in stator winding stands for nearly one third of reported faults. Broken rotor bar and end ring faults represent around 10 percent of induction motor faults. Early fault detection allows preventive maintenance to be scheduled for machines during scheduled downtimes and prevent an extended period of downtime caused by extensive motor failure, improving the reliability of motor driven system. With proper system monitoring and fault detection schemes, cost of maintaining the motors can be greatly reduced, while the availability of these machines can be significantly improved. Many Engineers and Researchers have focused their attention on incipient fault detection and preventive maintenance in recent years. Different methodologies based on current and vibration spectral analysis have been proposed using FFT and DWT for induction motor preventive monitoring of specific faults. FFT analysis has been utilized by Habetler et .al[1-2] for detecting thermal overload and bearing faults, analyzing the motor current signals. In [3] detection of broken rotor bar is done by applying Fourier transform, to improve the diagnosis and to permit the detection of incipient rotor bar , analysis is completed by Hilbert transform. Stator currents are analyzed via wavelet packet decomposition to detect bearing defects in [4]. A fault indicator, so called swing angle for broken rotor bar and interturn fault is investigated in [5]. This fault indicator is based on rotating magnetic field pendulous oscillations concept in faulty squirrel cage induction motor. FFT vibration analysis is used for detecting cracked rotor bar and inner race and outer race bearing defects. [6,7]. Time frequency domain techniques have been used for fault diagnosis of induction motor, which includes STFT,FFT, high resolution spectral analysis[8-12].Online induction motor diagnosis system using MCSA with signal and data processing algorithm is used to diagnose induction motor faults such as breakage of rotor bars, bearing defects and air gap eccentricity. [13]. Detection of broken rotor bars and interturn short circuit in stator windings based on analysis of three phase current envelopes of induction motor using reconstructed phase space transform is proposed in

[14]. Artificial Intelligence play a dominant role in field of conditioning monitoring and different techniques such as neural network, fuzzy inference systems, expert system, adoptive neural fuzzy inference system and genetic algorithm are being widely used for feature extraction and classification purpose [16 12]. It can be summarized that there are countless techniques for diagnosis and prognosis of specific induction motor faults, most of these techniques are applied offline, which demands a generalized technique that allows online multiple fault detection.

This paper presents an application of DWT and ANN to diagnose different faults in induction motor such as bearing and inter turn faults based on the analysis of three phase stator currents in both healthy and faulty condition**.** Since choice of particular wavelet plays a vital role for extracting features of generated harmonics, therefore an attempt is made to investigate threee different types of wavelets to establish the superiority of Db4 wavelet over other standard wavelets namely Daubechies(Db2 and Db6). Experimentation results demonstrate the suitability of proposed algorithm for multiple fault detection in induction motor namely inner and outer race bearing defects, stator Interturn short circuit, with 100 % classification accuracy.

II. WAVELET TRANSFORM

Wavelet analysis is about analyzing the signal with short duration finite energy functions which transform the considered signal into another useful form. This transformation is called Wavelet Transform (WT). Let us consider a signal *f*(t), which can be expressed as-

$$f(t) = \sum_{l} a_l \ \varphi_l(t) \qquad (1)$$

Where, l is an integer index for the finite or infinite sum. Symbol a_l are the real valued expansion coefficients, while $\varphi_l(t)$ are the expansion set.

If the expansion (1) is unique, the set is called a basis for the class of functions that can be so expressed. The basis is orthogonal if-

$$\langle \varphi_l(t), \varphi_k(t) \rangle = \int \varphi_l(t)\varphi_k(t)dt = 0 \quad k \neq l \qquad (2)$$

Then coefficients can be calculated by the inner product as-

$$\left\langle f(t), \varphi_k(t) \right\rangle = \int f(t)\, \varphi_k(t)\, dt \qquad (3)$$

If the basis set is not orthogonal, then a dual basis set $\varphi_k(t)$ exists such that using (3) with the dual basis gives the desired coefficients. For wavelet expansion, equation (1) becomes-

$$f(t) = \sum_{k}\sum_{j} a_{j,k}\ \varphi_{j,k}(t) \qquad (4)$$

In (4) j and k are both integer indices and φ_{jk} (t) are the wavelet expansion function that usually form an orthogonal basis. The set of expansion coefficients a_{jk} are called Discrete Wavelet Transform (DWT).

There are varieties of wavelet expansion functions (or also called as a Mother Wavelet) available for useful analysis of signals. Choice of particular wavelet depends upon the type of applications. If the wavelet matches the shape of signal well at specific scale and location, then large transform value is obtained, vice versa happens if they do not correlate. This ability to modify the frequency resolution can make it possible to detect signal features which may be useful in characterizing the source of transient or state of post disturbance system. In particular, capability of wavelets to spotlight on short time intervals for high frequency components improves the analysis of signals with localized impulses and oscillations particularly in the presence of fundamental and low order harmonics of transient signals. Hence, Wavelet is a powerful time frequency method to analyze a signal within different frequency ranges by means of dilating and translating of a single function called Mother wavelet.

The DWT is implemented using a multiresolution signal decomposition algorithm to decompose a given signal into scales with different time and frequency resolution. In this sense, a recorder-digitized function a0(n), which is a sampled signal of f(t), is decomposed into its smoothed version a1(n) (containing low-frequency components), and detailed version d1(n) (containing higher-frequency components), using filters h(n) and g(n), respectively. This is first-scale decomposition. The next higher scale decomposition is now based on signal a1(n) and so on, as demonstrated in Figure.1

PRATIBHA: INTERNATIONAL JOURNAL OF SCIENCE, SPIRITUALITY, BUSINESS AND TECHNOLOGY (IJSSBT), Vol. 1, No.1, March 2012
ISSN (Print) 2277—7261

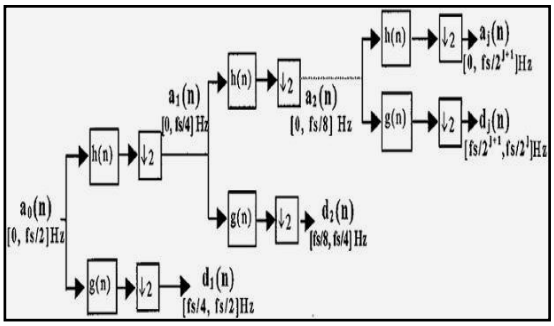

Figure:1

The analysis filter bank divides the spectrum into octave bands. The cut-off frequency for a given level j is found by –

$$fc = fs / 2^{j+1} \quad (5)$$

where fs is the sampling frequency. The sampling frequency in this paper is taken to be 10 kHz.

III. EXPERIMENT SETUP

For experimentation and data generation a 2 H.P, 3 phase, 4 pole, 415 volts, 50 Hz squirrel cage induction motor is used for staging different faults on the motor. Experimental set up is shown in Figure 2

Figure. 2:Experimental Set-up

Motor used for experiment has 24 coils and 36 slots. Each phase comprising of 8 coils has 300 turns. Each phase is tapped where tapping is made after 10 turns, starting from star point (neutral). Tapings are drawn from coils where each group comprises of approximately 70 to 80 turns. Spring and belt arrangement is used for mechanical loading of motor. With 10 Khz sampling frequency 200 samples per cycle are recorded for different load conditions and at different mains supply conditions for following cases.

1. Healthy: 2 H.P motor is fed from three phase balanced supply. Load on the motor is varied from 75 % of full load to full load with spring and belt arrangement .Stator current signals and phase voltages are captured for no load, 75 % of full load up to full load conditions.

2: Bearing Defects (Inner and Outer Race): Motor under test comprises of two bearings number 6204 and 6205. Bearings having natural defects caused by regular operation of motor are used in experimental study. Motor is fitted with different combinations of bearings having inner race or outer race defects. Stator currents and voltages for each combination of bearing are captured to compare it with healthy bearing condition. Different experiments are conducted with different combinations of rear side and load side bearings to assess the effect of bearings on performance of motor.

3: Stator Interturn Short Circuit
For this case study, stator windings of induction motor are modified to have several accessible tappings that can be used to introduce inter turn short circuits. For this experimentation phase A is tapped, where each tapping is made after 10 turns. Different experimentations are conducted with 10 turns, 20 turns and 30 turns short circuited in phase A of motor and for different loading conditions, phase voltage and stator current signals are recorded.

IV. FEATURE EXTRACTION USING DWT.

Current signals obtained for abnormal conditions of motor are similar to normal motor signals. Data acquired does not directly reveal any information usable for fault detection. For feature extraction Db4 is used as a mother wavelet since it has good performance results for fault analysis. To demonstrate the effectiveness of Db4 for accurate fault classification four different wavelets are used. Based on sampling rate of 10 KHz, current signals are decomposed into five levels using different wavelet transforms to obtain MRA coefficients. Table I gives range of frequency band for detail coefficient up to five levels.

Table I: Frequency levels of Wavelet Functions Coefficients

Level number	Wavelet component	Component type	Frequency band (Hz)
1	d1	Detail	5000:2500
2	d2	Detail	2500:1250
3	d3	Detail	1250:625
4	d4	Detail	625:312.5
5	d5	Detail	312.5:156.25
5	a5	Approximation	156.25:78.125

Figure 3 shows the decomposition of stator current up to five level for healthy and for different fault conditions.

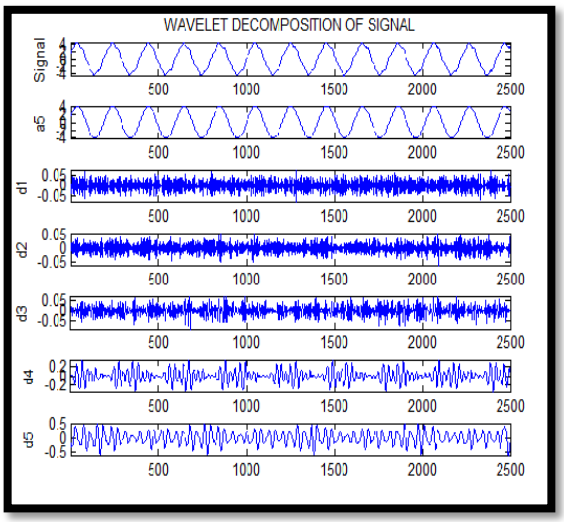

Figure 3.a Wavelet decomposition of stator current for healthy state of motor

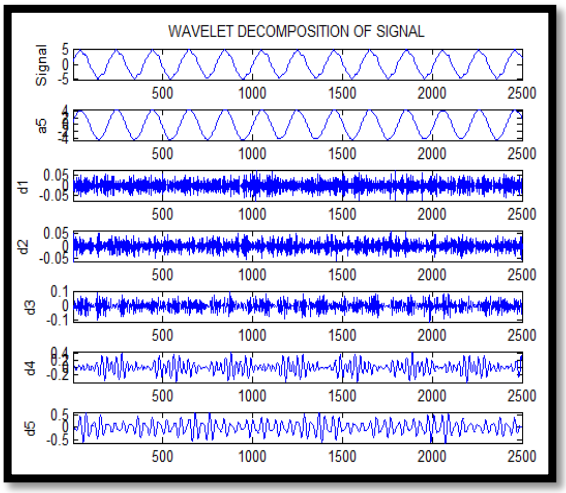

Figure 3.b Wavelet decomposition of stator current for the motor under bearing fault

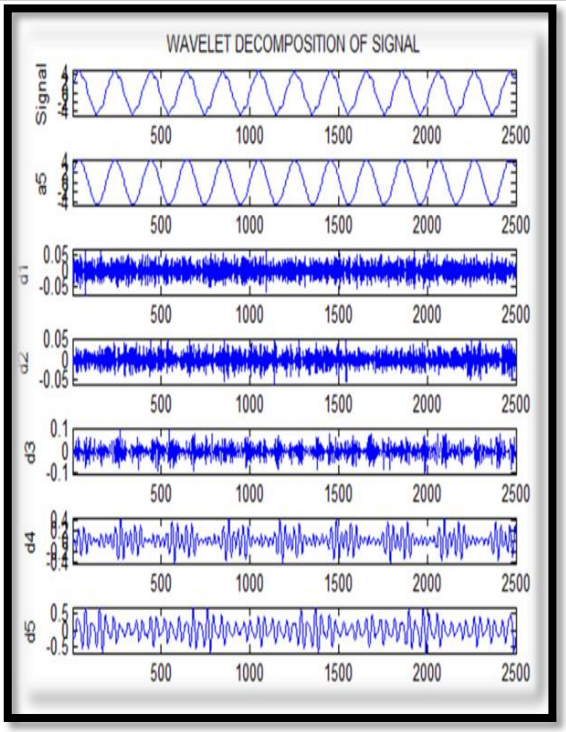

Figure 3.c Wavelet decomposition of stator current for the motor under stator interturn fault

These wavelet coefficients extracted from raw transient signal contains large amount of information. Though this information is useful, it is difficult for ANN to train that large data, another alternative is to input the energy content in the detailed coefficient according to Parseval's theorem. Parseval's theorem relates the energy of current signal to the wavelet coefficient. Norm of energy of signal can be partitioned in terms of expansion coefficients. The energy of signal is partitioned at different resolution levels in different ways depending on the signals to be analyzed.

Amongst different decomposition level levels 3-5 in MRA are seen to be the most dominant band hence feature extraction from level 3-5 could be effectively realized using MRA analysis technique. Energies of level d3-d5 are computed and used as input to neural network. Neural network is trained and further used for induction motor fault classification.

V. RESULTS AND DISCUSSION

An ANN with its excellent pattern recognition capabilities can be effectively employed for the fault classification of three phase induction motor. In this paper 3 layers fully connected FFANN is used and trained with supervised learning algorithm called back

propagation. FFANN consist of one input layer, one hidden layer, and one output layer. With respect to hidden layer it is customary that number of neurons in hidden layer is done by trial and error. Same approach is used in proposed algorithm. Randomized data is fed to neural network and number of processing elements in hidden layer is varied.

TanhAxon transfer function and Momentum learning rule is used for training the network and average minimum square error MSE on training and testing data is obtained. Momentum=0.7, data used for training purpose is 60 %, for testing is 40 %, step size in hidden layer and output layer=0.1.
Energies of level d3-d5 of stator currents are computed, and fed as input to neural network. Output layer consists of five neurons representing healthy, bearing fault, and stator Interturn short circuit condition. With these assumptions variation of percentage accuracy of classification for induction motor under healthy, bearing fault, Interturn fault condition with respect to number of processing elements in hidden layer is obtained. In order to demonstrate the superiority of Db4 wavelet, detail analysis of fault classification is done using different wavelets. Results tabulated in table II validate the efficacy of Db4 for fault classification.

Table II: Fault Classification Percentage Accuracy for Db4 Wavelet

Number of Processing Elements	Percentage Accuracy of Classification		
	Healthy	Bearing Fault	Interturn Fault
1	20	100	100
2	33	100	100
3	100	75	100
4	100	100	100

Figure 4 shows variation of percentage accuracy of classification with number of processing elements in hidden layer for the same

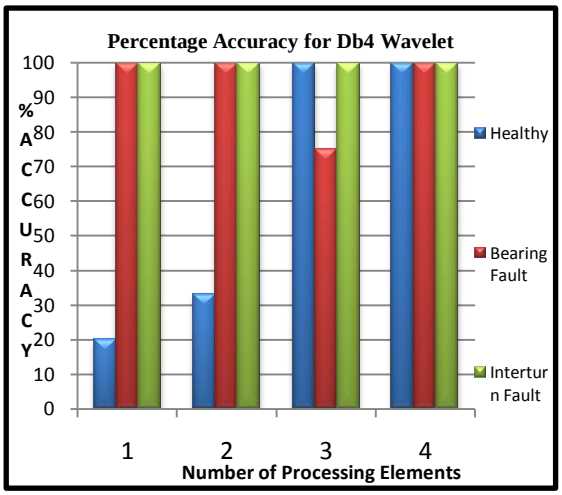

Figure 4: Percentage Accuracy with respect to number of processing elements

Table III-and IV shows the result obtained using other wavelets. From the results tabulated in table II to IV it is apparent that with four number of processing elements in hidden layer 100 percent classification accuracy is obtained with Db4,whereas other wavelets for the same number of processing elements fails to give 100 percent classification accuracy.

Table III: Fault Classification Percentage Accuracy for Db2 Wavelet

NO of Processing Elements	Percentage Accuracy of Classification				
	Healthy	Bearing Fault	Interturn Fault	Rotor bar crack	Voltage Unbalance
1	10	10	100	100	10
2	100	30	100	75	100
3	20	100	100	100	80
4	66	75	100	100	100
5	50	80	100	100	80
6	50	100	100	50	100
7	100	83	100	100	100
8	100	75	100	100	90
9	100	100	100	100	90

Table IV: Fault Classification Percentage Accuracy for Db6 Wavelet

NO of Processing Elements	Percentage Accuracy of Classification				
	Healthy	Bearing Fault	Interturn Fault	Rotor bar crack	Voltage Unbalance
1	10	100	55	100	10
2	33	50	100	100	100
3	100	100	83	100	66
4	100	80	100	90	100
5	100	83	100	100	80
6	50	100	100	100	100
7	100	75	100	100	100
8	100	75	100	100	100
9	100	100	100	100	75

VI. CONCLUSION

This paper proposes new approach to fault detection and classification of three phase induction motor, validating its effectiveness through different cases of study that considered the motor under diverse fault conditions like faulty bearings and stator interturn fault. Line current signals recorded under healthy and faulty conditions are passed through series of signal processing procedures .Subsequently DWT is utilized to extract the features which derive rich information about the fault from stator current signals. Since selection of particular wavelet plays an important role for extracting dynamic features of generated harmonics, therefore an investigation is carried out using three different wavelets to establish the efficacy of Db4 over other wavelets. Thus feature extraction using Db4, Feed Forward Artificial Neural Network with Momentum learning rule and TanhAxon transfer function and with four processing elements in hidden layer is the best network to classify multiple faults in induction motor.

REFERENCES

[1] T.G Habetter ,R.G.Hartley, R.M.Tallan, R.Sang Bin,L.Obaid &T.Stack,"Complete . Current based Induction motor condition monitoring , stator ,rotor, bearings, and load in Technical proceedings CIEP 2002 IEEE 2002, pp-3-8

[2] M.E.H. Benbouzid H. Nejjari R.Beguenane ,M.Vieira,"Induction motor asymmetrical fault detection using advanced signal processing Techniques", Transaction on Energy conversion IEEE volume 14,1999,pp147-152.

[3] G.Didier,E.Ternisien,O.Caspary,and H.Razik ,"A New Approach to Detect Broke n Rotors Bars in Induction Machines by Current Spectrum Analysis", Mechanical Systems and Signal Processing 21,2 (2007) pp1127-1142

[4] Levetnt Eren and Michael J Dvaney ,"Bearing damage detection via Wavelet packet decomposition of stator current" , IEEE Transaction on Instrumentation and measurement vol 533 N0-2 PP 431-436 April 2004

[5] Behrooz Mirafzal ,Nabeel A.O. Demerdash, "An Innovative Methods of Induction Motor Interturn and Broken bar Fault diagnostics IEEE Transactions on Industry Application , vol 42, No2 ,pp 405-410 March April 2006

[6] H.Oeak ,K.A.Loparo, "Estimation of running speed and bearing defect frequencies of an induction motor from vibration data.", Mechanical systems and signal processing Elsevier vol 18 2004 pp514-533

[7] J.J.Rangel Magdaleno,R.J.Romero Troncoso ,L.M. Contreras Medina and A.Garcia Perez ,"FPGA implementation of a novel algorithm for on line bar breakage detection on induction motor in proceedings of IMTC 2008 ,IEEE 2008,pp-720-725.

[8] Aderiano M.da Silva,Richard J.Povinelli and Nabeel A.O Demerdash,"Induction Machine broken bar and stator short fault diagnostic based on three phase stator current envelope" IEEE Transaction Ind Electronics , vol 55 no 3, pp 1310-1318 March 2008.

[9] H.Douglas,P Pillay ,A.K.Ziarani, " A new algorithm for transient motor current signature analysis using wavelet" IEEE transaction Industrial Application volume 40, no 5 ,pp1361-1368 september/October 2004

[10] M.E.H.Benbouzid et al, Induction motor's detection and localization using stator current advancd signal processing technique, "IEEE transaction on Power Electron vol 14, no1 ,pp 14-22 January 1999

[11] T.W.S.Chow & S.Hai , Induction Machine fault diagnostic analysis with wavelet technique, IEEE transaction Ind Electron vol 51,no 3 pp558-565 June 2004

[12] W.Thomson & M Fenger ," Current Sigature analysis to detect imduction motor faults IEEE Industrial Application Mag-vol 7, no 4 pp26-34 July//August 2001.

[13] Jee Hoon Jung,Jong –Jae Lee ,Bong Hwan Kwan, Member IEEE ,"Online diagnosis of induction motor using MCSA", IEEE Transaction on Industrial Electroncs vol 53, No-6 pp 1842-1852 Dec 2006

[14] A.M.Daselva ,R.J. Poveneli ,N.A. Odemer Dash ",Induction Machine Broken bar and stator current short circuit fault diagnosis based on three phase stator current envelope " IEEE transaction on Industrial Electronics ,2008 pp1310-1318.].

[15] Tian Han ,Bosuk,,Yang ,Won –Ho-Choi and Jae Sikkim ,"Fault diagnosis system of Induction Motor based on Neural Network and Genetic Algorithm using Stator Current signals , Hindavi publishing Corporation International Journal of Rotating Machinery vol 2006 Article I.D. 61690 pp 1-13.

[16] Paya.P.A Esal I. "Artificial Neural Network based fault diagnostics of rotating machinery using Wavelet Transforms as preprocessor ", Mechanical Systems and Signal Processing 1997 No 11, pp 751-765

[17] F.Zidani M.E.H. Benbouzid D.Dialllo ,M.S. Nailsaed ," Induction Motor Stator fault diagnosis by current Concordia Pattern based Fuzzy decision system IEEE Transaction on Energy Conversion 2003 pp 469-475.

PRATIBHA: INTERNATIONAL JOURNAL OF SCIENCE, SPIRITUALITY, BUSINESS AND TECHNOLOGY (IJSSBT), Vol. 1, No.1, March 2012
ISSN (Print) 2277—7261

Feature Extraction of Magnetizing Inrush Currents in Transformers by Discrete Wavelet Transform

Patil Bhushan Prataprao[1], M. Mujtahid Ansari[2], and S. R. Parasakar[3]
[1]Dept of Electrical Engg., R.C.P.I.T. Shirpur (MS) India
[2]Dept. of Electrical Engg. SSBT's C.O.E.T, Jalgaon (MS) India
[3]Dept. of Electrical Engg., S. S. G.M.C.E, Sheagaon. (MS) India
Emails: [1]bhushan.rcpit@gmail.com, [2]mujtahidansari@gmail.com, [3]srparaskar@gmail.com

Abstract: Transformers are essential and important elements of electric power system and their protection is critical. Traditional protection gives only terminal condition on the basis of protection of transformer. Discrimination between an internal fault and a magnetizing inrush current has long been recognized as a challenge for power transformer protection. In this paper a new method based on the Wavelet Transform techniques for discrimination of internal fault from magnetizing inrush current by considering different behavior of the differential current under fault and inrush current conditions is described. Wavelet analysis is about analyzing the signal with short duration finite energy functions. They transform the considered signal into another useful form. Wavelet decomposition is ideal for studying transient signals and obtaining a much better current characterization and a more reliable discrimination. This algorithm has been developed by considering different behaviors of the differential currents under fault and inrush current conditions obtained from test on custom built single phase transformer is presented. A discriminating function and feature extraction is defined in terms of difference of two-peak amplitude of wavelet coefficients in a specific band. This discrimination will aid in development of an automatic detection method and shall give information to predict the failure ahead of time so that the necessary corrective actions are taken to prevent outages and reduce down time. Tests are performed on 2KVA, 230/230Volt custom built single phase transformer. Discrete Wavelet Transform concept is used for feature extraction.

Index Terms: Inrush current, internal fault, second harmonic component power transformer, wavelet transform.

I. INTRODUCTION

Today's world of technology, the power transformer is one of the important links in a power system. Without it, the present power utilities would not at all be feasible [5], [16]. Differential relays are prone to maloperation in the presence of transformer inrush currents. Inrush currents result from transients in transformer magnetic flux .The conventional approach uses the second harmonic component of differential currents to restrain operation of differential relay to avoid tripping during magnetizing inrush conditions [4]. Harmonic restraint methods may not be adequate to prevent differential element operation for unique cases with very low harmonic content in the operating current. Modern methods for differentiating inrush current from fault current, may be required to ensure security without sacrificing fast and dependable operations when energizing a faulted transformer. In the modern power system, high performance relays are required, especially in terms of operating speed. Magnetizing inrush also exhibit a characteristic of peaked wave, which is caused by asymmetric saturation of transformer core. Identifying magnetizing inrush by these characteristics opens a new avenue of research for improving the operating speed of relays [15].

The presence of second harmonic component in the magnetizing inrush current can no longer be used as a means to discriminate between magnetizing inrush current and internal fault, since the second harmonic component may also be introduced during internal fault due to variety of other factors such as current transformer saturation or presence of a shunt capacitor etc [4],[13].

Transformer protection includes transformer inductance during saturation, flux calculated from the integral of voltage, and the

differential current. New methods have been adopted which include ANN, and fuzzy logic. Also, some techniques have been adopted to identify the magnetizing inrush and internal faults [16], [12]. A wavelet-based signal processing technique is an effective tool for power system transient's analysis and feature extraction [4]. Wavelet-based method can use to identify inrush current and internal faults. The second harmonic component is used as a characteristics component of the asymmetrical magnetization peculiar to the inrush. At first, the wavelet transform concept is used. The property of multi resolution in time and frequency provided by wavelets is described, which allows accurate time location of transient components while simultaneously retaining information about fundamental frequency and its lower order harmonics, which facilitates the detection of transformer inrush currents. The technique detects the inrush currents by extracting the wavelet components contained in the line currents using data window less than half power frequency cycle. The results prove that the proposed technique is able to offer the desired responses and could be used as a fast, reliable method to discriminate between inrush magnetizing and power frequency faults [8].In this paper a wavelet-based scheme is developed to identify inrush current and to distinguish it from internal faults. A custom-built single-phase transformer was used to collect the data from controlled experiments. In the experiments different faults were done on both primary and secondary windings of transformer. Method is independent of setting any threshold for discrimination amongst these. A discriminating function and feature extraction is defined in terms of difference of two-peak amplitude of wavelet coefficients in a specific band.

II. WAVELET TRANSFORM

The wavelet transforms associated with fast electromagnetic transients are typically no periodic signals, which contain both high-frequency oscillations and localized impulses superimposed on the power frequency and its harmonics. If signals are altered in a localized time instant, the entire frequency spectrum can be affected. To reduce the effect of non-periodic signals on the DFT, the short-time Fourier transform (STFT) is used. It assumes local periodicity within a continuously translated time window.Fig.1 illustrates the implementation procedure of a Discrete WT (DWT), in which S is the original signal; LPF and HPF are the low-pass and high pass filters respectively. At the first stage an original signal is divided in to two halves of the frequency bandwidth, and sent to both LPF and HPF. Then the output of LPF is further cut in half of the frequency bandwidth and then sent to the second stage, this procedure is repeated until the signal is decomposed to a pre-defined certain level. If the original signal were being sampled at Fs Hz, the highest frequency that the signal could contain, from Nyquist's theorem, would be Fs/2 Hz. This frequency would be seen at the output of the high pass filter, which is the first detail 1; similarly, the band of frequencies between Fs/4 and Fs/8 would be captured in detail 2, and so on. The sampling frequency in this paper is taken to be 10 kHz and Table I shows the frequency levels of the wavelet function coefficients.

Decomposition Level	Frequency Components, Hz
D1	5000-2500
D2	2500-1250
D3	1250-625
D4	625-312.5
D5	312.5-156.25
A5	0-156.25

Table No.1 Frequency levels of wavelet functions coefficients

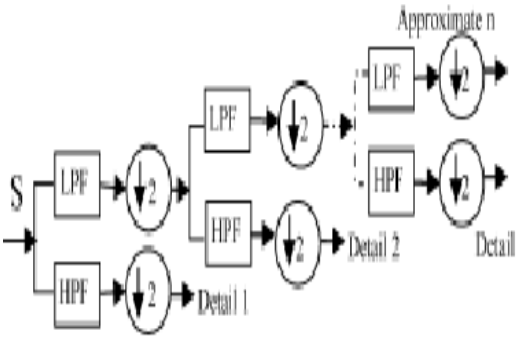

Fig No. 1 Implementation of DWT

II. PROPOSED METHOD

In figure 2, it is quite clear that slope of inrush differential waveform is lower at initial than its slope increases as time passes. The slop of fault differential waveform is higher than its slop decreases as time passes. A high value of slope indicates the presence of high frequency components. These features are independent of the connected power system and depend on the different nature of current and parameters of transformer.

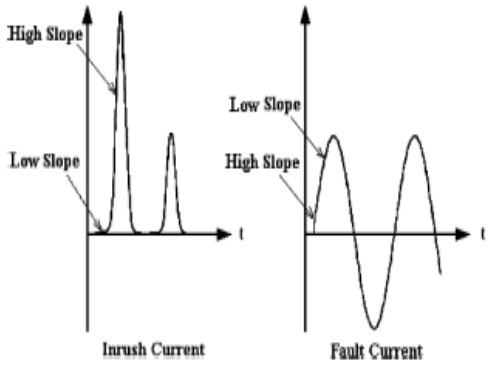

Fig No. 2: Different behavior of fault and inrush current

This significant marked difference between the initial slope of the differential current due to fault and that due to magnetizing inrush current has been used to discriminate between inter-urn fault and magnetizing inrush current. As per the proposed method for internal fault (in one case an inter-turn short circuit) the amplitude of high frequency is large initially and then it decreases. Hence high frequency components are captured in first two levels i.e. D1 and D2, as shown in Fig.3.1.Where as, in case of inrush current the amplitude of high frequency component initially is less and then increases. Therefore, in the first two levels that is D1, D2 nothing is seen where as in D3 high amplitude is observed in Fig.3.2.

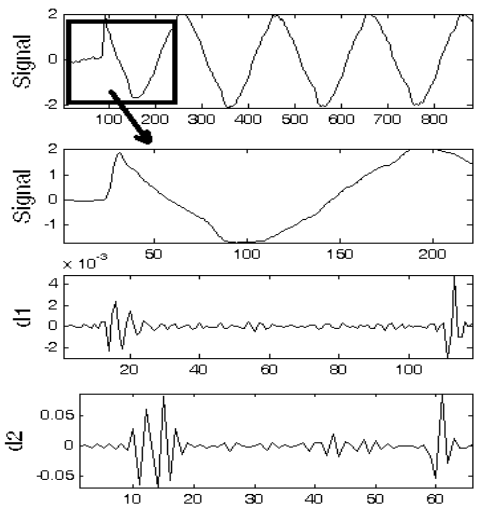

Fig No. 3.1 Illustration of Wavelet decomposition of fault Current

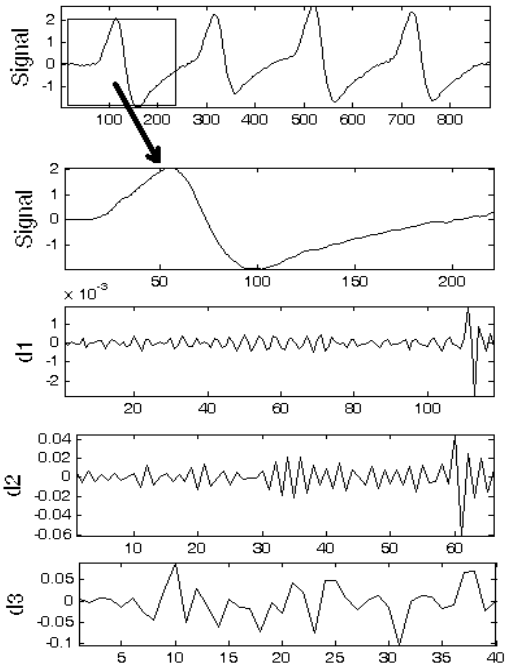

Fig No. 3.2 Illustration of Wavelet decomposition of inrush Current

A simplified flowchart of the proposed algorithm has been shown in Fig 3.3,block (1) implements the calculation of the differential current; the restraining currents are only used at the stage of blocks (1) and (2) to prevent false tripping due to, current-transformer (CT) mismatch, CT error between LV and HV sides and error caused by tap-changer. Block (2) signifies that the relay is activated if any one of three-phase differential currents is over a setting of the differential protection. If the output of block 2 is "Yes", there is an internal fault or inrush current which must be discriminated.

The proposed algorithm commences from block (3) and its aim is to discriminate internal fault from inrush current. Block (3) implements the WT to the differential currents. Block (4) estimates A, B, which are the amplitudes of the two first peak of differential current following the disturbance. The peaks are considered as A and B i.e. the absolute value of differential current. Finally the decision is made by block (5) to discriminate internal faults from inrush currents where in the case of inrush current A<B and in case of internal fault A>B. If an internal fault is detected, the relay will issue a tripping signal; otherwise, the relay will be restrained and does not operate.

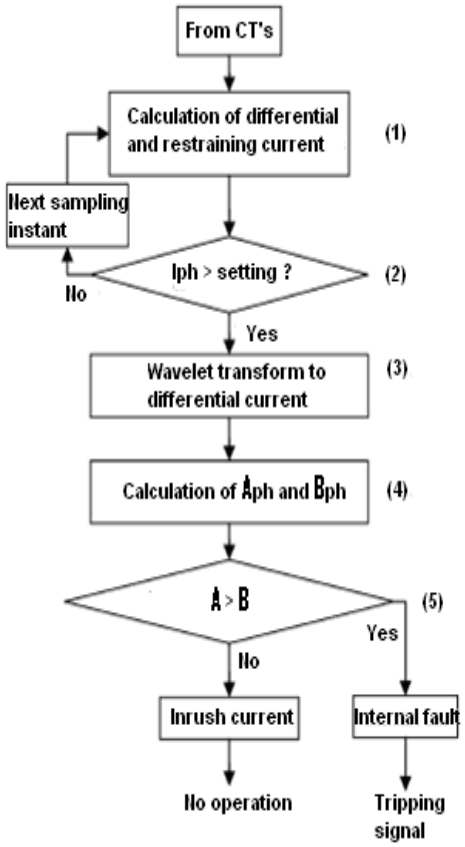

Fig No. 3.3 Flow chart of proposed algorithm

III. EXPERIMENTAL SETUP

The main components of the experiment setup are 230V/230V, 50Hz, 2KVA single phase transformer. The transformer is having 5 tap on primary winding, first four tap after each 10 turns and on secondary having total 27 tap, each of 10 turns. The taps are especially provided for turn to turn fault application. The application of fault on primary, secondary and both winding was done with the help of external contactor. A portable data acquisition system was used to collect the instant of faulted samples.

The Tektronix DSO, TPS 2014 B, with 100 MHz bandwidth and adjustable sampling rate of 1GHz is used to capture the currents. The Tektronix current probes of rating 100 mV/A, input range of 0 to 70 Amps AC RMS, 100A peak and frequency range DC to 100KHz are used. The current and voltage signal were recorded at appropriate sampling rate of 10Kz sample/s. Different cases of inter turn short circuit are staged, considering the effect of number of turns shorted on primary and secondary and load condition. The following experiments were conducted on the custom built transformer.

1. Primary current without load was acquired for healthy condition.
2. Four percentage (10 turns) of primary turns were kept short circuited on load and then the transformer was energized and differential current acquired.
3. The same procedure was also repeated for only secondary winding short-circuited.

The proposed algorithm was tested on the custom-built transformer .The experimental set up is as shown in Fig. 4.

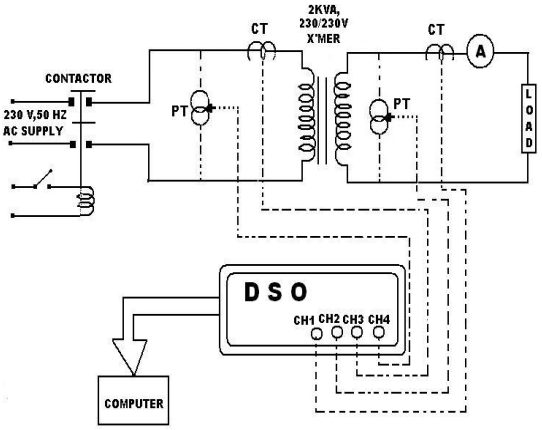

Fig No. 4 Experimental Setup

V. RESULTS AND DISCUSSIONS

Different cases of inrush current and inter turn short circuit were staged on the custom built transformer by varying the parameters, which significantly affects the characteristics of these currents. These parameters are the residual core flux, the voltage angle at the time of switching. Different cases of inter turn short circuit are staged, considering the effect of number of turns shorted on primary and secondary and load condition.

The following experiments were conducted on the custom built transformer.

1. Primary current was acquired without load for healthy condition.
2. Differential current was captured with load and four percent (10 turns) of primary turns were short circuited through contractor .
3. The same procedure was repeated for secondary winding.

Total 180 sets of signals were captured for different cases i.e. inrush and inter turn faults at different mains supply conditions. This captured data was then analyzed for the faults using discrete wavelet transform for classification of

Inrush and faults. Figure 5.1 shows the differential current (represented as 'Signal') due to inter-turn short circuit of 4% winding near to neutral in primary winding, with their detailed coefficients from Wavelet Transform up to D5 level. Here, the daub- 4-mother wavelet is used to obtain the desired wavelet coefficients. In figure 5.1, the respective signal and its |d5| is shown in the next consecutive figures. These figures illustrates usefulness and accuracy of proposed algorithms in classifying the inter turn fault and inrush currents of a transformer. At the bottom of this figure absolute value of d5 is given. The detailed description and interpretation of fig. 5.1 is given below-

a) Original Differential current signal is captured with data acquisition system discussed previously, and represented as 'Signal' in the figure 5.1. The fault is initiated at sample number 557 (Approx.) and it is marked as 'x' in figure.
b) In the fig. 5.1, the absolute value of |d5| as shown in figure, the first two consecutive peak values after the fault instant are the good approximations for the initial slope changes in the fault and inrush current.
c) The absolute value of the coefficients of d5 waveform is shown at the bottom of this figure. In this, A and B are the amplitudes of first two peaks following the disturbance. The fig. 5.1, It is seen that for inter-turn fault A>B. In the event of A>B trip command can be issued in quarter cycle.
d) The features used for diagnosis normally are seen in the high frequency range and not in lower frequency.
e) In the fig. 5.1,it is obvious that the amplitudes of wavelet coefficients in D5 are larger than that of D1-D4. Many wavelets were tried as an analyzing wavelet, but finally Daubochies 4 (Db4) gave encouraging and distinguishing features, magnitude of two consecutive peaks A and B, follows the same relation i.e. A>B.
f) In the fig. 5.2, Inrush current exhibits different behavior or feature than the fault current, though their amplitudes are comparable. Inrush current starts with low slope and increase rapidly afterwards.
g) The acquired inrush current signal is decomposed into five levels. No peaking was observed at the starting instant in d1-d2 level, as appeared in inter-turn fault. But high frequency oscillations can be noted in these levels, as high slope follows the low slope in inrush current.
h) In the fig. 5.2, the d5 and |d5|, the consecutive peaks A and B can be obtained and compared. For inrush, it can noted that A<B.

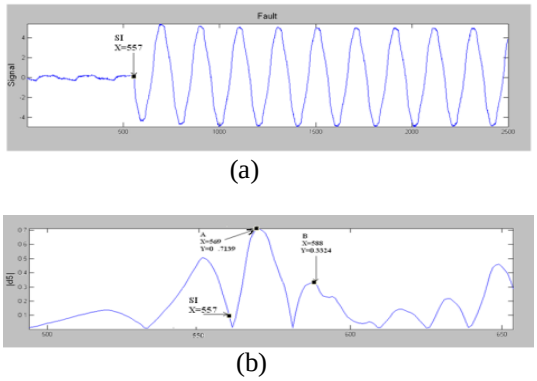

Fig No. 5.1 DWT decomposition of differential fault current (a) Fault current signal (b) |d5| coefficients

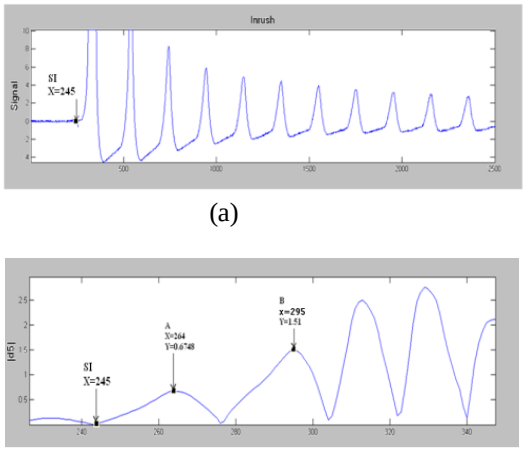

Fig No. 5.2: DWT decomposition of Inrush current (a) Inrush current signal (b) |d5| coefficients

Following the previous discussion, proposed technique does not require any threshold value for discrimination amongst the magnetizing inrush and inter-turn faults in the transformer. The algorithm for the discrimination is presented below-

1. Capture the differential current with appropriate sampling frequency under the previously said conditions.
2. Apply MRA technique to obtain the discrete wavelet transform up to 5th decomposition level.
3. Obtain |d5|
4. Find the first two peak values A and B of |d5|
5. Calculate ΔM=A-B
6. If ΔM<0 then it is Inrush Current.
7. If ΔM>0 then it is Fault and provide trip signal or alarm

VI. CONCLUSIONS

The second harmonic component is commonly used for blocking differential relay in power transformers, to avoid the needless trip by magnetizing inrush current. The major drawback of the differential protection of power transformer is the possibility for false tripping caused by the magnetizing inrush current during transformer energization. In this situation, the second harmonic component present in the inrush current is used as a discrimination factor between fault and inrush currents. In this paper, a new algorithm is presented which discriminate between the inter-turn fault and magnetizing inrush current. The algorithm used wavelet coefficients as a discriminating function. Two peak values corresponding to the |d5| level following the fault instant are used to discriminate the cases studied. As criterion compare the two peak values, hence no threshold settings are necessary in this algorithm. Proposed technique is discussed in depth and validated through the practical results obtained on custom-built transformer.

REFERENCES

[1] Benteng He,Xuesong Zhang,and Zhiqian Q.Bo "A New Method to Identify InrushCurrent Based on Error Estimation". *IEEE Transactions on power delivery*, Vol .21,No. 3 JULY 2006.

[2] C.K.Chui, ed: Wavelets *"A tutorial in theory and application academic"* Press. Inc. 1992.

[3] H.Wang and K.L.Butter "Modelling transformers with internal incipient faults." *IEE E Transactions on power delivery"*, Vol.17 PP 500-509 Apr-2002.

[4] Jawed Faiz, "A Novel Wavelet-based algorithm of internal faults from magnetizing inrush currents in power transformers." *IEEE Transactions on power delivery*, Vol.21 No.4 Oct 2006.

[5] Karen L Butter-pury & Mustafa Bagriyanik, "Characterization of transients in transformer using DWT" *IEEE Transactions on power system*, Vol.18 No.2 may 2003.

[6] Karen L Butter-pury, "Identifying Transformer Incipient Events fir maintaining Distribution system reliability" *Proceedings of the 36th Hawai International Conference on System Sciences* 2003.

[7] M.A.Rahman and B Jeyarurya "A state of art reviews of transformer protection Algorithm",*IEEE Transactions on power delivery*, Vol.3 PP 534-544 Apr-1988.

[8] O.A.S.Yousef, "A wavelet based technique for discrimination between faults and magnetizing inrush currents in transformer" *IEEE Transactions on power delivery* Vol.18 No.1 PP 170 – 176 Jan – 2003.

[9] P.M.Anderson, Power system protection. *Piscataway NJ: IEEE press* 1999.

[10] H.Wang and K.L.Butter "Modelling transformers with internal incipient faults." *IEEE Transactions on power delivery*, Vol.17 PP 500-509 Apr-2002.

[11] P.L.Mao and R.K Agrawal, "A wavelet transform based logic method for discrimination between internal faults and inrush currents in power transformers*," Electrical Power and Energy system*, Vol.22 PP 389 – 395, 2000.

[12] P.L.Mao and R.K.Agrawal "A novel approach to the classification of the transient phenomena's in power transformers using combine wavelet transform and neural network, "*IEEE Transactions on power delivery*, Vol.16 No.4 PP 654-660 Oct 2001.

[13] S.A.Saleh and M.A.Rahman , "Modelling and protection of three phase power Transformer using wavelet packet transform" *IEEE Transactions on power delivery*, Vol.20 No.2pt II PP 1273 – 1282 APR – 2005.

[14] S Mallat, "A theory for multi resolution signal decomposition: the wavelet Representation," *IEEE Transactions on power Anal and much Intel*, Vol.111 PP 674 – 693 Jul 1989.

[15] Y.Y.Hong and C.W.Wang, "Switching detection / classification using discrete wavelet transform and self organizing mapping network*" IEEE Transactions on power delivery*, Vol.20 No.2pt II PP 1662 – 1668 APR – 2005.

[16] Y Kukaki " Power differential method for discrimination between fault and magnetizing inrush current in transformer" *IEEE Transactions on power delivery*, Vol .12,pp1109-115, JULY 1197.

PRATIBHA: INTERNATIONAL JOURNAL OF SCIENCE, SPIRITUALITY, BUSINESS AND TECHNOLOGY (IJSSBT), Vol. 1, No.1, March 2012
ISSN (Print) 2277—7261

Pollution Control: A Techno-Spiritual Perspective

Dr M Husain[1], Dr K S Wani[2], and S P Pawar[3]
[1]SSBT's College of Engineering and Technology, Bambhori, Jalgaon, MS, India. (Corresponding author)
[2]SSBT's College of Engineering and Technology, Bambhori, Jalgaon, MS, India.
[3]SSVP's B S Deore Polytechnic College, Dhule, MS.
Email: ermujahidhusain@yahoo.com

Abstract: The previous century has seen a tremendous growth in Science and technology. This is followed by incredible industrial growth, population rise and radical transformation of life style making it more luxurious. At the same time, environmental degradation has appeared as a darker side of development. On one side the living standard is rising up but on the other side the quality of life is degrading. This has induced scientists all over the world to think over development without destruction. Indian mythology gives lot emphasis on environment friendly life style and sustainability. Ancient Indian peers have contemplated adequately on the issue of development without destruction. This paper highlights the spiritual guidelines given in the Indian mythology for environmental protection. The equivalence between modern environmental protection concepts and traditional Indian ideology is logically discussed here. The relevance of ancient mythological directives and wisdom in modern environmental problem solving is described. Thus this paper is an endeavor to look back to move ahead towards a world of no pollution.

Key words: E*nvironmental protection, Pollution control, Sustainability, Spirituality, and Mythology.*

I. INTRODUCTION

In the modern society environment and pollution are perhaps the most important, most relevant and most discussed issues. The present paper is also concerned with the environment and pollution. Lets first have and insight into the words environment and pollution:

The word environment is quite comprehensive and inclusive. Referring to the dictionary, the word environment simply means, whatever we see all around [1]. However this simple meaning is quite vast and contended. If we see all around, it includes- land, water, air, sky, vegetations, animals, human beings, microorganisms, property, time and space, electromagnetic flux and so on including ourselves. This includes everything of lithosphere to biosphere, living to non-living world. This infinite list can be replaced by a single word that is ENERGY. What we see all around is nothing but different forms of energy. So the word environment can be defined as *energy in time and space.* All our materialistic knowledge is based upon the concept that the *energy cannot be created it cannot be destroyed.* Similarly the basis of Indian spirituality is given in following couplet of Gita [2]:

Na enam chindanti shastrani, na enam dahti pawakah, Na ch enam cledyanti api, na enam shoshyati marutah.

The soul is eternal, weapons cannot damage it, fire cannot burn it, water cannot wet it and air cannot dry it.

So, what we see all around (environment) is energy in time and space. But this definition is incomplete. In fact what we see all around includes one more important phenomenon that is the cycles going on in nature. The cycles like C cycle, N cycle, P cycle, and so on. The list can be again infinite. In fact it is a very important feature of the environment that everything is inter-related with cycles. The cycles are also interwoven and quite complex. The Einstein's basic equation $E= mc^2$ in fact refers to this basic philosophy that the energy is subjected to cycles. Various elements of environment are in fact various forms of energy and are interrelated with cycles. Similarly, Gita [2] pronounces:

Vasansi Jirnani yatha vhay, annayni sanyati navani dehi, tatha sharinani vihay jirnani annayni snayati navani dehi.

As we change the old clothes, the eternal soul changes the body. Body is the physical manifestation of soul.

Thus the word environment can be more comprehensively defined as *energy cycles in time and space*. The universal energy subjected to cycles of creations and destructions.

Yet the definition is incomplete. There is one more important aspect of the environment that we see is

not included in the definition so evolved. This aspect can be explained by a simple example: air is a mixture of gases. In general it contains 21% Oxygen and 78% Nitrogen with minor proportion of few other gases. Now, these gases are various forms of energy. But it is very important to note that though the proportion of various gasses is fixed but is subjected to cycles. The Oxygen is continuously being inhaled by living creatures and carbon di oxide is being discharged. Yet another important aspect is that the cycles are tending to an *equilibrium*, more precisely, a *relative equilibrium* with other cycles. All cycles in the nature are subjected to a *dynamic equilibrium*. This is the complete definition of the word environment-energy subjected to dynamic equilibrium. When this equilibrium is disturbed, the pollution is created.

The concept of pollution can be evolved by a simple example: air has 21% Oxygen and 78% Nitrogen with 0.03% CO_2 and some other gasses. Now, Oxygen is a very important gas, can be termed as gas of life. Lets imagine if the proportion of Oxygen and Nitrogen is reverted. What will happen? The excess of Oxygen shall burn out everything due to its high oxidizing potential! While CO_2 is considered to be a pollution. It is responsible for a very important environmental problem called as global warming. Lets make CO_2 as 0%. What will be the consequence? Without CO_2 the plants cannot do photo-synthesis. So the Oxygen cycle shall be broken and the whole life will come to an end. Thus it can be seen that neither oxygen proportion can be increased nor CO_2 proportion can be decreased. Both are injurious to the environment. Obviously because the environment is defined as equilibrium of cycles. When this equilibrium is disturbed the pollution is created. This leads to a very important conclusion that *nothing as such is a pollution*. *Everything is a creation of God and as such cannot be pollution.* It is the concentration of anything that can be regarded as pollution. A *disturbed equilibrium is a pollution*. Universe is a dance of Lord Shiva. Dance has dynamism, dance has balance, dance has equilibrium. When the equilibrium is disturbed, the dance is disturbed, the environment is polluted.

The foregoing discussion has taken us to an spiritual insight into the conceptual meaning of the word environment and pollution.

II. THE GLOBAL POLLUTION SCENARIO:

The modern civilization has a history of over five thousand years. A remarkable technological development has taken place in the previous one and half century. This has been followed with global industrial revolution and population rise. This in sum has resulted in to the phenomenon of global warming and climatic changes [3] The basic phenomenon of global warming is shown as in fig 1:

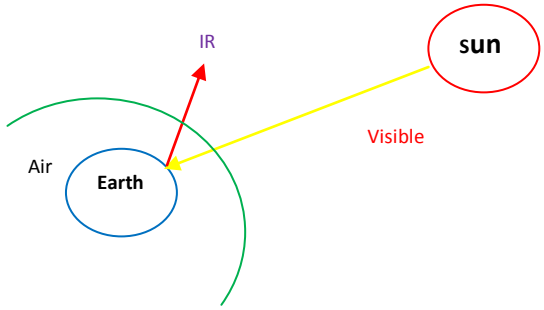

Fig 1: The basic phenomenon of global warming.

Global warming results in the rise of mean earth temperature consequently melting of polar ice. This causes rise in sea level followed by land submergence. At large scale this will result into mass migration and severe socio-economical consequences. The phenomenon is described in fig 2:

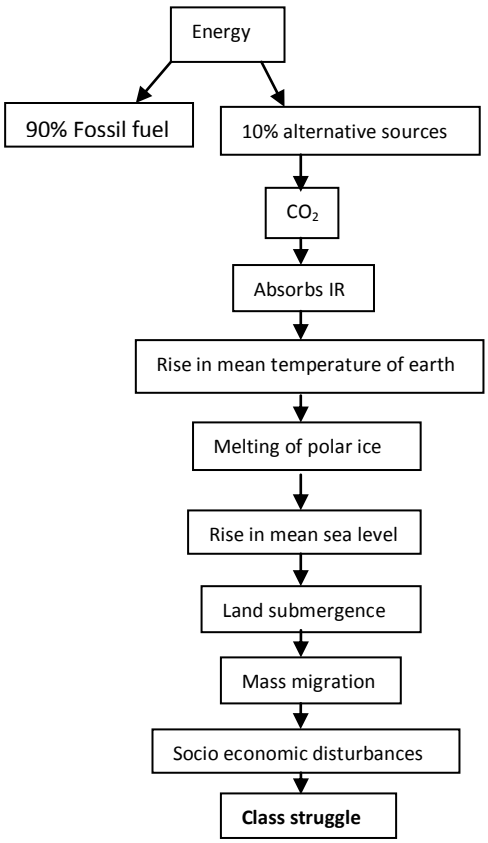

Fig 2: Process of global warming

Scientists are monitoring global warming data all over the world. The recorded rise in temperature is as shown in fig 3[3]: Based upon this, scientists have predicted rise in temperature of earth in coming years as shown in fig 4.

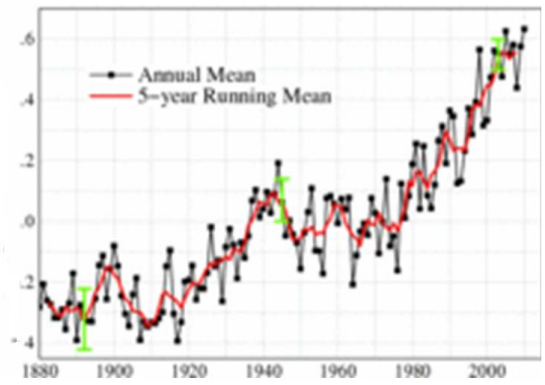

Fig 3: Rising mean temperature of earth.

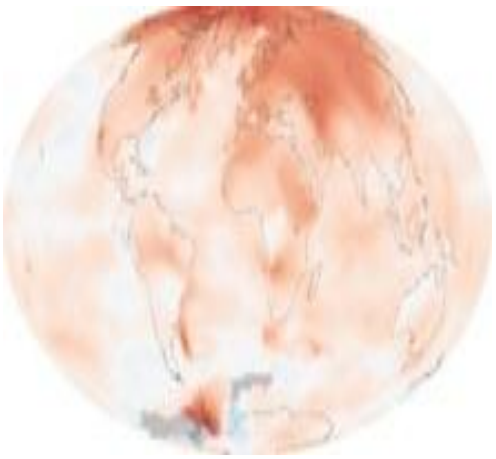

Fig 4: Predicted rise in earth's temperature due to global warming. From lightest to darkest colors indicate temperature rise from normal to $+7^0C$.

Global warming is not just an issue of environment it is an issue linked intimately with our very existence. The mass migration shall result into employment problems, loss or property cost etc. Migrated people shall be compelled to live in slums under malnutrition, unhygienic conditions, illiteracy and poverty. **Slum is the worst form of pollution.**

Apart from this, global warming shall result into disturbed climatic pattern. Climatic pattern is like steps of dance. As such dance is not a physical entity. It is the rhythm that makes its existence. Universe is like dance of Lord Shiva. Disturbed climatic pattern resembles to the "tandav nritya" of Shiva. It will kill the whole universe. The agriculture shall become impossible resulting into less food production. Coupled with the rising population it will be the worst situation in known history.

III. DIRECTION OF RESEARCH

The preceding paragraphs have described the problem of pollution which may be regarded the darker side of development. The global warming which has become a threat to the human existence, is due to CO_2 rising concentration. CO_2 is the by-product of fossil fuel combustion. Fossil fuel is the prime source of our energy. Our energy demands are increasing day by day to mechanized and luxurious life style, increased security requirements, and wars. Root cause of all this is the development in science and technology. Ultimately, this is due to the direction of research. In our mythology, one resemblance is given: once *devas* and *asuras* (Angels and Evils) decided to go for churning of sea. The first outcome was poison. It could have destroyed the universe. But *Shiva* consumed it and finally came out *amrit*. Had it been gone in the hands of *asuras*, they would have ruled the world with their grim. *Mohini* incarnated and skillfully distributed it to the devas. Now, it s the story of "Churning of sea". Research is the churning of brain. People with good and bad intention both do the research. The first outcome of the research is side effect. If the society has a shiva who can sustain these ill effects then only the churning can go ahead. Finally when the power of research is manifested, it is the conscious of society that has to decide how to use it. In this example, mohini resembles the conscious of mankind. For example, atomic power is superb in itself. It can be used for mass destruction as well as for large scale power generation. It is the conscious that will decide how to use this power. Unfortunately, mankind who is superior in terms of intellectual power, is inferior in terms of consciousness (*Chaitannya*). Even the dogs can recognize the arrival signs of earth quake or tsunami. But mankind has poor consciousness. It is the time when the we have to concentrate on improving our consciousness. Not only the individual consciousness (Vayashti chaitannay) but the collective consciousness (samashti chaitannya). Mankind is very poor in terms of collective consciousness. Imagine the orderly working of ants while making their hive. They do not have even vocabulary like us. Can mankind ever work like this in so orderly orientation?

Life style and environment: How to increase consciousness? It can be done only by meditation. Time has come when the society has to work in this direction. Mediation must be a part of school

curriculum. It must be a part of office working. It must be a compulsory practice in each house.

We have also seen that it is the rising energy demand that has resulted into global warming [4]. Our energy demand has increased because of three reasons: luxurious life style, wars, security requirement. Again, mediation only can make us strong enough and keep us from laziness so that we may not need luxury. And we may get rid of war-mentality.

Consciousness directs intellect:

Our laziness and luxurious life style has made au more dependent upon machines. This has increased the use of machines and consequently the consumption of energy. 75% of world's energy is used by the 25% population of developed world. Rest of the 75% population uses only 25% of the energy [5]. The higher consumption of energy has tremendously raised the *living standard*. Yet it has not necessarily enhanced the *quality of life* too. In fact it has posed the modern society with new kind of problems. Several new kinds of diseases and disorders have appeared. Most of them including diabetes are due to lack of physical work. The excessively mechanized lifestyle and rush for has increased hypertension problems. Pollution has caused early aging and several diseases. People have comfortable beds in sophisticated bedrooms but they depend upon medicines to sleep. People have mobile phones but yet facing communication gap problems in near relations. Sum total of all this has indeed degraded the modern life quality which earlier people used to have as a natural gift. Regular practicing of meditation and yoga can have combating effect of diseases and mental disorders. It can radically reorient the mass psychology. Development does not always mean mechanization. For instance "Mayan civilization" of American continent had developed mathematics and astronomy to a great extent. But they had not invented the *wheel*. It is even important they had not prohibited the invention of wheel, rather their collective consciousness was adequately developed so that their researcher did not get poised with the invention of wheel. It is the consciousness which is supreme. Consciousness supersedes intellect [6-7]. Consciousness directs intellect; for individual as well as for society.

IV. SUSTAINABLE DEVELOPMENT

Time has come when we have to learn sustainable development and environmental friendly life style [8].

What is exactly meant by sustainability? One has a right to harness the nature but not to exploit the nature. A simple well known example explains it: milking a cow harnessing, cutting the cow is exploiting. It is the basic philosophy applicable to all development projects. Rig Ved has pronounced in one of its hymn: thy bosom mountains, sky is your girdle, oceans sing your glory, O' mother earth forgive me as I touch you with my feet. If we recognize that nature is our mother, it care us like a mother, by none of our act we will pollute it. All our actions will be so humble, so gentle so soft that they will never hurt the nature.

REFERENCES

[1] Oxford English Dictionary: The definitive recording of the English Language, Oxford University Press, UK.
[2] Mythological literature including GEETA published by Geeta Press Gorakhpur, UP.
[3] Wikipedia of global warming.
[4] Pachauri R K and Sridharan P V (2008) Looking back to think ahead, TERI Publication Delhi.
[5] Wikipedia of Energy.
[6] Peter Russel (2006) From science to God: the mystery of consciousness and the meaning of life, New World Library, Navota.
[7] Peter Russel (2006) The evolution of consciousness, New World Library, Navota.
[8] Joann Loviglio (2007) Scientists bridging the spirituality gap, Associated Press, Philadelphia.

PRATIBHA: INTERNATIONAL JOURNAL OF SCIENCE, SPIRITUALITY, BUSINESS AND TECHNOLOGY (IJSSBT), Vol. 1, No.1, March 2012
ISSN (Print) 2277—7261

A NEW METHOD OF SPEED CONTROL OF A THREE-PHASE INDUCTION MOTOR INCORPORATING THE OVERMODULATION REGION IN SVPWM VSI

*S. K. Bhartari[1], Vandana Verma[2], Anurag Tripathi[3]**
[1,2]Author is with PSIT Engineering College, Kanpur
[3]Author is with Institute of Engineering. & Technology, Lucknow

Abstract: This paper proposes the matlab based model of a new scheme of speed control of the three phase induction motor under which the speed command is compared with the actual speed and the error is processed to generate the gating patterns for the space vector modulated voltage source inverter. The space vector modulation technique ensures linearity till an output of 90.7% of the installed inverter capacity. Beyond this value, if higher inverter output is desired, the operation is termed as overmodulation. The speed control scheme incorporates the two reported regions of overmodulation i.e. I & II and ensures a smooth transition of the motor till 100% of its rated speed and also beyond that in the field weakening region. Overmodulation is a non-linear process, and it involves two modes of operation depending on modulation index (MI). Mode I provides compensation of the voltage vector to be applied while mode II uses the concept of continuous application of a particular voltage vector in order to achieve the desired average voltage vector and hence angular velocity. In this paper, the range of mode I operation of overmodulation is extended beyond usual modulation index thus far reported (0.9535) in the literature, thus stretching the arrival of Mode II further towards six step. This delay in the arrival of overmodulation Mode II reduces the non-linearity effect as the lower order harmonics are minimized, thereby enhancing the controllability of the motor angular velocity. This helps in mitigating the current and torque ripples in the motor. The satisfactory operation of the extended range of mode I and the smooth transition into mode II and six step is verified using simulation results.

Keywords: Overmodulation, SVPWM, Volt–Second compensation.

I. INTRODUCTION

The basic advantage of SVPWM is that it increases the linear range of operation till a modulation index of 90.7% unlike the conventional sine PWM method having linear range till a modulation index of 78.5%. The concept of operation of linear or non-linear region is based on modulation index that indirectly provides information about the inverter utilization capability. . This feature of SVPWM puts on edge over other PWM techniques. Till M I $\leq$ 0.907 SVPWM inverter operates in the linear region meaning whereby that the modulation index is directly proportional to the fundamental component of the line side voltage. Beyond M I = 0.907 SVPWM inverter stands operating in the non-linear or in other words overmodulation region. This overmodulation region is further divided into two zones. Zone 1 lies between 0.907 < M I $\leq$ 0.9535 and zone II lies between 0.9535 < M I $\leq$ 1.0.

The main aim of any PWM technique is to utilize the inverter to its full capacity that is achieved only with six-step operation but at the cost of loss of controllability. In SVPWM, the operation from under modulation to overmodulation finally leads to the six-step operation.

The normal and six-step operating regions of a modulator can be easily programmed, but to maintain continuity between these two regions, overmodulation is required. Besides this, overmodulation helps in exploiting the voltage capability of the inverter and therefore is necessary to improve the dynamic response of the drive. To this end, several methods of achieving overmodulation are suggested.

In [1], the overmodulation range is divided into two sub-regions and the inverter switching is defined based upon the unique characteristics

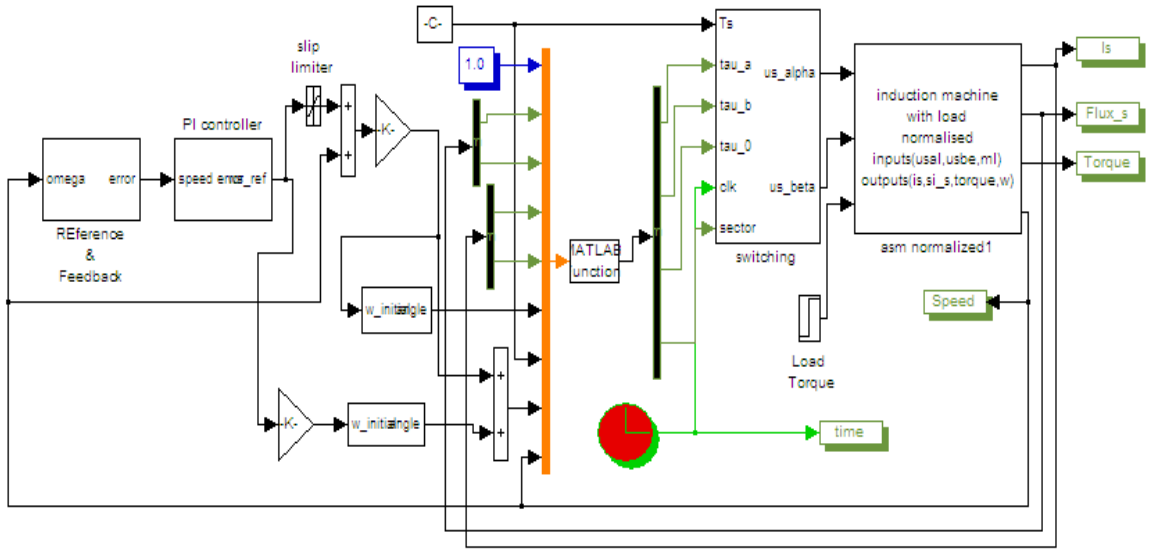

Figure 1: The complete SVM scheme applied to a three phase Induction motor

of the two regions. In the first sub-region, a pre-processor modifies the magnitude of the reference voltage vector before the conventional space vector modulator processes it. In the second sub-region, the pre-processor modifies both the angle and magnitude of the reference voltage vector. To avoid the solution of nonlinear equations, two look up tables are used and continuous control of voltage is obtained until six-step region. While the fundamental voltage cannot be obtained in every sampling period, [1] gets it in a fundamental cycle. The other overmodulation schemes like [2],[3],[4], [5] use the basic geometrical understanding provided in [1]. However, these methods differ from each other in the manner they implement the overmodulation switching strategy. In terms of minimum processing time, the method given in [4] is the fastest. However, due to large harmonic content in the voltage waveform, it results into distorted current and flux waveforms. The method described in [2] uses computationally intensive classification algorithms to achieve overmodulation. Instead of pre-processing the voltage vector as in [1], references [3] and [5] use approximated piecewise linearized equations to achieve overmodulation switching. All these methods have effectively extended the DC-bus utilization of the inverter until the six-step mode and are tested for the open loop V/f drives. During overmodulation, lower order harmonics are added to improve the fundamental cycle voltage gain of the modulator. However, when used in a closed loop torque and flux vector control scheme like FOC, these harmonics interfere with the working of linear current controllers, [6]. In reference [6], a method of compensation is proposed that uses an inverse model to estimate the harmonic component of the current vector during overmodulation. This harmonic content is then discarded from the inputs to the linear controllers. During dynamics at high angular velocities, the method developed by Mochikawa et al. selects the voltage vector that is vectorially closest to the reference [7]. This is achieved by projecting the reference voltage vector tip point on the closest inverter hexagon side. Another method implemented by Seidl et al. [8], uses neural networks for implementation, [7]. This approach however fails to utilize the voltage capability and requires a computationally intensive control algorithm. In the reference [9] an attempt is made to overcome the adverse effect of the nonlinear gain on the linear current controllers by utilizing the nonlinear inverter gain function model. This method appears to give a performance that is similar to a much simpler approach using look-up tables that are proposed in [1].

Besides the SVM based overmodulation methods discussed in the above paragraphs, a class of discontinuous PWM methods [10] have been described that extend the linear range of operation using the sine-triangle PWM scheme. In this category, the popular methods tested for V/f induction motor drives are the one by Ogasawara [11]. A hybrid method that combines the advantages of these methods is developed in [10]. However, the steady state FOC drive performance

using these methods in the overmodulation range is shown to be oscillatory.

II. CONTRIBUTION AND ORGANIZATION OF THE PAPER:

The proposed strategy of extending the range of overmodulation zone I and further achieving a smooth transition to overmodulation II and six step, considers the instantaneous value of stator voltage vector. The gating pattern is generated by the sampled error between the reference voltage vector and the estimated or actual voltage vector. Consideration of stator voltage vector error as the commanded value helps to achieve zero flux vector error in a fundamental cycle for all operating angular velocities. Figure 1 shows the complete scheme for the speed control of the three phase Induction motor.The achievement of the increased MI for zone I overmodulation, carried out right from the fundamental principle of calculating the switching times and selection of switching states is discussed in this paper. The mathematical equations developed are simulated through MATLAB / SIMULINK and the results of simulations are then validated through experimental results.

III. SPACE VECTOR MODULATION TECHNIQUE:

The figure 2 shows the three modes of operation of SVPWM. The operation within the inscribed circle of the regular hexagon is the linear region while operation outside the inscribed circle till the circumscribed circle around the hexagon depicts overmodulation region.

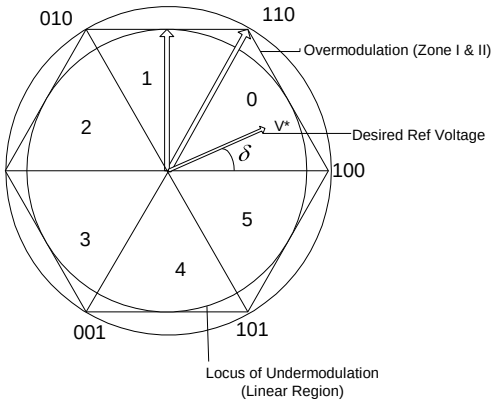

Figure 2: Showing the various regions of modulation

At the end of the liner modulation i.e. at a MI >0.907, the reference voltage vector tip traces a circle whose radius becomes greater than that of the inscribed circle of the hexagon representing the voltage vectors which can be applied in the six sectors.

IV. OVERMODULATION (ZONE I)

As can be seen from the figure 3, the whole situation in the OVMI stage can be divided into two regions. In region A, the value of the (desired) reference voltage vector $V_s^*(k)$ i.e. OD, is more than the actual available voltage vector $V_s(k)$ i.e. OC, which in region B is the other way round.

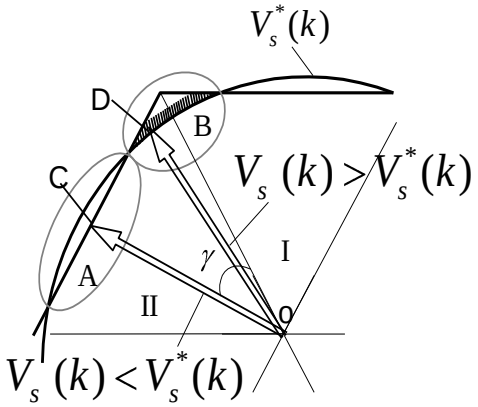

Figure 3: Overmodulation compensation

In region A, the maximum available reference voltage vector is $0.866 \times V_s(k)_{\max}$. So,

Max loss (of volt-sec) in region A =

$$V_s^*(k) - 0.866 \times V_s(k)_{\max} \quad (1)$$

Among the switching times τau_a, τau_b, and τau_0, τau_0 becomes negative in region A, which is not possible practically, so τau_0 is taken to be equal to zero and the switching is obtained by applying active states for τau_a and τau_b period only. The voltage vector in this region thus moves along the hexagon till the boundary of the region B starts.

In the region B, there is an ample available voltage vector $V_s(k)$ magnitude to accommodate tau_0 so all the three switching times are applied albeit in a modified manner. The loss of angular velocity in the region A is compensated in the region B. This compensation results in the modification of the switching times.

$$\text{Max.compensation} = k_c \times V_s(k)_{\max} - V_s^*(k) \quad (2)$$

Where k_c is a compensation factor which decides what percentage of the maximum voltage vector

ought to be required to compensate for the loss of angular velocity in the region A. Thus equating (1) and (2),

$$V_s^*(k) - 0.866V_s(k)_{\max} = k_c \times V_s(k)_{\max} - V_s^*(k) \quad (3)$$

This gives

$$k_c = \frac{2V_s^*(k)}{V_s(k)_{\max}} - 0.866$$

The rationale of the proposed method lies in the fact that since negative values of τau_0 are not possible to achieve in the region A, the value of τau_0 is kept zero in this region and only the two active voltage vectors are switched. The accompanying loss in the volt-seconds has to be compensated and this is done in the region B where the values of τau_a & τau_b have to be increased by applying the factor Kc, which is decided by equating the maximum loss (of volt-sec) in the region A with the maximum possible value of compensation that can be provided in the region B. Thus the average angular velocity can be made equal to the desired (reference) value in a sector rather than that in a complete cycle. It has been found that the modulation index at which negative values of τau_0 start occurring (during simulation) is the value at and beyond which compensation for the loss of volt-sec in the region A cannot be done.

The modified switching times are
τau_a1 = τau_a + 0.5 K_C *τau_0
τau_b1 = τau_b + 0.5K_C *τau_0
τau_01 = Ts – τau_a1 – τau_b1

The simulated results with the above switching times show that the overmodulation I region persists beyond a modulation index of 0.9535.

V. SIMULATION RESULTS AND DISCUSSION

The simulated results using MATLAB/SIMULINK are given in figures 4, 5 and 6. Typical values of MI=0.9535, 0.97 and 0.99 are considered for showing the difference in the various waveforms from the usual limit of overmodulation Zone I i.e. MI= 0.9535.

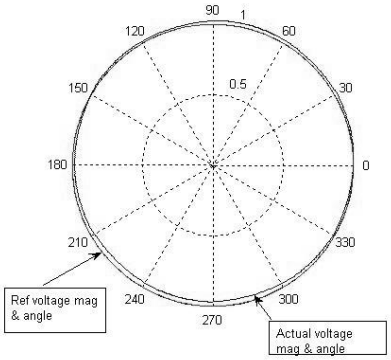

Figure 4(a)

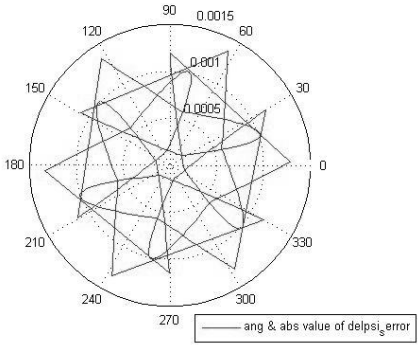

Figure 4(b)

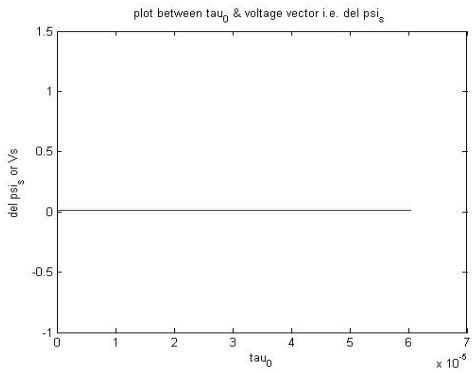

Figure 4(c)

The polar plots of voltages (both reference and actual) are shown in Figures 4(a), 5(a), 6(a) for MI = 0.9535, 0.97 and 0.99 respectively. Among the above modulation indices, that of MI=0.9535 is the existing value of MI which demarcates overmodulation zone I and zone II. Figure 4(a) proves that the actual value of voltage vector strictly tries to follow the reference voltage vector. Figure 4(b) shows that the flux error vector (which is actually equal to the applied voltage vector), is well within the normalized value of 0.0157. The same will be depicted for MI = 0.97 in Figure 5(a) where the maximum loss in actual voltage vector is successfully compensated by the maximum available voltage vector at the vertices of the hexagon. The same control and compensation is not possible for MI = 0.99 as is clear from figure

6(a). Here, clearly overmodulation Zone II exists and a continuous switching of a single voltage vector control technique are adopted to finally reach to six-step voltage level.

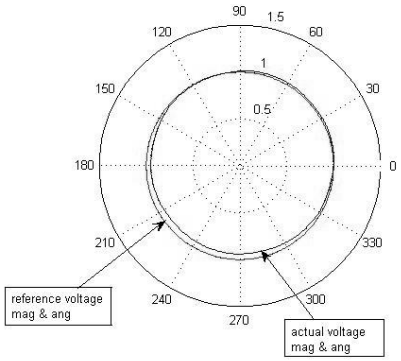

Figure 5(a)

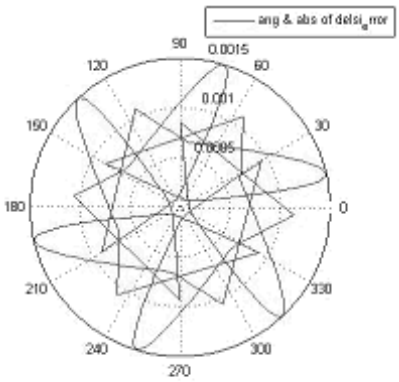

Figure 5(b)

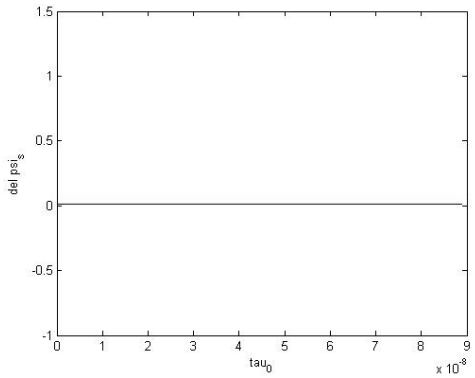

Figure 5(c)

Figures 5 (a-b) show the plots of same parameters considered in figure 4 but for MI = 0.97. Figures 4 (a, b) and figures 5(a, b) reflect the difference in value of magnitude of actual voltage vector. The increased value of voltage vector in figure 5(b) is still within the range where compensation is possible, whereas in figure 6(b) for MI=0.99 the magnitude of voltage vector crosses the boundary of the desired value and thus loses control through compensation process.

In figures 4(c), 5(c) and 6(c) the plots of voltage vectors verses zero switching times i.e. τau_0 are presented. In figure 4(c) the τau_0 = 60 microseconds. In figure 5(c) τau_0=0.09 microseconds and in figure 6(c) τau_0= a negative value. As can be seen that till modulation index of 0.97,the value of τau_0 is positive meaning that the compensation of the voltage vectors is still possible. For higher values of modulation index, overmodulation II region sets in. Thus we see that the arrival of overmodulation II is stretched further towards six step.

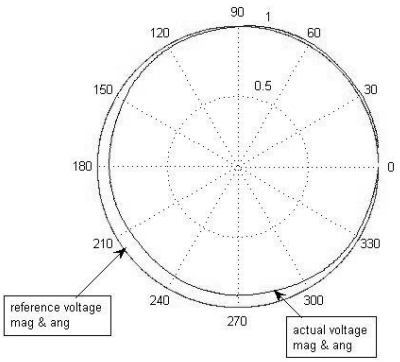

Figure 6(a)

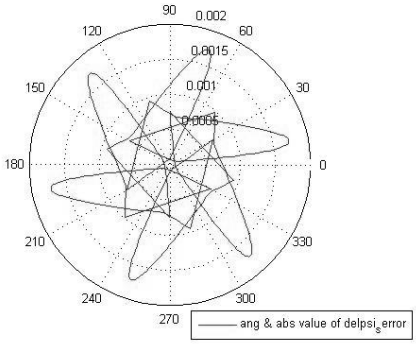

Figure 6(b)

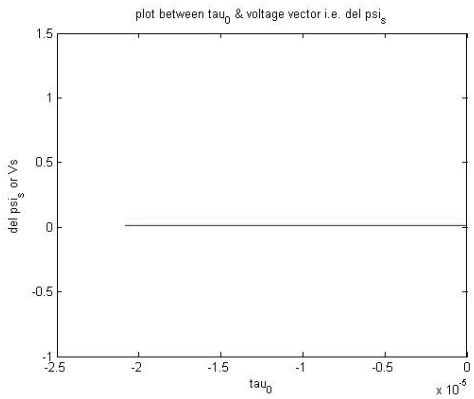

Figure 6(c)

The negative values of τau_0 directly reflect the zone of operation in overmodulation II region in SVPWM inverter. Since τau_0 cannot be negative so is kept zero and the control is achieved through active state vectors. Thus, the overmodulation zone II operation starts. The simulated results in figures 4(c), 5(c) and 6(c) define and conclude the extended range of operation of Zone I in overmodulation region.

The smooth control of torque and speed of three-phase induction motor is easily possible now with extended range of overmodulation Zone I. This gives greater flexibility in obtaining the required input voltage of the motor from the SVPWM inverter by generating the gating signals accordingly. It also helps in better and smooth transition from overmodulation to six-step operation. Moreover, extended range of Zone I improve the transient response of the torque and speed of the induction motor by reducing the pulsations in the torque in the dynamic condition.

VI. CONCLUSION

The novel approach towards the achievement of extended range of Zone I overmodulation presented in this paper when realized through simulations show the improved transient response of the induction motor with less effect of non linearity faced during overmodulation operation in SVPWM inverter. Since the Zone I range is stretched beyond the existing value of MI=0.9535, in turn, automatically reduces the range of operation in Zone II i.e. now zone II region starts at a much later value of MI. Hence, the control and transition to six step operation of the required voltage vector is much easy and even. The proposed approach removes the problem arising out of the extreme non linearity starting with the advent of overmodulation zone II by increasing the range of operation of zone I

REFERENCES

[1] J. Holtz, W. Lotzkat, and A. M. Khambadkone, "On continuous control of pwm inverters in overmodulation range including six-step," IEEE Transaction on Power Electronics, vol. 8, pp. 546–553, 1993.

[2] A. R. Bakhshai, G´eza, Jo´os, P. K.Jain, and H. Jin, "Incorporating the overmodulation range in space vector pattern generators using a classification algorithm,"
IEEE Trans. on Power Electronics, vol. 15, pp. 83 – 91, January 2000.

[3] D.-C. Lee and G.-M. Lee, "A novel overmodulation technique for space-vector pwm inverters," IEEE Trans. on Power Electronics, vol. 13, no. 6, pp. 1144–1151, 1998.

[4] S. Bolognani and M.Zigliotto, "Novel digital continuous control of svm inverters in the overmodulation range," IEEE Trans. on Industrial Applications, vol. 33, no. 2, pp. 525–530, 1997.

[5] G. Narayanan and V. T. Ranganathan, "Overmodulation algorithm for space vector modulated inverters and its application to low switching frequency pwm techniques," in Electric Power Applications, IEE Proceedings, vol. 148, November 2001.

[6] A. M. Khambadkone and J. Holtz, "Current control in overmodulation range for space vector modulation based vector controlled induction motor drives,"
(Nagoya, Japan), pp. 1334–1339, October 2000.

[7] H. Mochikawa, T. Hirose, and T. Umemoto, "Overmodulation of voltage source pwm inverter," in JIEE-Ind Society conference records, 1991.

[8] D. R. Seidl, D. A. Kaiser, and R. D. Lorenz, "One-step optimal space vector pwm current regulation using a neural network," in IEEE-Industrial Application Soc. Conf. Rec., 1994.

[9] R. J. Kerkman, T. M. Rowan, D. Leggate, and B. J. Seibel, "Control of pwm voltage inverters in pulse dropping range," IEEE Industry Application Magazine, vol. 2, pp. 24–31, Sept-Oct 1996.

[10] A. M. Hava, R. J. Kerkman, and T. A. Lipo., "Carrier-based PWM-VSI overmodulation strategies: analysis, comparison, and design," IEEE Transactions on Power Electronics, vol. 13, pp. 674–689, July 1998.

[11] S. Ogasawara, H. Akagi, and A. Nabae, "A novel PWM scheme of voltage source inverter based upon space vector theory," in European Power Electronics Conference records, 1989.

PRATIBHA: INTERNATIONAL JOURNAL OF SCIENCE, SPIRITUALITY, BUSINESS AND TECHNOLOGY (IJSSBT), Vol. 1, No.1, March 2012
ISSN (Print) 2277—7261

STUDY OF DYNAMIC PERFORMANCE OF RESTRUCTURED POWER SYSTEM WITH ASYNCHRONOUS TIE-LINES USING CONVENTIONAL PI CONTROLLERS

S. K. Pandey[1], V. P. Singh[2] , P. Chaubey[3]
[1,2,3]*Electrical Engineering Department, MNNIT, Allahabad – 211004, India*
Emails: [1]skp1111.1969@rediffmail.com, [2]vinaymnnit@gmail.com,
[3]prateekchaubey@gmail.com,
[1]*Corresponding Author*

Abstract: This paper presents a comprehensive study on dynamic performance of a two-area restructured power system interconnected via parallel ac/dc transmission links with conventional PI controllers. It has been observed that the dynamic performance i.e. frequency deviation and deviation in power tie-line improved with dc link in parallel with ac tie-line in terms of overshoot and settling time. The dynamic responses for small perturbation have been observed with PI controller with and without dc links and result of both have been compared.

Key words: Asynchronous tie-lines; Restructured power system; HVDC transmission links; Load frequency control.

I. INTRODUCTION

For large scale electrical power systems that normally consist of interconnected control areas representing coherent groups of generators, load frequency control is very important in power system operation and control for supplying sufficient and reliable electric power with good quality [1-3]. In case of area load changes and abnormal conditions, such as outages of generation and varying system parameters, mismatches in frequency and scheduled tie-line power flows between areas can be caused. These mismatches are corrected by controlling, which is defined as the regulation of the power output of generators within a prescribed area. The main objective of the LFC is to satisfy the requirements such as zero steady state errors in tie-line exchanges and frequency deviations, optimal transient behaviors and in steady state, the power generation levels should satisfy the optimal dispatch conditions. A little attention has been paid to use of HVDC transmission link as system interconnection. A favorable effect on system dynamic performance has been achieved considering such system interconnection [4-5].

Under restructured or open market system (deregulation) the power system structure changed in such a way that would allow the evolving of more specialized industries for generation (Genco), transmission (Transco) and distribution (Disco). In the restructured power system, DISCOs in each area can contract with GENCOs in its or other areas[3-5]. As there are several Gencos and Discos in the restructured power system, a Disco has the freedom to have a contract with any Genco for transaction of power. A Disco may have a contract with a Genco in another control area. Such transactions are called "bilateral transactions." All the transactions have to be cleared through an impartial entity called an independent system operator (ISO). The ISO has to control a number of so-called "ancillary services" one of which is load frequency control.

II. RESTRUCTURED POWER SYSTEM

The traditional power system industry has a "vertically integrated utility" (VIU) structure. In the restructured or open market system (deregulated), vertically integrated utilities no longer exist. In the restructured power system, GENCOs sell power to various DISCOs at competitive prices. Thus, DISCOs have the freedom to choose the GENCOs for contracts. They may or may not have contracts with the GENCOs in their own area. There can be various combinations of contracts between DISCOs and GENCOs which can be conveniently visualized by the concept of a 'DISCO participation matrix' (DPM). The rows of a DPM correspond to GENCOs and columns to DISCOs which contract power. Each entry in this matrix can be thought as a fraction of a total load contracted by a DISCO (column) towards a GENCO (row). The sum of all the entries in a column in this matrix is unity. Consider a two-area power system in which each area has two GENCOs and two DISCOs in it. Let $GENCO_1$, $GENCO_2$, $DISCO_1$, and $DISCO_2$ be in area1 and $GENCO_3$, $GENCO_4$, $DISCO_3$, and $DISCO_4$ be in area 2 as shown in Fig.1 [3-5].

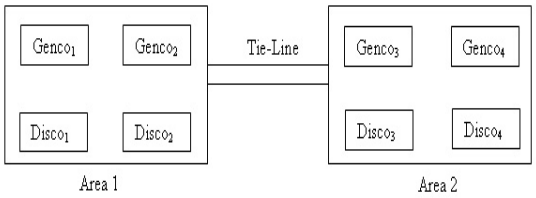

Fig.1. Block Diagram of two area restructured power system.

The corresponding DPM for a two-area power system will have the structure that follows:

$$\begin{bmatrix} cpf_{11} & cpf_{12} & cpf_{13} & cpf_{14} \\ cpf_{21} & cpf_{22} & cpf_{23} & cpf_{24} \\ cpf_{31} & cpf_{32} & cpf_{33} & cpf_{34} \\ cpf_{41} & cpf_{42} & cpf_{43} & cpf_{44} \end{bmatrix}$$

where cpf_{jd} is contract participation factor of j-th GENCO in the load following of d-th DISCO. DPM shows the participation of a DISCO in a contract with any GENCO, hence the name Disco Participation Matrix. The diagonal elements of DPM corresponding to the local demands and off diagonal elements corresponding to the demands of the DISCOs in one area to the GENCOs in another area.

III. TWO AREA POWER SYSTEM MODEL

The two area power system model used in this paper is as follows:

It is a two-area restructured or open system (deregulated) interconnected system consisting of identical thermal power plants. The two-areas are interconnected via AC tie-line in parallel with HVDC link.

The single line diagram of power system model under consideration is shown in Fig.2 [3-5]. The transmission links are considered as long transmission lines specifically of length greater than break even distance length of AC and HVDC transmission lines. The distance normally used as break even distance is about 600km.

The mathematical model of the two-area thermal systems under restructured or open market (deregulated) is shown in Fig.3.

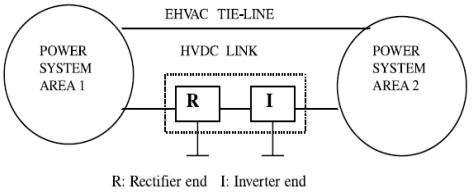

Fig.2. Two area power system with parallel AC/HVDC links.

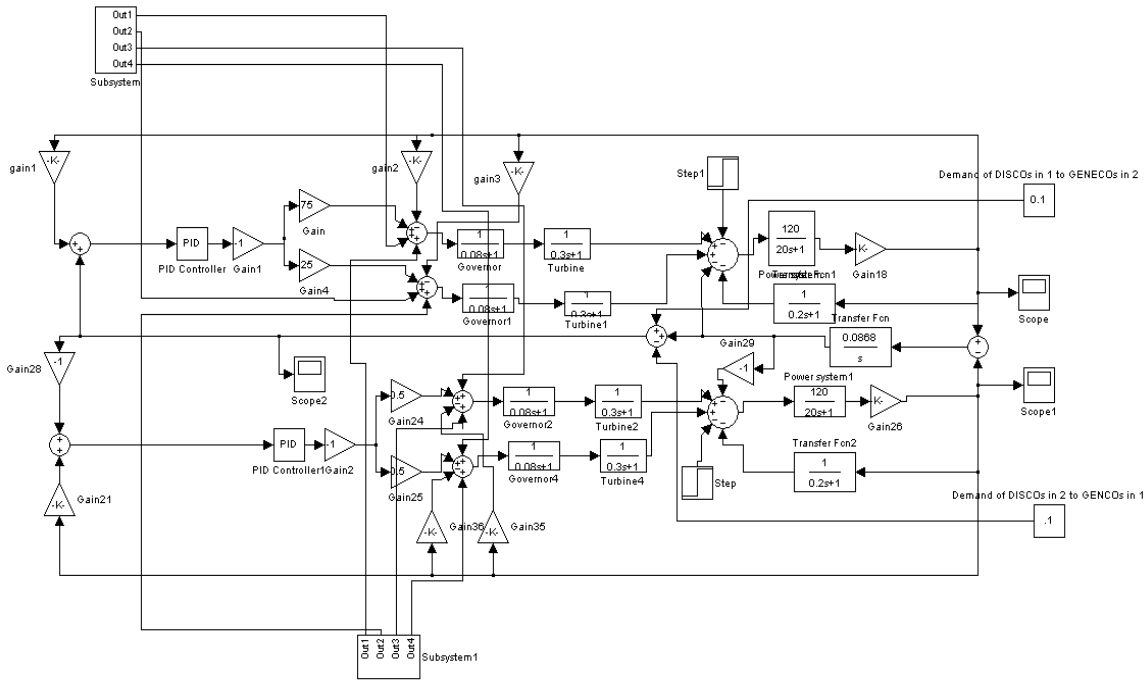

Fig.3 (A): Simulink model of Two-area restructured Asynchronous power system.

PRATIBHA: INTERNATIONAL JOURNAL OF SCIENCE, SPIRITUALITY, BUSINESS AND TECHNOLOGY (IJSSBT), Vol. 1, No.1, March 2012
ISSN (Print) 2277—7261

The structure of subsystem of Fig. 3(A) is shown in following Fig. 3(B).

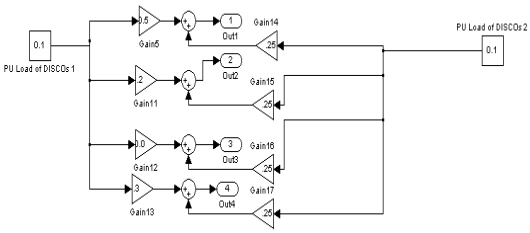

Fig. 3(B): The subsystem of Fig. 3(A).

IV. SIMULATION RESULTS OF A RESTRUCTURED TWO AREA ASYNCHRONOUS POWER SYSTEM

In this paper, a conventional PI controller has been applied to a restructured asynchronous two area power system. MATLAB 7.8 is used for simulation purpose. The values of system parameters are given in appendix.

Case 1: Base Case

Consider a case where the GENCOs in each area participate equally in AGC, i.e. ACE participation factors are apf_1 =0.5, apf_2=1-apf_1=0.5; apf_3=0.5, apf_4=1- apf_3=0.5.

Assume that the load change occurs only in area I. Thus, the load is demanded only by $DISCO_1$ and $DISCO_2$. Let the value of this load perturbation be 0.1 pu MW for each of them. The disco participation matrix (DPM) in this case taken as follows:

$$\begin{bmatrix} 0.5 & 0.5 & 0 & 0 \\ 0.5 & 0.5 & 0 & 0 \\ 0 & 0 & 0 & 0 \\ 0 & 0 & 0 & 0 \end{bmatrix}$$

Note that as $DISCO_3$ and $DISCO_4$ do not demand from any GENCOs, corresponding participation factors (columns 3 and 4) are zero. $DISCO_1$ and $DISCO_2$ demand identically from their local GENCOs viz. $GENCO_1$ and $GENCO_2$. The frequency deviations in area 1 and 2, tie line power flow following a step change in the loads of $DISCO_1$ and $DISCO_2$ are as shown in Fig 4.A, 4.B and 4.C respectively. A performance index which is denoted by $J= \int (\Delta f_1^2+\Delta f_2^2+\Delta P^2_{tie12})\, dt$ is taken into consideration in order to compare between with/without HVDC links. Fig.4D. shows the comparison of performance index between the with/without HVDC links. It can be seen that with HVDC link, the value of performance index (error values) indeed reduces drastically.

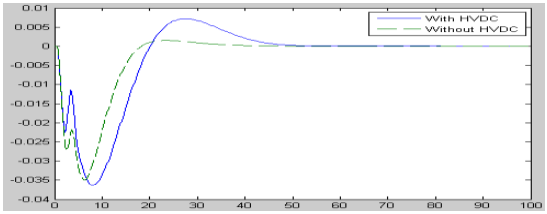

Fig. 4.A: Dynamic response of Δf_1 with and without HVDC links.

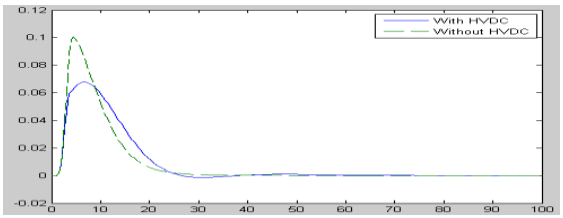

Fig. 4.B: Dynamic response of Δf_2 with and without HVDC links.

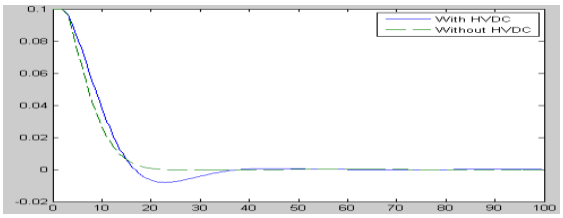

Fig. 4.C: Dynamic response of ΔP_{tie} with and without HVDC links.

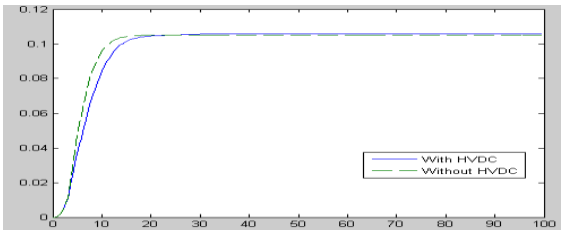

Fig. 4.D: Performance index values with and without HVDC links.

Case 2:

Consider a case where all the DISCOs contract with the
GENCOs for power as per the following DPM:

$$\begin{bmatrix} 0.5 & 0.25 & 0 & 0.3 \\ 0.2 & 0.25 & 0 & 0 \\ 0 & 0.25 & 1 & 0.7 \\ 0.3 & 0.25 & 0 & 0 \end{bmatrix}$$

Assume that the total load of each DISCO is perturbed by 0.1 pu and each GENCO participates in AGC as defined by following apfs: apf1=0.75, apf2=1-apf1=0.25; apf3=0.5, apf4=1-apf3=0.5. The dynamic responses in this case with/without HVDC links and performance index values are as shown in Fig. 5A-5D.

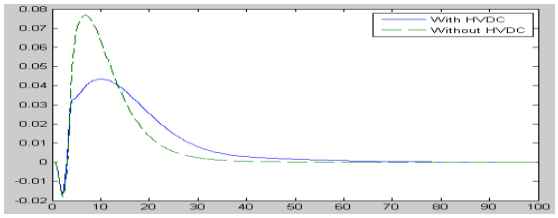

Fig. 5.A: Dynamic response of Δf1 with and without HVDC links.

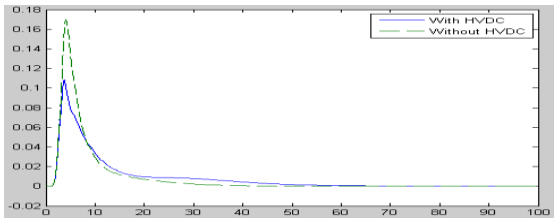

Fig. 5.B: Dynamic response of Δf2 with and without HVDC links.

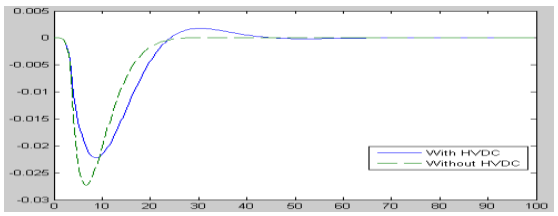

Fig. 5.C: Dynamic response of ΔPtie with and without HVDC links.

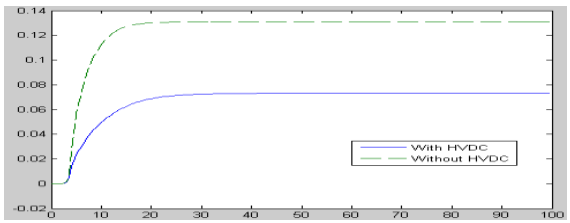

Fig. 5.D: Performance index values with and without HVDC links.

Case 3: Contract Violation

Consider case 2 again except that $DISCO_1$ demands an additional 0.1 pu MW which is not contracted out to any GENCO. The uncontracted load of $DISCO_1$ reflects in the generations of $GENCO_1$ and $GENCO_2$. Thus, this excess load is taken up by the GENCOs in the same area as that of the DISCO making the uncontracted demand. The dynamic responses in this case are as shown in Fig. 6A-6D.

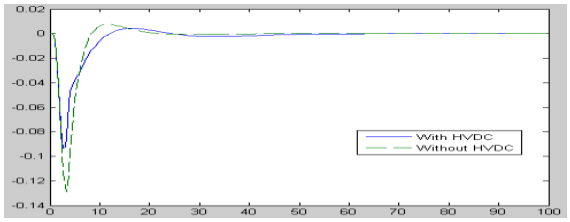

Fig. 6.A: Dynamic response of Δf1 with and without HVDC links.

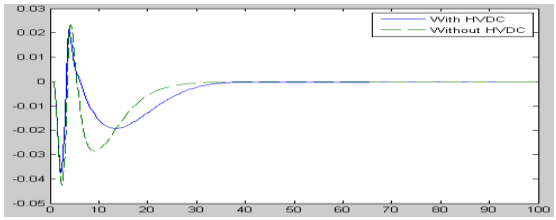

Fig. 6.B: Dynamic response of Δf2 with and without HVDC links.

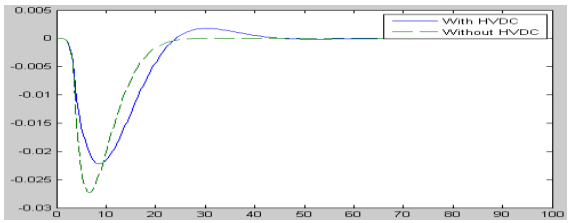

Fig. 6.C: Dynamic response of ΔPtie with and without HVDC links.

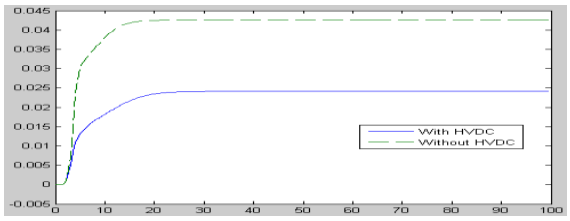

Fig. 6.D: Performance index values with and without HVDC links.

V. CONCLUSION

In this paper, power system model with identical thermal units under restructured scenario with and without HVDC links are considered for the study. By incorporating the HVDC links, the oscillations, peak overshoot and settling time are improved. The degradation in system dynamic performance of a restructured two area can be compensated effectively by incorporating HVDC links parallel with AC tie-line as area interconnection between two power system areas. It may be therefore concluded that, dynamic performance of the restructured two area power system enhanced with HVDC links.

REFERENCES

[1] N. Jaleel, D. N.Ewart and L. H. Fink, "Understanding automatic generation control", *IEEE Trans.on Power Systems*, vol.7, no.3, pp. 1106-1122, 1992.

[2] O. I. Elgerd and C. Fosha, "Optimum megawatt-frequency control of multiarea electric energy systems", *IEEE trans. Power Apparatus & system*, vol. 89, no. 4, pp. 556-563, 1970.

[3] V. Donde, M. A. Pai and I. A. Hiskens, "Simulation and optimization in an AGC system after deregulation", *IEEE Ttrans. power systems*, vol. 16, no. 3, 2001.

[4] C. S. Rao, Z. Naghizadeh and S. Mahadavi, "Improvement of dynamic performance of hydrothermal system under open market scenario using asynchronous tie-lines", *World J. of modeling and Simulation*, vol. 4, no. 2, pp 153-160, 2008.

[5] H. D. Mathur and H. V. Manjunath, "Study of dynamic performance of thermal units with asynchronous tie-liens using Fussy based controller, *J. Electrical systems*, vol. 3, no. 3, pp. 124-130, 2007.

APPENDIX

All the notations carry the usual meanings.

System Data:

$P_{r1} = P_{r2}$ = Rated area capacities = 1200 Mw

$T_{g1} = T_{g2}$ = Governor time constants = 0.08s

$K_{g1} = K_{g2}$ = Governor Gain constant= 1.0

$T_{t1} = T_{t2}$ =Turbine time constant= 0.3s

$K_{t1} = K_{t2}$ =Turbine gain constant=1.0

$T_{p1} = T_{p2}$ = Power system time constants = 20s

$K_{p1} = K_{p2}$ =System Gains = 120 Hz/p.u.Mw

$R_1 = R_2$ =Regulation parameter= 2.4Hz/p.u. Mw

$B_1 = B_2$ = Bias constants = 0.425p.u. Mw/Hz

T_{12} = Synchronizing coefficient= 0.0868s

Data for ac and dc Links:

K_{dc} =Gain associated with dc link= 1.0

T_{dc} = Time constant of dc link= 0.2s

Controller Gains:

$K_p = 1.0, K_I = 0.4, K_D = 0.0$

PRATIBHA: INTERNATIONAL JOURNAL OF SCIENCE, SPIRITUALITY, BUSINESS AND TECHNOLOGY (IJSSBT), Vol. 1, No.1, March 2012
ISSN (Print) 2277—7261

Performance Analysis of Various Image Compression Techniques

Dipeeka O. Kukreja[1], *S.R. Suralkar*[2], *A.H. Karode*[3]
S.S.B.T's College of Engineering And Technology, Bambhori, Jalgaon
Email: dipeeka.kukreja@gmail.com[1], shekhar_srs@rediffmail.com[2], atul_karode@rediffmail.com[3]

Abstract: Digital image compression has numerous practical applications to effectively utilize storage capacities & shorten transmission time. This paper aims at the analysis of various lossless and lossy image compression techniques. For lossless compression Huffman coding method and for lossy compression Discrete Cosine Transform (DCT), Discrete Wavelet Transform (DWT) using Embedded Zerotree Wavelet (EZW) and Block Truncation Coding (BTC) methods are described. These image compression strategies are examined for their relative effectiveness. Finally a performance comparison is made between these techniques based on different parameters like Peak Signal to Noise Ratio(PSNR), Compression Ratio (CR), Root Mean Square Error(RMSE) , Structural Similarity (SSIM) etc.

Keywords - Huffman coding, DCT, DWT, EZW coding, CR, SSIM.

I. INTRODUCTION

With the continual expansion of multimedia and Internet applications, the needs and requirements of the technologies used, grew and evolved. To address these needs and requirements in the specific area of still image compression, many efficient techniques with considerably different features have recently been developed for image compression. A common characteristic of most images is that the neighboring pixels are highly correlated and therefore contain highly redundant information. The basic objective of image compression is to find an image representation in which pixels are de-correlated.

The image compression may be lossless or lossy. In lossless compression, no loss of data is accepted & reconstructed image is identical to the original image while in lossy compression, some image information is lost & reconstructed image is similar but not identical to the original image.

Huffman method is one of the most commonly used lossless image compression technique .When coding the symbols of an information source individually, Huffman coding yields the smallest possible number of code symbols per source symbol. It provides the better quality of the reconstructed image but the value of CR is very small. The Lossless compression is mainly preferred for medical images where minor loss of data is not accepted. To obtain the high value of CR of the reconstructed image with some loss of data accepted, lossy image compression methods are used.

A Discrete Cosine Transformation (DCT) is similar to the Discrete Fourier Transform (DFT) [1] [3], but using only real numbers & widely used in signal processing. Joint Photographic Experts Group (JPEG) is a commonly used standard technique of compression for photographic images which utilizes DCT. DCT separates images into parts of different frequencies (i.e. dc & ac components) where less important frequencies are discarded through quantization and important frequencies are used to retrieve the image during decompression. But the disadvantage of DCT scheme is the "blocking artifacts" in reconstructed image at high compression ratio which degrades quality of reconstructed image. Hence In recent time, much of the research activities in image coding have been focused on the Discrete Wavelet Transform (DWT). It provides better image quality than DCT, especially at higher compression ratio [6]. JPEG 2000 image compression standard makes use of DWT. The discrete wavelet transform maps an image into a set of coefficients that constitute a multiscale representation of the image. Discrete Wavelet Transform (DWT) of a signal is computed by passing it through a series of filters giving approximation & detailed coefficients. Approximation coefficients are used to retrieve the image during decompression [1].

Also in DCT, edges of the reconstructed image are blurred but smooth. Hence to improve the sharpness of the edges in the reconstructed image BTC technique is used. It produces sharp edges; however, these edges do have a tendency to be ragged. This technique uses a one bit nonparametric quantizer to quantize pixels in an image while preserving the first two or three statistical moments.

II. IMAGE COMPRESSION TECHNIQUES

A. Huffman Coding

It is one of the most commonly used lossless image compression technique for removing coding redundancy. When coding the symbols of an information source individually, Huffman coding yields the smallest possible number of code symbols per source symbol [1]. In practice, the source symbols may be either the intensities of an image or the output of an intensity mapping operation. In Huffman coding, more frequently occurred symbols will have shorter code words than symbol that occur less frequently & the two symbols that occur least frequently will have the same length.

The first step in Huffman's approach is to create a series of source reductions by ordering the probabilities of the symbols in decreasing order and combining the two lowest probability symbols into a single symbol that replace them in the next source reduction .This compound symbol and its associated probability are placed in the first source reduction column so that the probabilities of the reduced source are also ordered from most to least probable. This process is repeated until only two probabilities of two compound symbols are left and thus a code tree is generated and Huffman codes are obtained from labeling of the code tree. This is illustrated with an example-

TABLE I: HUFFMAN SOURCE REDUCTIONS

Original source		Source reduction			
S	P	1	2	3	4
a_2	0.4	0.4	0.4	0.4	0.6
a_6	0.3	0.3	0.3	0.3	0.4
a_1	0.1	0.1	0.2	0.3	
a_4	0.1	0.1	0.1		
a_3	0.06	0.1			
a_5	0.04				

S-source, P-probability

TABLE II: HUFFMAN CODE ASSIGNMENT PROCEDURE

Original source		Source reduction							
S	P	1		2		3		4	
a_2	0.4	1	0.4	1	0.4	1	0.4	1	0.6 0
a_6	0.3	00	0.3	00	0.3	00	0.3	00	0.4 1
a_1	0.1	011	0.1	011	0.2	010	0.3	01	
a_4	0.1	0100	0.1	0100	0.1	011			
a_3	0.06	01010	0.1	0101					
a_5	0.04	01011							

At the far left of the table I the symbols are listed and corresponding symbol probabilities are arranged in decreasing order and now the least probabilities are merged as here 0.06 and 0.04 are merged, this gives a compound symbol with probability 0.1 and the compound symbol probability is placed in source reduction column1 such that again the probabilities should be in decreasing order. This process is continued until only two probabilities are left at the far right.

The next step in Huffman's procedure is to code each reduced source, starting with the smallest source and working back to its original source [6]. The minimal length binary codes for a two-symbol source are the symbols 0 and 1. As shown in table II these symbols are assigned to the two symbols on the right (the assignment is arbitrary; reversing the order of the 0 and would work just and well). As the reduced source symbol with probabilities 0.6 was generated by combining two symbols in the reduced source to its left, the 0 used to code it is now assigned to both of these symbols, and a 0 and 1 are arbitrary appended to each to distinguish them from each other. This operation is repeated until the original source is reached. The final code appears at the far-left in table II. The average length of the code is given by the average of the product of probability of the symbol and number of bits used to encode it. This is calculated as shown below

Lavg = (0.4)(1) + (0.3)(2) + (0.1)(3) + (0.1)(4) + (0.06)(5) + (0.04)(5) = 2.2 bits/ symbol and the entropy of the source is 2.14bits/symbol, the resulting Huffman code efficiency is 2.14/2.2 = 0.973.

Entropy is given by (1)

$$H = -\sum_{K=1}^{L} P(a_j) \log P(a_j) \qquad (1)$$

The a_j in this equation are called source symbols.

But if we use the natural coding than Lavg = 3 bits/symbol. Hence Huffman's procedure creates the optimal code for a set of symbols and probabilities subject to the constraint that the symbols be coded one at a time.

After the code has been created, decoding is accomplished in a simple look-up table manner [1] [6]. The code itself is an instantaneous uniquely decodable block code. It is called a block code, because each source symbol is mapped into a fixed sequence of code symbols. It is instantaneous, because each code word in a string of code symbols can be decoded without referencing

succeeding symbols. It is uniquely decodable, because any string of code symbols can be decoded in only one way. Thus, any string of Huffman encoded symbols can be decoded by examining the individual symbols of the string in a left to right manner. For the binary code of table II, a left-to-right scans of the encoded string 010100111100 reveals that the first valid code word is 01010, which is the code for symbol a_3. The next valid code is 011, which corresponds to symbol a_1. Valid code for the symbol a_2 is 1, valid code for the symbols a_6 is 00. Continuing in this manner reveals the completely decoded message a_3 a_1 a_2a_2 a_6, so in this manner the original image or data can be decompressed using Huffman decoding.

1) Proposed Algorithm

The proposed algorithm is as mentioned.

1. Read the input image.
2. Convert the given color image into grey level image.
3. Find the symbols (i.e. pixel value which is non-repeated).
4. Calculate the probability of each symbol.
5. Probability of symbols are arranged in decreasing order and lower probabilities are merged and this step is continued until only two probabilities are left and codes are assigned according to rule that the highest probable symbol will have a shorter length code.
6. Further Huffman encoding is performed i.e. mapping of the code words to the corresponding symbols will result in a compressed data.
7. The original image is reconstructed i.e. decompression is done by using Huffman decoding.

B. Discrete Cosine Transformation (DCT)

Currently the standard Discrete Cosine Transformation (DCT) based algorithm of the JPEG is the most widely used and accepted for image compression. It has excellent compaction for highly correlated data. DCT separates images into parts of different frequencies where less important frequencies are discarded through quantization and important frequencies are used to retrieve the image during decompression [3]. Compared to other input dependent transforms, DCT has many advantages: (1) It has been implemented in single integrated circuit; (2) It has the ability to pack most information in fewest coefficients.

In DCT the quality of the processed image is controlled by utilizing variable quantization matrix. The quantization matrix level varies from the range 1 to 100, where 1 gives the poorest image quality and highest compression, while 100 gives the best quality and lowest compression. As a result quality to compression ratio can be selected to meet different needs. JPEG committee suggests matrix with quality level 50 as standard matrix. For obtaining quantization matrices with other quality levels, scalar multiplications of standard quantization matrix are used. For a quality level greater than 50, the standard quantization matrix is multiply by (100-quality level)/50 & for a quality level less than 50, the standard quantization matrix is multiply by 50/quality level [9]. Values of the scaled quantization matrix are then rounded off & clipped to have the positive integer values between 1 to255.

1) Proposed Algorithm

The proposed algorithm is as mentioned.

1. Read the input image.
2. The algorithm can be tested for gray and color images.
3. The image is Level- shifted by subtracting 128 from each entry.
4. Check the dimensions of the input image as a multiple of blocksize. If not padding is done .
5. The given image is divided into blocks of 8X8.
6. Calculate DCT matrix.
7. DCT is applied to each block by multiplying the each block with DCT matrix on the left and transpose of DCT matrix on its right.
8. Each block is then compressed through quantization.

Depending upon quality level, quantization matrix is selected.

9. Encode the quantize coefficients in zigzag sequences.
10. The array of compression blocks that constitute the image is stored in a drastically reduced amount of space.
11. The image is reconstructed through decompression using Inverse-DCT.
12. Restore image to normal by Level-shift the image back by adding 128 from ach entry & Clip off padded rows and columns.
13 .Finally determine Image quality assessment parameters.

The 2-D DCT (2) shown computes the i, jth entry of the DCT of an image.

$$D(i,j) = \frac{1}{\sqrt{2N}} C(i)C(j) \sum_{x=0}^{N-1} \sum_{y=0}^{N-1} p(x,y) \cos\left[\frac{(2x+1)i\Pi}{2N}\right] \cos\left[\frac{(2y+1)i\Pi}{2N}\right] \quad (2)$$

Where

$$C(u) = \begin{cases} \frac{1}{\sqrt{2}} & if\ u = 0 \\ 1 & if\ u > 0 \end{cases}$$

For the standard 8 X 8 block that JPEG compression uses, N equals 8 and x and y range from 0 to 7. Hence D (i, j) would be as shown in (3)

$$D(i,j) = \frac{1}{4} C(i)C(j) \sum_{x=0}^{N-1} \sum_{y=0}^{N-1} p(x,y) \cos\left[\frac{(2x+1)i\Pi}{16}\right] \cos\left[\frac{(2y+1)i\Pi}{16}\right] \quad (3)$$

Since the DCT utilizes cosine functions , the resulting matrix depends on the horizontal, diagonal, and vertical frequencies. Hence, an image block with a lot of change in frequency has a very random looking resulting matrix, while an image matrix of just one color has a resulting matrix of a large value for the first element and zeros for the other elements.

To get the matrix form of (2), one must use the following equation shown in (4)

$$T_{ij} = \begin{cases} \frac{1}{\sqrt{N}} & if\ i = 0 \\ \sqrt{\frac{2}{N}} \cos\left[\frac{(2j+1)i\Pi}{2N}\right] & if\ i > 0 \end{cases} \quad (4)$$

The first row (i = 1) of the matrix has all the entries equals to $1/\sqrt{8}$ as expected from above equation.

The next step is to apply DCT to 8X8 block. The pixel values of 8×8 images range from 0 to 255, where 0 is for pure black and pure white is represented by 255. Thus, it can be seen how a photo illustration and so on can be accurately represented by these 256 shades of gray.

Now, let's start with DCT of a block image-pixel values. This particular block was chosen from the very upper left hand corner of an image. Since an image comprises hundreds or even thousands of 8×8 blocks of pixels, the following description for one 8×8 block is a part of the JPEG process. As DCT is designed to work on pixel values ranging from -128 to 127, the original block is leveled off by subtracting 128 from every entry & also checks the dimensions of the input image as a multiple of block size. If dimensions of the input image are not a multiple of block size, padding is done .This results in the generation of matrix 'M' given by (5).

$$D = TMT' \quad (5)$$

Here matrix 'M' is first multiplied by the DCT matrix 'T' on the left, this transforms the rows.

The columns are then transformed by multiplying by the transpose of the DCT matrix on the right. This yields the matrix 'D'. This block matrix now consists of 64-DCT co-efficient, Cij, where i and j range from 0 to 7. The top-left co-efficient, C00, correlates to the low frequencies of the original image block which contain the important image information. As one moves away from C00 in all the directions, the DCT correlate to higher and higher frequencies of the image block, where C77 corresponds to the highest frequency. These high-frequency coefficients contain the less-important image information. It is significant to note that the human eye is most sensitive to low frequencies, and results from the quantization step will reflect the said fact.

After the transformation, quantization is carried out by dividing transformed image matrix by the

quantization matrix & rounding to the nearest integer value. Mathematically it is given by (6).

$$C(i,j) = round\left(\frac{D(i,j)}{Q(i,j)}\right) \qquad (6)$$

It allows varying levels of image compression and quality through selection of specific quantization matrices. JPEG committee suggests matrix with quantization level 50 as standard matrix [8].

$$Q_{50} = \begin{bmatrix} 16 & 11 & 10 & 16 & 24 & 40 & 51 & 61 \\ 12 & 12 & 14 & 19 & 26 & 58 & 60 & 55 \\ 14 & 13 & 16 & 24 & 40 & 57 & 69 & 56 \\ 14 & 17 & 22 & 29 & 51 & 87 & 80 & 62 \\ 18 & 22 & 37 & 56 & 68 & 109 & 103 & 77 \\ 24 & 35 & 55 & 64 & 81 & 104 & 113 & 92 \\ 49 & 64 & 78 & 87 & 103 & 121 & 120 & 101 \\ 72 & 92 & 95 & 98 & 112 & 100 & 103 & 99 \end{bmatrix}$$

After quantization, only the few low frequency coefficients have significant values while most of the high frequency coefficients have zero values. In addition, the zeros representing the less important higher frequencies that have been discarded, giving rise to the lossy part of compression & only the remaining non-zero co-efficient will be used to reconstruct the image.

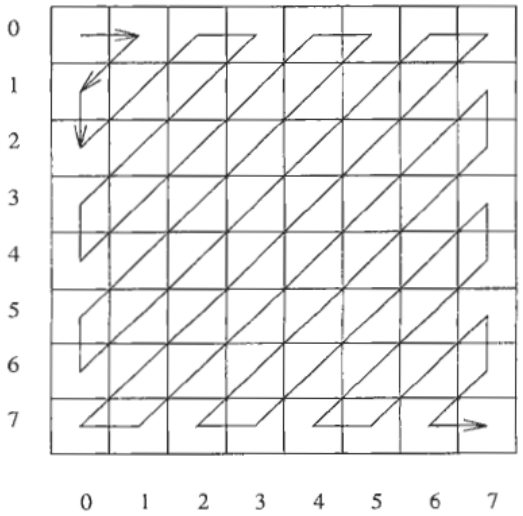

Fig 1: Zigzag Sequence

If we use different quantization matrices than use of Q10 would gives C significantly more zeros, while Q90 would result in very few zeros. After quantization most of the coefficients have zero values. JPEG takes advantage of this by encoding quantized coefficients in zigzag sequence as shown in figure 1.This zigzag process helps entropy coding by placing low-frequency coefficients (usually larger values) before the high-frequency coefficients (usually close to zero).

The original image is reconstructed using decompression technique. For that initially element of C is multiply by the corresponding element of quantization matrix using (7) shown below.

$$R(i,j) = Q(i,j) \times C(i,j) \qquad (7)$$

The IDCT is next applied to matrix R, which is rounded to the nearest integer. Also 128 is added to each element of that result.

$$N = round(T'RT) + 128 \qquad (8)$$

Finally Clip off padded rows and columns if padding is done, giving the decompressed version of original 8 X 8 image block M.

C. Discrete Wavelet Transform (DWT)

Wavelet Transform has become an important method for image compression. Wavelet based coding provides substantial improvement in picture quality at high compression ratios mainly due to better energy compaction property of wavelet transforms. In previous section, DCT transform the original pixels into a few large numbers and many small numbers. In contrast, the wavelet transforms of this section decompose an image into bands (regions or subbands) that correspond to different pixel frequencies.

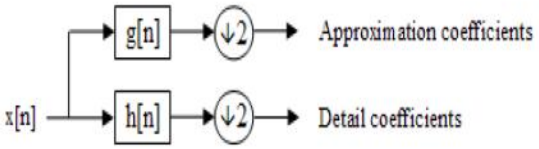

Fig 2: 1 level decomposition

Discrete wavelet transform (DWT) maps an image into a set of coefficients that constitute a multiscale representation of the image [1]. Discrete Wavelet Transform (DWT) of a signal is computed by passing it through a series of filters and down samplers. This wavelet filters are designed so that the coefficients in each subband are almost uncorrelated from the coefficients in other subbands. In DWT First the samples are passed through a low pass filter with impulse response g(n) giving approximation or average coefficients. The signal is decomposed simultaneously using a

high pass filter h(n), giving the detailed coefficients. Approximation is high scale, low frequency components of the signal. The details are low scale, high frequency components of the signal. Since half the frequencies of the signal are removed, the filter outputs are down sampled by 2. This constitutes 1 level of decomposition as shown in above figure 2.

Like the one dimensional discrete wavelet transform, the two-dimensional DWT can be implemented using digital filter and down samplers. Initially each row is filtered and then down sampled to obtain two subbands images. Then each column is filtered and down sampled to obtain four subbands images. The four subbands created are named as LL, LH, HL and HH, where the first letter corresponds to the filter applied to the rows, and the second letter corresponds to the filter applied to the columns. Here in the two-dimensional case, LL represents approximation coefficients while LH, HL and HH represent horizontal, vertical and diagonal detail coefficients. After first level of decomposition, the Approximation subband LL is then decomposed into four subbands at level two as shown in figure 4 and the process can be continued in the same manner for further levels. Reconstruction can be obtained from the approximation subband LL only. Thus the wavelet structure has potential for the image compression which is extensively used in JPEG 2000 standard [2][10].

The DWT scheme decomposed image into approximate & detail coefficients. After decomposition aside from quantizing away small coefficient, the next step is how to code the wavelet coefficients. The Embedded Zerotree Wavelet algorithm popularly known as EZW is an efficient coding scheme developed by Shapiro [3].It is an efficient coding scheme based on the multi-resolution nature of wavelet transforms. The resulting algorithm gave a better performance at higher compression ratio than the existing schemes. This scheme efficiently exploits the parent-child relationship of the DWT coefficients to code and compress them efficiently.

LL_1 HL_1

LH_1 HH_1

Fig 3: First stage of Discrete wavelet transform

LL_2 HL_2 HL_1

LH_2 HH_2

LH_1 HH_1

Fig 4: A two-scale wavelet decomposition

The two important features of the EZW coding are significance map coding and successive approximation quantization. The coding of the significance map is achieved using a new data structure known as zerotree. Figure 5 shows pictorial representation of the zerotree on 3-stage wavelet decomposition.

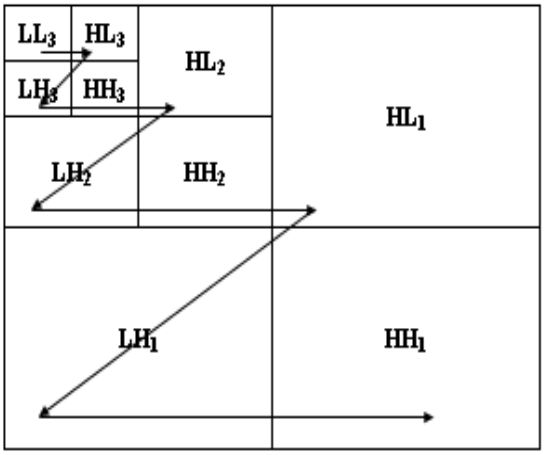

Fig5: Zerotree scanning for encoding significance map

The coefficient at coarse scale is called the parent while all corresponding coefficients at next finer scale of same spatial location and similar orientation are called children. For a given parent, the set of all coefficients at all finer scale are called descendants. Similarly for a given child, the set of all coefficients at all coarser scale are called ascentors. The scanning of the coefficients is performed in such a way that no child is scanned before its parent [3] [4].

In EZW initially a threshold level is selected. Depending upon a threshold level, significance map of symbols will be generated to indicate the significance of the coefficients. Usually, a 4-symbol alphabet (ZTR, IZ, POS, and NEG) is used to represent the significance map.

The four symbols are:
1) zerotree (ZTR),which means the coefficient and all its descendants are insignificant;
2) isolated zero (IZ), which means that the coefficient is insignificant but has some significant descendants;
3) positive significant(POS), which means a positive significant coefficient;

4) negative significant(NEG), which means a negative significant coefficient.

After significance mapping, Embedded coding is achieved using successive approximation quantization (SAQ) method. The SAQ method sequentially applies a sequence of thresholds $T_{0,\ldots\ldots,T_{N-1}}$ to determine the significance of each coefficient . The threshold are chosen such that $T_i = T_{i-1}/2$. The initial threshold are chosen such that $|x_j| < 2T_0$ [3].A dominant list and a subordinate list are maintained during encoding and decoding process. During a dominant pass, coefficients having their coordinates on the dominant list are compared to threshold T_i to determine their significance. If a coefficient is found to be significant, its magnitude is appended to the subordinate list and the coefficient in the wavelet transform array is set to zero to enable the possibility of zerotree occurring on future dominant passes at smaller thresholds. The resulting significance map is zerotree-coded.

The dominant pass is followed by subordinate pass .All coefficients on the subordinate list are scanned and their magnitude is refined. Effectively, the width of the uncertainty interval for the true magnitude of the coefficients is cut in half. For each magnitude on the subordinate list, the refinement can be encoded using a binary value with a 1 indicating that the true value falls in the upper half of the uncertainty interval and 0 indicating that it falls in the lower half. After the subordinate pass, the magnitudes of the subordinate list are sorted in decreasing order to the extent that decoder can perform the same sort. The process continues to alternate between the two passes, with the threshold halved before each dominant pass. The encoding stops when some target stopping criterion has been met.

1) Proposed Algorithm

The proposed algorithm is as follows:-

1. Read the input image.
2. Define the wavelet decomposition level and also type of wavelet (either Haar or biorthogonal wavelet) used.
3. Computes four filters associated with the selected wavelet.
4. Decomposes the input image into subbands using DWT at different level .
5. At each level of decomposition, determine it's approximate & detail (horizontal, vertical and diagonal) coefficients.
6. Define the initial threshold level & encode the Wavelet coefficients using EZW.
7. EZW decoding is than done to reconstruct the original input coefficients .
8. The image is reconstructed through decompression using Inverse- DWT.
9. Finally Determine Image quality assessment parameters.

D. Block Truncation Coding

Quantization is an important technique for image compression. Any quantization method should be based on a principle that determines what data items to quantize and by how much[5]. This technique uses a one bit nonparametric quantizer. The principle used by the block truncation coding (BTC) method and its variants is to quantize pixels in an image while preserving the first two *statistical moments*. In the basic BTC method, the image is divided into blocks (normally 4×4 or 8×8pixels each) .After dividing the picture into blocks, the blocks are coded individually, each into a two level signal[11]. The levels for each block are chosen such that the first two sample moments are preserved. Assuming that a block contains n pixels with intensities p_1 through p_n, *the* first two moments are the mean and variance is given by (9) & (11) shown below:

$$\bar{p} = \frac{1}{n}\sum_{i=1}^{n} p_i \qquad (9)$$

And

$$\overline{p^2} = \frac{1}{n}\sum_{i=1}^{n} p_i^{\,2} \qquad (10)$$

respectively. The standard deviation of the block is

$$\sigma = \sqrt{\overline{p^2} - \bar{p}^2} \qquad (11)$$

The principle of the quantization is to select three values, a threshold p_{thr}, a high value $p+$, and a low value $p-$. Each pixel is replaced by either $p+$ or $p-$, such that the first two moments of the new pixels (i.e., their mean and variance) will be identical to the original moments of the pixel block. The rule of quantization is that a pixel p_i is quantized to $p+$ if it is greater than the threshold, and is quantized to $p-$ if it is less than the threshold. Thus,

$$p_i = \begin{cases} p^+ & if\ \ p_i \geq p_{thr} \\ p^- & if\ \ p_i < p_{thr} \end{cases}$$

Intuitively, it is clear that the mean $\bar{p}$ is a good choice for the threshold[5][11]. The high and low values can be determined by writing equations that preserve the first two moments and solving them. We denote by n^+ the number of pixels in the

current block that are greater than or equal to the threshold. Similarly, n^- stands for the number of pixels that are smaller than the threshold. The sum $n^+ + n^-$ equals to the number of pixels n in the block. Once the mean $\bar{p}$ has been computed, both n^+ and n^- are easy to calculate. Preserving the first two moments is expressed by (12) & (13).

$$n\bar{p} = n^+ p^+ + n^- p^- \quad (12)$$

$$n\overline{p^2} = n^+ (p^+)^2 + n^- (p^-)^2 \quad (13)$$

Solving for $p+$ and $p-$:

$$p^- = \bar{p} - \sigma\sqrt{\frac{n^+}{n^-}}$$

$$p^+ = \bar{p} + \sigma\sqrt{\frac{n^-}{n^+}}$$

Each block is then described by the values of $\bar{p}$, σ and bit plane consisting of 1's and 0's indicating whether pixels are above or below p_{thr} [11]. These solutions are generally real numbers, but they have to be rounded to the nearest integer, which implies that the mean and variance of the quantized block may be somewhat different from those of the original block. In this type of coding techniques the block boundaries are not visible in the reconstructed pictures.

The basic BTC method is simple and fast. Its main drawback is the way it loses image information, which is based on pixel intensities in each block, and not on any properties of the human visual system. This led many researchers to develop enhanced and extended versions of the basic BTC. The original BTC is based on the principle of preserving the first two statistical moments of a pixel block. The variant described here changes this principle to preserving the first two absolute moments. The first absolute moment is given by (14)

$$\overline{p_a} = \frac{1}{n}\sum_{i=1}^{n}\left|p_i - \bar{p}\right| \quad (14)$$

The high & low values can also be written as

$$p^+ = \frac{1}{n^+}\sum_{p_i \geq \bar{p}} p_i \quad (15)$$

$$p^- = \frac{1}{n^-}\sum_{p_i < \bar{p}} p_i \quad (16)$$

The advantage of using a nonparametric quantizer is that the quantizer formulation is available in closed form; this greatly simplifies the computational load. But One especially annoying feature of the basic BTC is that straight edges in the original image become jagged in the reconstructed image.

1) Proposed Algorithm

The proposed algorithm is as mentioned.

1. Read the input image.
2. Define the block size.
3. The given image is divided in small no overlapping blocks of size as mentioned above.
4. Determine mean value of each block & assign threshold value is equal to the mean value.
5. Determine no. of pixels in the current block having p_i greater than p_{thr} & also determine p^+ value.
6. Determine no. of pixels in the current block having p_i less than p_{thr} & also p^- value.
7. A bit plane is constructed such that each pixel location is coded as a "1" or a "0" depending on whether that pixel is greater than p_{thr}.
8. The bit plane and mean value are sent to the receiver.
9. The picture block is reconstructed such that mean value is preserved. That is, pixels in the bit plane that are "1" are set to "p^+" and the "0" are set to "p^-".
10. Finally Determine Image quality assessment parameters.

III. SIMULATION RESULTS

The different image compression schemes discussed and elaborated here are simulated on MATLAB platform [2]. For performance analysis purpose we looked at 3-Standard Test Images. For lossless compression, Huffman method provides CR of 1.2, 1.1 & 1.14 for the images named lena, cameraman & mandril respectively. The result of huffman coding method for cameraman is shown in figure 6.

For lossy compression DCT, DWT& BTC methods are discussed & compared. The compression efficiency is measured using the CR. The quality of the image is analyzed by measuring PSNR and RMSE. SSIM index is a method for measuring the similarity between two images [12]. The variable quantization DCT technique when applied to the images will generate variable PSNR with compression. For instance, DCT application to lena image produces the PSNR of 27.25, 31.98, 39.06 and CR of 11.33, 6.42, 6.09 corresponding to Q10, Q50 and Q90 respectively. Fig. 7 shows the application of DCT algorithm to image, which in turn consists of original input image with reconstructed images using three different quantization levels Q10, Q50 and Q90. Table III represents performance summary of DCT algorithm to the images, and Table IV represents

performance summary of DWT algorithm. If we consider only PSNR values we can observe that DWT algorithm provides better image quality than DCT algorithm and if we consider CR, it provide the high compression than DCT. The DWT algorithm results better quality of reconstructed image than the DCT at high compression ratio because of the artifacts resulting from the block based DCT scheme as shown in figure 8. From fig 9 we observed that the edges of the reconstructed image are blurred but smooth in DCT while edges are sharp but ragged in BTC. Hence in BTC we get the artifacts but it is different from artifacts in DCT.

Original Image

Reconstructed Image

CR = 1.14

Fig 6: Image Compression results of Huffman Technique

Original image

Reconstructed Image (Q10)

CR =11.33, PSNR =27.25

Reconstructed Image (Q50)

CR =6.42, PSNR =31.98

Reconstructed Image (Q90)

CR =6.09, PSNR =39.06

Fig 7: Application of Discrete Cosine Transformation to image with $Q_{10,}$ Q_{50} and Q_{90}

Fig 8: Image Compression results of Discrete Cosine Transformation and Discrete Wavelet Transform

Fig9: Image Compression results of Discrete Cosine Transformation and Block Truncation Coding

TABLE III: PERFORMANCE SUMMARY OF DCT ALGORITHM

Image	**CR**	**PSNR**	**RMSE**	**MSSIM**
lena (256x256)	6.09	39.46	2.71	0.94
	7.43	38.13	3.15	0.91
	11.35	35.83	4.12	0.88
Cameraman (512x512)	7.33	48.70	0.93	0.98
	13.66	43.32	1.74	0.96
	21.3	40.00	2.54	0.94
Mandril (512x512)	4.99	41.61	2.11	0.97
	8.41	35.88	4.09	0.91
	14.96	32.82	5.82	0.82

TABLE IV: PERFORMANCE SUMMARY OF DCT ALGORITHM

Image	Q level	CR	PSNR	RMSE	MSSIM
lena (256x256)	90	6.09	39.06	2.83	0.96
	50	6.42	31.98	6.41	0.9
	10	11.33	27.25	11.06	0.78
Cameraman (512x512)	90	7.34	46.41	1.21	0.99
	50	7.94	38.88	2.89	0.96
	10	13.65	31.23	6.99	0.87
Mandril (512x512)	90	4.90	42.35	1.95	0.99
	50	4.94	34.21	4.96	0.95
	10	8.35	26.78	11.67	0.79

IV. CONCLUSION

The various image compression techniques compared and contrasted here reveals that images can be substantially compressed as application demands. Lossless method of image compression is mostly used to compress medical images where loss of data result in mislead in the diagnosis while lossy method is mostly used to compress photo graphics images . In an image as the redundant information gets added as more number of co-efficients considered. This in turn increases the computational time along with storage space requirements.

In image compression technique we expect the high compression ratio (CR) and also better quality of the reconstructed image. From the above results we conclude that as CR increases, value of PSNR decreases and RMSE increases. In DCT at high compression ratio quality of image degrades due to blocking artifacts. Hence at high compression ratio DWT technique is used which gives the better quality of the reconstructed image as compared to DCT. Also in DCT reconstructed image have the blurred but smooth edges .To get sharp edges BTC technique is used which result in reconstructed image having artifacts quite different from those produced by other techniques.

REFERENCES

[1] R.C Gonzalez, R.E Woods, “Digital Image Processing” (Third Edition), Pearson Education.
[2] R.C Gonzalez, R.E Woods, Steven L Eddins, “Digital Image Processing Using MATLAB”, Pearson Education.
[3] Ze-Nian Li, Mark S. Drew, “Fundamentals of Multimedia”, PHI Education.
[4] David Salomon, “A Concise Introduction to Data Compression”, Springer_Verlag , 2008.
[5] David Salomon, “Data Compression” (Fourth Edition), Springer-Verlag London Limited, 2007.
[6] J. H.Pujar, L.M.Kadlaskar, “ A New Lossless Method of Image Compression & Decompression using Huffman Coding Techniques” Journal of Theoretical and Applied Information Technology, Page No.1-nsformation, Haar Transformation, Simultaneous Encryption and Compression Techniques.” IEEE International Conference on Digital Image Processing , Page No.1-6, Nov 2009
[7] Mahendra M. Dixit1, Prof. Priyatamkumar, “Comparative Analysis of Variable Quantization DCT and Variable Rank Matrix SVD Algorithms for Image Compression Applications”, IEEE International Conference, Page No.1-5, 2010.
[8] Ken Cabeen & Peter Gent, “Image Compression and the Discrete Cosine Transform”, Page No.1-11.
[9] Andrew B. Watson, “Image Compression using the Discrete Cosine Transform”, NASA Research Center, Page No.1-8.
[10] J. M. Shapiro, "Embedded image coding using zerotree of wavelet coefficients”, IEEE Transactions on Signal Processing, Vol. 41, Page No.1 -18, Dec 1993.
[11] E.J. Delp & 0. Robert Mitchell, “Image Compression Using Block Truncation Coding IEEE Transactions on” Communication, Vol. 27,Page no 1 - 8 , September 1979.
[12] Zhou Wang , “Image Quality Assessment: From Error Visibility to Structural Similarity”, IEEE Transactions on Image Processing, Vol. 13, Page No.4, April 2004.

PRATIBHA: INTERNATIONAL JOURNAL OF SCIENCE, SPIRITUALITY, BUSINESS AND TECHNOLOGY (IJSSBT), Vol. 1, No.1, March 2012
ISSN (Print) 2277—7261

Discrimination Between Atrial Fibrillation (AF) & Normal Sinus Rhythm (NSR) Using Linear Parameters

Mayuri J. Patil[1], Bharati K. Khadse[2], S. R. Suralkar[3]
[1,2,3]Electronics and Telecommunication Dept. SSBT's COET Bambhori, Dist:Jalgaon.
Emails: [1]mayuri.deshmukh08@gmail.com, [2]bharatikhodpe@yahoo.co.in, [3]shekhar_srs@rediffmail.com

Abstract: Heart rate analysis method can be used for discern between atrial fibrillation (AF) and Normal Synus Rhythm (NSR). Atrial fibrillation is one of the common sustained cardiac arrhythmia diagnose by electrocardiogram (ECG). The Heart rate variability (HRV) and standard measurements techniques are used to detect QRS Complexes from ECG. All R peaks are detected for RR intervals. Various parameters can be measured using linear indexes of HRV like SDNN, SDANN, RMSSD, PNN50, LF, HF, VLF etc. It classifies NSR and AF patients using spectral parameter LF/HF ratio.

Keywords: Heart rate, ECG, QRS complex, RR interval, R peak

I. INTRODUCTION

One of the most common cardiac arrhythmias is atrial fibrillation. In Europe alone, about 4.5 million people are affected [2]. The probable prevalence is about 1% in the general population, increasing with age. Above the age of 50, the probability of developing atrial fibrillation doubles with every decade of life [1].Because of demographic expansion, the number of patients with atrial fibrillation will increase in the future. Atrial fibrillation has become a widespread disease in industrialized countries. This supraventricular tachyarrhythmia is characterized by ungraceful atrial commencement with the substantial decline of atrial mechanical function and hemodynamic devastation. Atrial fibrillation is not life aggressive but the most dreaded impediment is embolism, and strokes in particular. The rate of ischemic stroke among patients with atrial fibrillation is two to seven times higher than for people who don't suffer from atrial fibrillation [2]. One out of six ischemic strokes is caused by atrial fibrillation [1]. Unfortunately, AF remains under diagnosed, as it is often asymptomatic: up to 30% of all patients with AF are unaware of their diagnosis [3]. Thus, there are high risk patients, unaware of the disease. Atrial fibrillation is typically diagnosed by electrocardiogram (ECG). It is characterized by the substitution of reliable P waves by express oscillations or fibrillatory waves, associated with an irregular and often too rapid ventricular response when atrioventricular conduction is intact. As atrial fibrillation is often intermittent, it may not be detected on standard 12-lead ECG or even on a 24-hour ECG recording (Holter). But it is essential to identify these patients so that they can be medicated. Ischemic strokes can then be prevented.

II. QRS DETECTION METHODOLOGY

QRS detectors can be divided in to two stages: a filtering stage and a decision stage. The filtering stage is used to emphasize the QRS complex and to reduce noise and the influence of the other waves in the ECG signal (P and T waves). Typically first a bandpass filter is applied to the signal to reduce noise and to suppress P and T waves and then put through a non-linear stage to enhance the QRS complex. Then the QRS enhanced signal is thresholded and some decision logic is used for the final stage of detection. Wavelet transformation has proven to be a very efficient tool in the analysis of ECG signals. Its ability to automatically remove noise and to cancel out undesired fenomena such as baseline drift are a benefit over other techniques. When an arrhythmia appears, such a monitor can be programmed to immediately store an interval of the abnormal ECG for subsequent conduction to a central station where a physician can interpret it. Such a device requires a very accurate QRS recognition capability. False detection results in unnecessary transmission of data to the central station or requires an excessively large memory to store any ECG segments that are unnecessarily captured. Thus, an accurate QRS detector is an important part of many ECG instruments. QRS detection is difficult, not only because of the physiological variability of the QRS complexes, but also because of the various types of noise that can be present in the ECG signal.

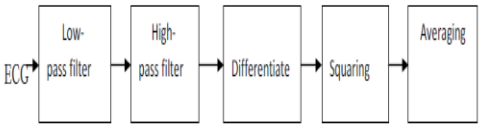

Figure.1 Block diagram of QRS detector algorithm

Noise sources include muscle noise, artifacts due to electrode motion, power-line involvement, baseline wander, and T waves with high-frequency characteristics similar to QRS complexes. In given approach, digital filters reduce the influence of these noise sources, and thereby improve the signal-to-noise ratio. Of the many QRS detectors proposed in the literature, few give serious enough concentration to noise reduction.

Software QRS detectors typically include one or more of three different types of processing steps: linear digital filtering, nonlinear transformation, and decision rule algorithms [2]. Linear processes include a band pass filter, a derivative, and a moving window integrator. The nonlinear transformation that is used is signal amplitude squaring. Applying thresholds provide part of the decision rule algorithm.

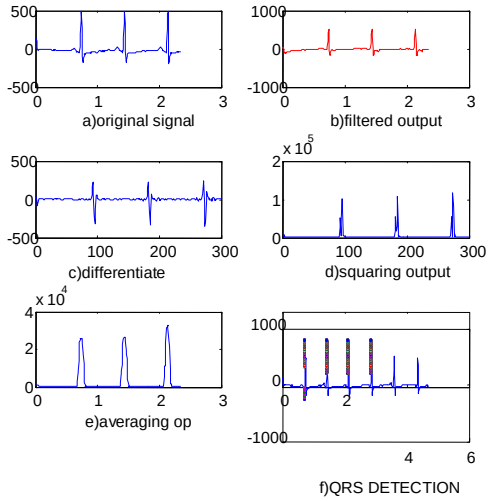

Figure 2.A Output of QRS Detection Algorithm for NSR a) Original signal b) Filter output c) derivative output d) squaring output e) averaging f) QRS detection

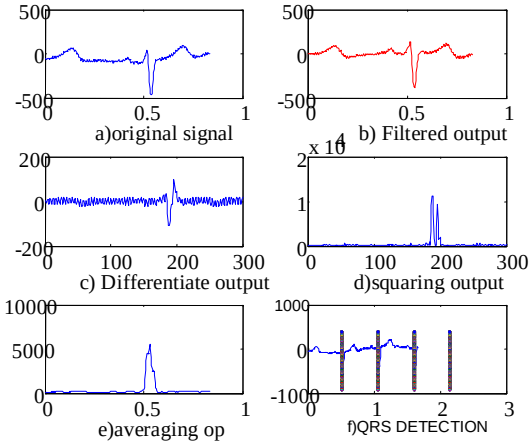

Figure 2.B Output of QRS Detection Algorithm for AF a) Original signal b) Filter output c) derivative output d) squaring output e) averaging f) QRS detection

Fig. 2.A and Fig.2.B shows signals at various steps in digital signal processing of Normal Sinus Rhythm and Atrial fibrillation. A real-time QRS detection algorithm was developed by Pan and Tompkins [2].First, in order to ease noise, the signal passes through a digital band pass filter composed of cascaded high-pass and low-pass filters. Fig. 2.A.(b) shows the output of this filter. The next process after filtering is differentiation [Fig. 2.A.(c)], followed by squaring [Fig.2.A. (d)], and then moving window integration [Fig. 2.A.(e)]. Information about the slope of the QRS is obtained in the derivative stage. The squaring process intensifies the slope of the frequency response curve of the derivative and helps restrict false positives caused by T waves with higher than usual spectral energies. The moving window integrator produces a signal that includes information about both the slope and the width of the QRS complex. Fig. 2.A.(f) shows the final output stream of pulses marking the locations of the QRS complexes after application of the adaptive thresholds.

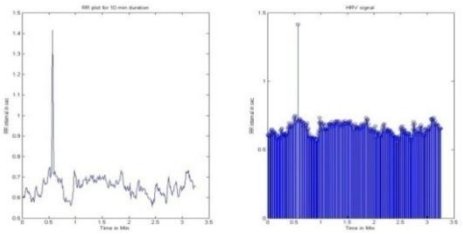

Figure 3.RR interval time series for 10 min duration and HRV signal

PRATIBHA: INTERNATIONAL JOURNAL OF SCIENCE, SPIRITUALITY, BUSINESS AND TECHNOLOGY (IJSSBT), Vol. 1, No.1, March 2012
ISSN (Print) 2277—7261

III. HEART RATE VARIABILITY

The distance between adjacent QRS complexes is termed as the normal to normal (NN) or the R to R (RR) intervals. Heart rate variability (HRV) refers to the beat-to-beat alterations in heart rate. Under inactive conditions, the ECG of healthy individuals exhibits periodic variation in R-R intervals. The HRV measurements are captured noninvasively from the ECG signal. The results from this HRV data are capable of portraying physiological condition of the patient and are an important indicator of cardiac disease. Variability in heart rate is clinically linked to lethal arrhythmias, hypertension, coronary artery disease, congestive heart failure, organ transplant, tachycardia, neuropathy, and diabetes.There are two methods in linear analysis time domain and frequency domain analysis.

A. Time Domain Analysis

The easiest inference of HRV is portrayed by the time domain measures. Originally, HRV was measured manually from the mean R-R interval in time domain and its standard deviation measured on short-term 5 minute ECG segment. With these methods either the heart rate or each QRS complex or the RR intervals between successive normal complexes are determined. Simple time–domain variables include the mean RR interval, the mean heart rate, the difference between maximum and minimum heart rate, etc. Table I shows in detail the various time domain HRV parameters [3].Recordings for a longer period of 24 hours allow complex statistical time-domain analysis. These statistical parameters may be derived from direct measurements of the RR intervals or from the differences between RR intervals. The simplest variable to calculate is square root of variance i.e. the standard deviation of the NN interval (SDNN). Since variance is mathematically equal to total power under the curve, SDNN covers complete variability in the ECG recording.

$$NN50 = \sum_{i=1}^{N} \left| RR_{i+1} - RR_i \right| > 50ms \quad [count; -]$$

$$pNN50 = \frac{NN50}{N} . 100 \quad [\%; -]$$

$$SDNN = \sqrt{\frac{1}{N} \sum_{i=1}^{N} (RR_i - \overline{RR})^2} \quad [ms; -, ms, ms]$$

$$\overline{RR} = \frac{RR_1 + RR2 .... R_N}{N} = \frac{1}{N} \sum_{i=1}^{N} RR_i \quad [ms; -, ms]$$

$$SDANN = \sqrt{\frac{1}{N} \sum_{i=1}^{N} (RR_i - \overline{\overline{RR_i}})^2} \quad [ms; -, ms, ms]$$

$$RMSSD = \sqrt{\frac{1}{N-1} \sum_{i=1}^{N-1} (RR_{i+1} - RR_i)^2} \quad [ms; -, ms, ms]$$

TABLE I. TIME DOMAIN HRV PARAMETERS

Variables	Unit	Description
		Statistical measures
SDNN	ms	Standard deviation of all NN intervals
SDANN	ms	Standard deviation of averages of NN intervals in all 5 min. segments of the entire reading.
RMSSD	ms	The square root of mean of the sum of the square of differences between adjacent NN intervals
NN50 count		Number of pairs of adjacent NN intervals differing by more than 50ms in the entire recording
pNN50	%	NN50 count divided by the total number of all NN intervals

B. Frequency Domain Analysis:

In distinction to the time domain measures of HRV mentioned above, recent developments in microprocessor technology has enabled the calculation of frequency measures on the same ECG data. Frequency measures involve the spectral analysis of HRV. The RR interval time series is an irregularly time-sampled signal. This is not an issue in time domain, but in the frequency-domain it has to be taken into account. If the spectrum estimate is calculated from this irregularly time-sampled signal, additional harmonic components appear in the spectrum. Therefore, the RR interval signal is usually interpolated before the spectra analysis to recover an evenly sampled signal from the irregularly sampled event series. The HRV spectrum contains the high frequency (0.18 to 0.4 Hz) component, which is due to respiration and the low frequency (0.04 to 0.15 Hz) component that appears due to both the vagus and cardiac sympathetic nerves [3]. Ratio of the low-to-high frequency spectra is used as an index of parasympathetic sympathetic balance. Frequency domain HRV variables are detailed in Table II [3]. In the frequency-domain analysis power spectral density (PSD) of the RR series is calculated. Methods for calculating the PSD may be divided into Fast Fourier transform (FFT) based and autoregressive (AR) model based methods. The PSD is analyzed by calculating powers and peak frequencies for different

frequency bands. For the FFT based spectrum analysis powers are calculated by integrating the entire spectrum. The spectrum in AR model methods can be divided into components and the band powers are obtained as powers of these components [3].

TABLE II. FREQUENCY DOMAIN HRV PARAMETERS

Variables	Unit	Description	Frequency Range
Total Power	ms^2	Variance of all NN intervals	Approx.≤0.4 Hz
VLF	ms^2	Power in the low frequency range	0.003-0.04Hz
LF	ms^2	Power in the low frequency range	0.04-0.15Hz
HF	ms^2	Power in high frequency range	0.15-0.4Hz

IV. RESULTS

We have used ECG signals from the MIT-BIH Atrial Fibrillation Database (MIT-BIH AF DB) and the MIT-BIH Normal Sinus Rhythm Database (MIT-BIH NSR DB), which are derived from the archive of PhysioBank [6]. The MIT-BIH AF DB includes 25 ECG recordings of 10 hours each. These ECGs are from patients with paroxysmal atrial fibrillation. The MIT-BIH Sinus Rhythm Database consists of 18 ECG records, of 24 hours each. These ECGs originate from healthy persons who do not have significant arrhythmias.

The results of the algorithm are summarized in Tables III and IV.

TABLE III: TIME-FREQUENCY DOMAIN MEASURE OF NORMAL SINUS RHYTHM

Signal	Time domain measures					Frequency domain measures				
	SDNN	***SDANN***	***RMSSD***	***PNN50***	***HR***	***TF***	***LF***	***HF***	***VLF***	***LF/HF***
17453	129.350	58.72208	4.5427	11.6700	82.87	1.31E+07	3.34E+04	5.35E+04	3.17E+04	0.62
16273	108.29	66.8916	7.254	9.903	79.6333	1.31E+07	8.23E+03	5.26E+03	2.56E+04	1.56
16786	68.792	61.4817	4.9623	13.5589	73.4144	1.30E+07	1.16E+04	6.27E+03	1.28E+04	1.84
18184	102.3229	74.1323	4.5579	6.866	86.80411	1.31E+07	1.88E+04	1.41E+04	3.52E+04	1.33
19093	93.5589	73.2916	9.47599	9.6547	69.05033	1.28E+07	1.22E+04	2.60E+03	2.74E+04	4.68

TABLE IV Time-frequency domain measure of atrial fibrillation

Signal	Time domain measures					Frequency domain measures				
	SDNN	***SDANN***	***RMSSD***	***PNN50***	***HR***	***TF***	***LF***	***HF***	***VLF***	***LF/HF***
08455	755.8688	35.4495	1.6275	1.05226	77.4012	4.39001E+006	2.75529E+005	6.2450E+005	9.39005E+004	0.44088
06995	172.5533	55.4949	6.22889	4.09000	222.6845	3.517E+006	3.81446E+005	9.05537E+005	2.11003E+004	0.42133
04043	632.4581	152.3067	2.5981	17.43667	109.2900	4.38761E+006	2.69714E+005	6.2531E+005	9.38038E+004	0.43044
06426	338.1285	165.1368	22.6916	78.23133	83.0707	1.32E+07	5.81E+04	1.18E+05	2.14E+04	0.49277
08378	310.701	249.3951	39.9613	25.73773	70.546	6.27E+07	1.31E+07	2.47E+07	9.99E+06	0.32885

V. CONCLUSION

Time domain measures SDNN, SDANN, RMSSD, NN50 and pNN50 randomly varies in analyzed signals. For this reason these parameters are not appropriate for atrial fibrillation detection. Also SDNN is not a well defined statistical quantity because of its dependence on length of recording period. Parameter LF/HF ratio can be used as atrial fibrillation indicator. Ratio varies from 0.28± 0.25 for atrial fibrillation and 2.63±2.09 for normal sinus rhythm. The discrimination between NSR and AF patient using LF/HF is not satisfactory. ECG recordings without atrial fibrillation, but of patients who suffer from

atrial fibrillation, will be analyzed in more detail to improve the algorithm. When the ECG recording time is extended, the detection rate increases. But this procedure is time-consuming for patients, as well as for physicians, and even then, not all patients will be identified . This algorithm allows patients suffering from atrial fibrillation to be identified in an easier and more convenient way.

REFERENCES

[1] Patrick S. Hamilton and Willis J. Tompkins, "*Quantitative investigation of QRS detection rules using the MIT-BIH arrhythmia database*" IEEE Trans. Biomed. Eng., vol. BME-33, no. 12, pp. 1157-1165, 1986.

[2] J. Pan and W. J. Tompkins, "*A real-time QRS detection algorithm*,"IEEE Trans. Biomed. Eng., vol. BME-32, no. 3, pp. 230-236, 1985.

[3] Dipali bansal,Munna khan,A.K.Salhan, "*A Review of measurement and analysis of Heart Rate variability*"Internation conference on computer and automation Engineering.

[4] Task force of the European society of cardiology and the North American society of spacing and electrophysiology. "*Heart rate variability: standards of measurement, physiological interpretation and clinical use"*.Circulation,vol93,no.5,1043-1065,1996.

[5] European Heart Journal(1996) 17,354-381

[6] Database:- MIT-BIH Normal Sinus Rhythm & MIT-BIH Atrial Fibrillation from www.physionet.org

[7] Fe smith, Ej bowers Langley, j Allen, A Murray medical physics, Freeman hospital, Newcastle upon Tyne,UK '*Heart rate variability characteristics required for simulation of interval sequence'.*

[8] Gari D.Clifford St.Cross College "Signal Processing Methods For Heart Rate Variability".

[9] Rangaraj M. Rangayan "Biomedical Signal Analysis, A case-study approach".

[10] W.J.Tompkins, Ed.,"Biomedical Digital Signal processing".

[11] Nicole Kikillus, Gerd Hammer, Steven Wieland and Armin Bolz," Algorithm for Identifying Patients with Paroxysmal Atrial Fibrillation without Appearance on the ECG "Proceedings of the 29th Annual International Conference of the IEEE EMBS Cité Internationale, Lyon, France August 23-26, 2007.

[12] M. Brennan, M. Palaniswami*, and P. Kamen" Communications", IEEE Transactions On Biomedical Engineering, Vol. 48, No. 11, November 2001.

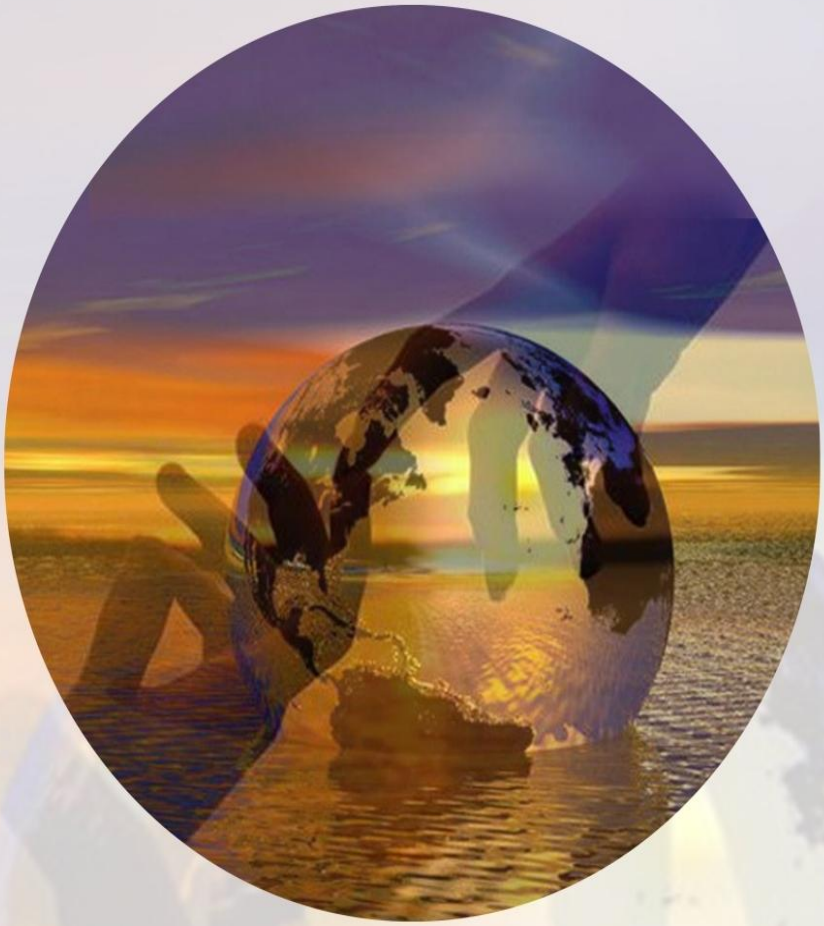

PRATIBHA : INTERNATIONAL JOURNAL OF SCIENCE, SPIRITUALITY, BUSINESS & TECHNOLOGY (IJSSBT)

Vol.1, No.1, March 2012

ISSN (Print) : 2277-7261

http : www.ijssbt.org

SHRAM SADHANA BOMBAY TRUST's
COLLEGE OF ENGINEERING & TECHNOLOGY,
BAMBHORI, JALGAON (INDIA)

ISSN 2277-7261

PRATIBHA : INTERNATIONAL JOURNAL OF SCIENCE,SPIRITUALITY, BUSINESS & TECHNOLOGY (IJSSBT) Vol.1,No.1, March 2012 ISSN (Print) : 2277-7261